UNIVERSIDADE FEDERAL DE LAVRAS

THAIS APARECIDA SALES

COMPUTATIONAL DESIGN OF CHEMICAL SENSORS: from molecules to molecularly imprinted polymers

LAVRAS - MG
2022

THAIS APARECIDA SALES

COMPUTATIONAL DESIGN OF CHEMICAL SENSORS: from
molecules to molecularly imprinted polymers

Thesis submitted to the Federal
University of Lavras, as part of the
requirements of the Graduate Program in
Agrochemistry, area of concentration in
Computational Chemistry, for the degree
of Doctor.

Advisor: Dr. Teodorico de Castro Ramalho

LAVRAS – MG
2022

THAIS APARECIDA SALES

DESIGN COMPUTACIONAL DE SENSORES QUÍMICOS: DE MOLÉCULAS A POLÍMEROS MOLECULARMENTE IMPRESSOS

COMPUTATIONAL DESIGN OF CHEMICAL SENSORS: FROM MOLECULES TO MOLECULARLY IMPRINTED POLYMERS

> Tese apresentada à Universidade Federal de Lavras, como parte das exigências do Programa de Pós-Graduação em Agroquímica, área de concentração em Química Computacional, para obtenção do título de Doutor.

APROVADA em 11 de fevereiro de 2022.
Dr. Arnaldo César Pereira UFSJ
Dra. Adélia Aquino TTU
Dra. Daiana Teixeira Mancini UFLA
Dr. Guilherme Luiz Dotto UFSM

Prof. Dr. Teodorico de Castro Ramalho
Orientador

LAVRAS – MG
2022

Aos meus filhos, por serem o motivo das minhas maiores lutas, e por serem o futuro do mundo. Futuro não se faz sem ciência.
À todas as meninas e mulheres que já sonharam ou sonham em fazer ciência e produzir conhecimento.
Dedico.

Agradecimentos

Desafio tão grande quanto escrever toda essa tese é conseguir agradecer a tudo e a todos que contribuíram de alguma forma para que eu chegasse até aqui. Talvez o mais importante de toda jornada não seja somente a chegada, mas também perceber que não se faz nada sozinho; e que quanto mais aprendemos, mais percebemos o quão primitivos ainda permanecemos.

Inicialmente, gostaria de agradecer à Deus, inteligência suprema e a causa primária de todas as coisas, e aos espíritos de luz que sempre me orientam e me guiam, transmitindo força e sabedoria para seguir evoluindo e fazendo o bem;

Aos meus filhos, de sangue e de coração, Davi e Raul, Yuri e Gabriel, por ressignificar em mim o amor e todo o resto das coisas da vida;

Ao meu grande companheiro de vida, Régis, pelo imenso amor, cuidado, respeito e carinho, por ser o marido mais maravilhoso e meu principal apoiador em tudo que me disponho a fazer;

Aos meus familiares, em especial minha mãe, minha vó, meu irmão e minha cunhada por serem minha rede de apoio; sem vocês o caminho seria mais duro e triste, e essa conquista não seria possível;

Ao meu avô que partiu recentemente e que me mostrou como tudo sempre é muito maior do que conseguimos enxergar;

Ao meu orientador Teodorico de Castro Ramalho, por toda atenção, dedicação e ensinamentos, por me incentivar sempre a crescer e explorar novos caminhos e oportunidades, me fazendo evoluir cada vez mais. Obrigada por me mostrar que o mais importante não é o que se fala, mas como se fala; e por ser um exemplo de pessoa e profissional, não só para seus alunos, mas para todos que o conhecem;

Aos professores do Grupo Molecc Elaine e Matheus, e à todos aos demais colegas do grupo, em especial aos amigos Alexandre, Ander, Aquino, Bruna, Francisco, Joyce, Jéssica, Lethícia Braga, Lethícia Assis, Dani, Daiana, Lucas, Taináh e Dani pelo excelente trabalho em equipe, pelo enorme conhecimento transmitido e compartilhado, pela companhia e pelos momentos de descontração que tornaram o trabalho mais leve e feliz.

À Universidade Federal de Lavras (UFLA), pela infraestrutura oferecida e por proporcionar esta conquista;

À minha grande amiga Monalisa, por ser e estar nas horas boas e ruins, mesmo distante fisicamente;

Aos amigos, professores e funcionários da UFLA e do Departamento de Química, pelo grande aprendizado, amizade e serviços prestados;

A todos os professores que tive ao longo da vida que me ensinaram e me deram grandes exemplos, pessoais e profissionais, e que me mostraram não só a importância do conhecimento, mas também a beleza da ciência;

E por fim, como a vida não é nada linear, desejo agradecer à todas as pessoas que fizeram parte desta jornada direta e indiretamente, seja no doutorado ou fora dele.

Obrigada!

ABSTRACT

Computational methods can be employed at various stages in the development of different types of chemical sensors. The use of theoretical tools can drastically accelerate the development process of new sensors, as well as helping to obtain a more robust, cheaper, and selective end product. This thesis discusses the employment of different computational chemistry methods in the design of chemical sensors. The first approach deals with the study of electrochemical sensors. Initially, the density functional theory (DFT) method was employed to perform the design of a molecularly imprinted polymer (MIP) for detection of the drug of abuse MDMA. This theoretical method was used to simulate several steps in the synthesis of a MIP in addition to selectivity tests. The set of computational analyses obtained constitutes a very useful protocol to predict the optimal experimental conditions, saving time and financial resources in the process. Still in the electrochemical sensors approach, an electrochemical sensor based on the same MIP technology was developed for detection of progesterone and 17-β Estradiol. The developed material responded to the concentrations of the analytes in the ranges from 10 to 50 µM, and also has a single current range response, which improves the selectivity of the material. The second chemical sensor approach addressed in this thesis was spectroscopic probes. In this part, both computational methods based on classical mechanics such as molecular dynamics (MD) and quantum methods such as DFT were employed to explore the photochemical and spectroscopic properties of the ciprofloxacin molecule. From the calculations performed, it was possible to observe the changes that can occur in the UV-Vis, fluorescence and fluorine[19] NMR spectra of the antibacterial agent when it interacts with the human topoisomerase-II beta enzyme. Such results indicate a possibility of using ciprofloxacin as a spectroscopic probe for cancer detection, since this enzyme is related to the disease. From all the tests performed, it can be concluded that computational methods are able to predict many properties and behaviors that can be useful in the design of new chemical sensors. The manipulation of molecules and systems in a theoretical way can assist in obtaining crucial information that often cannot be obtained experimentally. Moreover, it is also possible to conclude that chemical sensors are an extremely useful and versatile technology that can be developed for various purposes.

Keywords: Electrochemical sensors. MIPs. Spectroscopic probe. Computational design. Ciprofloxacin.

RESUMO

De maneira ampla, os métodos computacionais podem ser empregados em diversas etapas do desenvolvimento de diferentes tipos sensores químicos. O uso de ferramentas teóricas pode acelerar drasticamente o processo de desenvolvimento de novos sensores, além de auxiliar na obtenção de um produto final mais resistente, barato e seletivo. Esta tese discute o emprego de diferentes métodos de química computacional no design de sensores químicos. A primeira abordagem trata do estudo de sensores eletroquímicos. Inicialmente, o método de teoria do funcional da densidade (DFT) foi empregado para realizar o design de um polímero molecularmente impresso (PIM) para detecção da droga de abuso MDMA. O referido método teórico foi utilizado para simular diversas etapas da síntese de um PIM, além de testes de seletividade. O conjunto de análises computacionais obtidos constitui um protocolo muito útil para predizer as condições experimentais ótimas, economizando tempo e recursos financeiros no processo. Ainda na abordagem dos sensores eletroquímicos, foi desenvolvido um sensor eletroquímico baseado na mesma tecnologia de MIP, para detecção de progesterona e 17-β Estradiol. O material desenvolvido respondeu às concentrações dos analitos nas faixas de 10 a 50 µM, além de possuir resposta em faixa de corrente única, o que melhora a seletividade do material. A segunda abordagem de sensor químico tratada nesta tese foram as sondas espectroscópicas. Nesta parte, foram empregados tanto métodos computacionais baseados na mecânica clássica, como a dinâmica molecular (DM) quanto métodos quânticos como o DFT, para explorar as propriedades fotoquímicas e espectroscópicas da molécula de ciprofloxacina. A partir dos cálculos realizados, foi possível observar as mudanças que podem ocorrer nos espectros de UV-Vis, de fluorescência e de RMN de flúor[19] do agente antibacteriano quando este interage com a enzima topoisomerase-II beta humana. Tais resultados indicam uma possibilidade de uso da ciprofloxacina como sonda espectroscópica para detecção de câncer, uma vez que esta enzima está relacionada à doença. A partir de todos os testes realizados, é possível concluir que os métodos computacionais são capazes de predizer muitas propriedades e comportamentos que podem ser úteis no design de sensores químicos. A manipulação de moléculas e sistemas de forma teórica pode auxiliar na obtenção de informações cruciais, que muitas vezes não podem ser obtidas de forma experimental. Além disso, é possível concluir também que os sensores químicos constituem uma tecnologia extremamente útil e versátil, podendo ser desenvolvidos para diversas finalidades.

Palavras-chave: Sensor eletroquímico. MIPs. Sonda espectroscópica. Design computacional. Ciprofloxacina.

TABLE OF CONTENTS

PART I- OUTLINE AND SCOPE

1. GENERAL INTRODUCTION

The need to monitor biologically important molecules is one of the many justifications for the development of new chemical sensors (LI, Q. Y. *et al.*, 2022). Chemical sensors are molecules or measuring devices used in various types of analysis, which allows the real-time monitoring and *in situ* information capture, since they require minimal manipulation of the studied system. In addition, they have several other advantages, such as portability, ease of automation, and the possibility of miniaturization (LOWINSOHN; BERTOTTI, 2006; YANG, B. *et al.*, 2016). A traditional chemical sensor is basically composed of a recognition material, a transducer, and a detector that will interpret the signal. For selective recognition, molecules or materials that can react specifically with the target molecule are employed, generating a signal that allows its identification or quantification. This received signal is maximized to minimize environmental effects on detection (LOWINSOHN; BERTOTTI, 2006).

In most cases, the development of chemical sensors requires a high amount of financial resources and time in their production, since the process is quite complex, and the final product can still present low selectivity and stability, especially with sensors that use biological macromolecules as recognition part (SALES; RAMALHO, 2020). Additionally, other aspects must be considered such as sensor regeneration that may be laborious, making reuse unfeasible or even impossible. Besides all these disadvantages, there is also the problem of biocompatibility with sensors for *in vivo* use (ASADIAN; GHALKHANI; SHAHROKHIAN, 2019). Thus, a chemical sensor cheap, simple to obtain and stable, easy to handle and made by means of biocompatible material is of great interest not only for medical applications but in various industrial processes. It should be kept in mind, however, that obtaining a material or compound with most of these advantages is difficult. In order to develop a chemical sensor many possible and available resources should be evaluated (PENDLEY; LINDNER, 2017).

In this sense, computational chemistry tools can drastically accelerate the chemical sensor design. With the help of computational modeling techniques, it is possible to control the desired properties to develop chemical sensors of high

selectivity, which is advantageous when compared to the process of obtaining sensors based on chemical intuition (COWEN; KARIM; PILETSKY, 2016; VIVEIROS et al., 2017). Additionally, computational methods are able to make predictions more effectively, avoiding the use of empirical testing methods, which saves time and financial resources (PILETSKY et al., 2001). For this purpose, both quantum (FONSECA; NASCIMENTO; BORGES, 2016) and classical (VIVEIROS et al., 2017) methods can be employed.

2. JUSTIFICATION

The central part of a chemical or biosensor is the recognition element, called receptor, which is responsible for specifically recognizing and binding the target molecule in a complex sample. The recognition element is in close contact with the transducer. To rationally design better recognition elements, it is important to obtain the maximum of information at the molecular level as possible. In this context, computational chemistry techniques can be very useful to design new sensors (HAUPT; MOSBACH, 2000; KHAN; PAL; KRUPADAM, 2015; SALES; RAMALHO, 2020).

The use of computational tools in rational design of chemical sensors can help in the prediction of the most proper recognition elements (FONSECA; NASCIMENTO; BORGES, 2016), and also for the best size (NICHOLLS *et al.*, 2015), molar ratio (KHAN; PAL; KRUPADAM, 2015), prevalent molecular interactions (FONSECA; NASCIMENTO; BORGES, 2016), energy (LV *et al.*, 2008), selectivity (GHOSH *et al.*, 2017) and the best solvent to be employed both in synthesis and in analysis (KHAN; PAL; KRUPADAM, 2015). A lot of this information cannot be obtained experimentally, and for some experimental data, there is a significant cost in many cases. In this way, computational methods have advantages of low cost, time saving, clinical and environmental safety as no disposal of chemicals is needed (ABDEL GHANI *et al.*, 2016).

3. OBJECTIVE

3.1. General

To explore applications of several computational chemistry methods to rationalize the chemical sensors design, employing both molecular mechanics and quantum mechanics methods.

3.2. Specific

- To perform a rational design for the Molecularly Imprinted Polymer (MIP) preparation, for 3,4-methylenedioxymethamphetamine (MDMA) detection, employing computational chemistry methods.

- To synthesize a hybrid material consisting of molecularly imprinted polymer (MIP) and magnetic nanoparticles, as a recognizable part of an electronic system used as a sensor for progesterone and 17-β Estradiol.

- To investigate theoretically, the behavior of ciprofloxacin (CPX) in the human topoisomerase-II β (hTOPO-II) active site, evaluating how this interaction affects the ^{19}F NMR chemical shift of CPX to propose the use of CPX as a spectroscopic NMR probe for cancer diagnosis.

- To analyze theoretically the potential of ciprofloxacin as a dual UV-Vis/fluorescent probe to be used in cancer diagnosis.

PART II- THEORETICAL BACKGROUND

1. CHEMICAL SENSORS

The modern era is an era of science and technology, which strongly influences all aspects of life (KUMAR; PATHAK; CHAUDHARY, 2021). The new generation of sensing technologies is closely related to the development of new functional synthetic materials, both of which have a direct impact on expanding the hardware capabilities available today (SWAGER, 2018). A simpler physical manifestation of the term "technology" comes as a simple, user-friendly device, with the design and development of a smart equipment capable of optimal performance at reduced costs and guaranteed wide deployment (KUMAR; PATHAK; CHAUDHARY, 2021). The emergence of nanoscience and nanotechnology have provided more and more resources for measurement techniques as well. In addition, the current moment is opening new horizons for researchers in the field of sensing technologies, allowing the development of chemical sensors that are increasingly efficient and technological (ASADIAN; GHALKHANI; SHAHROKHIAN, 2019; WANG, C. *et al.*, 2022).

The origin of the word "sensor" comes from the Latin *sentire*, to feel (SIMÕES; XAVIER, 2017). Considering the semantics of the word, sensors have the attribute of feeling into their surrounding environment to define a coupling relationship. Now, in a more pragmatic interpretation, the term "sensor" can cover many definitions. According to the International Union of Pure and Applied Chemistry (IUPAC), a chemical sensor is "a device that transforms chemical information, ranging from the con-centration of a specific sample component to total composition analysis, into an analytically useful signal. The chemical information, mentioned above, may originate from a chemical reaction of a molecule or from a physical property of the system investigated" (LEIBL *et al.*, 2021). Usually, a sensor is defined as a device that responds to a physical stimulus, and as a result transmits an electrical impulse aimed at measuring some change in any intrinsic property of the constituent material, whose magnitude is normally proportional to this change. This stimulus can be as light intensity or wavelength, heat, motion, pressure, magnetic signal, chemical composition, or even sound (HILLBERG; BRAIN; ALLENDER, 2005; SIMÕES; XAVIER, 2017).

Basically, a sensor is composed of a recognition material, a transducer and a detector, as can be seen in Figure 1. The recognition material is responsible for reacting to stimuli, which can be the amount, property or condition that is received and will be converted into an electrical signal. The transducer is the part responsible for converting that stimulus that was received into an electrical signal. Finally, the detector is responsible for identifying this electrical signal. Besides the basic parts, a sensor can also contain many other components, such as processors, other detectors and transducers, signal conditioners, processors, memory devices, data recorders, actuators, among others (FRADEN, 2015). For the selective recognition of molecules or materials that react specifically with the molecule of interest, recognition elements are generally employed and allow the signal transduction to the detector. This signal is then maximized in order to minimize errors (LOWINSOHN; BERTOTTI, 2006).

Figure 1 – Basic structure of a generic sensor.
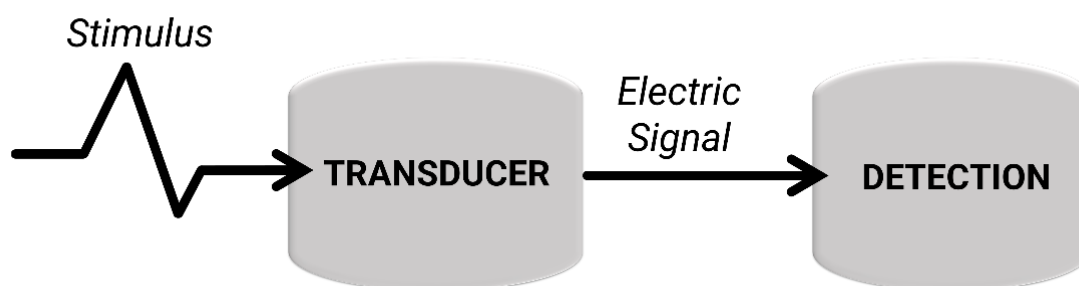
Sensors can be classified in many ways, one way to classify these sensors is based on some of their properties, such as the sensing material, the conversion phenomenon, field of application, stimulus type, among others (YURISH, 2017). In the case of chemical sensors, they are defined as materials that respond to stimuli produced by means of chemical reactions or any chemical compound, intended for the identification and quantification of chemical species (FRADEN, 2015). A chemical sensor can act either as an isolated device or as part of larger or more complex systems (HUSSAIN *et al.*, 2021; LI, R. *et al.*, 2018).

The use of chemical sensors allows real-time monitoring and *in situ* information capture, since they require minimal manipulation of the system to be

studied (LOWINSOHN; BERTOTTI, 2006). Such devices have the potential to complement or even replace many of the classical analytical methods, having many advantages, such as easier sample preparation, reduced analysis costs, and the possibility of miniaturization of the systems, which favors the portability and use of this equipment (MERCANTE *et al.*, 2017).

The optimization process of a chemical sensor is closely related to the selectivity improvement process, which allows a more efficient detection of certain chemical species in complex samples, and consequently minimizes the manipulation of the sample (HILLBERG; BRAIN; ALLENDER, 2005). Furthermore, aspects related to robustness, sensitivity and stability of the chemical sensor should also be considered in the development of an efficient chemical sensor (LOWINSOHN and BERTOTTI, 2006).

Considering the wide range of materials, technologies, and purposes that can be employed in the preparation of sensors that fall into the category of chemical sensors, there is no universally accepted method for categorizing the complete list of this type of detector (FRADEN, 2015). Usually, chemical sensors are divided into two main categories, one based on transduction methods and the other class based on implementation methods. The classification of chemical sensors based on transduction method can be further subdivided into those that measure electrical or electrochemical properties (SILAMBARASAN; MOON, 2022), those that measure a change in a physical property (YURISH, 2017), and finally those that rely on absorption or emission of optical or other wavelengths of electromagnetic radiation (TIKUM *et al.*, 2019).

1.1. Chemical sensors based on spectroscopic signals

One sensing technology that has been widely investigated in many fields, is the use of spectroscopic probes (SPs) (J LLOYD-HUGHES1 *et al.*, 2021; LI, H.; MA, 2018; XUE *et al.*, 2021). SPs can be described as molecules that react with a specific target and this interaction results in changes in their spectroscopic properties, which in turn can identify this target (ZHOU, J.; MA, 2016). The spectroscopic change can be

in chromogenic, fluorescent, or chemiluminescent properties (CHEN, X.; SUN; MA, 2006). The increasing development and implementation of SPs can be attributed to the advantages of offering greater temporal and spatial sampling capability, as well as to the powerful ability of these compounds to improve analytical sensitivity. In addition, it is important to emphasize their special photochemical stability, unique electronic and self-assembly properties (SHI; MA, 2012; YU, Q. *et al.*, 2021). The use of SPs has gained a lot of prominence, especially in the field of medical diagnostics as a crucial part of molecular imaging (PEREIRA *et al.*, 2019). Molecular imaging constitutes a powerful tool to investigate the intact living samples in real time with great spatial resolution by the use of synthetic SPs and biological imaging instrumentation (BRITTON, 2017). These probes are able to respond selectively to its intended target even in a complex system that contains a host of competing analyte (CHAN; DODANI; CHANG, 2012).

Generally, SPs are composed of three parts, which are the spectroscopic half and the recognition half, and the binding part that connects the first two. The most common reaction mechanisms employed in SP design strategies are the protonation-deprotonation mechanism, complexation, cleavage and formation of covalent bond, non-covalent (supramolecular) interactions and redox reactions. In addition, design strategies of SP are chosen according to the different purposes of detection. For example, to detect analytes with redox properties, redox-based spectroscopic probes can be designed, while to detect physical environmental factors, such as viscosity, polarity or temperature; the environment-sensitive spectroscopic probes are more suitable (LI, X. *et al.*, 2014). Beyond all of this information, other important assignment in the SP design is to identify the best reactions that have high chemoselectivity, biorthogonality and fast rate. This is important once that for SP to be suitable for detection and imaging applications, the reaction must proceed with suitable kinetics under biological constraints or that have short lifetimes (YANG, YOUJUN *et al.*, 2010).

Among the various photophysical processes in which the SP can be based, fluorescence sensing is attractive for its potentially very high sensitivity, excellent temporal-spatial resolution and fairly simple technical implementation (NIU *et al.*, 2015). There are three basic kinds of SP response modes in fluorescence spectroscopy,

which are the *on-off* mode, in which there is a decrease of fluorescence intensity of the probe; the *off-on*, in which there is an increase of the fluorescence intensity; and the ratiometric response, which refers to a shift in the emission or excitation spectra of a probe upon reaction with an analyte. As can be seen, each kind of probe has its own advantage and drawback, and the correct choice of the design strategy is the key point in the SP development (ZHOU, J.; MA, 2016).

Many are the applications of these molecules in different areas. Just in the beginning of 2022, more than 200 researches were developed in order to aim the design of fluorescent probes (ANALYTICS, 2022), and the molecular targets range from ions (AHMED, N. *et al.*, 2022; CUI *et al.*, 2022; GUO *et al.*, 2022; XIANG *et al.*, 2022; ZHANG, C.; PAN; HE, 2022) to biological macromolecules (LI, Y. *et al.*, 2022; LIU, D. *et al.*, 2022; YAN *et al.*, 2022).

Speaking more in depth about probes for biological applications, the implementation of this technique has enabled *in situ* and real-time monitoring of many biological processes (CHEN, X.; SUN; MA, 2006) . In this context, several inhibitors have been developed and tested as fluorescent probes, aiming the identification (KANAGARAJ *et al.*, 2020; LEE, Y.-A. *et al.*, 2018), localization (LIU, H.-W. *et al.*, 2017; YU, Q. *et al.*, 2021), tracing (MA *et al.*, 2020), imaging (HONG *et al.*, 2019; WANG, HUAIMIN *et al.*, 2018) and possibly the treatment of many diseases (TANG *et al.*, 2019). Regarding the latter, a very promising example worths mentioning are the PI3K inhibitors. Phosphoinositide 3-kinases (PI3Ks), also called phosphatidylinositol 3-kinases, are a family of enzymes known to be related to several types of cancer (JANKU; YAP; MERIC-BERNSTAM, 2018). Based on this relevant feature, some PI3K inhibitors with specific spectroscopic properties that can be used as probes for early cancer diagnosis have been proposed, as a case of Pt complexes (PEREIRA *et al.*, 2019). Some other applications for SPs can be found in Figure 2.

Figure 2 – Representative bioimaging applications with reaction-based small-molecule fluorescent probes for highly reactive species and metal ions.
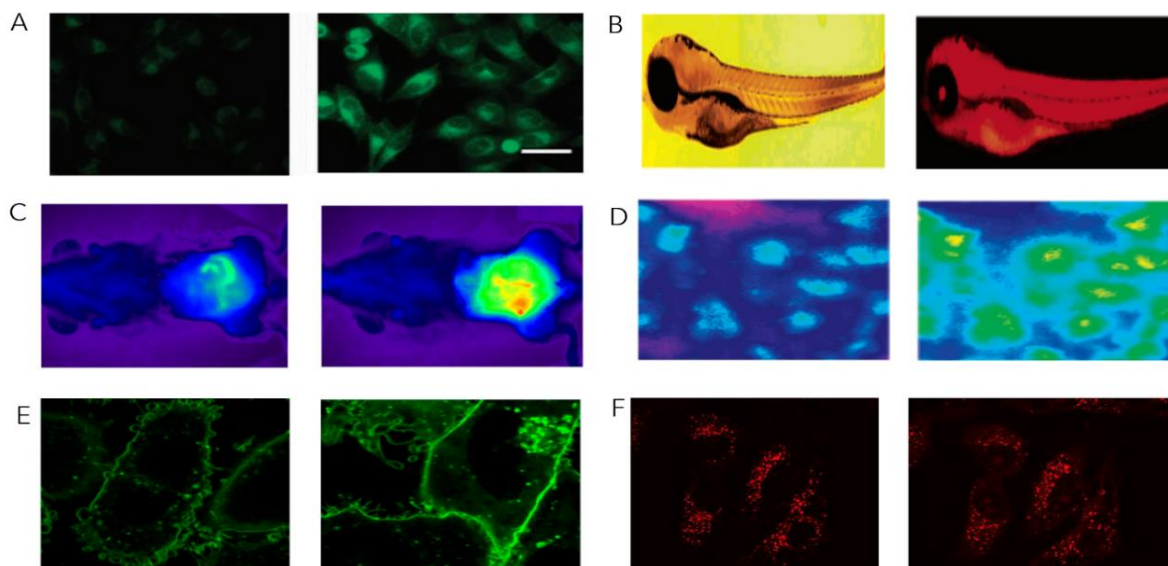
Source: (CHAN; DODANI; CHANG, 2012).
Legend: **(A)** Detection of H2S in mammalian cells with SFP-2 (QIAN et al., 2011). **(B)** Visualizing accumulation of mercury pools in zebrafish with a spirorhodamine-based probe (SUNG-KYUN KO et al., 2006). **(C)** Visualization of myeloperoxidase-derived HOCl in a mouse model for peritonitis with SNAPF (SHEPHERD, J. et al., 2007). **(D)** Levels of NO in a rat kidney visualized with DAC-P (EITA SASAKI et al., 2005) **(E)** Imaging of Saos-2 cells with phosphotyrosine-based probe (WANG, HUAIMIN et al., 2018). **(F)** ATP detection in HeLa cells with rhodamine-based probe (TIKUM et al., 2019).

1.1.1. Fluorescence Spectroscopy

Although some famous figures in science have studied this phenomenon in the past, it was in the year 1852 that British physicist G. G. Stokes began to determine the nature of fluorescent emission. Stokes published some interesting results involving several samples, both organic, using a quinine solution, and inorganic, using the mineral fluorite (STOKES, 1852). His reports were based on earlier results presented by J. Herschel (HERSCHEL, 1843, 1845), who describes that the quinine solution shows an arc of pale blue light when sunlight enters the tube. Stokes also observed that the mineral fluorite exhibits fluorescence when illuminated with ultraviolet light, employing the word "fluorescence" for the first time (STOKES, 1852; VALEUR; ARIO; BERBERAN-SANTOS, 2011).

Like quinine, many other compounds can not only absorb light, but also emit part of the absorbed light at different wavelengths (GODBEY, 2014). Fluorescent molecules, also called fluorophores, have a wide range of applications being used in detergents, fluorescent lighting, synthetic fibers in credit cards, banknotes, fluorine in toothpastes among others (GARCÍA *et al.*, 2012).

If a molecule absorbs a photon with an adequate amount of energy, many photophysical events can occur, such as phosphorescence, internal conversion (IC) or vibrational relaxation, intersystem crossing (ISC), or fluorescence, both shown in the Jablonski diagram for organic molecules (Figure 3). The figure is an example of the general scheme of a Jablonski Diagram showing the formation of an excited state S_1 or S_2, which can decay to the ground state S_0 while maintaining the singlet state. This decay can be radiative resulting in the photophysical process of fluorescence or non-radiative, which are the IC process. The diagram also shows that decay from a triplet state T_1 formed earlier by ISC energy transfer, which can occur with the emission of a photon by the process called phosphorescence (LAKOWICZ, 2006).

Figure 3 − Simplified Jablonski diagram for organic molecules.
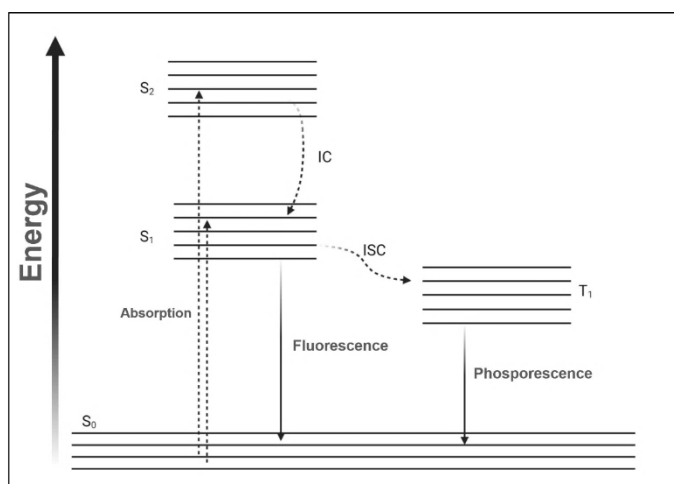
Legend: In the figure, the abbreviations S_0, S_1, and S_2 correspond to the fundamental, first, and second excited states, respectively. T_1 corresponds to the first triplet state. The acronym IC corresponds to the internal crossing process, and ISC corresponds to the intersystem crossing phenomenon.

Each of the above processes occurs with a certain probability given by the decay rate constants (k). This decay rate is inversely proportional to the lifetime of the

photophysical process, also called the average length of time (τ) for a set of molecules to decay from one state to another. In the case of fluorescence, the lifetime is an intrinsic property and therefore, regardless of the measurement method, it can be considered a state function since it does not depend on the initial perturbation conditions of the system. The fluorescence lifetime is understood as the time required for a population of excited fluorophores to decrease exponentially to N/e through energy loss via fluorescence and other non-radiative processes (BEREZIN; ACHILEFU, 2010).

The processes described above are called photophysical processes, since there is electronic excitation of a molecule by absorption of radiation, and this process does not result in chemical changes in the molecule. There are also chemical reactions that occur due to the absorption of UV, Vis or IR radiation. In this case, the process is called photochemical (LIU, SIMIN; KOKOT; WILL, 2009). The presence of certain functional groups that are sensitive to light brings great probabilities for inducing a photochemical process. The main functional groups that exhibit photoreactivity are the carbonyl group, aryl chloride, nitroaromatic group, n-oxides, weakened C-H bonds, sulfide groups, alkenes, phenolic groups and polyenes, mainly with conjugated double bonds (GRANIZO, 2012).

1.1.2. Nuclear Magnetic Resonance Spectroscopy (NMR)

Besides the fluorescence technique, another spectroscopic technique that is widely used as a basis for developing SPs is the Nuclear Magnetic Resonance (NMR) spectroscopy. NMR spectroscopy is one of the most powerful tools currently available not only for determining structural and other properties of molecules, but also in many fields of science, where it is increasingly being considered as a tool, especially in the clinical context (HATZAKIS, 2019; SEDAGHAT DOOST *et al.*, 2019; SPEYER; BALEJA, 2021). Together with liquid chromatography-mass spectrometry (LC-MS) and Fourier Transform ion cyclotron resonance (FT-MS), NMR is one of the most important spectroscopic techniques applied for analysis of metabolic profiling (SERKOVA; NIEMANN, 2006). NMR technique has a variety of applications ranging

from materials, biological sciences and food sciences to medicine (GHOSH *et al.*, 2017; GLADDEN, 1994; HATZAKIS, 2019; RAMALHO; TAFT , 2005).

This technique was first developed in 1946 in Stanford and M.I.T. by the physicists Felix Bloch and Edward Purcell and their collaborators (BLOCH, 1946; PURCELL; TORREY; POUND, 1946), who received the Nobel Prize (EDWARDS, 2019; WÜTHRICH, 1995, 2003). Some phenomena in NMR can be explained only using quantum mechanics, but the basis of the theory can be understood through the principles of classical mechanics and magnetism. The phenomenon of nuclear magnetic resonance is based on the fact that the nucleus of some atoms has magnetic properties, which in the presence of an external magnetic field, behave in such a way that chemical information can be obtained (PELLECCHIA; SEM; WÜTHRICH, 2002).

In order to start, it is necessary to explain some basic concepts such as the nuclear *spin* property. Generally, atomic nuclei contain protons and neutrons except for the ^{1}H atom. Such core constituents have an intrinsic angular momentum and this property is called *spin*. There is a quantized number of spin states that can be adopted for each nuclear *spin.* This number of allowed states is determined by the quantum number of nuclear spin *I*. For each nucleus, there are $2I + 1$ allowed states. In a nucleus, the pairs of protons or neutrons when aligned makes that the *spins* of these particles to cancel each other. Thus, there is not cancellation of spins when there are unpaired protons or neutrons in the nucleus, i.e. when the atomic number or atomic mass has odd number. Similarly, nuclei with even numbers of protons and neutrons have zero nuclear spin (HATZAKIS, 2019; PYKETT *et al.*, 1982). With this in mind, it is already possible to anticipate that only some nuclei will be active in NMR, which are those that do not have null spin.

Due to the fact that there is distribution of electric charges, the rotation of these particles around some axis generates a magnetic field. This means that each nucleus can then be considered a magnetic dipole, or magnet (VEEMAN, 1997). Thus, the nucleus has a magnetic moment μ generated by its charge and spin. In the absence of an external magnetic field, the dipoles orientation is random, and all spin states have the same energy, which is said to be degenerate. Also, in a group of atoms all *spin* states must be almost equally occupied and must have allowed *spins*. However, in the

presence of a uniform magnetic field, called B_0, these dipoles reorient themselves aligning with or opposite the field. This means that the previously degenerate *spin* states split into two states of unequal energy, and the particles will be arranged in these two states according to the Boltzman distribution. Continuing with the example of the ^{1}H nucleus, the state *spin* +1/2 is the state that is aligned with the field, and thus has the least energy (PAVIA, 2015).

In addition, when an external magnetic field is applied, the nucleus begins to precess, that is, to change of direction on its own rotation axis, with angular frequency ω, as can be seen in Figure 4. The frequency intensity is proportional to the magnetic field. Therefore, the more intense is the applied magnetic field, the higher is the frequency.

Figure 4 – Precession of a spinning nucleus as a result of the presence of an external magnetic field.
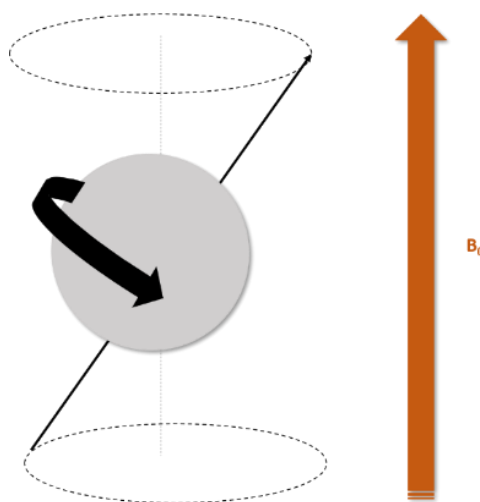
Adapted from PAVIA et al., 2015.

Since the nucleus is charged this precession generates an oscillating electric field of the same frequency. Thus, if radiofrequency reaches in this nucleus, the change of the *spin* state will occur when the frequency of the incident radiofrequency (ν) is equivalent to the frequency of the electric field generated by the preceding nucleus (ω) (i.e. if ν = ω). As there is a small population excess in the lower energy state this change will occur to equalize number of particles in both states. When nuclei

aligned with the external magnetic field are induced to absorb energy and change spin orientation relative to the field, the nuclear magnetic resonance phenomenon occurs (PYKETT *et al.*, 1982). Since this absorption is a quantized process, the energy absorbed is equivalent to energy difference between the two states, as shown in the equation **(1)**:

$$\Delta E = E2 - E1 = h\nu \tag{1}$$

Moreover, this energy difference is also proportional to the field strength B_0, and this proportionality is given by the equations **(2 and 3):**

$$\Delta E = f(B_0) \tag{2}$$
$$\Delta E = f(\gamma B_0) = h\nu \tag{3}$$

Since μ is quantized in h / 2π units, we have:

$$\Delta E = \gamma \frac{h}{2\pi} B_0 = h\nu \tag{4}$$

and

$$\nu = \frac{h}{2\pi} B_0 \tag{5}$$

Where γ is the gyromagnetic ratio, mentioned previously. This ratio determines the energy dependence on the magnetic field. From the equation, it can be concluded that the frequency required for the transition is proportional to the magnetic field created (PAVIA, 2015).

At the end of radiofrequency irradiation, nuclei that have changed to the higher energy state return to their initial state, releasing the portion of energy absorbed for the transition, giving rise to the signal. Thus, it can be concluded that only a small percentage of all nuclei will give rise to the signal, since only the excess population in the lowest energy state will carry out the state transition. To have an idea, for a 60 MHz instrument there are 1,000,009 nuclei in the lowest spin state for every 1,000,000

nuclei in the highest spin. This means that in approximately 2 million cores, only 9 that are left in the lowest energy state and will absorb energy, making the transition, allowing resonance to be observed (GLADDEN, 1994).

This phenomenon is what generates the signal, but this whole theory would not be of much use in obtaining chemical information if all nuclei absorbed the same amount of energy. Therefore, another important piece of information to understand NMR spectroscopy is that hydrogen nuclei absorb different amounts of energy depending on the chemical environment in which they are located, i.e. the electron density around them. Surrounding electrons around the nucleus form the so-called *local diamagnetic current*, and create a magnetic field that opposes the external magnetic field B_0. Thus, when the hydrogen atom is, for example, close to electronegative atoms, the absorbed frequency is changed, and consequently there is a change in the signal. This means that hydrogen atoms that are in different chemical environments in a molecule will not be magnetically equivalent and will give rise to different signals (POPLE, J. A., 1957).

These different signals will originate a characteristic spectrum for each compound, which will allow the deduction of various information such as structural elucidation, stereochemistry, among others. Since different intensities of the magnetic field generate different energy gaps, a measure of this displacement that is not field dependent is required. For this, a field independent measure was adopted, called *chemical shift* (δ). This measure expresses how much a proton resonance differs from a standard, which is the tretramethylsilane (TMS) molecule in parts per million (ppm) (SILVERSTEIN; WEBSTER; KIEMBLE, 2005).

In addition to electron density-related absorption interference, the amount of energy absorbed by a nucleus can also change due to the presence of other magnetically different ^{1}H nuclei that are nearby. When this happens, the signal unfolds into n + 1 signals, where n is the number of magnetically inequivalent hydrogen nuclei that are adjacent to the nucleus in question. So, besides knowing which atoms are neighboring the ^{1}H nucleus, it is also possible to know how many other active ^{1}H are in the vicinity. The distance between the generated peaks is called the *coupling constant* represented by the letter J. This constant is then a measure of how much the nucleus is affected by the *spin* of its active neighbors in the NMR (BRUICE, 2004).

Therefore, it can be concluded that the number of signals will show how many types of magnetically different nuclei are present in the molecule. The location of the signals will tell how much a nucleus is protected or unprotected by the surrounding electronic density; the signal strength will give information about the number of hydrogen nuclei of the same type, and finally, the signal unfolding will show the hydrogen number of the adjacent atoms (SILVERSTEIN; WEBSTER; KIEMBLE, 2005).

This technique is an extremely valuable tool in the structural elucidation of organic compounds (GIMENEZ *et al.*, 2021). Furthermore, the NMR bases allow its application in several technologies, such as imaging diagnostics (BRITTON, 2017), spectroscopic probes (GONÇALVES *et al.*, 2019), among others (BELDA *et al.*, 2013; GHOSH *et al.*, 2017; XIAO *et al.*, 2015). In relation to cancer cells, some studies have been developed applying NMR techniques to detect and quantify low molecular weight metabolites excreted by them, such as pancreatic cancer metabolites (OUYANG; DAI, 2017) and prostate cancer (MADHU *et al.*, 2016). In addition, compounds that are active in NMR can act as imaging markers, as the case of cancer diagnosis (MANCINI, 2014; OUYANG; DAI, 2017; PEREIRA *et al.*, 2019; SALEEM *et al.*, 2018).

1.1.2.1. Spectroscopic sensors and F^{19} NMR Spectroscopy

Since the fluorine atom has only one naturally occurring isotope, ^{19}F, with spin ½ and a high magnetogyric ratio (γ), fluorine-19 nuclei have a good sensitivity to NMR analysis, with 83% sensitivity, when compared to ^{1}H (SCOTT; HENNIG, 2016). Minor changes in the chemical environment cause a great change in the chemical shift. This is one of its most useful features of the use of fluorine nucleus in NMR. For most fluorine-organic compounds, the chemical shift range is of 400 ppm. The standard reference compound for ^{19}F is the trichlorofluoromethane (CFCl$_3$), but other compounds are frequently used. In this case, the data must be converted. Organic compounds of natural origin difficultly have ^{19}F as substituent, but considering that the fluorine is monovalent, it can be used as substitute of ^{1}H atoms in organic synthetic compounds (STANLEY, 2002). The ^{19}F spectra of organic fluorinated compounds

besides possess large chemical shifts, are also characterized by strong spin-spin interactions of the ^{19}F-^{19}F and ^{19}F- ^{1}H types (GUNTHER, 2014). Due to all of these characteristics, the ^{19}F NMR has a most pronounced shifts and consequently, the signals are good solved and prevent the overlapping of the peaks. This is crucial, for example, in differentiation of analytes with similar structures (DAL POGGETTO *et al.*, 2014).

In relation to the applications of this technique, ^{19}F NMR has emerged as a versatile tool both in biological and in pharmaceutical studies and several libraries of fluorinated compounds have been used to search potential ligands that bind to target proteins (CANTRELLE *et al.*, 2021; GIMENEZ *et al.*, 2021). For *in vivo* applications, ^{19}F NMR is particularly attractive, since the natural occurrence of fluorine is very low and natural biological molecules do not contain this atom in their composition. As such, there is essentially no endogenous signal from the tissues, which ensures greater reliability of results (NUSSBAUMER *et al.*, 2020; YU, J. X. *et al.*, 2013). These characteristics are particularly advantageous in the development of fluorine-based Magnetic Resonance Imaging (MRI) contrast agents, producing a very clear signal (BAILEY *et al.*, 2012). Moreover, the technique has several other no less important applications that can be mentioned such as in conformational analysis (GE *et al.*, 2021), reaction monitoring (OJHA *et al.*, 2021), metal ions detection, and many others (AGBENYEGAH *et al.*, 2022; ANARAKI *et al.*, 2021; BUNCHUAY *et al.*, 2021; SHANINA *et al.*, 2021; ZHAO, Y.; MARKOPOULOS; SWAGER, 2014).

1.2. Chemical sensors based on electrochemical signal

The second type of chemical sensor based on the signal transduction method that will be discussed here is the electrochemical signal-based sensor. The signal from an electrochemical sensor (ESs) is usually derived from an electrical response given in the presence of an analyte. An electrochemical-based method involves the transfer of charge from an electrode to another phase, which can be a solid or liquid sample. The charge resulting from the chemical changes that occur at the electrodes during this process is conducted through most of the sample phase. The detection process can be

based on both the electrode reactions and the charge transport reactions, since both can be modulated chemically (NOVAC, 2013). In general, the electrochemical responses monitored by different methods are mainly based on potential resistance, and electric current (SIMÕES; XAVIER, 2017).

When compared with most standard analytical tools, ESs have many advantages. The first important advantage is that ESs are relatively easy to fabricate in different sizes, which allows for analysis ranging from single small molecule to millions of cells. This is possible because electrochemistry is a surface phenomenon, and therefore analytical measurements with miniaturized devices in ultra-small volumes are relatively easy to make (HEINEMAN; KISSINGER; WEHMEYER, 2021). The second great advantage considers the use of reagents for the detection of analytes. ESs can detect the molecular target without the need to load the cells with reagents, which can be helpful since the use of reagents can change the properties of the medium to be investigated. Third, ESs have a relatively small response time, which allows for more efficient analysis, and consequently faster diagnosis and possible resolution of the problem (MUNTEANU *et al.*, 2020). All the advantages already mentioned, added to its low cost and the short time required for the analysis, as well as the possibility of detecting two or more analytes simultaneously makes the use of electrochemical sensors an excellent analytical approach (TAVAKOLIAN-ARDAKANI *et al.*, 2019).

Taking into account all these advantages, many areas have invested in the development and production of ESs, which has been greatly benefited by the fast development not only of microelectronics and microengineering but also of nanoscience and nanotechnology (SIMÕES; XAVIER, 2017). Modern equipment uses various properties to detect physical, chemical, or biological parameters in many aspects of daily life. In this context, sensors for environmental monitoring (RAHMAN *et al.*, 2019; ZHENG *et al.*, 2021), health (ERTUĞRUL UYGUN *et al.*, 2020; XU, Z. *et al.*, 2021) and sensors related to machines, such as cars, airplanes, cell phones, and technological means, can be mentioned (DUNN-RANKIN; LEAL; WALTHER, 2005; HE *et al.*, 2021; SILAMBARASAN; MOON, 2022; XIA; ZHAO; ZENG, 2020; ZHANG, G. *et al.*, 2020). Another important example between the many interesting applications to the ESs is the *in vivo* monitoring. The *in vivo* ESs approach is as

increasingly technology, both for fundamental research and practical applications. The continuous monitoring of certain analytes enables researches to better understand biological structure and functions of normal and abnormal states of metabolism, which, in turn can help in the identification and treatment of any alteration in the organism. Moreover, continuous monitoring also enables the development of personal databases for the purpose of customizer health managing (XU, C. *et al.*, 2019).

Having in mind the vast possibility of applications and analytes that an ES can detect, it is expected that there is a multitude of materials that can be used with great efficiency in the preparation of ESs. The electrode modification ensures highest selectivity and sensitivity of the sensor (HEINEMAN; KISSINGER; WEHMEYER, 2021). In this context, some of the most known materials that are used in electrode modifications are the 2D materials, such as graphene based materials (MUNTEANU *et al.*, 2020); enzymes (SATOMURA *et al.*, 2018); antibodies (TUTEJA; NEETHIRAJAN, 2018); carbon nanoparticles (ASADIAN; GHALKHANI; SHAHROKHIAN, 2019) and synthetic receptors, such as molecularly imprinted polymers (MIPs) (BANGALEH *et al.*, 2019). For the latter, electrochemical sensors represent one of the most successful applications for MIP-based sensors (LEIBL *et al.*, 2021).

1.2.1. Molecularly imprinted polymers (MIPs)

Since the late 1990s, the development of Molecularly Imprinted Polymers (MIPs) for use in chemo-biosensors has been on a continuous rise. These materials are very attractive both for their recognition properties, which are close to those of natural receptors, for their availability for a wide range of molecular targets, and also for their superior chemical and physical stability when compared to biological receptors (LEIBL *et al.*, 2021). The idea of molecular imprinting came in the 1950s and was initially inspired by Pauling's theories about the formation of antibodies in the human immune system. According to him, the antibodies behaved like denatured proteins where their chains were free to move. Upon geting into contact with an antigen, the attraction of the amino acids would occur by specific groups of the antigen from which

the antibody could memorize the structure of the antigen. The idea was later disapproved, but it served as the basis for the MIPs (BERGMANN *et al.*, 2008; MOSBACH; RAMSTRÖM, 1996).

MIPs are novel class of synthetic receptors capable of selectively recognizing their analyte (APPELL; MARAGOS; KENDRA, 2008; VIVEIROS *et al.*, 2018). This is made possible by using the molecular imprinting approach, which is a polymerization technique used to produce artificial sorbents for a template molecule in a polymeric matrix. In other words, the technique allows the synthesis of polymers with cavities of specific size and shape, as if they were specific receptors to the target molecule (SAJINI; THOMAS; MATHEW, 2019).

In general, MIPs are prepared employing specific template molecules, functional monomers and cross-linking agents. The basic scheme of the synthesis can be seen in Figure 5. The polymerization occurs in the presence of the analyte, enabling the formation of cavities extremely similar to the target molecules during the synthesis. For this, it is necessary to prepare the pre-polymerization complex, that consists in the functional monomer complex making specific intermolecular interactions with the template molecule. Next, it is employed the cross-linking agent, which must be thinking for do not disrupt the functional monomer-template interactions. After the polymerization, the final step is the washing of this polymer, in order to remove the template molecule of the cavities, and then the material is ready for use (FAROOQ *et al.*, 2018). In this way, the formed cavities have a specific size and shape, which makes the adsorption selective for molecules structurally similar to the analyte (FONSECA; NASCIMENTO; BORGES, 2016).

The stability of template-monomer complex is directly related to the quality of imprinted sites (LIU, Z. *et al.*, 2021). This concept is the foundation of the computational MIP design, and is represented in equation (**6**). In this equation, E_C, E_T and E_M are the lowest calculable energies of the template-monomer complex, template, and monomer respectively (SALES; RAMALHO, 2020).

The comparison of the relative stability of different components in the system is given by the analysis of the different values of ΔE (Equation 6), which may then provide an appropriate guide for the selection of the best monomer or even to find the most suitable proportion of template-monomer (KARIM *et al.*, 2017).

$$\Delta E = E_C - [\Sigma E_M + E_T] \tag{6}$$

With all of this in mind, it can be inferred that if the material is theoretically designed before of experimental preparation, the time and cost of preparation as well as selectivity and quality of the material can be improved (SURYANA *et al.*, 2021). In this context, the use of computational techniques has made the design of this type of material increasingly efficient (COWEN; KARIM; PILETSKY, 2016; KHAN; PAL; KRUPADAM, 2015).

Figure 5 – Simplified scheme of the molecular imprinting process.
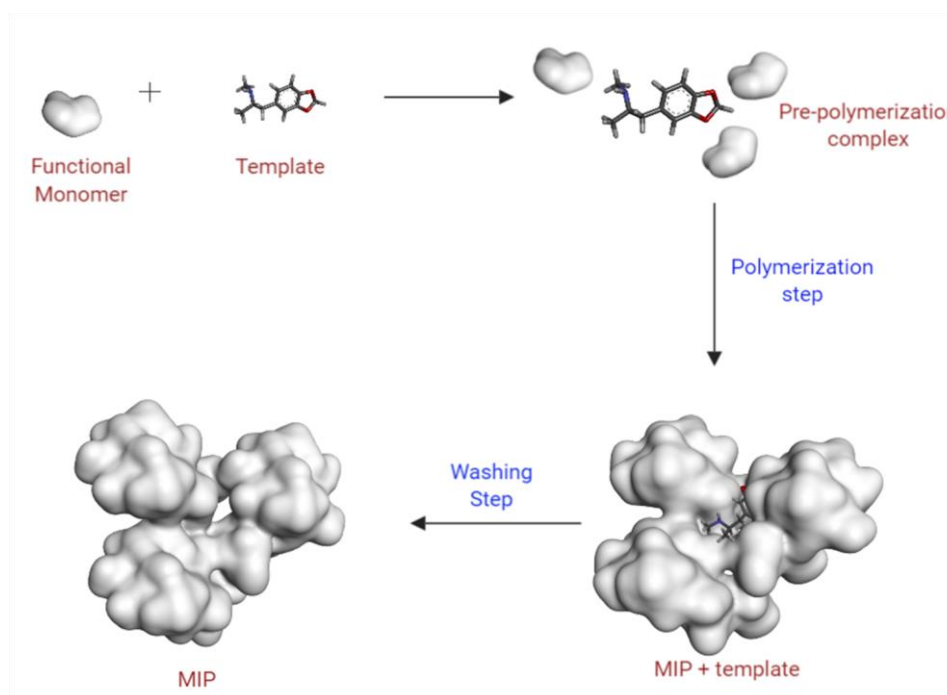
The use of computational methods in the design of MIPs allows for a better understanding of the complexation model that occurs between the monomer and the target molecule. It also allows greater visualization of the impact of polymerization on the structure of the binding site. This makes easier for the production of new materials, with advanced dynamics and reactivity able to respond to their binding targets in more efficient ways (NICHOLLS *et al.*, 2021).

2. COMPUTATIONAL CHEMISTRY METHODS IN THE CHEMICAL SENSORS DESIGN

Computational chemistry tools can drastically accelerate the development of chemical sensors. The protocol of a rational design through computational techniques has enabled efficient preparation of high-affinity chemical sensors with the possibility to design and control their final properties (LIU, Z. *et al.*, 2021). In addition, the increased availability of high-performance computing resources has also contributed to the design of new materials optimizing the experimental phase (ABBURU; VENKATRAMAN; ALSBERG, 2016). From computational chemistry techniques, it is possible to analyze the interactions between the monomer and the template, allowing a proper selection of the material to be used. In addition, computational methods are able to make predictions more efficiently at all stages of the sensor production process avoiding the execution of empirical test methods, which can save time and financial resources (PILETSKY *et al.*, 2001; SURYANA *et al.*, 2021).

Beyond MIP design, the use of computational chemistry techniques offers enormous contributions for the development of many types of chemical sensors, as in the investigation of the molecular recognition between the ligand and biological macromolecules, which is fundamental for the development of biosensors and for the design of spectroscopic probes (DA ROCHA *et al.*, 2016; GANJALI *et al.*, 2009; GHOSH *et al.*, 2017; LEE, N. *et al.*, 2019; LOOGER *et al.*, 2003).

In this context, several computational methods can be employed within a wide variety of methods currently available including classical and quantum methods, such as density functional theory (DFT), semi-empirical, hybrid methods and molecular dynamics (MD). Some of them are better described in the next subsections.

2.1. Density functional Theory (DFT) method

Most of the computational methods used to solve the Schrödinger equation (SE), despite their great accuracy, have a high computational demand, and their use is generally restricted to relatively small systems. DFT is an extremely popular method

that can in principle guarantee not only a good accuracy, but also a greater versatility to be employed in various types and sizes of systems (CAPELLE, 2006).

The DFT method was established in the 1980s as a convenient alternative to solving the SE, showing electronic structure information comparable to Hartree-Fock methods. The basis of the DFT method is the theory developed by Hohenberg and Khon (HOHENBERG; KOHN, 1964; KOHN; SHAM, 1965) around the 1960s which states that the ground state properties of an interacting electron in gaseous form can be calculated from its electronic density, independent of the nature of the external potential. Using this approximation, the many-body problem can then be reformulated into a single-particle problem, which will be expressed in terms of the electronic density (TSE, 2002). The contribution of DFT can be attested by the 1998 Nobel Prize in Chemistry, received by Walter Khon (KOHN, 1999) e John Pople (POPLE, JOHN A., 1999), who developed and implemented the DFT method, respectively.

To better understand the fundamentals of the theory, it is necessary to briefly touch upon the conventional method used to solve the SE. The wave function Ψ is employed as the central quantity. Once this quantity is known, it then becomes possible to access all the information that can be obtained about a particular target system (KOCH; HOLTHAUSEN, 2001). In the simplified form, the usual quantum mechanics (QM) approximation for the SE can be understood by the sequence **(7)**. The system can be specified by choosing a potential $v(r)$, which is entered into the SE, and then the equation for the wave function Ψ is solved, and the observables are calculated. One of the important observables that can be calculated in this way is the particle density **(8)** (CAPELLE, 2006). The density, represented by $\rho(r)$, determines the probability of finding any of N electrons in a given space. Unlike the wave function, $\rho(r)$ is an observable, and therefore can be measured experimentally.

$$v(\boldsymbol{r}) \stackrel{SE}{\Rightarrow} \Psi(\boldsymbol{r_1}, \boldsymbol{r_2} \dots, \boldsymbol{r_n}) \xrightarrow{\langle \boldsymbol{\Psi}|\dots|\boldsymbol{\Psi}\rangle} \text{observables} \tag{7}$$

$$\rho(\mathbf{r}) = N \int \rho^3 \mathbf{r}_2 \int \rho^3 \mathbf{r}_3 \dots \int \rho^3 \mathbf{r}_N \psi^*(\mathbf{r}, \mathbf{r}_2, \dots, \mathbf{r}_N) \tag{8}$$

The conceptual structure of density functional theory can be well summarized by the sequence **(9)** below, which demonstrates that knowledge of $\rho(r)$ implies

knowledge of the wave function and potential, and consequently of all other observables.

$$\rho(r) \Longrightarrow \psi(r_1, \ldots, r_n) \Longrightarrow v(r) \tag{9}$$

To understand the theory in more depth, it is necessary to further highlight the Hohenberg-Kohn (HK) theorem, which is the heart of DFT. Originally, the theorem states that " $V_{ext}(\vec{r})$ is (to within a constant) a unique functional of $\rho(\vec{r})$; since, in turn $V_{ext}(r)$ fixes $\hat{H}$ we see that the full many particle ground state is a unique functional of $\rho(\vec{r})$". (HOHENBERG; KOHN, 1964). In other words, this theorem states that the ground state density ρ_0 uniquely provides an external potential, which is called V_{ext}. This can be stated on the assumption that only two variables (N and $v(r)$) can sufficiently describe any property of the ground state of an electronic system (LIU, 2009), and considering both equation (10), which shows that N can be obtained from ρ_0; and the first KS theorem. It becomes possible to conclude that ρ_0 is a property that contains information about N and V_{ext}, and consequently can be used to calculate the ground state energy and all other properties. All this information can be summarized in equation (11).

$$\int \rho(\vec{r})d\,\vec{r} = N \tag{10}$$

$$\rho_0 \Longrightarrow \{N, V_{ext}\} \Rightarrow \hat{H} \Rightarrow \Psi_0 \Longrightarrow E_0 \tag{11}$$

This is the key point of the computational cost advantage of this theory: a function of one (vectorial) variable **r** becomes "equivalent" to a function of **N** (vectorial) variables **r₁, ...r_N**. Some assumptions are crucial to make the theory possible (CAPELLE, 2006). To certify that a certain density is really the ground state density, it is important to introduce the second KH-theorem. This theorem follows the variational principle (equation 12), and states that the lowest energy can be obtained from the functional $F_{HK}(\rho)$. But this is true if and only if the initial density is the density of the ground state ρ_0. This means that the energy obtained from any other test density $\tilde{\rho}(\vec{r})$, always represents a value above the ground state energy value E_0.

$$E_0 \leq \mathrm{E}[\tilde{\rho}] = \mathrm{T}[\tilde{\rho}] + \mathrm{E}_{\mathrm{Ne}}[\tilde{\rho}] + \mathrm{E}_{\mathrm{ee}}[\tilde{\rho}] \tag{12}$$

In equation 12, *T[ρ]* represents the kinetic energy, $E_{Ne}[\rho]$ is the attraction between the nucleus and the electrons, while $E_{ee}[\rho]$ represents the electron-electron repulsion (following the Born-Oppenheimer approximation, the nucleus-nucleus repulsion can be considered a constant) (KOCH; HOLTHAUSEN, 2001).

Consequently, it follows that:

$$\langle \widetilde{\Psi} | \hat{H} | \widetilde{\Psi} \rangle = \mathrm{T}[\tilde{\rho}] + \mathrm{V}_{\mathrm{ee}}[\tilde{\rho}] + \int \widetilde{\rho(\vec{r})} \mathrm{V}_{\mathrm{ext}} \mathrm{d}\vec{r} = \mathrm{E}[\tilde{\rho}] \leq E_0[\rho_0] = \langle \Psi_0 | \hat{H} | \Psi_0 \rangle \tag{13}$$

However, this variational principle is applied for an exact functional *F[ρ]*, and in the real implementation of DFT there are only approximations for this functional(KOCH; HOLTHAUSEN, 2001). It was at this point that the second contribution of DFT appeared in 1965, when Khon and Shan (KOHN; SHAM, 1965) suggested the first approximation for the calculation of this functional. Kohn and Sham considered fictitious reference systems of non-interacting electrons, showing a way to calculate the kinetic energy with a good accuracy, which was the major obstacle of the energy calculation using the density functional approach. Equation **(14)** was proposed to obtain the kinetic energy term, while equation **(15)** was proposed to separate the *F[ρ]* functional. The last term, called the exchange and correlation functional (E_{xc}), is defined by equation **(16)** and contains all the unknown information, such as the non-classical effects of the self-interaction correction, exchange and correlation, and a portion related to the kinetic energy (JENSEN, F., 2007)**.**

$$T_s = -\frac{1}{2} \sum_i^N \langle \varphi_i | \nabla^2 | \varphi_i \rangle \tag{14}$$

$$F[\rho(\vec{r})] = T_s[\rho(\vec{r})] + J[\rho(\vec{r})] + E_{XC}[\rho(\vec{r})] \tag{15}$$

$$E_{XC}[\rho] \equiv (T[\rho] - T_S[\rho]) + (E_{ee}[\rho] - J[\rho]) = T_C[\rho] + E_{ncl}[\rho] \tag{16}$$

As can be expected, the most difficult part is solving equation **(16)**, since the exact analytic form of the E_{xc} functional is not yet known, and the orbitals have to be constructed with a finite linear combination of the basis sets (ZHAO, J.; DJURABEKOVA, 2020). In this sense, many approximations have been made in an

attempt to solve it (ABREU, 2004). The difference between the DFT methods lies precisely in the form of the E_{xc} functional. The right choice of the type of functional is of great importance. Mostly the E_{xc} functionals are empirical (JENSEN, F., 2007). The most basic model is the Local Density Approximation (LDA) which assumes that the exchange and correlation energy of a system corresponds to the exchange and correlation energy of a homogeneous electron gas with the same density. In this case, E_{xc} is given by the Dirac formula (DIRAC, 1930).

Later, many other exchange correlation functionals were developed, such as Local Spin Density Approximation (LSDA) (KARASIEV *et al.*, 2013), which take into account the spin density; Generalized Gradient Approximation (GGA) (BECKE, AXEL D., 1993; PERDEW *et al.*, 1992), which considers the first derivative of the density to better predict the inhomogeneous form of the actual density; the higher order gradient or meta-GGA (BECKE, A. D.; ROUSSEL, 1989), which considers even the second derivative of the density function; and hybrid or hyper-GGA methods (BECKE, AXEL D, 1997), which use an exact energy exchange part of the Hartree-Fock method in conjunction with GGA methods.

2.2. Time-Dependent Density Functional Theory (TD-DFT)

As mentioned above, the theory on which the DFT method is based also serves as a basic principle for describing dynamic events and analyzing the behavior of the system as a function of time (JACQUEMIN *et al.*, 2009). Over the years, time-dependent density functional theory (TD-DFT) has become a very popular tool for a wide range of applications enabling better investigation of the properties of atoms, molecules, nanostructures, and materials. In various research areas, such as the study of nuclear dynamics (NAKATSUKASA *et al.*, 2016), electronic excitations (ROSSI *et al.*, 2017; VAN BAY *et al.*, 2019), charge transfer process (DONG *et al.*, 2021; JANKOWSKA; SOBOLEWSKI, 2021), optical properties (ALI *et al.*, 2021; WOPPERER; DE GIOVANNINI; RUBIO, 2017), electronic properties (MUNIZ-MIRANDA, 2021) and many others (DERBENYOVA; KONAKOV; BURDOV, 2021; HWANG; SCHLENKER, 2021; TELPOUKHOVSKAIA *et al.*, 2015; YI;

NAKATANI; NOMURA, 2020). The number of publications addressing TD-DFT has increased from 37 in 1997 to over 8.500 in 2021, and continues to grow (SCIENCE, 2021).

The TD-DFT method is becoming increasingly popular. This growing popularity can mainly be attributed to the fact that it is used as a tool to extract energies from the electronic excited state of molecules (LEE, G. H.; CHOI; KIM, 2019a, b; LIU, SONGSONG *et al.*, 2019; SANZ-RODRIGO; OLIVIER; SANCHO-GARCÍA, 2020; SOLOVYEV *et al.*, 2019; SUKPATTANACHAROEN, C.; SALAEH, R.; PROMARAK, V.; ESCUDERO, D.; KUNGWAN, 2019). The importance of processes related to electronically excited states, not only in chemistry and physics but also in technology development research, has been constantly growing and TD-DFT is probably the most widely used theoretical approach for this kind of purpose (JACQUEMIN D, 2011). The calculation of electronically excited states is always a challenge demanding relatively more work compared to a theoretical calculation of ground state properties (VAN BAY *et al.*, 2019). In this context, TD-DFT has the advantage of being a simpler method, as well as allowing the study of larger systems when compared to methods based on wave function (VAN BAY *et al.*, 2019).

As in the time-independent DFT described earlier, the time-dependent wave function is equivalent to the electron density. The fundamental existence theorem, like the HK theorem in time-independent DFT, on which this method is based was developed by Runge and Gross in 1984 (RUNGE; GROSS, 1984) which states that for a given system of electrons in a given initial state, there is a relationship between the external potential and the time-dependent electron density. Thus, as in the DFT, all the physical properties of a system of many interacting electrons can be determined from its time-dependent density (CRAWFORD-URANGA *et al.*, 2014).

The main equations for TD-DFT simulations are the time-dependent Khon-Shan equations (TDKS), defined by equation **(17)** as follows:

$$\dot{\varphi_m}(t) = -i\hat{H}[n(t)](t)\varphi_m(t), \quad (m = 1, \dots, N) \tag{17}$$

In this equation, $\dot{\varphi}_m$ represents the derivatives with respect to time, $\hat{H}[n(t)](t)$ is the KS Hamiltonian; $\varphi \equiv \{\varphi_m\}_{m=1}^{N}$ are the KS orbitals, N is the number of electrons while n corresponds to the electronic electron density, obtained from equation **(18)** below (PUEYO *et al.*, 2018):

$$n(\vec{r}, t) = \sum_{\sigma=\uparrow,\downarrow} \sum_{m=1}^{N} |\varphi_m(\vec{r}\sigma, t)|^2 \qquad \textbf{(18)}$$

The KS Hamiltonian is a linear Hermitian operator that can have time dependence either explicitly, as in the presence of a laser field or if atoms are moving, for example, or implicitly, through the density, which in turn is written in terms of KS orbitals. The KS equation gives the correct density of the system if the exact KS potential is known. The KS potential is divided into three terms, v_{ext} which is the external potential; $v_{Hartree}$, which considers the classical electrostatic interaction between electrons; and the third, v_{XC}, which comprises all non-trivial many-body effects, as in the static DFT (MARQUES; GROSS, 2004). The KS potential is shown in equation **(19)** below**:**

$$v_{KS}(r, t) = v_{ext}(r, t) + v_{Hartree}(r, t) + v_{XC}(r, t) \qquad \textbf{(19)}$$

The price of this huge simplification, as can be expected, is that the exact expression v_{XC} as a density functional is unknown and needs to be approximated. Unlike DFT, approximate time-dependent v_{XC} functionals are still in their infancy. There are a few approaches the simplest being the adiabatic local density approximation (ALDA), which states that the Hamiltonian KS at time *t* depends only on the instantaneous density at the same time. Another approximation is the time-dependent exact exchange functional (EXX), which belongs to the family of time-dependent optimized effective potential functionals (ULLRICH; GOSSMANN; GROSS, 1995). There are also some functional of the "memory-including" type (DOBSON; BÜNNER; GROSS, 1997), considering that the time *t* of the KS Hamiltonian depends on the complete history of the density at all times. This type of functional tries to include this kind of information in a simplified way. The TD-DFT method is extremely promising, since functionals are constantly being created, or even

improved, allowing the accuracy of the method to always increase, besides reducing the computational cost. This makes its use possible in larger and larger systems, in an increasingly efficient way (VAN BAY *et al.*, 2019). However, for the analysis of very large systems, such as the simulation of macromolecules, a classical approach needs to be employed even TD-DFT becomes infeasible.

2.3. Classical Molecular Dynamics (MD) simulations

A MD simulation comprises analyzing the evolution of the molecular system over time, considering that the whole molecule is rotating, atoms are continuously moving, angles are bending and bonds are vibrating (MORRIS; CORTE, 2021). For a classical simulation, it is necessary to prepare an initial model that contains the coordinates of the constituent atoms of that system, which can be done by means of Nuclear Magnetic Resonance (NMR), crystallography or another method. The first Molecular Dynamics (MD) simulations were performed by Alder and Wainwright (ALDER; WAINWRIGHT, 1957, 1959) using a perfect elastic rigid sphere model to represent atomic interactions. Since then, considerable advances have been made (BATES *et al.*, 2017; PRANDI; RAMALHO; FRANÇA, 2019; RAMALHO *et al.*, 2016; RAMALHO; TAFT, 2005; ZHANG, K. *et al.*, 2021).

In a simplified form, the MD procedure can be summarized in five steps. First, the initial molecular geometry, the initial atomic velocities, and the ambient temperature must be obtained. The next step is to calculate the force as the potential gradient. After that, it is necessary to calculate the new molecular geometry or atomic position by integration of Newton's equations. The fourth step is to redefine the atomic velocities using the virial theorem, and finally save the information obtained for statistics and repeat the procedure until stabilization of the molecular energy is achieved. When the total energy remains constant, or differs by a predetermined amount, this is the end of the simulation (KALYAANAMOORTHY; CHEN, 2014; MUNDIM; ELLIS, 1999).

In more detail, for the simulation the molecule is assumed to be a collection of spherical atoms, and the chemical bonds are considered as springs. The atoms of the system are represented by a spherical body where the mass of the particle is equivalent

to the atomic mass, described only by the coordinates of the nucleus, following the Born-Oppenheimer Approximation. In this approximation, it is considered that, due to the large mass difference, electrons move on a much faster time scale than nuclei, which allows decoupling their motion (ADCOCK; MCCAMMON, 2006; HASSANALI; VERDOLINO; PARRINELLO, 2014; PALERMO *et al.*, 2019). Furthermore, different solvation models are employed, including explicit or implicit solvent (CHANG *et al.*, 2016).

The simulation is performed by numerically solving the Newtonian equations of motion, for each atom, using evolution in time intervals from *n* to *n + 1*, where a long series of these steps generates a trajectory through space. For an atom *i*, with mass m_i, the Newtonian equation of motion is given by equation **(20)**:

$$\frac{d\vec{p_i}}{dt} = \vec{F_i} \tag{20}$$

The relationship between velocity and momentum are given by equation **(21)**, as shown below:

$$\frac{d\vec{r_i}}{dt} = \frac{\vec{p_i}}{m_i} \tag{21}$$

Where the three-dimensional vector r_i indicates the position of the atom. The resultant force that the system exerts on atom *i* can also be obtained by the negative gradient of the potential energy function with respect to the position of atom *i*, as shown in Equation **(22)**:

$$\vec{F_i} = \frac{d\vec{V}}{d\vec{r_i}} \tag{22}$$

The Second law of Newton is then used to calculate the acceleration of the system (equation **23**).

$$\frac{d^2x(t)}{dt^2} = \frac{\vec{F_x}}{m} \tag{23}$$

Once the values for *x(t)*, *v(t),* and the acceleration are got, it becomes possible to solve numerically the classical equations of motion (ADCOCK; MCCAMMON, 2006). The numerical integration of these equations can be performed using different approximations. Currently, there are several algorithms for this purpose, such as Verlet's algorithm (VERLET, 1967). These equations are relatively complex, so their integration is performed over very short discrete time intervals, in the call of a continuous analysis. The approximations assume that for each discrete time interval, the atomic coordinates are fixed. These fixed coordinates are then used to calculate the intra and intermolecular interaction potentials, which determine the forces acting on each atom, such as the atomic partial charge, bond length, bond angle, among others (BECK; DAGGETT, 2004).

It is generally assumed that the interaction potential between two molecules can be described as the sum of the interactions between each pair of atoms, and that the interaction depends only on the distance between these atoms. In addition, in cases of internal motion of the molecule, terms related to the deformation of the molecular geometry are included. The set of parameters needed to describe all these interactions is called the force field (MORGON, N.H.; COUTINHO, K. 2007). There are several force fields available for MD simulations, which have appropriate parameters for different types of molecules, and the correct choice of this set of parameters is crucial for an accurate determination of the potential energy function, which will give reliability to the DM simulation (MALDE *et al.*, 2011).

To describe the parameters, most force fields separates the potential energy function in terms of the contribution of bonded atoms (Equation **24**) and unbonded atoms (Equation **25**), as shown below.

$$V_{Bond} = \sum_{i=1}^{N_b} \frac{1}{2} K_{bi}(b_n - b_{0i})^2 + \sum_{i=1}^{N_\theta} \frac{1}{2} K_{\theta i}(\theta_n - \theta_{0i})^2 + \sum_{i=1}^{N_\varepsilon} \frac{1}{2} K_{\varepsilon i}(\varepsilon_n - \varepsilon_{0i})^2 +$$

$$\sum_{i=1}^{N_\varphi} \frac{1}{2} K_{\varphi i}[1 + \cos(n_i \varphi_i - \delta_i)] \quad \textbf{(24)}$$

$$V_{unbond} = \sum_{i<j}^{N} 4\varepsilon_{ij} \left[\left(\frac{\sigma_{ij}}{r_{ij}}\right)^{12} - \left(\frac{\sigma_{ij}}{r_{ij}}\right)^{6} \right] + \sum_{i<j}^{N} \frac{q_i q_j}{D r_{ij}} \quad \textbf{(25)}$$

Where:

K_b = harmonic constant of energy associated with the chemical bond between two atoms and b_o is the equilibrium distance of that bond;

K_θ = harmonic energy constant associated with the angle between two chemical bonds and θ_0 is the equilibrium angle;

K_ε = harmonic energy constant associated with the angle formed between two planes (defined by four atoms) and ε_0 is the equilibrium angle between these two planes;

K_φ = energy constant associated with the torsion term between two planes defined by four atoms and φ is the torsion angle between these two planes;

n = multiplicity;

δ = phase angle;

r_{ij} = distance between atoms i and j;

ε_{ij} and σ_{ij} = Lennard-Jones parameters;

q_i and q_j = partial charges located on the respective atoms

D = effective dielectric constant of the medium

The most commonly used force fields are AMBER (DUAN *et al.*, 2003), OPLS (WILLIAM L. JORGENSEN; DAVID S. MAXWELL; TIRADO-RIVES, 1996), GROMOS (CHRISTEN *et al.*, 2005) and CHARMM (MACKERELL *et al.*, 1998). The correct choice of force fields is one of the most important and critical parts in performing MD simulations, since the quality of these force fields has a huge impact on the physical quantities extracted from the simulations. Despite the great usefulness of classical dynamics simulations for large systems, most standard force fields have some limitations (WU *et al.*, 2020). Most of them do not explicitly explain the polarizability of electrons, which can be essential, for example, in describing the solvation phenomenon of certain ions. Furthermore, most force fields cannot deal with chemical processes involving bond breaking and bond formation, such as a case of proton transport in water (HASSANALI; VERDOLINO; PARRINELLO, 2014). To try to get around these limitations, some approaches have been proposed, such as combining *ab initio* and MD methods (WU *et al.*, 2020). In this case, the statistical information from the studied system is explored by MD simulations and some

representative conformations from the MD simulation are selected and evaluated by QM calculations.

2.4. The Optimal Wavelet Signal Compression Algorithm (OWSCA)

The optimal wavelet signal compression algorithm (OWSCA) (GONÇALVES *et al.*, 2017) is an efficient method for selection of MD conformations (GONÇALVES *et al.*, 2019, 2021). Therefore, conformations obtained for a previous MD calculations need to be used as input. This algorithm is based on a wavelet compression strategy and is applied to compress the maximum number of wavelet coefficients, instead of using heuristically chosen parameters. This method contains four steps, described below:

Discrete wavelet transform:

$$d_{j,k} = \int_{-\infty}^{+\infty} x(t)\psi_{j,k}(t)dt, \; j = 0, \dots, N-1; k = 0, \dots, 2^n - 1 \tag{26}$$

Optimization on order to find δ_j* j=0,...,N-1

Wavelet compression, for each J

$$d_{j,k} = 0 \; if \; d_{j,k} \leq \delta_j^* j = 0, \dots, N-1; k = 0, \dots, 2^n - 1 \tag{27}$$

Inverse discrete wavelet transform:

$$y(t) = \sum_{j=0}^{N-1} \sum_{k=0}^{2^n-1} \int_{-\infty}^{+\infty} d_{j,k}\psi_{j,k}(t) \tag{28}$$

As can be seen, the algorithm uses the discrete wavelet transform to convert the signal. Equation **(29)** defines the discrete wavelet transform, for a given data set *x(t)*:

$$d_{j,k} = \int_{-\infty}^{+\infty} x(t)\psi_{j,k}(t)dt \tag{29}$$

In which $d_{j,k}$ is the wavelet coefficient, t is the variable time (normalized between 0 and 1), j represents the scaling parameter (resolution), which determines the time and frequency resolutions of the scaled wavelet function ψ, and k represents the shifting parameter, which translates the scaled wavelet along the time axis. Typically, j and k are correlated, where $j = 0\ldots N - 1$ and $k = 0\ldots M$, where N denotes the maximum resolution and $M = 2N - 1$.

The discrete wavelet transform, defined above, results in a vector of wavelet coefficients, d, where $d = \{d_{0,0}, d_{0,1}, \ldots, d_{N,M}\}$ and each wavelet level represents a frequency, or resolution, and has its own coefficients.

$\psi_{j,k}$ can be defined by equation **(30)**, being ψ the mother wavelength:

$$\psi_{j,k}(t) = \frac{1}{\sqrt{2^j}}\psi\left(\frac{t-k2^j}{k2^j}\right) \tag{30}$$

In this algorithm, the simplest wavelet function, H_{aar} wavelet, also known as Daubechies-1, is used, and its definition can be seen in equation **(31):**

$$\psi_{Haar}(t) = \begin{cases} -1 & 0 \leq t < 0.5 \\ 1 & 0.5 \leq t < 1 \\ 0 & otherwise \end{cases} \tag{31}$$

By using this algorithm, the configuration generated in the simulation can be drastically reduced without loss of statistical information. The structures are selected more correctly, besides the great reduction of computational cost when the generated results need to be inputs for later calculations.

3. FIELDS OF APPLICATION FOR CHEMICAL SENSORS

Sensors for measuring and detecting chemical and biological substances are present in almost every part of everyday life. They are used to help to run the cars more efficiently, promote greater security, speed up research processes, track criminals, and monitor the environment and health of humans, animals and plants. Examples of endless applications include monitoring oxygen in car exhaust systems, glucose levels in diabetic samples, and CO_2 levels in the environment. In the laboratory, chemical detectors are the key pieces of analytical equipment used to develop new chemicals, drugs, or even to monitor industrial processes (FRADEN, 2015). Progress has been impressive and the literature is full of interesting developments. Recent developments include a wide spectrum of technologies, such as chemical analysis (LIU, H. *et al.*, 2020), food safety (CHEN, S. *et al.*, 2022; SANT'ANNA *et al.*, 2022), clinical diagnosis (LI, Q. Y. *et al.*, 2022), environmental monitoring (SILAMBARASAN; MOON, 2022), industrial analysis (HUSSAIN *et al.*, 2021) and mineral resources detection (ABDOLLAHZADEH *et al.*, 2022; YANG, B. *et al.*, 2016). In the pharmaceutical and medical field, for example, chemical sensors can be employed for continuous monitoring of electrolytes and metabolites (BANDODKAR *et al.*, 2019; XU, Z. *et al.*, 2021).

Beyond these interesting applications, there are also several opportunities in using chemical sensors for security and forensic applications, and towards monitoring drugs of abuse (BARFIDOKHT *et al.*, 2019; DE JONG *et al.*, 2016; MAHMUD *et al.*, 2018). Additionally, molecules with spectroscopic properties can also be employed for sensing technologies, where medical diagnosis is one of the main applications (LI, Q. Y. *et al.*, 2022; TU *et al.*, 2022; WANG, N. *et al.*, 2022).

3.1. Medical diagnosis

The diagnosis is a fundamental step of the medical system as a whole. It is from early and accurate diagnosis that the forms of treatment are defined, the necessary care and treatment are chosen, and the crucial information about the state of

the disease is obtained. For a correct diagnosis, the acquisition of accurate physiological information is vital. In this way, it is necessary that there is always an optimization of the medical diagnostic processes in general, aiming to minimize errors as much as possible, to get the results in a faster and more reliable way, enabling an efficient treatment and consequent increase of the chances of cure (BHAVSAR; ABUGABAH; *et al.*, 2021; BHAVSAR; SINGLA; *et al.*, 2021). For this purpose, chemical sensors have been widely developed and employed (LEIBL *et al.*, 2021; LI, Q. Y. *et al.*, 2022; PROMPHET *et al.*, 2021).

Using chemical sensors can be helpful once they can improve healthcare services, as well as to minimize errors in diagnostic process and provide treatment to patients (PENDLEY; LINDNER, 2017). Another very important function of chemical sensors in medical areas is a real-time monitoring. Chemical sensors are able to measure quickly and selectively, with minimal preparation of the environment, and therefore have great potential to be used in daily monitoring systems. These devices provide clinically critical information for early detection of diseases and allow the capture of body activities. They can measure health-related signals such as respiration rate, pronation, intracranial pressure, intraocular pressure, and blood flow, and external stimuli for tactile sensing, among others (KANG *et al.*, 2021).

For the design of chemical sensors capable of diagnosing diseases, known biological markers of these diseases are usually employed(TUTEJA; NEETHIRAJAN, 2018). Based on this context, many sensors are developed, and one of the most explored areas is certainly the diagnosis of cancer, which is a disease with high incidence and that remains without cure, in which early diagnosis is critical for patient survival (SIMON, 2010).

3.1.1. Cancer disease

A living organism is a complex machine, which requires constant keeping, reconstruction and restructuration. For this, millions of subunits in the live organism, such as cells, are produced, altered, used and continuously killed (RYBCZYNSKA *et al.*, 2018). Normal cells that form the tissues of the human body are capable of

multiplying in a continuous natural process. Most normal cells grow, multiply, and die ordered. When, instead of dying, the cells continue to grow disorderly, giving rise to other abnormal cells, occur functional disturbs, such as cancer. Cancer is the name given to a set of diseases, which has as fundamental characteristic the disordered growth of cells (INCA, 2019).

The process of cancer formation is called carcinogenesis or oncogenesis. In general, this process occurs slowly, and it can take several years for a cancer cell to proliferate and give rise to a visible tumor. The effects of different carcinogenic agents, when acting cumulatively, handle the initiation, promotion, tumor progression and inhibition (THUN *et al.*, 2010). Carcinogenesis is determined by exposure to these agents, at a given frequency and time period, and by the interaction between them. The carcinogenesis consists of three stages, as seen in Figure 6. These stages are initiation, where the genes are exposed to the action of carcinogens; promotion stage, in which the oncopromotor agents act on the already altered cell and lastly the progression stage, characterized by the uncontrolled and irreversible multiplication of the cell (INCA, 2011).

Figure 6 – Carcinogenesis stages.

Initiation stage
Exposure to carcinogenic agents

Progression stage
Uncontrolled and irreversible multiplication of the cell.

Promotion stage
Oncopromotor agents act on the already altered cell.
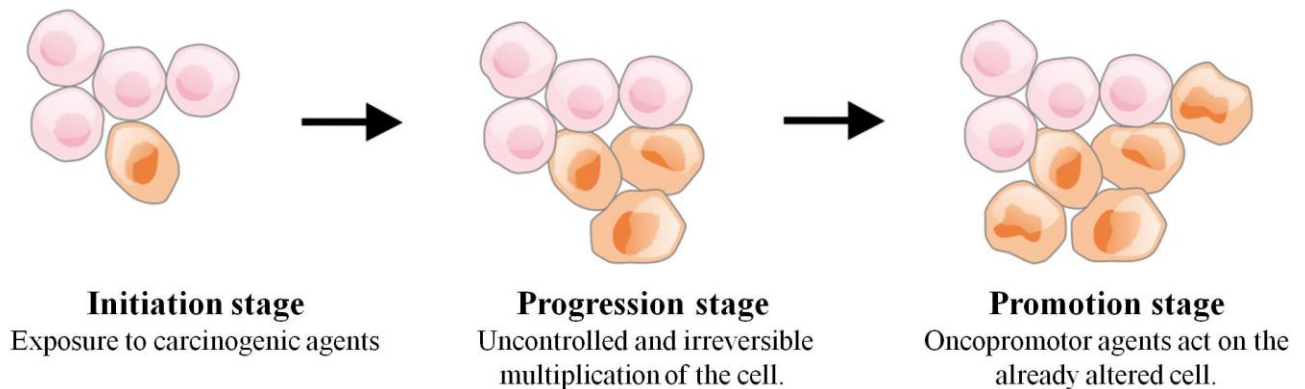
Globally, cancer is the second most deadly disease, responsible for about 9.6 million deaths per year (INCA, 2019). These data are from the most recent global estimate, for the year of 2018, which also indicates that 18 million new cases of cancer occurred in the world. Among these, lung cancer is the most incident (2.1 million),

followed by breast cancer, with 2.1 million of cases, and after colon and rectum cancer, with total 1.8 million. Lastly prostate cancer represents 1.3 million of cases. Considering the incidence between sexes, the incidence in men represents 53% of new cases, being a little lower in women, with 8.6 million (47%) of new cases. The most frequent types of cancer in men were lung cancer (14.5%), prostate (13.5%), colon and rectum (10.9%), stomach (7.2%) and liver (6.3%). In women the highest incidences were breast cancer (24.2%), colon and rectum (9.5%), lung (8.4%), and cervix (6.6%) (BRAY *et al.*, 2018). In addition, it is estimated that in the year of 2030 there will be the occurrence of 26 million new cases and 17 million of deaths caused by cancer disease per year in all word (THUN *et al.*, 2010).

For Brazil, the estimate for each year of the triennium 2020-2022 points out that there should be approximately 625,000 new cases of cancer, with non-melanoma skin cancer being the most common, with 177,000 cases, followed by breast and prostate cancer, 66,000 cases each. About the incidence by sex, prostate cancer accounts for 29.2% of all cases in men while female breast represents 29.7% of all cases in women. Figure 7 shows in more detail the estimates for cancer incidence in 2020 by sex, only for Brazil (INCA, 2019).

Figure 7 – Proportional distribution of the ten most incident cancers estimated for 2020 in Brazil, by sex, except non-melanoma skin.

Estimated New cases

	Males			Females		
Prostate	65.840	29,2%		Female breast	66.280	29,7%
Colon and rectum	20.520	9,1%		Colon and rectum	20.470	9,2%
Trachea, bronchus and lung	17.760	7,9%		Cervix	16.590	7,4%
Stomach	13.360	5,9%		Trachea, bronchus and lung	12.440	5,6%
Oral cavity	11.180	5,0%		Thyroid gland	11.950	5,4%
Esophagus	8.690	3,9%		Stomach	7.870	3,5%
Bladder	7.590	3,4%		Ovary	6.650	3,0%
Non Hodgkin lymphoma	6.580	2,9%		Uterine body	6.540	2,9%
Larynx	6.470	2,9%		Non-Hodgkin lymphoma	5.450	2,4%
Leukemias	5.920	2,6%		Central Nervous System	5.220	2,3%

From the data, it can be concluded that cancer is a disease with a very high incidence and mortality rate worldwide. Furthermore, it is already clear today that cancer diagnosis, being the image diagnosis the most common, when it occurs in its early stages of disease progression, significantly increases the chances of cure (NAJAFI; KOUCHAKZADEH, 2019). One of the challenges of image diagnosis is to develop a system capable of locating species in different environments to detect outbreaks of cancer in the surgical margins for clinical use with high resolution (LUE *et al.*, 2012). In this line, many spectroscopic techniques have been proposed for detecting tumor cells, for example NMR (PEREIRA *et al.*, 2019), Infra-Red (BELEITES *et al.*, 2005; ZHEN *et al.*, 2019), Raman (NEETIKA SINGH, PRABHAT KUMAR, 2019; WANG, J. *et al.*, 2019), Diffuse Reflectance Spectroscopy and Fluorescence Spectroscopy (LEE, Y.-A. *et al.*, 2018; LI, J.-Y. *et al.*, 2013; LI, Y. *et al.*, 2022).

 Despite great advancement today, achieving successful imaging with high efficiency and sensitivity at the cellular and molecular level remains a challenge. The development of increasingly sophisticated diagnostic techniques, less invasive and with fewer side effects, is a growing demand in healthcare, especially in cancer diagnosis (NAJAFI; KOUCHAKZADEH, 2019). To optimize this process, many biological markers are being researched, such as cancer-related enzymes. These are one of the most promising targets, since compounds that interact with these macromolecules can serve both for the treatment and detection of diseases (PEREIRA *et al.*, 2019). In this context, there are many enzymes whose overproduction is related to cancer. Among these, one of the best known are the topoisomerase enzymes (CINELLI, 2019).

3.1.2. Topoisomerase enzymes

The double helical structure and the complementarity between the sister strands of DNA has many benefits, such as a stable storage of genetic information, as well as the willingness to identify and correct errors and discontinuities in the genome. However, some problems can arise in this magnificent structure, and these problems

can pose serious challenges to the cell, interfering with gene expression, DNA duplication, and chromosome segregation (IZUMI, 2016; SUZANNE CLANCY & KENNA M. SHAW, 2008; TROESTER *et al.*, 2016). For example, the occurrence of DNA knotting and catenation during DNA metabolic processes, and also supra-helical tension in vital genetic processes that require strand separation, such as replication and transcription, where DNA strands have no apparent free ends. Thus, the cell needs to invest a considerable amount of energy in maintaining the topology of its chromosomes. For this, there is a class of specialized nuclear enzymes responsible for maintaining the chromosomes in an adequate topological state, the so-called topoisomerases (topos) (KHADKA; CHO, 2013; SCHOEFFLER; BERGER, 2008).

The first Topoisomerase enzyme was discovered by James Wang (WANG, J. C., 1971). This protein was found in *Escherichia colli* microorganism and was named "omega" by him. Since then, many other topoisomerases have been discovered and isolated of many organisms, from plants to archeabacteria (CINELLI, 2019). The different topos enzymes are distinguished by their catalytic mechanisms and are divided into two class, type I and type II (FIEF *et al.*, 2019). Type I topoisomerases are involved in maintaining genomic integrity and act by generating a transient single-stranded break in the double helix and consequently, these enzymes are able to alleviate torsional stress in duplex DNA. Type II topoisomerases are able to remove superhelical twists for DNA and resolve knotted or tangled duplex molecules, acting by the generation a transient double-stranded DNA-break, followed by double-stranded DNA passage event (LIANG *et al.*, 2019; MCCLENDON; OSHEROFF, 2007). In humans, two isoforms are expressed, which are called topoisomerase IIα (TOPO2A)(TSAI-PFLUGFELDER *et al.*, 1988) and IIβ (TOPO2B)(AUSTIN; FISHER, 1990; CHUNG *et al.*, 1989). A structure of a human Topoisomerase IIβ in complex with DNA ca be viewed in Figure 8.

Topos enzymes have their catalytic function by creating a single or double stranded break in DNA through the nucleophilic attack of a Tyr residue on the phosphodiester backbone, creating a phosphotyrosyl bond that links the protein to the newly generated 5′-terminus of the DNA chain. Figure 9 shows the cleavage of the DNA double-strand mediated by topoisomerase II. During cleavage, the active Tyr residue of each subunit covalently binds to the 5' phosphate moiety on each strand.

The bond formed preserves the sugar-phosphate DNA backbone. The newly generated 3′-hydroxyl group interacts non-covalently with topoisomerase II, such binding represents the reverse process (DEWEESE; OSHEROFF, 2009).

Figure 8 – Structure of topoisomerase IIβ in complex with DNA. PDB ID 5ZAD.

Figure 9 – DNA double-strand cleavage mediated by topoisomerase II enzyme.
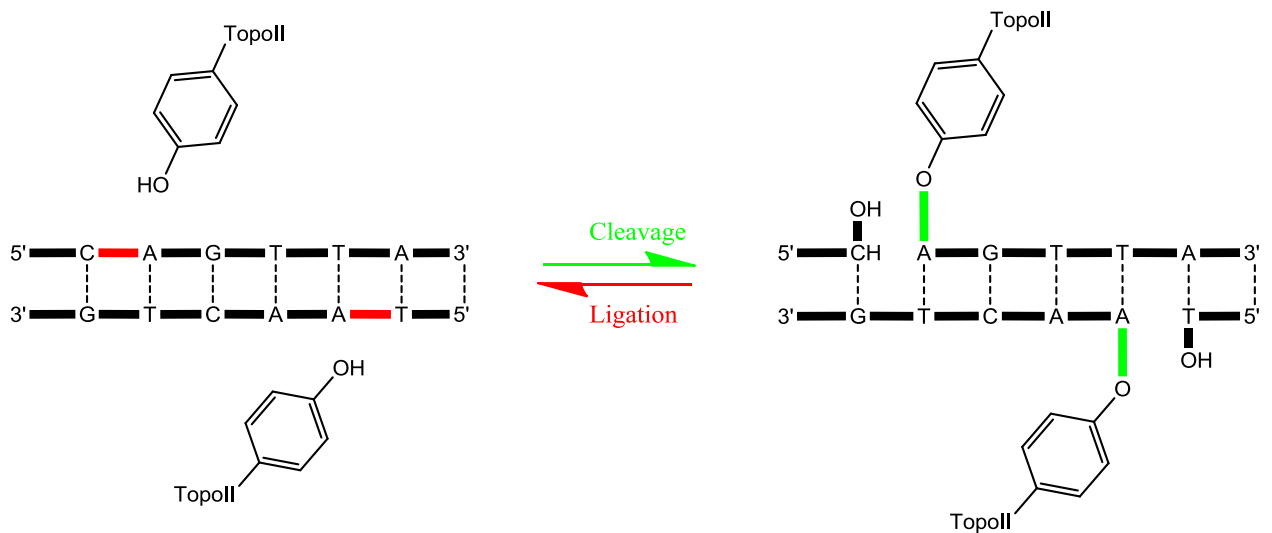
In general, the DNA cleavage is undesirable, but in other cases it is very necessary. As can be observed, topos has an essential function, helping in the

maintenance of genetic coding and the functioning of the body. However, DNA breaks can be subverted to give rise to mutagenic or cytotoxic lesions. Because of this, many Topo inhibitors have been used as frontline antibiotic or anticancer agents (CINELLI, 2019; WENDORFF *et al.*, 2012). Moreover, these enzymes are under continuous investigation for the development of new anticancer and antibiotic drugs (KIRK E. HEVENERN; TATSIANA A. VERSTAK; DANIEL L. RIGGSBEE, 2018).

3.1.2.1. Topoisomerase II and its involvement in cancer disease

Topoisomerase enzymes have been described as an important target for anticancer drug discovery for more than 30 years (CINELLI, 2019). The Topo-II levels is highly increased in proliferating cancer cells, which is essential to cancer cell survival (ZHOU, D.-C. *et al.*, 2019). In the past decade, several organic chemists, biologists and medicinal chemists all around the word have been try to design, identify, synthesize and test a series of novel bioactive compounds with Topoisomerase enzyme as target (LIANG *et al.*, 2019). However, it is important to mention that despite the efficiency of topo inhibitors in current anticancer therapies, this type of treatment is still limited by some important negative consequences. In the case of treatment with topo-II inhibition, there is the problem of selectivity. The inhibitors used can also inhibit the topo Iβ isoform, which can result in secondary malignancies such as acute myeloid leukemia (LIANG *et al.*, 2019; MISTRY *et al.*, 2005; TURKSEN *et al.*, 1992). Because of this, it is still of great importance the development of new inhibitors, more selective and with less side effects.

The main inhibitors currently available can act by different mechanisms of action. The Topo II- targeting agents can be classified into two major groups, namely "Topo-II poisons" and "Topo-II catalytic inhibitors", being both able to interfere at least in one step of the catalytic cycle. The first group, Topo-II poisons, exercise their activity through stabilization of the covalent DNA-topoisomerase II complex while the second group, the Topo-II catalytic inhibitors, are a heterogeneous group of compounds, being able to act in any of the other steps in the catalytic cycle of the Topo II. As example, these inhibitors can act on interference in the binding between

DNA and Topos II, in stabilization of noncovalent DNA-Topos II complexes, or even in inhibition of ATP binding. Regarding the clinical uses, the Topo II poisons are the most used as antitumor agents, and Topo II catalytic inhibitors are most used as antineoplastic agents (LARSEN; ESCARGUEIL; SKLADANOWSKI, 2003).

Among the various compounds studied for inhibiting topoisomerase enzymes, there are also drugs already on the market, such as the fluoroquinolones (BEBEROK; WRZEŚNIOK; MINECKA; *et al.*, 2018). This arpoach of proposing new uses for already known drugs is called drug repositioning and has several advantages, culminating in the main one, which is to accelerate the drug design process (NOVAC, 2013).
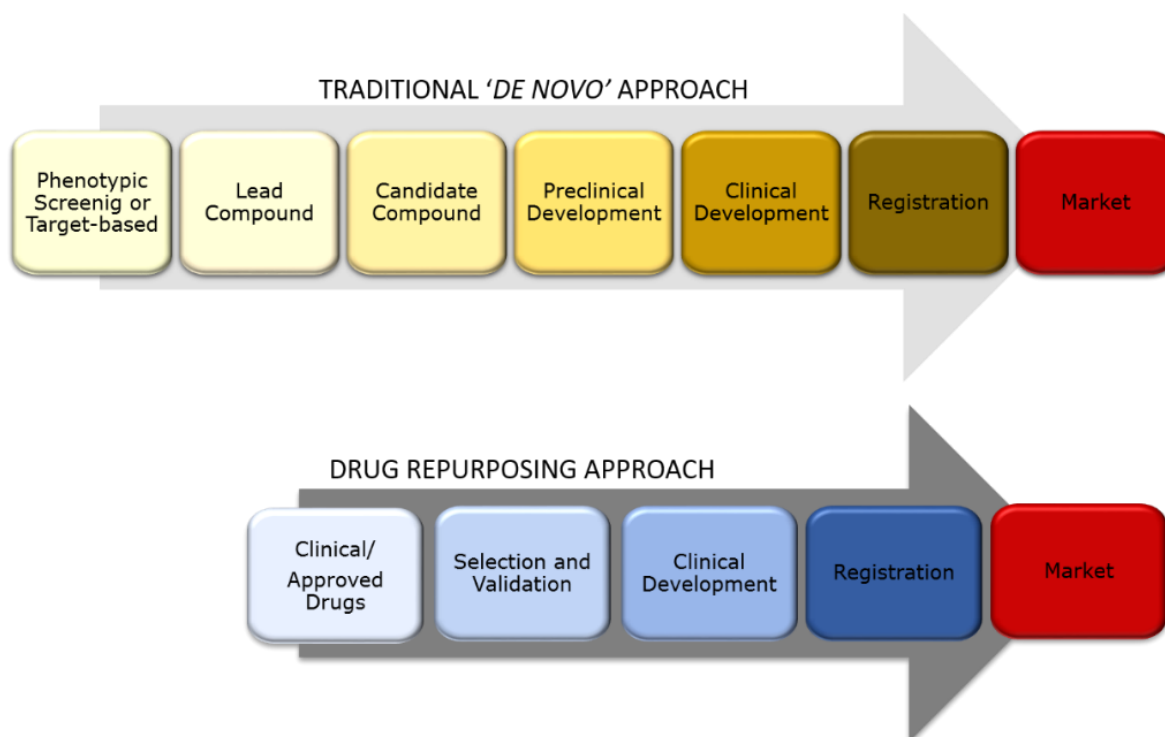
3.1.3. Drug Repositioning

The pharmaceutical industry cannot keep up with the enormous demand for the production of new drugs, since the costs of both the production and development of new drugs can be very expensive. Because of this, there is a productivity gap, even with the considerable amounts of resources invested by the pharma industry in new discovery technologies such as combinatorial chemistry, high-throughput screening (HTS) and genomics, and also structure-based drug design. This gap causes drug developers to look for novel approaches in drug design, combining complementary therapeutic drugs in a single tablet, improving existing versions of drugs, or even finding new attributes for them. In this context, one alternative is the strategy of drug repositioning (ASHBURN; THOR, 2004).

Drug repositioning approach, also called drug repurposing, redirect and reprofiling, in a nutshell, it comprises the process of "recycling old drugs", which includes identifying new uses for existing or approved drugs. This strategy is an attractive opportunity from both business and social standpoints, once it reduces the time and costs of the drug development process in comparison with de *de novo* drug discovery approach, as can be seen in Figure 10. The savings in time and money mentioned above can occur in many stages of the process, such as development, clinical trials, or even drug approval and launch, since the pharmacokinetic,

toxicological, and safety data of the existing drug are already done. This technique offers the possibility, for example, to recycle drugs that have been shown to be safe but not effective in the initial indications for which they were originally developed (KIM, 2015). It is important to mention that drug repositioning studies need to be solidly grounded in science to be successful. In order to ensure higher success rates, the process can rely on more refined methodologies, as is the case with computational methods and more detailed mechanistic models that can be integrated with experimental methods. (JIN; WONG, 2014).

Figure 10 – Schematic Representation of the traditional de novo drug discovery versus drug repositioning strategy.

By this approach, several drugs have been successfully repositioned, once the repositioning strategy constitutes 10-50% of all R&D spending and is viewed as an important part of product-life cycle management. One of the best known examples are the sildenafil citrate, or Viagra®, which has repurposed from a hypertension drug to a therapy for erectile disfunction, and thalidomide, which has repositioned from morning sickness to multiple myeloma (NOVAC, 2013). Despite all positive

characteristics of this process, several obstacles need to be overcome, such as patent protection and market exclusivity in commercial terms, and the choice of repurposing strategy to be adopted to select the best candidates (ASHBURN; THOR, 2004; KIM, 2015).

Another example of a drug that has been widely studied in repositioning is the fluoroquinolones (SONG *et al.*, 2016). Fluoroquinolones (FQs) are a class of broad-spectrum antibiotics derived from quinolones (FIEF *et al.*, 2019). The class of FQs remains one of the most important classes of antibiotics, currently used worldwide (EZELARAB *et al.*, 2018). Data from 2019 shows that FQ prescriptions represent 14% of all antibiotic prescriptions (YIMENU *et al.*, 2019). Fluoroquinolones possess many desirable pharmacokinetic properties, such as their prolonged bioavailability and half-life. In addition, they have a broad spectrum of activity, including coverage of intracellular and atypical organisms (CHO *et al.*, 2018).

In order to take advantage of these desirable characteristics, numerous researches have highlighted other biological activities of this class of molecules, including anticancer activities (ABDEL-AZIZ *et al.*, 2013; GUPTA *et al.*, 2019), antimalarial (LI, J. *et al.*, 2013), antiviral (AHMED, A.; DANESHTALAB, 2011) and anti-Alzheimer (PUDLO *et al.*, 2014). The many secondary biological activities have been studied for several drugs belonging to this class, such as levofloxacin (SONG *et al.*, 2016) lomefloxacin and ofloxacin (PERUCCA *et al.*, 2014), moxifloxacin (YADAV *et al.*, 2015) and ciprofloxacin (ALI *et al.*, 2021).

3.1.4. Ciprofloxacin

Among the fluoroquinolones, compound 1-cycloprppyl-6-fluoro-4-oxo-7-(piperazin-1-yl)-1,4-dihydroquinoline-3-carboxylic acid, most known as Ciprofloxacin, was developed by Bayer as the second-generation fluoroquinolone, and was introduced into clinical practice to treat various bacterial infections around three decades. The chemical structure can be seen in Figure 11. This molecule exhibits notable antimicrobial activity, with an excellent pharmacokinetics and a few side effects (ZHANG, G. F. *et al.*, 2018).

Figure 11 – Chemical structure of Ciprofloxacin (1-cycloprppyl-6-fluoro-4-oxo-7-(piperazin-1-yl)-1,4-dihydroquinoline-3-carboxylic acid).
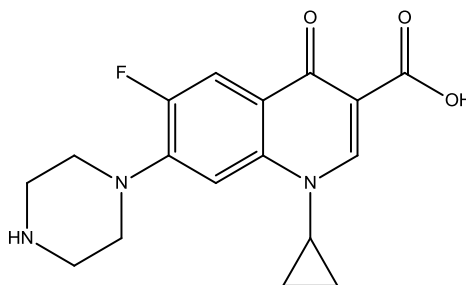
Ciprofloxacin molecule has molecular weight of 331.33 g mol^{-1}, *pKa* of 6.09 and a temperature-dependent partition coefficient (log P =0.28). The hydrophobicity of this molecule plays a key role in the cell's penetration. The insertion of fluorine substituent together with the 1-piperazinyl group increases the activity of Ciprofloxacin, when compared with cinoxacin, nalidixic acid and oxolinic acid. Besides that, the N-1 position cyclopropyl substitution plays an important role in antimicrobial effect and DNA gyrase activity (PERUCCA *et al.*, 2014; VANCE-BRYAN; GUAY; ROTSCHAFER, 1990).

As other fluoroquinolones, ciprofloxacin possess many other biological activities, in addition to antibacterial activity. One example is its anticancer properties. It is already known that fluoroquinolones as ciprofloxacin, enrofloxacin, moxifloxacin and gatifloxacin exhibit inhibitory activity not only in bacterial Topoisomerase II. Due to this fact, these antibiotics exhibit market toxicity against many cancer cells (BEBEROK; WRZEŚNIOK; ROK; *et al.*, 2018). Talking specifically of ciprofloxacin, there are several reports in literature retracting its anticancer activity (PERUCCA *et al.*, 2014; SUAIFAN; MOHAMMED, 2019; SURESH *et al.*, 2018). The effects where observed in many cell lines, such as lung cancer cells (PHIBOONCHAIYANAN; KIRATIPAIBOON; CHANVORACHOTE, 2016); breast cancer MDA-MB-231 cells (BEBEROK; WRZEŚNIOK; ROK; *et al.*, 2018) and pancreatic cancer cells (YADAV *et al.*, 2015). When compared with conventional topoisomerase II chemotherapeutics, such as doxorubicin and etoposide, ciprofloxacin have been shown to be less susceptible to efflux-mediated resistance (BISACCHI; HALE, 2016).

3.2. Drug of abuse detection

According to global data, drug use killed nearly half a million people in 2019, while disorders caused by their use resulted in the loss of 18 million years of healthy life, mainly due to opioids. Each year, drug use directly and indirectly is responsible for 11.8 million deaths, which is more than the number of deaths caused by all cancers. For illicit drugs, the number of deaths, directly and indirectly, is more than 750,000 annually. Aside from the deaths, serious and often lethal diseases are more common among people who use drugs, many of whom are living with HIV and hepatitis C, especially injecting drug users (DWYER-LINDGREN *et al.*, 2019; UNODC, 2021). Social development is also a factor compromised by the illicit drug commerce, affecting mainly the most marginalized and economically vulnerable population. Even with all the problems caused by the commerce and consumption of illicit drugs, this use persists and even increases. In the year 2020 about 275 million people used drugs, an increase of 22% compared to 2010. Moreover, it is estimated that by 2030, there will be an 11% increase in this number, and more than a 40% increase in Africa alone (UNODC, 2021).

Considering the great social and economic impact caused by drug abuse, the control of prescriptions and the use of these compounds is a demand of clinical and forensic toxicology. Currently, the detection of these substances requires analysis with biological samples, either blood or urine. The classical methods employed for substance detection range from simple colorimetric tests to more complex techniques such as gas chromatography and mass spectrometry (GC-MS). These methods are very accurate and reliable, but they require more time to perform, need sample treatment in most cases, are relatively expensive and difficult to operate, factors that make it unfeasible to use them for *in situ* and real-time monitoring (MORADI *et al.*, 2021).

In this context, the development of portable devices for easy, selective, sensitive, and cost-effective detection of abuse drugs in complex biological environments is a very promising alternative, since it facilitates early recognition, improves treatment outcomes, and may help prevent relapse. The high sensitivity and selectivity of this equipment is essential, considering that the concentrations of psychotropic drugs in biological matrices such as saliva, blood or urine are low,
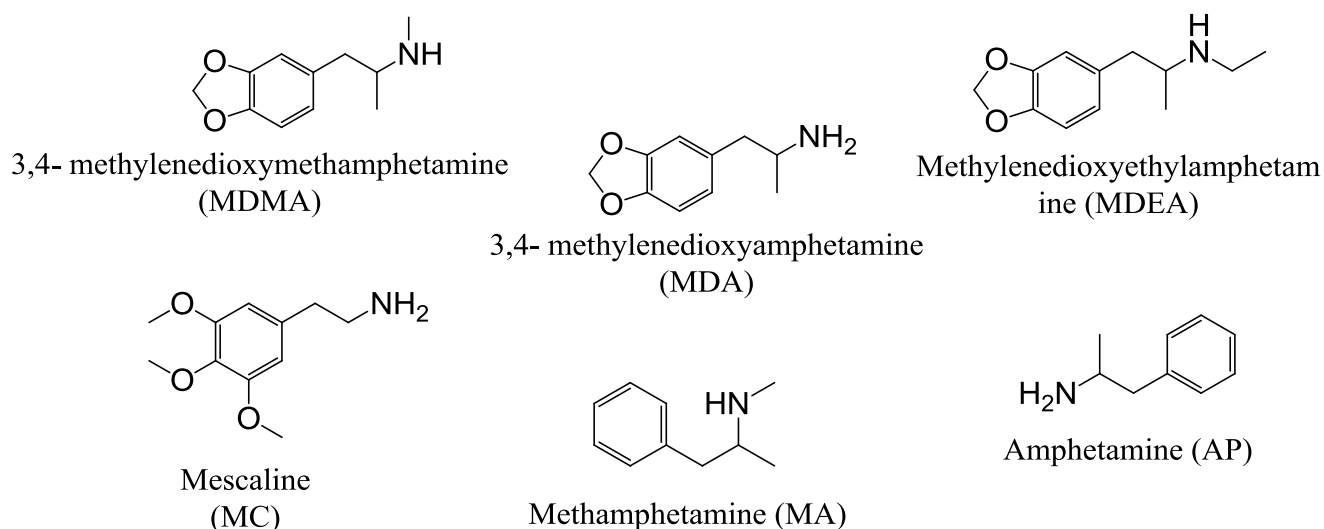
requiring very appropriate methods for their detection and quantification (QRIOUET *et al.*, 2021).

A series of multidisciplinary discoveries in fields such as chemistry, physics, biological and material sciences have led to the development of a variety of sensing tools with a range of analytical characteristics (MCNEILL *et al.*, 2021; MORADI *et al.*, 2021; SOEIRO *et al.*, 2021). Considering the large number of existing substances, the molecular targets are also variable, some examples are opioids (MISHRA *et al.*, 2020; SAICHANAPAN *et al.*, 2021; SOEIRO *et al.*, 2021), morphine (HUANG *et al.*, 2020), cocaine and heroin (D'AURELIO *et al.*, 2020; MASEMOLA *et al.*, 2020), amphetamines (YANG, YUPING; SUN; ESLAMI, 2021) and amphetamine-type stimulants such as MDMA, also known as "ecstasy" (DRAGAN *et al.*, 2021; ZHANG, R. *et al.*, 2021).

3.2.1. MDMA (3,4-methylenedioxymethamphetamine)

The origin of the 3,4-methylenedioxymethamphetamine (MDMA) (Figure 12) has some divergences, but a systematic analysis of the original documents points that Dr Anton Köllisch made the first description of the synthesis of MDMA molecule (FREUDENMANN; ÖXLER; BERNSCHNEIDER-REIF, 2006). MDMA was firstly synthesized at Merck around 1912 under the name "Methylsafrylamin" (MEAD; PARROTT, 2020). The most common history in literature is that this molecule was produced in order to develop an appetite suppressor. However, the official documents do not indicate this. The substance was only a precursor in a pathway, patented to avoid other patent of the clotting agent hydrastinine synthesis. Concomitant with synthesis, MDMA was studied in animals, with the first basic pharmacological test taking place decades later while human tests occurred only in 1960 (FREUDENMANN; ÖXLER; BERNSCHNEIDER-REIF, 2006).

Figure 12 – Molecular structures of MDA, MDEA, MA, AP, Mescaline and MDMA.

3,4- methylenedioxymethamphetamine
(MDMA)

3,4- methylenedioxyamphetamine
(MDA)

Methylenedioxyethylamphetam
ine (MDEA)

Mescaline
(MC)

Methamphetamine (MA)

Amphetamine (AP)

This psychoactive compound has a MW= 193.24 g.mol^{-1}, logP = 2.050 and is an amphetamine-type stimulant, structurally related to MDA, MDEA, MA, AP and mescaline, both presented in Figure 12. MDMA differs from AP and MA by an methylenedioxy group attached to positions 3 and 4 of the aromatic ring of the AP molecule. In this part, MDMA is similar to mescaline, and as a result, the effects of MDMA are a mix of the AP and mescaline effects. MDMA molecule is a principal component of "ecstasy", which is a synthetic illegal drug with potential to generate dependence (KALANT, 2001; SILVA, A. T. M. DA *et al.*, 2018).

Structurally, MDMA poses a single stereocenter, and can easily penetrate the Blood Brain Barrier (BBB) because of its small size and hydrophobic nature (DUNLAP; ANDREWS; OLSON, 2018). This molecule produces psychostimulants and hallucinogens effects, and the interoceptive effects are distinct from other class of psychoactive compounds. For produce subjective effects for several hours, 75-150 mg of this molecule is sufficient. The effects include reduced social inhibition, positive mood, increased alertness, feeling of closeness with other, among others. Regarding to hallucinogen effects, 20% of recreational users reports experiencing visual hallucinations, often described as flashes of light in the peripheral visual field (DUNLAP; ANDREWS; OLSON, 2018). In addition to psychedelic and hallucinogen effects, MDMA can also induce several neurological, cardiovascular, hepatic and renal

toxic symptoms, both acute and chronic, such as hepatotoxicity, hyperthermia, hypertension, tachycardia and even fatal intoxications (MONKS *et al.*, 2004).

Most of these effects and biological actions can arise of the structural similarity of these drugs with adrenaline, dopamine and serotonin. The MDMA is broken down metabolically by the action of several enzymes, such as CYP2D6 enzyme (PAPASEIT *et al.*, 2020). Even after metabolism, some MDMA metabolites are pharmacologically active, especially MDA, the first metabolite, which prolongs the drug's effect on the body (KALANT, 2001).

3.3. Animal Health Monitoring

The third important field of application for chemical sensors discussed here is animal health monitoring. It is estimated that for the next three decades the global demand for various meat and animal products can increase by more than 70%. To satisfy this high demand, it is necessary to find the most efficient ways and systems for animal husbandry, since resources like land, water and other natural resources are also increasingly limited (NEETHIRAJAN, 2020). In addition to the high demand for animal products and the scarcity of natural resources, the improvement of animal management techniques also contributes significantly to the economy of producing countries (WANG, HAI; FAPOJUWO; DAVIES, 2016). Animal diseases can cause significant economic losses, especially in countries where agribusiness is the engine of the economy, as is the case in Brazil, in which agribusiness accounted for 26.6% of GDP in the year 2020 (CNA, 2021).

In this context, optimized technologies for real-time and continuous monitoring of animal health as a chemical sensor offers a practical solution for many problems in animal management, constituting a very important requirement in the animal production industry. Since the sensors are able to provide crucial information, quickly and efficiently, with optimum reliability, the use of these devices, besides decreasing the health and economic costs associated with the occurrence of diseases, are also important to reduce the time for diagnosis of pathologies or even for early treatment.

As a consequence, there is an increase in production and animal welfare (FUTAGAWA *et al.*, 2011; KIANI, 2018).

The development of technologies to monitor animal behavior and health has been the subject of a wide range of studies, mainly for chemical sensing technologies. Within this field many sensors have already been developed for various purposes, such as sensors for detect metabolic disorders (GAREIS *et al.*, 2018; MOTTRAM, TOBY, 1997), biomarkers for common diseases (PELED *et al.*, 2012; SHEPHERD *et al.*, 2016), immune status (KNOBLOCH *et al.*, [S.d.]; SILVA, M. G. *et al.*, 2008), hormone levels or other fertility markers (MANZOLI *et al.*, 2019), among others.

3.3.1. Fertility hormones β- Estradiol and Progesterone

Two physiological components that are key molecules not only for the female reproductive system but also for the functioning of the whole organism are the hormones progesterone and β-estradiol (Figure 13). The first of these, progesterone, is essential in the menstrual cycle, in reproduction, and in the biosynthesis of steroidal hormones. In addition, it also acts in the central nervous system, the immune system, and in the development of the mammary glands. The second, β-estradiol, is the main female sex hormone and the more potent among estrogenic hormones, being essential for the development and maintenance of female reproductive tissues, acting in regulating the menstrual cycle (JENSEN, E. V.; DESOMBRE, 2003; NAGY *et al.*, 2021).

Figure 13 – Chemical structures of female sex hormones β-estradiol and progesterone.

17 beta-Estradiol   Progesterone
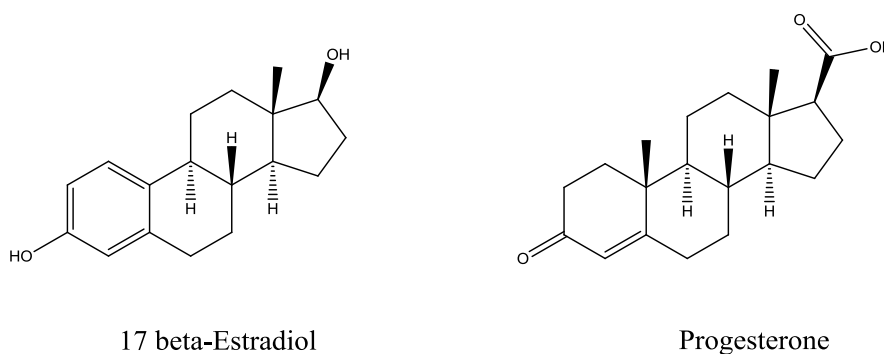
Briefly, the onset of the reproductive cycle occurs in response to low estrogen levels in the body. The hypothalamus sends a signal to the anterior pituitary gland, which secretes follicle-stimulating hormone (FSH), which in turn induces an increase in estrogen production. This increase in estrogen production ends up stimulating the luteinizing hormone (LH), which has its peak concentration in a period of 2 to 24 hours before ovulation. In the case of absence of pregnancy, after the maximum peaks of estrogen, FSH and LH occur, the secretion of LH continues, thus stimulating the production of progesterone for a period of approximately 10 days. Finally, hemorrhage occurs, which is a result of the rapid decrease in progesterone and estrogen production. Once estrogen drops, the cycle then starts again (SERAFÍN *et al.*, 2019).

As can be seen, despite acting at different stages and performing different functions in the reproductive cycle, both progesterone and β-estradiol are markers of fertility, and therefore can be used as molecular targets for the development of sensors for this purpose. In this sense, some chemical sensors have already been developed, such as the sensor to monitor ovulation and fertility of cows, increasing the chance of successful pregnancy (CERRI *et al.*, 2021; MOTTRAM, T., 2016).

BIBLIOGRAPHY

ABBURU, S.; VENKATRAMAN, V.; ALSBERG, B. K. **TD-DFT based fine-tuning of molecular excitation energies using evolutionary algorithms †**. 2016. Disponível em: <www.rsc.org/advances>. Acesso em: 4 jul. 2019.

ABDEL-AZIZ, M. *et al.* **Novel N-4-piperazinyl-ciprofloxacin-chalcone hybrids: Synthesis, physicochemical properties, anticancer and topoisomerase i and II inhibitory activity**. *European Journal of Medicinal Chemistry*, v. 69, p. 427–438, 2013.

ABDEL GHANI, N. T. *et al.* **Computational Design, Synthesis and Application of a New Selective Molecularly Imprinted Polymer for Electrochemical Detection**. *Electroanalysis*, v. 28, n. 7, p. 1530–1538, 1 jul. 2016.

ABDOLLAHZADEH, M. *et al.* **Highly stable Li+ selective electrode with metal-organic framework as ion-to-electron transducer**. *Sensors and Actuators B: Chemical*, v. 350, p. 130799, 1 jan. 2022.

ABREU, H. A. *ESTUDO DE SISTEMAS QUÍMICOS APLICANDO-SE A TEORIA DO FUNCIONAL DE DENSIDADE*. 2004. 163 f. UFMG, 2004.

ADCOCK, S. A.; MCCAMMON, J. A. **Molecular Dynamics: Survey of Methods for Simulating the Activity of Proteins**. *Chemical Reviews*, v. 106, n. 5, p. 1589–1615, maio 2006. Disponível em: <https://pubs.acs.org/doi/10.1021/cr040426m>. Acesso em: 13 jun. 2019.

AGBENYEGAH, G. *et al.* **Adsorption of HF on gibbsite calcined at various temperatures: A solid-state NMR study of low-level fluorinated systems**. *Journal of Physics and Chemistry of Solids*, v. 160, p. 110355, 1 jan. 2022.

AHMED, A.; DANESHTALAB, M. *Nonclassical biological activities of quinolone derivatives*. *Journal of Pharmacy and Pharmaceutical Sciences*. [S.l: s.n.]. , 9 dez. 2011.

AHMED, N. *et al.* **Irreversible coumarin based fluorescent probe for selective detection of Cu2+ in living cells**. *Spectrochimica Acta Part A: Molecular and Biomolecular Spectroscopy*, v. 264, p. 120313, 5 jan. 2022.

ALDER, B. J.; WAINWRIGHT, T. E. **Phase Transition for a Hard Sphere System**. *The Journal of Chemical Physics*, v. 27, n. 5, p. 1208–1209, 13 nov. 1957. Disponível em: <http://aip.scitation.org/doi/10.1063/1.1743957>. Acesso em: 8 fev. 2019.

ALDER, B. J.; WAINWRIGHT, T. E. **Studies in Molecular Dynamics. I. General Method**. *The Journal of Chemical Physics*, v. 31, n. 2, p. 459–466, 6 ago. 1959. Disponível em: <http://aip.scitation.org/doi/10.1063/1.1730376>. Acesso em: 8 fev. 2019.

ALI, R. *et al.* **Ratiometric ultrasensitive optical chemisensor film based antibiotic drug for Al(III) and Cu(II) detection**. *Talanta*, v. 221, 1 jan. 2021.

ANALYTICS, C. *Citation Report Web of Science 2022: Fluorescent Probes*. . [S.l: s.n.]. Disponível em: <https://www-webofscience.ez26.periodicos.capes.gov.br/wos/woscc/citation-report/b6aeb58e-2a4c-4108-ab4c-e5eb6f203a50-17ada0b9>2022.

ANARAKI, M. T. *et al.* **NMR spectroscopy of wastewater: A review, case study, and future potential**. *Progress in Nuclear Magnetic Resonance Spectroscopy*, v. 126–127, p. 121–180, 1 out. 2021.

APPELL, M.; MARAGOS, C. M.; KENDRA, D. F. Molecularly Imprinted Polymers for Mycotoxins. [S.l: s.n.], 2008. p. 152–169. Disponível em: <http://pubs.acs.org/doi/abs/10.1021/bk-2008-1001.ch008>. Acesso em: 22 jun. 2018.

ASADIAN, E.; GHALKHANI, M.; SHAHROKHIAN, S. **Electrochemical sensing based on carbon nanoparticles: A review**. *Sensors and Actuators B: Chemical*, v. 293, p. 183–209, 15 ago. 2019.

ASHBURN, T. T.; THOR, K. B. **Drug repositioning: identifying and developing new uses for existing drugs**. *Nature Reviews Drug Discovery*, v. 3, n. 8, p. 673–683, ago. 2004. Disponível em: <http://www.ncbi.nlm.nih.gov/pubmed/15286734>. Acesso em: 15 out. 2019.

AUSTIN, C. A.; FISHER, L. M. **Isolation and characterization of a human cDNA clone encoding a novel DNA topoisomerase II homologue from HeLa cells**. *FEBS Letters*, v. 266, n. 1–2, p. 115–117, 18 jun. 1990. Disponível em: <https://www.sciencedirect.com/science/article/pii/001457939081520X>. Acesso em: 10 out. 2019.

BAILEY, M. M. *et al.* **Chemically modifiable fluorinated copolymer nanoparticles for 19F-MRI contrast enhancement**. *Journal of Applied Polymer Science*, v. 126, n. 4, p. 1218–1227, 15 nov. 2012. Disponível em: <https://onlinelibrary-wiley.ez26.periodicos.capes.gov.br/doi/full/10.1002/app.36889>. Acesso em: 8 dez. 2021.

BANDODKAR, A. J. *et al.* **Wearable Sensors for Biochemical Sweat Analysis**. *https://doi-org.ez26.periodicos.capes.gov.br/10.1146/annurev-anchem-061318-114910*, v. 12, p. 1–22, 12 jun. 2019. Disponível em: <https://www-annualreviews-org.ez26.periodicos.capes.gov.br/doi/abs/10.1146/annurev-anchem-061318-114910>. Acesso em: 6 dez. 2021.

BANGALEH, Z. *et al.* **A New Potentiometric Sensor for Determination and Screening Phenylalanine in Blood Serum Based on Molecularly Imprinted Polymer.** *Iranian journal of pharmaceutical research : IJPR*, v. 18, n. 1, p. 61–71, 2019. Disponível em: <http://www.ncbi.nlm.nih.gov/pubmed/31089344>. Acesso em: 11 dez. 2019.

BARFIDOKHT, A. *et al.* **Wearable electrochemical glove-based sensor for rapid and on-site detection of fentanyl**. *Sensors and Actuators B: Chemical*, v. 296, p. 126422, 1 out. 2019. Disponível em: <https://www.sciencedirect.com/science/article/pii/S0925400519305763>. Acesso em: 20

ago. 2019.

BATES, F. *et al.* **Computational design of molecularly imprinted polymer for direct detection of melamine in milk**. *Separation Science and Technology*, v. 52, n. 8, p. 1441–1453, 24 maio 2017. Disponível em: <https://www.tandfonline.com/doi/full/10.1080/01496395.2017.1287197>. Acesso em: 26 ago. 2019.

BEBEROK, A.; WRZEŚNIOK, D.; MINECKA, A.; *et al.* **Ciprofloxacin-mediated induction of S-phase cell cycle arrest and apoptosis in COLO829 melanoma cells**. *Pharmacological Reports*, v. 70, n. 1, p. 6–13, 1 fev. 2018. Disponível em: <http://www.ncbi.nlm.nih.gov/pubmed/29306115>. Acesso em: 21 abr. 2020.

BEBEROK, A.; WRZEŚNIOK, D.; ROK, J.; *et al.* **Ciprofloxacin triggers the apoptosis of human triple-negative breast cancer MDA-MB-231 cells via the p53/Bax/Bcl-2 signaling pathway**. *International Journal of Oncology*, v. 52, n. 5, p. 1727–1737, 2018. Disponível em: <http://www.spandidos-publications.com/10.3892/ijo.2018.4310>. Acesso em: 16 out. 2019.

BECK, D.; DAGGETT, V. **Methods for molecular dynamics simulations of protein folding/unfolding in solution**. *Methods*, v. 34, n. 1, p. 112–120, set. 2004. Disponível em: <http://www.ncbi.nlm.nih.gov/pubmed/15283920>. Acesso em: 13 jun. 2019.

BECKE, A. D. **A new mixing of Hartree–Fock and local density-functional theories**. *The Journal of Chemical Physics*, v. 98, n. 2, p. 1372–1377, 15 jan. 1993. Disponível em: <http://aip.scitation.org/doi/10.1063/1.464304>. Acesso em: 24 jun. 2019.

BECKE, A. D. **Density-functional thermochemistry. V. Systematic optimization of exchange-correlation functionals**. *The Journal of Chemical Physics*, v. 107, p. 1040, 1997. Disponível em: <https://doi.org/10.1063/1.475007>. Acesso em: 24 jun. 2019.

BECKE, A. D.; ROUSSEL, M. R. **Exchange holes in inhomogeneous systems: A coordinate-space model**. *Physical Review A*, v. 39, n. 8, p. 3761–3767, 1 abr. 1989. Disponível em: <https://link.aps.org/doi/10.1103/PhysRevA.39.3761>. Acesso em: 24 jun. 2019.

BELDA, R. *et al.* **Homo- and heterobinuclear Cu2+ and Zn2+ complexes of abiotic cyclic hexaazapyridinocyclophanes as SOD mimics**. *Dalton Transactions*, v. 42, n. 31, p. 11194–11204, 2013.

BELEITES, C. *et al.* **Classification of human gliomas by infrared imaging spectroscopy and chemometric image processing**. *Vibrational Spectroscopy*, v. 38, n. 1–2, p. 143–149, 29 jul. 2005. Disponível em: <https://www.sciencedirect.com/science/article/pii/S0924203105000366>. Acesso em: 10 set. 2018.

BEREZIN, M. Y.; ACHILEFU, S. **Fluorescence Lifetime Measurements and Biological Imaging**. *Chemical Reviews*, v. 110, n. 5, p. 2641–2684, 12 maio 2010. Disponível em: <https://pubs.acs.org/doi/10.1021/cr900343z>. Acesso em: 1 ago. 2019.

BERGMANN, N. M. *et al.* **Molecularly imprinted polymers with specific recognition for macromolecules and proteins**. *Prog. Polym. Sci*, v. 33, p. 271–288, 2008. Disponível em: <https://ac.els-cdn.com/S0079670007001141/1-s2.0-S0079670007001141-main.pdf?_tid=36424f60-d646-4110-907f-5b0969dd4259&acdnat=1529694086_463da86594627506eadc2567a1a10d21>. Acesso em: 22 jun. 2018.

BHAVSAR, K. A.; ABUGABAH, A.; *et al.* **A comprehensive review on medical diagnosis using machine learning**. *Computers, Materials and Continua*, v. 67, n. 2, p. 1997–2014, 2021.

BHAVSAR, K. A.; SINGLA, J.; *et al.* **Medical diagnosis using machine learning: a statistical review**. *Computers, Materials and Continua*, v. 67, n. 1, p. 107–125, 2021.

BISACCHI, G.; HALE, M. **A "Double-Edged" Scaffold: Antitumor Power within the Antibacterial Quinolone**. *Current Medicinal Chemistry*, v. 23, n. 6, p. 520–577, 3 mar. 2016. Disponível em: <http://www.ncbi.nlm.nih.gov/pubmed/26695512>. Acesso em: 16 out. 2019.

BLOCH, F. *Nuclear Induction. Physical Review*. [S.l: s.n.]. , 1946

BRAY, F. *et al.* **Global cancer statistics 2018: GLOBOCAN estimates of incidence and mortality worldwide for 36 cancers in 185 countries**. v. 68, n. 6, p. 394–424, nov. 2018. Disponível em: <https://pubmed.ncbi.nlm.nih.gov/30207593/>. Acesso em: 4 nov. 2019.

BRITTON, M. M. *MRI of chemical reactions and processes. Progress in Nuclear Magnetic Resonance Spectroscopy*. [S.l.]: Elsevier B.V. , 1 ago. 2017.

BRUICE, P. Y. ET AL. *Quimica orgânica*. [S.l.]: Ed. Prendice Hall, 2004.

BUNCHUAY, T. *et al.* **A new halogen bonding 1,2-iodo-triazoliu-triazole benzene motif for anion recognition**. *Polyhedron*, v. 209, p. 115482, 15 nov. 2021.

CANTRELLE, F.-X. *et al.* **NMR Spectroscopy of the Main Protease of SARS-CoV-2 and Fragment-Based Screening Identify Three Protein Hotspots and an Antiviral Fragment**. *Angewandte Chemie International Edition*, v. 60, n. 48, p. 25428–25435, 22 nov. 2021. Disponível em: <https://onlinelibrary-wiley.ez26.periodicos.capes.gov.br/doi/full/10.1002/anie.202109965>. Acesso em: 8 dez. 2021.

CAPELLE, K. *A Bird's-Eye View of Density-Functional Theory. Brazilian Journal of Physics*. [S.l: s.n.], 2006. Disponível em: <http://arxiv.org/archive/cond-mat,>. Acesso em: 1 abr. 2019.

CERRI, R. L. A. *et al.* **Symposium review: Linking activity-sensor data and physiology to improve dairy cow fertility**. *Journal of Dairy Science*, v. 104, n. 1, p. 1220–1231, 1 jan. 2021.

CHAN, J.; DODANI, S. C.; CHANG, C. J. **Reaction-based small-molecule fluorescent probes for chemoselective bioimaging**. *Nature Chemistry*, v. 4, n. 12, p. 973–984, 23 dez. 2012. Disponível em: <http://www.nature.com/articles/nchem.1500>. Acesso em: 2 out. 2019.

CHANG, C. *et al.* **Investigation of Structural Dynamics of Enzymes and Protonation States of Substrates Using Computational Tools**. *Catalysts*, v. 6, n. 6, p. 82, 31 maio 2016. Disponível em: <http://www.ncbi.nlm.nih.gov/pubmed/27885336>. Acesso em: 13 jun. 2019. CHEN, S. *et al.* **Rapid recognition of di-n-butyl phthalate in food samples with a near infrared fluorescence imprinted sensor based on zeolite imidazolate framework-67**. *Food Chemistry*, v. 367, p. 130505, 15 jan. 2022.

CHEN, X.; SUN, M.; MA, H. **Progress in Spectroscopic Probes with Cleavable Active Bonds**. *Current Organic Chemistry*, v. 10, n. 4, p. 477–489, 28 fev. 2006.

CHO, J. C. *et al.* *What Is Old Is New Again: Delafloxacin, a Modern Fluooquinolone. Pharmacotherapy.* [S.l.]: Pharmacotherapy Publications Inc. , 1 jan. 2018

CHRISTEN, M. *et al.* **The GROMOS software for biomolecular simulation: GROMOS05**. *Journal of Computational Chemistry*, v. 26, n. 16, p. 1719–1751, 1 dez. 2005. Disponível em: <http://doi.wiley.com/10.1002/jcc.20303>. Acesso em: 13 jun. 2019.

CHUNG, T. D. *et al.* **Characterization and immunological identification of cDNA clones encoding two human DNA topoisomerase II isozymes.** *Proceedings of the National Academy of Sciences of the United States of America*, v. 86, n. 23, p. 9431–5, 1 dez. 1989. Disponível em: <http://www.ncbi.nlm.nih.gov/pubmed/2556712>. Acesso em: 10 out. 2019.

CINELLI, M. A. **Topoisomerase 1B poisons: Over a half-century of drug leads, clinical candidates, and serendipitous discoveries**. *Medicinal Research Reviews*, v. 39, n. 4, p. 1294–1337, 19 jul. 2019. Disponível em: <https://onlinelibrary.wiley.com/doi/abs/10.1002/med.21546>. Acesso em: 4 out. 2019.

CNA, C. DA A. E P. DO B. **PIB do Agronegócio**. 2021.

COWEN, T.; KARIM, K.; PILETSKY, S. **Computational approaches in the design of synthetic receptors – A review**. *Analytica Chimica Acta*, v. 936, p. 62–74, 14 set. 2016. Disponível em: <http://www.ncbi.nlm.nih.gov/pubmed/27566340>. Acesso em: 5 abr. 2018.

CRAWFORD-URANGA, A. *et al.* **Time-dependent density-functional theory of strong-field ionization of atoms by soft x rays**. *Physical Review A*, v. 90, n. 3, p. 033412, 11 set. 2014. Disponível em: <https://link.aps.org/doi/10.1103/PhysRevA.90.033412>. Acesso em: 1 jul. 2019.

CUI, W.-L. *et al.* **A novel and stable fluorescent probe for tracking Hg2+ with large Stokes shift and its application in cell imaging**. *Spectrochimica Acta Part A: Molecular and Biomolecular Spectroscopy*, v. 267, p. 120516, 15 fev. 2022.

D'AURELIO, R. *et al.* **Molecularly Imprinted Nanoparticles Based Sensor for Cocaine**

Detection. *Biosensors 2020, Vol. 10, Page 22*, v. 10, n. 3, p. 22, 4 mar. 2020. Disponível em: <https://www.mdpi.com/2079-6374/10/3/22/htm>. Acesso em: 15 dez. 2021.

DA ROCHA, E. P. *et al.* **Probing kinetic and thermodynamic parameters as well as solvent and substituent effects on spectroscopic probes of 2-amino-1,4-naphthoquinone derivatives**. *Computational and Theoretical Chemistry*, v. 1096, p. 17–26, 2016. Disponível em: <http://dx.doi.org/10.1016/j.comptc.2016.09.028>.

DAL POGGETTO, G. *et al.* **^{19}F DOSY NMR analysis for spin systems with $^{n}J_{FF}$ couplings**. *Magnetic Resonance in Chemistry*, v. 52, n. 4, p. 172–177, 1 abr. 2014. Disponível em: <http://doi.wiley.com/10.1002/mrc.4047>. Acesso em: 12 set. 2018.

DE JONG, M. *et al.* **Electrochemical fingerprint of street samples for fast on-site screening of cocaine in seized drug powders**. *Chemical Science*, v. 7, n. 3, p. 2364–2370, 22 fev. 2016. Disponível em: <http://xlink.rsc.org/?DOI=C5SC04309C>. Acesso em: 20 ago. 2019.

DERBENYOVA, N. V.; KONAKOV, A. A.; BURDOV, V. A. **Recombination, multiplication, and transfer of electron-hole pairs in silicon nanocrystals: Effects of quantum confinement, doping, and surface chemistry**. *Journal of Luminescence*, v. 233, p. 117904, 1 maio 2021.

DEWEESE, J. E.; OSHEROFF, N. **The DNA cleavage reaction of topoisomerase II: wolf in sheep's clothing**. *Nucleic Acids Research*, v. 37, n. 3, p. 738, 2009. Disponível em: </pmc/articles/PMC2647315/>. Acesso em: 14 dez. 2021.

DIRAC, P. A. M. **Note on Exchange Phenomena in the Thomas Atom**. *Mathematical Proceedings of the Cambridge Philosophical Society*, v. 26, n. 3, p. 376–385, 24 jul. 1930. Disponível em: <https://www.cambridge.org/core/product/identifier/S0305004100016108/type/journal_article>. Acesso em: 24 jun. 2019.

DOBSON, J. F.; BÜNNER, M. J.; GROSS, E. K. U. **Time-Dependent Density Functional Theory beyond Linear Response: An Exchange-Correlation Potential with Memory**. *Physical Review Letters*, v. 79, n. 10, p. 1905–1908, 8 set. 1997. Disponível em: <https://link.aps.org/doi/10.1103/PhysRevLett.79.1905>. Acesso em: 1 jul. 2019.

DONG, H. *et al.* **Modulation of excited state proton transfer**. *Journal of Luminescence*, v. 231, p. 117840, 1 mar. 2021.

DRAGAN, A. M. *et al.* **Electrochemical Fingerprints of Illicit Drugs on Graphene and Multi-Walled Carbon Nanotubes**. *Frontiers in Chemistry*, v. 9, p. 67, 16 mar. 2021.

DUAN, Y. *et al.* **A point-charge force field for molecular mechanics simulations of proteins based on condensed-phase quantum mechanical calculations**. *Journal of Computational Chemistry*, v. 24, n. 16, p. 1999–2012, 1 dez. 2003. Disponível em: <http://doi.wiley.com/10.1002/jcc.10349>. Acesso em: 13 jun. 2019.

DUNLAP, L. E.; ANDREWS, A. M.; OLSON, D. E. **Dark Classics in Chemical Neuroscience: 3,4-Methylenedioxymethamphetamine**. *ACS Chemical Neuroscience*, v. 9, n. 10, p. 2408–2427, 17 out. 2018. Disponível em: <http://www.ncbi.nlm.nih.gov/pubmed/30001118>. Acesso em: 23 nov. 2018.

DUNN-RANKIN, D.; LEAL, E. M.; WALTHER, D. C. **Personal power systems**. *Progress in Energy and Combustion Science*, v. 31, n. 5–6, p. 422–465, 1 jan. 2005.

DWYER-LINDGREN, L. *et al.* **Drug Use**. *Our World in Data*, v. 319, n. 10, p. 1013–1023, 5 dez. 2019. Disponível em: <https://ourworldindata.org/drug-use>. Acesso em: 15 dez. 2021.

EDWARDS, J. C. *Principles of NMR [online]. .* [S.l: s.n.], 2019. Disponível em: <http://www.process-nmr.com/pdfs/NMR Overview.pdf>. Acesso em: 14 out. 2019.

ERTUĞRUL UYGUN, H. D. *et al.* **Non-invasive cortisol detection in saliva by using molecularly cortisol imprinted fullerene-acrylamide modified screen printed electrodes**. *Talanta*, v. 206, 1 jan. 2020.

EZELARAB, H. A. A. *et al. Recent updates of fluoroquinolones as antibacterial agents. Archiv der Pharmazie*. [S.l.]: Wiley-VCH Verlag. Disponível em: <https://pubmed.ncbi.nlm.nih.gov/30048015/>. Acesso em: 7 jun. 2021. , 1 set. 2018.

FAROOQ, S. *et al.* **Molecularly imprinted polymers' application in pesticide residue detection**. *The Analyst*, v. 143, n. 17, p. 3971–3989, 20 ago. 2018. Disponível em: <http://xlink.rsc.org/?DOI=C8AN00907D>. Acesso em: 18 set. 2018.

FIEF, C. A. *et al.* **Examining the Impact of Antimicrobial Fluoroquinolones on Human DNA Topoisomerase IIα and IIβ**. *ACS Omega*, v. 4, n. 2, p. 4049–4055, 22 fev. 2019.

FONSECA, M. C.; NASCIMENTO, C. S.; BORGES, K. B. **Theoretical investigation on functional monomer and solvent selection for molecular imprinting of tramadol**. *Chemical Physics Letters*, v. 645, p. 174–179, 1 fev. 2016. Disponível em: <https://www.sciencedirect.com/science/article/pii/S0009261416000026>. Acesso em: 22 jun. 2018.

FRADEN, J. *Handbook of Modern Sensors: Physics, Designs, and Applications*. Fifth Edit ed. San Diego, CA, USA: Springer, 2015. Disponível em: <doi: 10.1007/978-3-319-19303-8>. Acesso em: 6 dez. 2021.

FREUDENMANN, R. W.; ÖXLER, F.; BERNSCHNEIDER-REIF, S. **The origin of MDMA (ecstasy) revisited: the true story reconstructed from the original documents**. *Addiction*, v. 101, n. 9, p. 1241–1245, 1 set. 2006. Disponível em: <http://doi.wiley.com/10.1111/j.1360-0443.2006.01511.x>. Acesso em: 22 nov. 2018.

FUTAGAWA, M. *et al.* **Study of a wireless multimodal sensing system integrated with an electrical conductivity sensor and a temperature sensor for the health control of cows**. *IEEJ Transactions on Electrical and Electronic Engineering*, v. 6, n. 2, p. 93–96, 1 mar. 2011. Disponível em: <https://onlinelibrary-

wiley.ez26.periodicos.capes.gov.br/doi/full/10.1002/tee.20629>. Acesso em: 17 dez. 2021.

GANJALI, M. R. *et al.* **Design and construction of a naltrexone selective sensor based on computational study for application in pharmaceutical analysis**. *International Journal of Electrochemical Science*, v. 4, n. 8, p. 1153–1166, 2009.

GARCÍA, J. A. *et al. Fluorescence: An Interdisciplinary Phenomenon for Different Education Levels. European J of Physics Education*. [S.l: s.n.], 2012. Disponível em: <https://files.eric.ed.gov/fulltext/EJ1052006.pdf>. Acesso em: 1 ago. 2019.

GAREIS, N. C. *et al.* **Alterations in key metabolic sensors involved in bovine cystic ovarian disease**. *Theriogenology*, v. 120, p. 138–146, 15 out. 2018.

GE, M. *et al.* **Octahedral Trifluoromagnesate, an Anomalous Metal Fluoride Species, Stabilizes the Transition State in a Biological Motor**. *ACS Catalysis*, v. 11, n. 5, p. 2769–2773, 5 mar. 2021. Disponível em: <https://pubs-acs-org.ez26.periodicos.capes.gov.br/doi/full/10.1021/acscatal.0c04500>. Acesso em: 8 dez. 2021.

GHOSH, D. *et al.* **Spectroscopic investigation of bis-appended 1,2,3-triazole probe for the detection of Cu(II) ion**. *Journal of Molecular Structure*, v. 1134, p. 638–648, 15 abr. 2017. Disponível em: <https://www.sciencedirect.com/science/article/pii/S0022286016314156>. Acesso em: 4 fev. 2019.

GIMENEZ, D. *et al.* **19F NMR as a tool in chemical biology**. *Beilstein Journal of Organic Chemistry 17:28*, v. 17, n. 1, p. 293–318, 28 jan. 2021. Disponível em: <https://www.beilstein-journals.org/bjoc/articles/17/28>. Acesso em: 21 out. 2021.

GLADDEN, L. F. **Nuclear magnetic resonance in chemical engineering: Principles and applications**. *Chemical Engineering Science*, v. 49, n. 20, p. 3339–3408, 1994.

GODBEY, W. T. Fluorescence. *An Introduction to Biotechnology*. [S.l.]: Elsevier, 2014. p. 173–186. Disponível em: <https://linkinghub.elsevier.com/retrieve/pii/B9781907568282000083>. Acesso em: 1 ago. 2019.

GONÇALVES, M. A. *et al.* **Investigating an efficient and accurate protocol for sampling structures from molecular dynamics simulations: a close look by different wavelet families**. *Theoretical Chemistry Accounts 2021 140:8*, v. 140, n. 8, p. 1–12, 16 jul. 2021. Disponível em: <https://link.springer.com/article/10.1007/s00214-021-02816-y>. Acesso em: 22 out. 2021.

GONÇALVES, M. A. *et al.* **NMR relaxation and relaxivity parameters of MRI probes revealed by optimal wavelet signal compression of molecular dynamics simulations**. *International Journal of Quantum Chemistry*, v. 119, n. 10, p. e25896, 15 maio 2019. Disponível em: <https://onlinelibrary.wiley.com/doi/full/10.1002/qua.25896>. Acesso em: 22 out. 2021.

GONÇALVES, M. A. *et al.* **Optimal wavelet signal compression as an efficient alternative to investigate molecular dynamics simulations: application to thermal and solvent effects of MRI probes**. *Theoretical Chemistry Accounts*, v. 136, n. 1, p. 15, 22 jan. 2017. Disponível em: <http://link.springer.com/10.1007/s00214-016-2037-z>. Acesso em: 11 set. 2018.

GRANIZO, P. E. R. *Avaliação da fotoestabilidade deacetazolamida e lorantadina e da capacidade de fotoproteção de seus complexos com ciclodextrinas*. 2012. 199 f. Universidade de São Paulo, 2012. Disponível em: <https://www.teses.usp.br/teses/disponiveis/9/9139/tde-18042013-154107/publico/Tese_Doutorado_Patricia_Elizabeth_Rivas_Granizo_1002012.PDF>.

GUNTHER, H. *Nmr spectroscopy : basic principles, concepts and applications in chemistry*. Third ed. Weinheim, Germany: Wiley-VCH, 2014. Disponível em: <https://download.e-bookshelf.de/download/0004/9997/85/L-G-0004999785-0019264820.pdf>. Acesso em: 16 out. 2019.

GUO, Y. *et al.* **Detection, detoxification, and removal of multiply heavy metal ions using a recyclable probe enabled by click and declick chemistry**. *Journal of Hazardous Materials*, v. 423, p. 127242, 5 fev. 2022.

GUPTA, P. *et al.* **Ciprofloxacin Enhances the Chemosensitivity of Cancer Cells to ABCB1 Substrates**. *International Journal of Molecular Sciences*, v. 20, n. 2, p. 268, 11 jan. 2019. Disponível em: <http://www.mdpi.com/1422-0067/20/2/268>. Acesso em: 16 out. 2019.

HASSANALI, A. A.; VERDOLINO, V.; PARRINELLO, M. **Aqueous solutions: state of the art in ab initio molecular dynamics**. 2014.

HATZAKIS, E. *Nuclear Magnetic Resonance (NMR) Spectroscopy in Food Science: A Comprehensive Review*. *Comprehensive Reviews in Food Science and Food Safety*. [S.l.]: Blackwell Publishing Inc. , 1 jan. 2019.

HAUPT, K.; MOSBACH, K. **Molecularly imprinted polymers and their use in biomimetic sensors**. *Chemical Reviews*, v. 100, n. 7, p. 2495–2504, jul. 2000.

HE, J. *et al.* **Scalable production of high-performing woven lithium-ion fibre batteries**. *Nature 2021 597:7874*, v. 597, n. 7874, p. 57–63, 1 set. 2021. Disponível em: <https://www-nature.ez26.periodicos.capes.gov.br/articles/s41586-021-03772-0>. Acesso em: 9 dez. 2021.

HEINEMAN, W. R.; KISSINGER, P. T.; WEHMEYER, K. R. **Editors' Choice—Review—From Polarography to Electrochemical Biosensors: The 100-Year Quest for Selectivity and Sensitivity**. *Journal of The Electrochemical Society*, v. 168, n. 11, p. 116504, 11 nov. 2021. Disponível em: <https://iopscience-iop.ez26.periodicos.capes.gov.br/article/10.1149/1945-7111/ac33e3>. Acesso em: 9 dez. 2021.

HERSCHEL, J. F. W. **Αμο'ρφωτα, No. 2. On the Epipolic Dispersion of Light; Being a Supplement to a Paper Entitled on a Case of Superficial Colour Presented by a**

Homogeneous Liquid Internally Colourless. *Proceedings of the Royal Society of London*, v. 5, n. 0, p. 549–549, 1 jan. 1843. Disponível em: <http://rspl.royalsocietypublishing.org/cgi/doi/10.1098/rspl.1843.0042>. Acesso em: 1 ago. 2019.

HERSCHEL, J. F. W. **IV. ’Αμόρφωϒα, no. I.— on a case of superficial colour presented by a homogeneous liquid internally colourless**. *Philosophical Transactions of the Royal Society of London*, v. 135, p. 143–145, 31 jan. 1845. Disponível em: <http://www.royalsocietypublishing.org/doi/10.1098/rstl.1845.0004>. Acesso em: 1 ago. 2019.

HILLBERG, A.; BRAIN, K.; ALLENDER, C. **Molecular imprinted polymer sensors: Implications for therapeutics**. *Advanced Drug Delivery Reviews*, 27 out. 2005. Disponível em: <https://linkinghub.elsevier.com/retrieve/pii/S0169409X05001560>. Acesso em: 20 ago. 2019.

HOHENBERG, P.; KOHN, W. **Inhomogeneous Electron Gas**. *Physical Review*, v. 136, n. 3B, p. B864–B871, 9 nov. 1964. Disponível em: <https://link.aps.org/doi/10.1103/PhysRev.136.B864>. Acesso em: 8 fev. 2019.

HONG, J. *et al.* **A red to near-infrared fluorescent probe featuring a super large Stokes shift for light-up detection of endogenous H2S**. *Dyes and Pigments*, v. 160, p. 787–793, 1 jan. 2019. Disponível em: <https://www.sciencedirect.com/science/article/pii/S014372081831742X>. Acesso em: 3 out. 2019.

HUANG, L. *et al.* **Discrimination of narcotic drugs in human urine based on nanoplasmonics combined with chemometric method**. *Journal of Pharmaceutical and Biomedical Analysis*, v. 186, p. 113174, 15 jul. 2020.

HUSSAIN, M. *et al.* **Oxygen vacancies boosted vanadium doped ZnO nanostructures-based voltage-switchable binary biosensor**. *Nanotechnology*, v. 33, n. 2, p. 025502, 22 out. 2021. Disponível em: <https://iopscience-iop.ez26.periodicos.capes.gov.br/article/10.1088/1361-6528/ac2c44>. Acesso em: 6 dez. 2021.

HWANG, D.; SCHLENKER, C. W. **Photochemistry of carbon nitrides and heptazine derivatives**. *Chemical Communications*, v. 57, n. 74, p. 9330–9353, 16 set. 2021. Disponível em: <https://pubs-rsc-org.ez26.periodicos.capes.gov.br/en/content/articlehtml/2021/cc/d1cc02745j>. Acesso em: 10 dez. 2021.

INCA. *ABC do câncer : abordagens básicas para o controle do câncer*. [S.l: s.n.], 2011. Disponível em: <www.inca.gov.br>. Acesso em: 9 nov. 2018.

INCA. *Estimativa 2020: incidência de câncer no Brasil | INCA - Instituto Nacional de Câncer*. COORDENAÇÃ ed. Rio de Janeiro: [s.n.], 2019. Disponível em: <https://www.inca.gov.br/publicacoes/livros/estimativa-2020-incidencia-de-cancer-no-

brasil>. Acesso em: 13 dez. 2021.

IZUMI, K. **Disorders of Transcriptional Regulation: An Emerging Category of Multiple Malformation Syndromes**. *Molecular Syndromology*, v. 7, n. 5, p. 262–273, 1 out. 2016. Disponível em: <https://www.karger.com/Article/FullText/448747>. Acesso em: 27 dez. 2021.

J LLOYD-HUGHES1, 19,∗ , P M OPPENEER2,19,∗ *et al.* **The 2021 ultrafast spectroscopic probes of condensed matter roadmap**. *J. Phys.: Condens. Matte*, v. 22, n. 353001, p. 1–43, 2021. Disponível em: <http://uu.diva-portal.org/smash/get/diva2:1594643/FULLTEXT01>. Acesso em: 8 dez. 2021.

JACQUEMIN, D. *et al.* **Extensive TD-DFT Benchmark: Singlet-Excited States of Organic Molecules**. *Journal of Chemical Theory and Computation*, v. 5, n. 9, p. 2420–2435, 8 set. 2009. Disponível em: <https://pubs.acs.org/doi/10.1021/ct900298e>. Acesso em: 4 jul. 2019.

JACQUEMIN D, M. B. AND A. C. **Excited-state calculations with TD-DFT: from benchmarks to simulations in complex environments**. *Physical Chemistry Chemical Physics*, v. 13, n. 38, p. 16987–98, 2011. Disponível em: <file:///C:/Users/Dani/Desktop/178-PCCP13201116987.pdf>. Acesso em: 10 out. 2019.

JANKOWSKA, J.; SOBOLEWSKI, A. L. **Modern Theoretical Approaches to Modeling the Excited-State Intramolecular Proton Transfer: An Overview**. *Molecules 2021, Vol. 26, Page 5140*, v. 26, n. 17, p. 5140, 25 ago. 2021. Disponível em: <https://www.mdpi.com/1420-3049/26/17/5140/htm>. Acesso em: 10 dez. 2021.

JANKU, F.; YAP, T. A.; MERIC-BERNSTAM, F. *Targeting the PI3K pathway in cancer: Are we making headway? Nature Reviews Clinical Oncology*. [S.l.]: Nature Publishing Group. , 1 maio 2018

JENSEN, F. *Introduction to computational Chemistry*. Second ed. [S.l: s.n.], 2007. v. 1. Disponível em: <http://dx.doi.org/10.1007/s00214-011-0895-y%5Cnhttp://dx.doi.org/10.1007/s00214-013-1372-6%5Cnhttp://www.bibsonomy.org/bibtex/242a63c877d539b0eb710239a715f0eb1/bronckobuster%5Cnhttp://www.sciencedirect.com/science/article/pii/B9780444517197500792%5Cnhttp:>.

JENSEN, E. V.; DESOMBRE, E. R. **Mechanism of Action of the Female Sex Hormones**. *http://dx.doi.org/10.1146/annurev.bi.41.070172.001223*, v. 41, p. 203–230, 28 nov. 2003. Disponível em: <https://www.annualreviews.org/doi/abs/10.1146/annurev.bi.41.070172.001223>. Acesso em: 21 dez. 2021.

JIN, G.; WONG, S. T. C. **Toward better drug repositioning: prioritizing and integrating existing methods into efficient pipelines**. *Drug Discovery Today*, v. 19, n. 5, p. 637–644, 1 maio 2014. Disponível em: <https://www.sciencedirect.com/science/article/pii/S1359644613003991>. Acesso em: 15

out. 2019.

KALANT, H. **The pharmacology and toxicology of "ecstasy" (MDMA) and related drugs.** *CMAJ : Canadian Medical Association journal = journal de l'Association medicale canadienne*, v. 165, n. 7, p. 917–28, 2 out. 2001. Disponível em: <http://www.ncbi.nlm.nih.gov/pubmed/11599334>. Acesso em: 23 nov. 2018.

KALYAANAMOORTHY, S.; CHEN, Y.-P. P. **Modelling and enhanced molecular dynamics to steer structure-based drug discovery**. *Progress in Biophysics and Molecular Biology*, v. 114, n. 3, p. 123–136, 1 maio 2014. Disponível em: <https://www.sciencedirect.com/science/article/pii/S0079610713000552?via%3Dihub>. Acesso em: 24 jun. 2019.

KANAGARAJ, K. *et al.* **A Quinoline-Appended Cyclodextrin Derivative as a Highly Selective Receptor and Colorimetric Probe for Nucleotides**. *iScience*, v. 23, n. 3, p. 100927, 27 mar. 2020.

KANG, K. *et al.* **Recent developments of emerging inorganic, metal and carbon-based nanomaterials for pressure sensors and their healthcare monitoring applications**. *Nano Research 2021 14:9*, v. 14, n. 9, p. 3096–3111, 26 abr. 2021. Disponível em: <https://link-springer-com.ez26.periodicos.capes.gov.br/article/10.1007/s12274-021-3490-0>. Acesso em: 13 dez. 2021.

KARASIEV, V. V. *et al.* **Local Spin-density Approximation Exchange-correlation Free-energy Functional**. 19 nov. 2013. Disponível em: <http://arxiv.org/abs/1311.4903>. Acesso em: 24 jun. 2019.

KARIM, K. *et al.* **A Protocol for the Computational Design of High Affi nity Molecularly Imprinted Polymer Synthetic Receptors**. *Glob J Biotechnol Biomater Sci*, v. 3, n. 1, p. 1–7, 2017.

KHADKA, D. B.; CHO, W.-J. **Topoisomerase inhibitors as anticancer agents: a patent update**. *Expert Opinion on Therapeutic Patents*, v. 23, n. 8, p. 1033–1056, 23 ago. 2013. Disponível em: <http://www.tandfonline.com/doi/full/10.1517/13543776.2013.790958>. Acesso em: 7 out. 2019.

KHAN, M. S.; PAL, S.; KRUPADAM, R. J. **Computational strategies for understanding the nature of interaction in dioxin imprinted nanoporous trappers**. *Journal of Molecular Recognition*, v. 28, n. 7, p. 427–437, 1 jul. 2015. Disponível em: <http://doi.wiley.com/10.1002/jmr.2459>. Acesso em: 24 abr. 2019.

KIANI, F. **Animal behavior management by energy-efficient wireless sensor networks**. *Computers and Electronics in Agriculture*, v. 151, p. 478–484, 1 ago. 2018.

KIM, T.-W. **Drug Repositioning Approaches for the Discovery of New Therapeutics for Alzheimer's Disease**. *Neurotherapeutics*, v. 12, n. 1, p. 132–142, 31 jan. 2015. Disponível em: <http://link.springer.com/10.1007/s13311-014-0325-7>. Acesso em: 27 ago. 2018.

KIRK E. HEVENERN; TATSIANA A. VERSTAK, K. E. L.; DANIEL L. RIGGSBEE, J. W. M. **Recent developments in topoisomerase-targeted cancer chemotherapy**. *Acta Pharmaceutica Sinica B*, v. 8, n. 6, p. 844–861, 2018. Disponível em: <https://www.ncbi.nlm.nih.gov/pmc/articles/PMC6251812/pdf/main.pdf>. Acesso em: 16 out. 2019.

KNOBLOCH, H. ; *et al.* **Electronic nose responses and acute phase proteins correlate in blood using a bovine respiratory infection Journal Item How to cite**. [S.d.]. Disponível em: <http://dx.doi.org/>. Acesso em: 17 dez. 2021.

KOCH, W.; HOLTHAUSEN, M. C. *A Chemist's Guide to Density Functional Theory*. Second ed. Federal Republic of Germany: Wiley-VCH Verlag GmbH, 2001. v. 3.

KOHN, W. **Nobel Lecture: Electronic structure of matter—wave functions and density functionals**. *Reviews of Modern Physics*, v. 71, n. 5, p. 1253–1266, 1 out. 1999. Disponível em: <https://link.aps.org/doi/10.1103/RevModPhys.71.1253>. Acesso em: 1 abr. 2019.

KOHN, W.; SHAM, L. J. **Self-Consistent Equations Including Exchange and Correlation Effects**. *Physical Review*, v. 140, n. 4A, p. A1133–A1138, 15 nov. 1965. Disponível em: <https://link.aps.org/doi/10.1103/PhysRev.140.A1133>. Acesso em: 8 fev. 2019.

KUMAR, R.; PATHAK, D. K.; CHAUDHARY, A. **Current status of some electrochromic materials and devices: a brief review**. *Journal of Physics D: Applied Physics*, v. 54, n. 50, p. 503002, 28 set. 2021. Disponível em: <https://iopscience-iop.ez26.periodicos.capes.gov.br/article/10.1088/1361-6463/ac10d6>. Acesso em: 6 dez. 2021.

LAKOWICZ, J. R. Solvent and Environmental Effects. *Principles of Fluorescence Spectroscopy*. [S.l.]: Springer Boston, MA, 2006. p. 205–235. Disponível em: <https://link.springer.com/chapter/10.1007/978-0-387-46312-4_6>. Acesso em: 20 jan. 2021.

LARSEN, A. K.; ESCARGUEIL, A. E.; SKLADANOWSKI, A. **Catalytic topoisomerase II inhibitors in cancer therapy**. *Pharmacology & Therapeutics*, v. 99, n. 2, p. 167–181, 1 ago. 2003. Disponível em: <https://www.sciencedirect.com/science/article/pii/S0163725803000585?via%3Dihub>. Acesso em: 10 out. 2019.

LEE, G. H.; CHOI, D. H.; KIM, Y. S. **Molecular Design of Triazole Based Thermally Activated Delayed Fluorescence Hosts for Blue Electrophosphorescence**. *Journal of Nanoscience and Nanotechnology*, v. 19, n. 10, p. 6791–6795, 1 out. 2019a. Disponível em: <https://www.ingentaconnect.com/content/10.1166/jnn.2019.17118>. Acesso em: 31 jul. 2019.

LEE, G. H.; CHOI, D. H.; KIM, Y. S. **Theoretical Study of Benzofuro-Pyridine Derivatives-Based Organic Light-Emitting Diodes Exhibiting Thermally Activated Delayed Fluorescence**. *Journal of Nanoscience and Nanotechnology*, v. 19, n. 8, p. 4787–4790, 1 ago. 2019b. Disponível em: <http://www.ncbi.nlm.nih.gov/pubmed/30913788>. Acesso em: 31 jul. 2019.

LEE, N. *et al.* **A selective triarylmethine-based spectroscopic probe for Zn2+ ion monitoring**. *Dyes and Pigments*, v. 171, p. 107721, 1 dez. 2019. Disponível em: <https://www.sciencedirect.com/science/article/pii/S0143720819312689>. Acesso em: 2 out. 2019.

LEE, Y.-A. *et al.* **Identification of Tumor Initiating Cells with a Small-Molecule Fluorescent Probe by Using Vimentin as a Biomarker**. *Angewandte Chemie International Edition*, v. 57, n. 11, p. 2851–2854, 5 mar. 2018. Disponível em: <http://doi.wiley.com/10.1002/anie.201712920>. Acesso em: 3 out. 2019.

LEIBL, N. *et al.* **Molecularly Imprinted Polymers for Chemical Sensing: A Tutorial Review**. *Chemosensors 2021, Vol. 9, Page 123*, v. 9, n. 6, p. 123, 26 maio 2021. Disponível em: <https://www.mdpi.com/2227-9040/9/6/123/htm>. Acesso em: 13 dez. 2021.

LI, H.; MA, H. **New progress in spectroscopic probes for reactive oxygen species**. *Journal of Analysis and Testing 2018 2:1*, v. 2, n. 1, p. 2–19, 21 mar. 2018. Disponível em: <https://link-springer-com.ez26.periodicos.capes.gov.br/article/10.1007/s41664-018-0049-5>. Acesso em: 8 dez. 2021.

LI, J.-Y. *et al.* **A highly specific tetrazole-based chemosensor for fluoride ion: A new sensing functional group based on intramolecular proton transfer**. *Spectrochimica Acta Part A: Molecular and Biomolecular Spectroscopy*, v. 102, p. 66–70, 1 fev. 2013. Disponível em: <https://www.sciencedirect.com/science/article/pii/S1386142512010852>. Acesso em: 10 set. 2018.

LI, J. *et al.* **Structural requirements of 3-carboxyl-4(1H)-quinolones as potential antimalarials from 2D and 3D QSAR analysis**. *Journal of Molecular Graphics and Modelling*, v. 44, p. 266–277, 2013.

LI, Q. Y. *et al.* **Array-based sensing of amyloidogenic proteins and discrimination of cancer by using different oxidants doped carbon nanodots as fluorescent probes**. *Chemical Engineering Journal*, v. 430, p. 132696, 15 fev. 2022.

LI, R. *et al.* **A fluorescence and UV/vis absorption dual-signaling probe with aggregation-induced emission characteristics for specific detection of cysteine**. *RSC Advances*, v. 8, n. 43, p. 24346–24354, 2018.

LI, X. *et al.* **Design Strategies for Water-Soluble Small Molecular Chromogenic and Fluorogenic Probes**. *Chemical Reviews*, v. 114, n. 1, p. 590–659, 8 jan. 2014. Disponível em: <http://www.ncbi.nlm.nih.gov/pubmed/24024656>. Acesso em: 1 out. 2019.

LI, Y. *et al.* **A new near-infrared excitation/emission fluorescent probe for the detection of β-galactosidase in living cells and in vivo**. *Talanta*, v. 237, p. 122952, 15 jan. 2022.

LIANG, X. *et al.* **A comprehensive review of topoisomerase inhibitors as anticancer agents in the past decade**. *European Journal of Medicinal Chemistry*, v. 171, p. 129–168, jun. 2019. Disponível em: <https://linkinghub.elsevier.com/retrieve/pii/S0223523419302521>. Acesso em: 4 out. 2019.

LIU, D. *et al.* **A turn on fluorescent assay for real time determination of β-galactosidase and its application in living cell imaging**. *Spectrochimica Acta Part A: Molecular and Biomolecular Spectroscopy*, v. 265, p. 120345, 15 jan. 2022.

LIU, H.-W. *et al.* **In Situ Localization of Enzyme Activity in Live Cells by a Molecular Probe Releasing a Precipitating Fluorochrome**. *Angewandte Chemie International Edition*, v. 56, n. 39, p. 11788–11792, 18 set. 2017. Disponível em: <http://doi.wiley.com/10.1002/anie.201705747>. Acesso em: 3 out. 2019.

LIU, H. *et al.* **Progress in Research on VOC Molecule Recognition by Semiconductor Sensors**. *Acta Phys.-Chim Sin.*, v. 38, n. 5, p. 2008018–0, 3 set. 2020. Disponível em: <http://www.whxb.pku.edu.cn/CN/abstract/abstract35994.shtml>. Acesso em: 6 dez. 2021.

LIU, S.-B. **Conceptual Density Functional Theory and Some Recent Developments**. *Acta Phys. -Chim. Sin*, v. 25, n. 3, p. 590–600, 2009. Disponível em: <https://www.ingentaconnect.com/content/apcs/apcs/2009/00000025/00000003/art00033#>. Acesso em: 30 maio 2019.

LIU, S. *et al.* **The novel excited state intramolecular proton transfer broken by intermolecular hydrogen bonds in HOF system**. *Spectrochimica Acta Part A: Molecular and Biomolecular Spectroscopy*, v. 219, p. 164–172, 5 ago. 2019. Disponível em: <https://www.sciencedirect.com/science/article/pii/S1386142519304342>. Acesso em: 31 jul. 2019.

LIU, S.; KOKOT, S.; WILL, G. **Photochemistry and chemometrics—An overview**. *Journal of Photochemistry and Photobiology C: Photochemistry Reviews*, v. 10, n. 4, p. 159–172, 1 dez. 2009.

LIU, Z. *et al.* **A Review on Molecularly Imprinted Polymers Preparation by Computational Simulation-Aided Methods**. *Polymers 2021, Vol. 13, Page 2657*, v. 13, n. 16, p. 2657, 10 ago. 2021. Disponível em: <https://www.mdpi.com/2073-4360/13/16/2657/htm>. Acesso em: 9 dez. 2021.

LOOGER, L. L. *et al.* **Computational design of receptor and sensor proteins with novel functions**. *Nature*, v. 423, n. 6936, p. 185–190, 8 maio 2003. Disponível em: <http://www.nature.com/articles/nature01556>. Acesso em: 4 fev. 2019.

LOWINSOHN, D.; BERTOTTI, M. *SENSORES ELETROQUÍMICOS: CONSIDERAÇÕES SOBRE MECANISMOS DE FUNCIONAMENTO E APLICAÇÕES NO MONITORAMENTO DE ESPÉCIES QUÍMICAS EM AMBIENTES MICROSCÓPICOS*. *Quim. Nova*. [S.l: s.n.], 1318. Disponível em: <http://quimicanova.sbq.org.br/imagebank/pdf/Vol29No6_1318_28-RV05268.pdf>. Acesso em: 17 set. 2018.

LOWINSOHN, D.; BERTOTTI, M. **SENSORES ELETROQUÍMICOS: CONSIDERAÇÕES SOBRE MECANISMOS DE FUNCIONAMENTO E APLICAÇÕES NO MONITORAMENTO DE ESPÉCIES QUÍMICAS EM AMBIENTES MICROSCÓPICOS**. *Quim. Nova*, v. 29, n. 6, p. 1318–1325, 2006.

Disponível em: <http://quimicanova.sbq.org.br/imagebank/pdf/Vol29No6_1318_28-RV05268.pdf>. Acesso em: 11 jun. 2018.

LUE, N. *et al.* **Portable Optical Fiber Probe-Based Spectroscopic Scanner for Rapid Cancer Diagnosis: A New Tool for Intraoperative Margin Assessment**. *PLoS ONE*, v. 7, n. 1, p. e30887, 27 jan. 2012. Disponível em: <http://dx.plos.org/10.1371/journal.pone.0030887>. Acesso em: 10 set. 2018.

LV, Y. *et al.* **Application of molecular dynamics modeling for the prediction of selective adsorption properties of dimethoate imprinting polymer**. *Sensors and Actuators B: Chemical*, v. 133, n. 1, p. 15–23, 28 jul. 2008. Disponível em: <https://www.sciencedirect.com/science/article/pii/S0925400508000890>. Acesso em: 26 mar. 2019.

MA, J. *et al.* **Correction to Near-Infrared Fluorescence Probe for Evaluating Acetylcholinesterase Activity in PC12 Cells and In Situ Tracing AChE Distribution in Zebrafish**. *ACS Sensors*, v. 5, n. 4, p. 1246, 24 abr. 2020. Disponível em: <https://pubs-acs-org.ez26.periodicos.capes.gov.br/doi/full/10.1021/acssensors.0c00436>. Acesso em: 8 dez. 2021.

MACKERELL, A. D. *et al.* **All-Atom Empirical Potential for Molecular Modeling and Dynamics Studies of Proteins †**. 1998. Disponível em: <https://pubs.acs.org/doi/10.1021/jp973084f.>. Acesso em: 13 jun. 2019.

MADHU, B. *et al.* **Response of Degarelix treatment in human prostate cancer monitored by HR-MAS 1 H NMR spectroscopy**. *Metabolomics*, v. 12, n. 120, 2016. Disponível em: <https://link-springer-com.ez26.periodicos.capes.gov.br/content/pdf/10.1007%2Fs11306-016-1055-0.pdf>. Acesso em: 11 set. 2018.

MAHMUD, M. S. *et al.* **Wearables technology for drug abuse detection: A survey of recent advancement**. *Smart Health*, p. 100062, 29 out. 2018. Disponível em: <https://www.sciencedirect.com/science/article/pii/S2352648318300011?via%3Dihub>. Acesso em: 20 ago. 2019.

MALDE, A. K. *et al.* **An Automated force field Topology Builder (ATB) and repository: Version 1.0**. *Journal of Chemical Theory and Computation*, v. 7, n. 12, p. 4026–4037, 13 dez. 2011.

MANCINI, D. T. *FENILBENZOTIAZÓIS COMO SONDA ESPECTROSCÓPICA PARA BIOMOLÉCULAS: CÁLCULO DE PROPRIEDADES ESTRUTURAIS E ELETRÔNICAS*. 2014. 158 f. Federal University of Lavras, 2014. Disponível em: <http://repositorio.ufla.br/bitstream/1/3022/1/TESE Fenilbenzotiazois como sonda espectroscópica para   biomoléculas cálculo de propriedades estruturais e eletrônicas.pdf>. Acesso em: 11 set. 2018.

MANZOLI, A. *et al.* **Volatile compounds monitoring as indicative of female cattle fertile period using electronic nose**. *Sensors and Actuators B: Chemical*, v. 282, p. 609–616, 1 mar. 2019.

MARQUES, M. A. L.; GROSS, E. K. U. **Time-dependent Density Functional Theory**. *Annual review of physical chemistry*, p. 427–455, 2004. Disponível em: <https://pdfs.semanticscholar.org/ad8c/36cd6ddf288a879db7a8d2ae026c22e61391.pdf>. Acesso em: 1 jul. 2019.

MASEMOLA, D. P. *et al.* **Gold nanoparticles modified exfoliated graphite electrode as electrochemical sensor in the determination of psychoactive drug**. *https://doi-org.ez26.periodicos.capes.gov.br/10.1080/03601234.2020.1713670*, v. 55, n. 5, p. 455–461, 3 maio 2020. Disponível em: <https://www-tandfonline.ez26.periodicos.capes.gov.br/doi/abs/10.1080/03601234.2020.1713670>. Acesso em: 15 dez. 2021.

MCCLENDON, A. K.; OSHEROFF, N. **DNA topoisomerase II, genotoxicity, and cancer**. *Mutation Research/Fundamental and Molecular Mechanisms of Mutagenesis*, v. 623, n. 1–2, p. 83–97, 1 out. 2007. Disponível em: <http://www.ncbi.nlm.nih.gov/pubmed/17681352>. Acesso em: 8 out. 2019.

MCNEILL, L. *et al.* **Lab-on-a-Chip approaches for the detection of controlled drugs, including new psychoactive substances: A systematic review**. *Forensic Chemistry*, v. 26, p. 100370, 1 dez. 2021.

MEAD, J.; PARROTT, A. **Mephedrone and MDMA: A comparative review**. *Brain Research*, v. 1735, p. 146740, 15 maio 2020.

MERCANTE, L. A. *et al.* **Electrospinning-based (bio)sensors for food and agricultural applications: A review**. *TrAC Trends in Analytical Chemistry*, v. 91, p. 91–103, 1 jun. 2017. Disponível em: <https://linkinghub.elsevier.com/retrieve/pii/S0165993617300493>. Acesso em: 11 dez. 2018.

MISHRA, R. K. *et al.* **Continuous Opioid Monitoring along with Nerve Agents on a Wearable Microneedle Sensor Array**. *Journal of the American Chemical Society*, v. 142, n. 13, p. 5991–5995, 1 abr. 2020. Disponível em: <https://pubs-acs-org.ez26.periodicos.capes.gov.br/doi/full/10.1021/jacs.0c01883>. Acesso em: 15 dez. 2021.

MISTRY, A. R. *et al.* **DNA Topoisomerase II in Therapy-Related Acute Promyelocytic Leukemia**. *New England Journal of Medicine*, v. 352, n. 15, p. 1529–1538, 14 abr. 2005. Disponível em: <http://www.nejm.org/doi/abs/10.1056/NEJMoa042715>. Acesso em: 10 out. 2019.

MONKS, T. J. *et al.* **The role of metabolism in 3,4-(+)-methylenedioxyamphetamine and 3,4-(+)-methylenedioxymethamphetamine (ecstasy) toxicity.** *Therapeutic drug monitoring*, v. 26, n. 2, p. 132–6, 1 abr. 2004. Disponível em: <https://www.ncbi.nlm.nih.gov/pubmed/15228153>. Acesso em: 23 nov. 2018.

MORADI, R. *et al.* **Nanoarchitectonics for Abused-Drug Biosensors**. *Small*, p. 2104847, 9 dez. 2021. Disponível em: <https://onlinelibrary-wiley.ez26.periodicos.capes.gov.br/doi/full/10.1002/smll.202104847>. Acesso em: 15 dez. 2021.

MORGON, N.H.; COUTINHO, K. *Methods of theoretical chemistry and molecular modeling*. São Paulo: Physics Bookstore, 2007.

MORRIS, C. J.; CORTE, D. DELLA. **Using molecular docking and molecular dynamics to investigate protein-ligand interactions**. *Modern Physics Letters B*, v. 35, n. 8, p. 2130002, 20 mar. 2021. Disponível em: <www.worldscientific.com>. Acesso em: 10 dez. 2021.

MOSBACH, K.; RAMSTRÖM, O. **The Emerging Technique of Molecular Imprinting and Its Future Impact on Biotechnology**. *Nature Biotechnology*, v. 14, n. 2, p. 163–170, 1 fev. 1996. Disponível em: <http://www.nature.com/doifinder/10.1038/nbt0296-163>. Acesso em: 22 jun. 2018.

MOTTRAM, T. **Animal board invited review: precision livestock farming for dairy cows with a focus on oestrus detection**. *Animal*, v. 10, n. 10, p. 1575–1584, 1 jan. 2016.

MOTTRAM, T. **Automatic monitoring of the health and metabolic status of dairy cows**. *Livestock Production Science*, v. 48, n. 3, p. 209–217, 1 jun. 1997.

MUNDIM, K.; ELLIS, D. **Stochastic classical molecular dynamics coupled to functional density theory: Applications to large molecular systems**. *Brazilian journal of physics*, v. 29, n. 1, p. 199–214, 1999. Disponível em: <http://www.scielo.br/scielo.php?pid=S0103-97331999000100018&script=sci_arttext&tlng=es>.

MUNIZ-MIRANDA, F. **Computational Approaches to the Electronic Properties of Noble Metal Nanoclusters Protected by Organic Ligands**. *Nanomaterials 2021, Vol. 11, Page 2409*, v. 11, n. 9, p. 2409, 16 set. 2021. Disponível em: <https://www.mdpi.com/2079-4991/11/9/2409/htm>. Acesso em: 10 dez. 2021.

MUNTEANU, R. E. *et al.* **2D materials in electrochemical sensors for in vitro or in vivo use**. *Analytical and Bioanalytical Chemistry*, v. 413, n. 3, p. 701–725, 10 ago. 2020. Disponível em: <https://link-springer-com.ez26.periodicos.capes.gov.br/article/10.1007/s00216-020-02831-1>. Acesso em: 9 dez. 2021.

NAGY, B. *et al.* **Key to Life: Physiological Role and Clinical Implications of Progesterone**. *International Journal of Molecular Sciences 2021, Vol. 22, Page 11039*, v. 22, n. 20, p. 11039, 13 out. 2021. Disponível em: <https://www.mdpi.com/1422-0067/22/20/11039/htm>. Acesso em: 21 dez. 2021.

NAJAFI, P.; KOUCHAKZADEH, H. **BSA nanoparticles loaded with IONPs for biomedical applications: fabrication optimization, physicochemical characterization and biocompatibility evaluation**. *Nanomedicine Journal*, v. 6, n. 1, p. 55–66, 1 jan. 2019. Disponível em: <http://nmj.mums.ac.ir/article_12159.html>. Acesso em: 8 out. 2019.

NAKATSUKASA, T. *et al.* **Time-dependent density-functional description of nuclear dynamics**. 15 jun. 2016. Disponível em: <http://arxiv.org/abs/1606.04717>. Acesso em: 1 jul.

2019.

NEETHIRAJAN, S. **The role of sensors, big data and machine learning in modern animal farming**. *Sensing and Bio-Sensing Research*, v. 29, p. 100367, 1 ago. 2020.

NEETIKA SINGH, PRABHAT KUMAR, U. R. **Applications of near infrared and surface enhanced Raman scattering techniques in tumor imaging: A short review**. *Spectrochimica Acta Part A: Molecular and Biomolecular Spectroscopy*, v. 222, p. 117279, 5 nov. 2019. Disponível em: <https://www-sciencedirect.ez26.periodicos.capes.gov.br/science/article/pii/S1386142519306699?via%3Dihub>. Acesso em: 8 out. 2019.

NICHOLLS, I. A. *et al.* **The Use of Computational Methods for the Development of Molecularly Imprinted Polymers**. *Polymers 2021, Vol. 13, Page 2841*, v. 13, n. 17, p. 2841, 24 ago. 2021. Disponível em: <https://www.mdpi.com/2073-4360/13/17/2841/htm>. Acesso em: 9 dez. 2021.

NICHOLLS, I. A. *et al.* Theoretical and Computational Strategies for the Study of the Molecular Imprinting Process and Polymer Performance. [S.l.]: Springer, Cham, 2015. p. 25–50. Disponível em: <http://link.springer.com/10.1007/10_2015_318>. Acesso em: 11 jul. 2019.

NIU, L.-Y. *et al.* **Design strategies of fluorescent probes for selective detection among biothiols**. *Chemical Society Reviews*, v. 44, n. 17, p. 6143–6160, 17 ago. 2015. Disponível em: <http://xlink.rsc.org/?DOI=C5CS00152H>. Acesso em: 2 out. 2019.

NOVAC, N. **Challenges and opportunities of drug repositioning**. *Trends in Pharmacological Sciences*, v. 34, n. 5, p. 267–272, 1 maio 2013. Disponível em: <https://www.sciencedirect.com/science/article/pii/S016561471300045X>. Acesso em: 15 out. 2019.

NUSSBAUMER, F. *et al.* **Aromatic 19F–13C TROSY—[19F, 13C]-Pyrimidine Labeling for NMR Spectroscopy of RNA**. *Angewandte Chemie International Edition*, v. 59, n. 39, p. 17062–17069, 21 set. 2020. Disponível em: <https://onlinelibrary-wiley.ez26.periodicos.capes.gov.br/doi/full/10.1002/anie.202006577>. Acesso em: 8 dez. 2021.

OJHA, R. *et al.* **Diverse and unexpected outcomes from oxidation of the platinum(II) anticancer agent [Pt{(p-BrC6F4)NCH2CH2NEt2}Cl(py)] by hydrogen peroxide**. *Journal of Inorganic Biochemistry*, v. 218, p. 111360, 1 maio 2021.

OUYANG, D.; DAI, Q. **Metabolomics analysis of human pancreatic cancer tissue and paired adjacent tissue samples**. *Biomedical Research*, v. 28, n. 8, p. 3580–3582, 2017. Disponível em: <www.biomedres.info>. Acesso em: 11 set. 2018.

PALERMO, G. *et al.* **Understanding the mechanistic basis of non-coding RNA through molecular dynamics simulations**. *Journal of Structural Biology*, v. 206, n. 3, p. 267–279, jun. 2019. Disponível em:

<https://linkinghub.elsevier.com/retrieve/pii/S1047847719300498>. Acesso em: 13 jun. 2019.

PAPASEIT, E. *et al.* **MDMA interactions with pharmaceuticals and drugs of abuse**. *https://doi-org.ez26.periodicos.capes.gov.br/10.1080/17425255.2020.1749262*, v. 16, n. 5, p. 357–369, 3 maio 2020. Disponível em: <https://www-tandfonline.ez26.periodicos.capes.gov.br/doi/abs/10.1080/17425255.2020.1749262>. Acesso em: 16 dez. 2021.

PAVIA, D. L. ET AL. *Introdução à Espectroscopia - Tradução da 5a ed. norte americana by Cengage Brasil - issuu*. [S.l: s.n.], 2015. Disponível em: <https://issuu.com/cengagebrasil/docs/9788522123384_introducao_espectrosc>. Acesso em: 15 out. 2019.

PELED, N. *et al.* **Detection of volatile organic compounds in cattle naturally infected with Mycobacterium bovis**. *Sensors and Actuators B: Chemical*, v. 171–172, p. 588–594, 1 ago. 2012.

PELLECCHIA, M.; SEM, D. S.; WÜTHRICH, K. **NMR in drug discovery**. *Nature Reviews Drug Discovery*, v. 1, n. 13, p. 211–219, 2002.

PENDLEY, B. D.; LINDNER, E. **Medical Sensors for the Diagnosis and Management of Disease: The Physician Perspective**. *ACS Sensors*, v. 2, n. 11, p. 1549–1552, 22 nov. 2017.
PERDEW, J. P. *et al.* **Atoms, molecules, solids, and surfaces: Applications of the generalized gradient approximation for exchange and correlation**. *Physical Review B*, v. 46, n. 11, p. 6671–6687, 15 set. 1992. Disponível em: <https://link.aps.org/doi/10.1103/PhysRevB.46.6671>. Acesso em: 24 jun. 2019.

PEREIRA, B. T. L. L. *et al.* **First attempts of the use of 195Pt NMR of phenylbenzothiazole complexes as spectroscopic technique for the cancer diagnosis**. *Molecules*, v. 24, n. 21, p. 3970, 2 nov. 2019. Disponível em: <https://www.mdpi.com/1420-3049/24/21/3970/htm>. Acesso em: 22 out. 2021.

PERUCCA, P. *et al.* **Structure-activity relationship and role of oxygen in the potential antitumour activity of fluoroquinolones in human epithelial cancer cells**. *Journal of Photochemistry and Photobiology B: Biology*, v. 140, p. 57–68, 1 nov. 2014.

PHIBOONCHAIYANAN, P. P.; KIRATIPAIBOON, C.; CHANVORACHOTE, P. **Ciprofloxacin mediates cancer stem cell phenotypes in lung cancer cells through caveolin-1-dependent mechanism**. *Chemico-Biological Interactions*, v. 250, p. 1–11, 25 abr. 2016. Disponível em: <http://www.ncbi.nlm.nih.gov/pubmed/26947806>. Acesso em: 16 out. 2019.

PILETSKY, S. A. *et al.* **Recognition of ephedrine enantiomers by molecularly imprinted polymers designed using a computational approach**. *The Analyst*, v. 126, n. 10, p. 1826–1830, 9 out. 2001. Disponível em: <http://xlink.rsc.org/?DOI=b102426b>. Acesso em: 5 jul. 2018.

POPLE, J. A. **Nobel Lecture: Quantum chemical models**. *Reviews of Modern Physics*, v.

71, n. 5, p. 1267–1274, 1 out. 1999. Disponível em:
<https://link.aps.org/doi/10.1103/RevModPhys.71.1267>. Acesso em: 1 abr. 2019.

POPLE, J. A. **The theory of chemical shifts in nuclear magnetic resonance I. Induced current densities**. *Proceedings of the Royal Society of London. Series A. Mathematical and Physical Sciences*, v. 239, n. 1219, p. 541–549, 9 abr. 1957.

PRANDI, I. G.; RAMALHO, T. C.; FRANÇA, T. C. C. **Esterase 2 as a fluorescent biosensor for the detection of organophosphorus compounds: docking and electronic insights from molecular dynamics**. *Molecular Simulation*, v. 45, n. 17, p. 1432–1436, 2019.
PROMPHET, N. *et al.* **Non-invasive wearable chemical sensors in real-life applications**. *Analytica Chimica Acta*, v. 1179, p. 338643, 22 set. 2021.

PUDLO, M. *et al.* **Quinolone-benzylpiperidine derivatives as novel acetylcholinesterase inhibitor and antioxidant hybrids for Alzheimer Disease**. *Bioorganic and Medicinal Chemistry*, v. 22, n. 8, p. 2496–2507, 15 abr. 2014.

PUEYO, A. G. ; A. *et al.* **Propagators for the Time-Dependent Kohn−Sham Equations: Multistep, Runge−Kutta, Exponential Runge−Kutta, and Commutator Free Magnus Methods**. 2018. Disponível em: <https://pubs.acs.org/doi/10.1021/acs.jctc.8b00197.>. Acesso em: 1 jul. 2019.

PURCELL, E. M.; TORREY, H. C.; POUND, R. V. *Resonance absorption by nuclear magnetic moments in a solid. Physical Review*. [S.l: s.n.]. , 1946

PYKETT, I. L. *et al.* **Principles of nuclear magnetic resonance imaging.** *Radiology*, v. 143, n. 1, p. 157–168, abr. 1982. Disponível em:
<http://pubs.rsna.org/doi/10.1148/radiology.143.1.7038763>. Acesso em: 15 out. 2019.

QRIOUET, Z. *et al.* **Monoclonal Antibodies Application in Lateral Flow Immunochromatographic Assays for Drugs of Abuse Detection**. *Molecules 2021, Vol. 26, Page 1058*, v. 26, n. 4, p. 1058, 18 fev. 2021. Disponível em: <https://www.mdpi.com/1420-3049/26/4/1058/htm>. Acesso em: 15 dez. 2021.

RAHMAN, M. M. *et al.* **Development of 3-methoxyaniline sensor probe based on thin Ag2O@La2O3 nanosheets for environmental safety**. *New Journal of Chemistry*, v. 43, n. 11, p. 4620–4632, 2019.

RAMALHO, T. C. *et al.* **Computational Enzymology and Organophosphorus Degrading Enzymes: Promising Approaches Toward Remediation Technologies of Warfare Agents and Pesticides.** *Current medicinal chemistry*, v. 23, n. 10, p. 1041–61, 2016. Disponível em: <http://www.ncbi.nlm.nih.gov/pubmed/26898655>. Acesso em: 1 mar. 2018.

RAMALHO, T. C.; TAFT, C. A. **Thermal and solvent effects on the NMR and UV parameters of some bioreductive drugs**. *The Journal of Chemical Physics*, v. 123, n. 5, p. 054319, 9 ago. 2005. Disponível em: <http://aip.scitation.org/doi/10.1063/1.1996577>. Acesso em: 31 jul. 2019.

ROSSI, T. P. *et al.* **Kohn−Sham Decomposition in Real-Time Time-Dependent Density-Functional Theory: An Efficient Tool for Analyzing Plasmonic Excitations**. 2017. Disponível em: <https://pubs.acs.org/doi/10.1021/acs.jctc.7b00589.>. Acesso em: 1 jul. 2019.

RUNGE, E.; GROSS, E. K. U. *PHYSICAL REVIEW LETTERS Density-Functional Theory for Time-Dependent Systems*. . [S.l: s.n.], 1984. Disponível em: <http://karin.fq.uh.cu/~lmc/ref/old/runge84.pdf>. Acesso em: 25 jun. 2019.

RYBCZYNSKA, A. A. *et al.* **Avenues to molecular imaging of dying cells: Focus on cancer**. *Medicinal Research Reviews*, v. 38, n. 6, p. 1713–1768, set. 2018. Disponível em: <http://www.ncbi.nlm.nih.gov/pubmed/29528513>. Acesso em: 9 nov. 2018.

SAICHANAPAN, J. *et al.* **Voltammetric Determination of Tramadol Using a Hierarchical Graphene Oxide Nanoplatelets Modified Electrode**. *Journal of The Electrochemical Society*, v. 168, n. 11, p. 117512, 18 nov. 2021. Disponível em: <https://iopscience-iop.ez26.periodicos.capes.gov.br/article/10.1149/1945-7111/ac3529>. Acesso em: 15 dez. 2021.

SAJINI, T.; THOMAS, R.; MATHEW, B. **Rational design and synthesis of photo-responsive molecularly imprinted polymers for the enantioselective intake and release of l-phenylalanine benzyl ester on multiwalled carbon nanotubes**. *Polymer*, v. 173, p. 127–140, maio 2019. Disponível em: <https://linkinghub.elsevier.com/retrieve/pii/S0032386119303519>. Acesso em: 11 jul. 2019.

SALEEM, H. *et al.* **Design, synthesis, characterization and computational docking studies of novel sulfonamide derivatives**. *EXCLI Journal*, v. 17, p. 169–180, 1 fev. 2018. Disponível em: <https://www.excli.de/index.php/excli/article/view/448>. Acesso em: 4 jun. 2021.

SALES, T. A.; RAMALHO, T. C. **Computational design of synthetic receptors for drug detection: interaction between molecularly imprinted polymers and MDMA (3,4-methylenedioxymethamphetamine)**. *Theoretical Chemistry Accounts*, v. 139, n. 2, 2020.

SANT'ANNA, M. V. S. *et al.* **Selective carbonaceous-based (nano)composite sensors for electrochemical determination of paraquat in food samples**. *Food Chemistry*, v. 373, p. 131521, 30 mar. 2022. Disponível em: <https://linkinghub.elsevier.com/retrieve/pii/S0308814621025279>. Acesso em: 6 dez. 2021.

SANZ-RODRIGO, J.; OLIVIER, Y.; SANCHO-GARCÍA, J. C. **Computational Studies of Molecular Materials for Unconventional Energy Conversion: The Challenge of Light Emission by Thermally Activated Delayed Fluorescence**. *Molecules 2020, Vol. 25, Page 1006*, v. 25, n. 4, p. 1006, 24 fev. 2020. Disponível em: <https://www.mdpi.com/1420-3049/25/4/1006/htm>. Acesso em: 10 dez. 2021.

SATOMURA, T. *et al.* **D-Lactate electrochemical biosensor prepared by immobilization of thermostable dye-linked D-lactate dehydrogenase from Candidatus Caldiarchaeum subterraneum**. *Journal of Bioscience and Bioengineering*, v. 126, n. 4, p. 425–430, 1 out. 2018. Disponível em: <https://pubmed.ncbi.nlm.nih.gov/29691195/>. Acesso em: 25 mar. 2021.

SCHOEFFLER, A. J.; BERGER, J. M. **DNA topoisomerases: harnessing and constraining energy to govern chromosome topology**. *Quarterly Reviews of Biophysics*, v. 41, n. 1, p. 41–101, 29 fev. 2008. Disponível em: <https://www.cambridge.org/core/product/identifier/S003358350800468X/type/journal_article>. Acesso em: 7 out. 2019.

SCIENCE, W. OF. *Core-colection Web of Science reports*. Disponível em: <https://www-webofscience.ez26.periodicos.capes.gov.br/wos/woscc/summary/6746b171-fc30-4a60-9c7d-06b9512e306c/date-descending/1>.

SCOTT, L. G.; HENNIG, M. **[19]F-Site-Specific-Labeled Nucleotides for Nucleic Acid Structural Analysis by NMR**. *Methods in enzymology*, v. 566, p. 59–87, 2016. Disponível em: <https://pubmed.ncbi.nlm.nih.gov/26791976/>. Acesso em: 8 dez. 2021.

SEDAGHAT DOOST, A. *et al. A review on nuclear overhauser enhancement (NOE) and rotating-frame overhauser effect (ROE) NMR techniques in food science: Basic principles and applications. Trends in Food Science and Technology*. [S.l.]: Elsevier Ltd. , 1 abr. 2019.

SERAFÍN, V. *et al.* **Enhanced determination of fertility hormones in saliva at disposable immunosensing platforms using a custom designed field-portable dual potentiostat**. *Sensors and Actuators B: Chemical*, v. 299, p. 126934, 15 nov. 2019.

SERKOVA, N. J.; NIEMANN, C. U. **Pattern recognition and biomarker validation using quantitative [1] H-NMR-based metabolomics**. *Expert Review of Molecular Diagnostics*, v. 6, n. 5, p. 717–731, 9 set. 2006. Disponível em: <http://www.ncbi.nlm.nih.gov/pubmed/17009906>. Acesso em: 11 set. 2018.
SHANINA, E. *et al.* **Protein-observed 19F NMR of LecA from Pseudomonas aeruginosa**. *Glycobiology*, v. 31, n. 2, p. 159–165, 9 fev. 2021. Disponível em: <https://academic-oup-com.ez26.periodicos.capes.gov.br/glycob/article/31/2/159/5861409>. Acesso em: 27 dez. 2021.

SHEPHERD, M. A. *et al.* **Evaluation of refractive index for measuring urinary nitrogen concentration in a sensor worn by grazing female cattle**. *http://dx-doi.ez26.periodicos.capes.gov.br/10.1080/00288233.2016.1237979*, v. 60, n. 1, p. 23–31, 2 jan. 2016. Disponível em: <https://www-tandfonline.ez26.periodicos.capes.gov.br/doi/abs/10.1080/00288233.2016.1237979>. Acesso em: 17 dez. 2021.

SHI, W.; MA, H. **Spectroscopic probes with changeable π-conjugated systems**. *Chemical Communications*, v. 48, n. 70, p. 8732, 6 ago. 2012. Disponível em: <http://xlink.rsc.org/?DOI=c2cc33366j>. Acesso em: 20 ago. 2019.

SILAMBARASAN, P.; MOON, I. S. **Enhancing the mediated electrochemical reduction process combined with developed liquid-gas electrochemical flow sensors for sustainable N2O removal at room temperature**. *Environmental Research*, v. 204, p. 111912, 1 mar. 2022.

SILVA, A. T. M. DA *et al.* **Bioanalytical methods for determining ecstasy components in biological matrices: A review**. *TrAC Trends in Analytical Chemistry*, v. 108, p. 323–346, 1 nov. 2018. Disponível em: <https://linkinghub.elsevier.com/retrieve/pii/S0165993618302917>. Acesso em: 22 nov. 2018.

SILVA, M. G. *et al.* **An impedance spectroscopy method for the detection and evaluation of Babesia bovis antibodies in cattle**. *Sensors and Actuators B: Chemical*, v. 135, n. 1, p. 206–213, 10 dez. 2008.

SILVERSTEIN, R. M.; WEBSTER, F. X.; KIEMBLE, D. J. *Spectrometric identification of organic compunds*. . [S.l.]: John Wiley and Sons Inc. , 2005.

SIMÕES, F. R.; XAVIER, M. G. **Electrochemical Sensors**. *Nanoscience and its Applications*, p. 155–178, 1 jan. 2017.

SIMON, E. *Biological and chemical sensors for cancer diagnosis. Measurement Science and Technology*. [S.l.]: Institute of Physics Publishing. , 2010.

SOEIRO, T. *et al.* **Early Detection of Prescription Drug Abuse Using Doctor Shopping Monitoring From Claims Databases: Illustration From the Experience of the French Addictovigilance Network**. *Frontiers in Psychiatry*, v. 12, p. 552, 17 maio 2021.

SOLOVYEV, A. I. *et al.* **Photochemistry of dithiophosphinate Ni(S2P(i-Bu)2)2 complex in CCl4. Transient species and TD-DFT calculations**. *Journal of Photochemistry and Photobiology A: Chemistry*, v. 381, p. 111857, 1 ago. 2019. Disponível em: <https://www.sciencedirect.com/science/article/pii/S1010603018317866>. Acesso em: 31 jul. 2019.

SONG, M. *et al.* **Antibiotic drug levofloxacin inhibits proliferation and induces apoptosis of lung cancer cells through inducing mitochondrial dysfunction and oxidative damage**. *Biomedicine & Pharmacotherapy*, v. 84, p. 1137–1143, dez. 2016. Disponível em: <https://linkinghub.elsevier.com/retrieve/pii/S0753332216310745>. Acesso em: 16 out. 2019.

SPEYER, C. B.; BALEJA, J. D. **Use of nuclear magnetic resonance spectroscopy in diagnosis of inborn errors of metabolism**. *Emerging Topics in Life Sciences*, v. 5, n. 1, p. 39–48, 14 maio 2021. Disponível em: </emergtoplifesci/article/5/1/39/227734/Use-of-nuclear-magnetic-resonance-spectroscopy-in>. Acesso em: 8 dez. 2021.

STANLEY, P. D. **Principles and Topical Applications of 19F NMR Spectrometry**. *Organofluorines*, p. 1–61, 14 mar. 2002. Disponível em: <https://link.springer.com/chapter/10.1007/10721878_1>. Acesso em: 22 out. 2021.

STOKES, G. G. **XXX. On the change of refrangibility of light**. *Philosophical Transactions of the Royal Society of London*, v. 142, p. 463–562, 31 jan. 1852. Disponível em: <http://www.royalsocietypublishing.org/doi/10.1098/rstl.1852.0022>. Acesso em: 1 ago. 2019.

SUAIFAN, G. A. R. Y.; MOHAMMED, A. A. M. *Fluoroquinolones structural and medicinal developments (2013–2018): Where are we now? Bioorganic and Medicinal Chemistry*. [S.l.]: Elsevier Ltd. , 2019.

SUKPATTANACHAROEN, C.; SALAEH, R.; PROMARAK, V. ; ESCUDERO, D.; KUNGWAN, N. **Heteroatom substitution effect on electronic structures, photophysical properties, and excited-state intramolecular proton transfer processes of 3-hydroxyflavone and its analogues: A TD-DFT study**. *Journal of Molecular Structure*, v. 1195, p. 280–292, 5 nov. 2019. Disponível em: <https://www-sciencedirect.ez26.periodicos.capes.gov.br/science/article/pii/S0022286019306854?via%3Dihub>. Acesso em: 31 jul. 2019.

SURESH, N. *et al.* **Anti-proliferative activity, molecular modeling studies and interaction with calf thymus DNA of novel ciprofloxacin analogues**. *Journal of Chemical Sciences*, v. 130, n. 9, p. 1–11, 1 set. 2018. Disponível em: <https://link.springer.com/article/10.1007/s12039-018-1528-y>. Acesso em: 8 fev. 2021.

SURYANA, S. *et al.* **An Update on Molecularly Imprinted Polymer Design through a Computational Approach to Produce Molecular Recognition Material with Enhanced Analytical Performance**. *Molecules 2021, Vol. 26, Page 1891*, v. 26, n. 7, p. 1891, 26 mar. 2021. Disponível em: <https://www.mdpi.com/1420-3049/26/7/1891/htm>. Acesso em: 9 dez. 2021.

SUZANNE CLANCY & KENNA M. SHAW. **DNA Deletion and Duplication and the Associated Genetic Disorders** . *Nature Education*, v. 1, n. 23, 2008. Disponível em: <https://www.nature.com/scitable/topicpage/dna-deletion-and-duplication-and-the-associated-331/>. Acesso em: 27 dez. 2021.

SWAGER, T. M. **Sensor Technologies Empowered by Materials and Molecular Innovations**. *Angewandte Chemie International Edition*, v. 57, n. 16, p. 4248–4257, 9 abr. 2018. Disponível em: <http://doi.wiley.com/10.1002/anie.201711611>. Acesso em: 11 dez. 2018.

TANG, Z.-Y. *et al.* **The first small fluorescent probe as Tyrosyl-DNA phosphodiesterase 1 (TDP1) substrate**. *Dyes and Pigments*, v. 169, p. 45–50, 1 out. 2019. Disponível em: <https://www.sciencedirect.com/science/article/pii/S0143720819304942>. Acesso em: 2 out. 2019.

TAVAKOLIAN-ARDAKANI, Z. *et al.* **Latest Trends in Electrochemical Sensors for Neurotransmitters: A Review**. *Sensors 2019, Vol. 19, Page 2037*, v. 19, n. 9, p. 2037, 30 abr. 2019. Disponível em: <https://www.mdpi.com/1424-8220/19/9/2037/htm>. Acesso em: 9 dez. 2021.

TELPOUKHOVSKAIA, M. A. *et al.* **3-Hydroxy-4-pyridinone derivatives designed for fluorescence studies to determine interaction with amyloid protein as well as cell permeability**. *Bioorganic & Medicinal Chemistry Letters*, v. 25, n. 17, p. 3654–3657, 1 set. 2015. Disponível em: <http://www.ncbi.nlm.nih.gov/pubmed/26141772>. Acesso em: 21 jan. 2019.

THUN, M. J. *et al.* **The global burden of cancer: priorities for prevention**. *Carcinogenesis*, v. 31, n. 1, p. 100–110, 1 jan. 2010. Disponível em: <http://www.ncbi.nlm.nih.gov/pubmed/19934210>. Acesso em: 7 nov. 2018.

TIKUM, A. F. *et al.* **Rhodamine-based near-infrared probe for emission detection of ATP in lysosomes in living cells**. *Sensors and Actuators B: Chemical*, v. 292, p. 40–47, 1 ago. 2019. Disponível em: <https://www.sciencedirect.com/science/article/pii/S0925400519306458>. Acesso em: 2 out. 2019.

TROESTER, M. A. *et al.* **DNA defects, epigenetics, and gene expression in cancer-adjacent breast: a study from The Cancer Genome Atlas**. *NPJ breast cancer*, v. 2, n. 1, 14 dez. 2016. Disponível em: <https://pubmed.ncbi.nlm.nih.gov/28721375/>. Acesso em: 27 dez. 2021.

TSAI-PFLUGFELDER, M. *et al.* **Cloning and sequencing of cDNA encoding human DNA topoisomerase II and localization of the gene to chromosome region 17q21-22.** *Proceedings of the National Academy of Sciences of the United States of America*, v. 85, n. 19, p. 7177–81, 1 out. 1988. Disponível em: <http://www.ncbi.nlm.nih.gov/pubmed/2845399>. Acesso em: 10 out. 2019.

TSE, J. S. **A <scp>B</scp> I <scp>NITIO</scp> M <scp>OLECULAR</scp> D <scp>YNAMICS WITH</scp> D <scp>ENSITY</scp> F <scp>UNCTIONAL</scp> T <scp>HEORY</scp>**. *Annual Review of Physical Chemistry*, v. 53, n. 1, p. 249–290, 2002. Disponível em: <http://www.annualreviews.org/doi/10.1146/annurev.physchem.53.090401.105737>.

TU, Y.-X. *et al.* **Specific two-photon fluorescent probe for cysteine detection in vivo**. *Spectrochimica Acta Part A: Molecular and Biomolecular Spectroscopy*, v. 267, p. 120521, 15 fev. 2022.

TURKSEN, K. *et al.* **Interleukin 6: insights to its function in skin by overexpression in transgenic mice.** v. 89, n. 11, 1 jun. 1992. Disponível em: <http://www.ncbi.nlm.nih.gov/pubmed/1375756>. Acesso em: 10 out. 2019.

TUTEJA, S. K.; NEETHIRAJAN, S. **Exploration of two-dimensional bio-functionalized phosphorene nanosheets (black phosphorous) for label free haptoglobin electro-immunosensing applications**. *Nanotechnology*, v. 29, n. 13, 14 fev. 2018.

ULLRICH, C. A.; GOSSMANN, U. J.; GROSS, E. K. U. **Time-Dependent Optimized Effective Potential**. *Physical Review Letters*, v. 74, n. 6, p. 872–875, 6 fev. 1995. Disponível em: <https://link.aps.org/doi/10.1103/PhysRevLett.74.872>. Acesso em: 1 jul. 2019.

UNODC, U. NA. O. ON D. AND C. DRUG MARKET TRENDS: CANNABIS OPIOIDS. *World Drug Report 2021*. 21. ed. [S.l: s.n.], 2021. p. 1–121. Disponível em: <www.unodc.org/unodc/en/data-and-analysis/wdr2021.html>. Acesso em: 15 dez. 2021.

VALEUR, B.; ARIO, M.; BERBERAN-SANTOS, N. **A Brief History of Fluorescence and**

Phosphorescence before the Emergence of Quantum Theory. *J. Chem. Educ*, v. 88, p. 731–738, 2011. Disponível em: <https://pubs.acs.org/sharingguidelines>. Acesso em: 10 jun. 2021.

VAN BAY, M. *et al.* **Using calculations of the electronically excited states for investigation of fluorescent sensors: A review**. *Vietnam Journal of Chemistry*, v. 57, n. 4, p. 389–400, 1 ago. 2019. Disponível em: <https://onlinelibrary-wiley.ez26.periodicos.capes.gov.br/doi/full/10.1002/vjch.201900089>. Acesso em: 3 jun. 2021.

VANCE-BRYAN, K.; GUAY, D. R. P.; ROTSCHAFER, J. C. **Clinical Pharmacokinetics of Ciprofloxacin**. *Clinical Pharmacokinetics*, v. 19, n. 6, p. 434–461, 1990.

VEEMAN, W. S. **Nuclear magnetic resonance, a simple introduction to the principles and applications**. *Geoderma*, v. 80, n. 3–4, p. 225–242, nov. 1997.

VERLET, L. **Computer "Experiments" on Classical Fluids. I. Thermodynamical Properties of Lennard-Jones Molecules**. *Physical Review*, v. 159, n. 1, p. 98–103, 5 jul. 1967. Disponível em: <https://link.aps.org/doi/10.1103/PhysRev.159.98>. Acesso em: 13 jun. 2019.

VIVEIROS, R. *et al.* **Green Strategies for Molecularly Imprinted Polymer Development**. *Polymers*, v. 10, n. 3, p. 306, 12 mar. 2018. Disponível em: <http://www.mdpi.com/2073-4360/10/3/306>. Acesso em: 18 set. 2018.

WANG, C. *et al.* **A review and outlook of ratiometric optical thermometer based on thermally coupled levels and non-thermally coupled levels**. *Journal of Alloys and Compounds*, v. 894, p. 162494, 15 fev. 2022. Disponível em: <https://linkinghub.elsevier.com/retrieve/pii/S0925838821039049>. Acesso em: 6 dez. 2021.

WANG, H. *et al.* **Active Probes for Imaging Membrane Dynamics of Live Cells with High Spatial and Temporal Resolution over Extended Time Scales and Areas**. *Journal of the American Chemical Society*, v. 140, n. 10, p. 3505–3509, 14 mar. 2018. Disponível em: <https://pubs.acs.org/doi/10.1021/jacs.7b13307>. Acesso em: 3 out. 2019.

WANG, H.; FAPOJUWO, A. O.; DAVIES, R. J. **A wireless sensor network for feedlot animal health monitoring**. *IEEE Sensors Journal*, v. 16, n. 16, p. 6433–6446, 1 ago. 2016.

WANG, J. *et al.* **Multicolor Cocktail for Breast Cancer Multiplex Phenotype Targeting and Diagnosis Using Bioorthogonal Surface-Enhanced Raman Scattering Nanoprobes**. *Analytical Chemistry*, v. 91, n. 17, p. 11045–11054, 3 set. 2019. Disponível em: <https://pubs.acs.org/doi/10.1021/acs.analchem.9b01382>. Acesso em: 8 out. 2019.

WANG, J. C. **Interaction between DNA and an Escherichia coli protein ω**. *Journal of Molecular Biology*, v. 55, n. 3, p. 523-IN16, 14 fev. 1971. Disponível em: <https://www.sciencedirect.com/science/article/pii/0022283671903342>. Acesso em: 7 out. 2019.

WANG, N. *et al.* **Diketopyrrolopyrrole-based sensor for over-expressed peroxynitrite in drug-induced hepatotoxicity via ratiometric fluorescence imaging**. *Sensors and Actuators B: Chemical*, v. 352, p. 130992, 1 fev. 2022. Disponível em: <https://linkinghub.elsevier.com/retrieve/pii/S0925400521015604>. Acesso em: 6 dez. 2021.

WENDORFF, T. J. *et al.* **The Structure of DNA-Bound Human Topoisomerase II Alpha: Conformational Mechanisms for Coordinating Inter-Subunit Interactions with DNA Cleavage**. *Journal of Molecular Biology*, v. 424, n. 3–4, p. 109–124, 7 dez. 2012. Disponível em: <http://www.ncbi.nlm.nih.gov/pubmed/22841979>. Acesso em: 10 out. 2019.

WILLIAM L. JORGENSEN, *; DAVID S. MAXWELL, AND; TIRADO-RIVES, J. **Development and Testing of the OPLS All-Atom Force Field on Conformational Energetics and Properties of Organic Liquids**. 1996. Disponível em: <https://pubs.acs.org/doi/10.1021/ja9621760>. Acesso em: 13 jun. 2019.

WOPPERER, P.; DE GIOVANNINI, U.; RUBIO, A. **Efficient and accurate modeling of electron photoemission in nanostructures with TDDFT**. *The European Physical Journal B*, v. 90, n. 3, p. 51, 22 mar. 2017. Disponível em: <http://link.springer.com/10.1140/epjb/e2017-70548-3>. Acesso em: 1 jul. 2019.

WU, X. *et al.* **Molecular dynamics simulations of BSA absorptions on pure and formate-contaminated rutile (1 1 0) surface**. *Applied Surface Science*, v. 533, p. 147574, 15 dez. 2020.

WÜTHRICH, K. *NMR in Structural Biology*. [S.l.]: WORLD SCIENTIFIC, 1995. v. 5. Disponível em: <https://www.worldscientific.com/worldscibooks/10.1142/2732>. Acesso em: 15 out. 2019. (World Scientific Series in 20th Century Chemistry).
WÜTHRICH, K. NMR studies of structure and function of biological macromolecules (Nobel Lecture). 28 jul. 2003, [S.l: s.n.], 28 jul. 2003. p. 3340–3363.

XIA, Y.; ZHAO, F.; ZENG, B. **A molecularly imprinted copolymer based electrochemical sensor for the highly sensitive detection of L-Tryptophan**. *Talanta*, v. 206, p. 120245, 1 jan. 2020.

XIANG, H. *et al.* **A novel hydrazone-based fluorescent "off-on-off" probe for relay sensing of Ga3+ and PPi ions**. *Spectrochimica Acta Part A: Molecular and Biomolecular Spectroscopy*, v. 267, p. 120510, 15 fev. 2022.

XIAO, Y. *et al.* **Abeta(1-42) fibril structure illuminates self-recognition and replication of amyloid in Alzheimer's disease**. *Nature structural & molecular biology*, v. 22, n. 6, p. 499–505, jun. 2015.

XU, C. *et al.* **In Vivo Electrochemical Sensors for Neurochemicals: Recent Update**. 2019. Disponível em: <https://pubs.acs.org/sharingguidelines>. Acesso em: 9 dez. 2021.

XU, Z. *et al.* **A conducting polymer PEDOT:PSS hydrogel based wearable sensor for accurate uric acid detection in human sweat**. *Sensors and Actuators B: Chemical*, v. 348, p. 130674, 1 dez. 2021.

XUE, S. *et al.* **In Situ Spectroscopic Probes for Structures and Processes at the Surface of Noble Metallic Nanoparticles**. *Particle & Particle Systems Characterization*, v. 38, n. 5, p. 2000316, 1 maio 2021. Disponível em: <https://onlinelibrary-wiley.ez26.periodicos.capes.gov.br/doi/full/10.1002/ppsc.202000316>. Acesso em: 8 dez. 2021.

YADAV, V. *et al.* **Moxifloxacin and ciprofloxacin induces S-phase arrest and augments apoptotic effects of cisplatin in human pancreatic cancer cells via ERK activation**. *BMC Cancer*, v. 15, n. 1, p. 581, 11 dez. 2015. Disponível em: <http://bmccancer.biomedcentral.com/articles/10.1186/s12885-015-1560-y>. Acesso em: 16 out. 2019.

YAN, C. *et al.* **Facile design of multifunction-integrated linear oligonucleotide probe with multiplex amplification effect for label-free and highly sensitive GMO biosensing**. *Talanta*, v. 236, p. 122821, 1 jan. 2022.

YANG, B. *et al.* **Progress of Mimetic Enzymes and Their Applications in Chemical Sensors**. *Critical Reviews in Analytical Chemistry*, v. 46, n. 6, p. 469–481, 23 nov. 2016. Disponível em: <https://www.tandfonline.com/doi/full/10.1080/10408347.2016.1151767>. Acesso em: 11 dez. 2018.

YANG, Y. *et al.* **A Highly Selective Low-Background Fluorescent Imaging Agent for Nitric Oxide**. *Journal of the American Chemical Society*, v. 132, n. 38, p. 13114–13116, 29 set. 2010. Disponível em: <https://pubs.acs.org/doi/10.1021/ja1040013>. Acesso em: 2 out. 2019.

YANG, Y.; SUN, A.; ESLAMI, M. **A density functional theory study on detection of amphetamine drug by silicon carbide nanotubes**. *Physica E: Low-dimensional Systems and Nanostructures*, v. 125, p. 114411, 1 jan. 2021.

YI, J.; NAKATANI, N.; NOMURA, K. **Solution XANES and EXAFS analysis of active species of titanium, vanadium complex catalysts in ethylene polymerisation/dimerisation and syndiospecific styrene polymerisation**. *Dalton Transactions*, v. 49, n. 24, p. 8008–8028, 23 jun. 2020. Disponível em: <https://pubs-rsc-org.ez26.periodicos.capes.gov.br/en/content/articlehtml/2020/dt/d0dt01139h>. Acesso em: 10 dez. 2021.

YIMENU, D. K. *et al.* **Assessment of Antibiotic Prescribing Patterns at Outpatient Pharmacy Using World Health Organization Prescribing Indicators**. *Journal of Primary Care and Community Health*, v. 10, 2019. Disponível em: </pmc/articles/PMC6836303/>. Acesso em: 7 jun. 2021.

YU, J. X. *et al.* **New Frontiers and Developing Applications in 19F NMR**. *Progress in nuclear magnetic resonance spectroscopy*, v. 70, p. 25, 2013. Disponível em: </pmc/articles/PMC3613763/>. Acesso em: 8 dez. 2021.

YU, Q. *et al.* **Developments of spectroscopic biosensors for cholinesterase and its**

inhibitors in the last decade: an overview. *https://doi-org.ez26.periodicos.capes.gov.br/10.1080/05704928.2021.1990080*, 2021. Disponível em: <https://www-tandfonline.ez26.periodicos.capes.gov.br/doi/abs/10.1080/05704928.2021.1990080>. Acesso em: 8 dez. 2021.

YURISH, S. Advances in Sensors: Reviews, Vol.4. In: YURISH, S. Y. (Org.). . *Sensors and Applications in Measuring and Automation Control Systems*. Vol 4 ed. [S.l.]: International Frequency Sensor Association (IFSA), 2017. v. 4. p. 504.

ZHANG, C.; PAN, G.; HE, Y. **Conjugated microporous organic polymer as fluorescent chemosensor for detection of Fe3+ and Fe2+ ions with high selectivity and sensitivity**. *Talanta*, v. 236, p. 122872, 1 jan. 2022.

ZHANG, G. *et al.* **Precise detection of prostate specific antigen in serum: A surface molecular imprinted sensor based on novel cooperated signal amplification strategy**. *Sensors and Actuators, B: Chemical*, v. 302, p. 1269982, 1 jan. 2020. Disponível em: <https://www.sciencedirect.com/science/article/pii/S0925400519311979>. Acesso em: 11 dez. 2019.

ZHANG, G. F. *et al. Ciprofloxacin derivatives and their antibacterial activities*. *European Journal of Medicinal Chemistry*. [S.l.]: Elsevier Masson SAS. , 25 fev. 2018.

ZHANG, K. *et al.* **Advances on Quasi-classical Molecular Dynamics of Organic Reaction Mechanisms**. *Chinese Journal of Organic Chemistry*, v. 41, n. 10, p. 3995, 25 out. 2021. Disponível em: <http://sioc-journal.cn/Jwk_yjhx/EN/10.6023/cjoc202102036>. Acesso em: 10 dez. 2021.

ZHANG, R. *et al.* **Highly sensitive electrochemical sensor based on Pt nanoparticles/carbon nanohorns for simultaneous determination of morphine and MDMA in biological samples**. *Electrochimica Acta*, v. 370, p. 137803, 20 fev. 2021.

ZHAO, J.; DJURABEKOVA, F. **Computational modeling of nanoparticles in inert environment**. *Frontiers of Nanoscience*, v. 17, p. 5–26, 1 jan. 2020.

ZHAO, Y.; MARKOPOULOS, G.; SWAGER, T. M. **19 F NMR Fingerprints: Identification of Neutral Organic Compounds in a Molecular Container**. *Journal of the American Chemical Society*, v. 136, n. 30, p. 10683–10690, 30 jul. 2014. Disponível em: <https://pubs.acs.org/doi/10.1021/ja504110f>. Acesso em: 16 out. 2019.

ZHEN, S. *et al.* **Drug delivery micelles with efficient near-infrared photosensitizer for combined image-guided photodynamic therapy and chemotherapy of drug-resistant cancer**. *Biomaterials*, v. 218, p. 119330, out. 2019. Disponível em: <http://www.ncbi.nlm.nih.gov/pubmed/31301577>. Acesso em: 8 out. 2019.

ZHENG, T. *et al.* **A portable, battery-powered photoelectrochemical aptasesor for field environment monitoring of E. coli O157:H7**. *Sensors and Actuators B: Chemical*, v. 346, p. 130520, 1 nov. 2021.

ZHOU, D.-C. *et al.* **Design, synthesis and biological evaluation of novel perimidine o-quinone derivatives as non-intercalative topoisomerase II catalytic inhibitors**. *Bioorganic Chemistry*, v. 91, p. 103131, 1 out. 2019. Disponível em: <https://www.sciencedirect.com/science/article/pii/S0045206819307308>. Acesso em: 10 out. 2019.

ZHOU, J.; MA, H. **Design principles of spectroscopic probes for biological applications**. *Chemical Science*, v. 7, n. 10, p. 6309–6315, 19 set. 2016. Disponível em: <https://pubs-rsc-org.ez26.periodicos.capes.gov.br/en/content/articlehtml/2016/sc/c6sc02500e>. Acesso em: 30 set. 2019.

PART III: ARTICLES

1. DRUG OF ABUSE DETECTION

1.1. Computational design of synthetic receptors for drug detection: interaction between molecularly imprinted polymers and MDMA (3,4-methylenedioxymethamphetamine)

Abstract:

For many decades, synthetic receptors have been used as sensor elements, and are a promising alternative to natural receptors, which despite its great selectivity, are so complex and instable. The rational design of this kind of receptors is currently one of the most researched topics in molecular recognition. Molecular imprinted polymers (MIPs) have become a growing highlight in polymer chemistry, once they possess a wide range of applications and can be used in several environments, due to their high chemical and thermal stability. The aim of this study was to perform a rational design for the Molecularly Imprinted Polymer (MIP) preparation, for 3,4-methylenedioxymethamphetamine (MDMA) detection. The theoretical measurements were employed at several stages of the process, using DFT, and B3LYP/6-31G(d,p) level of theory, by means of optimization and frequency calculations. Among the several functional monomers tested, the itaconic acid was the most appropriated for MIP preparation with MDMA template, and the proper molar ratio found theoretically was 3:1 (itaconic acid: MDMA). In the preparation of pre-polymerization complex, polar solvents were found to perform a better stabilization, mainly those which are not protic solvents. As cross-linking agents, the better results were obtained for trimethylolpropane trimethacrylate (TRIM) and ethylene glycol dimethacrylate (EGDMA) molecules, respectively. Finally, selectivity tests showed a high affinity of the studied MIP for MDMA and chemically similar molecules. The proposal theoretical strategy yielded novel, experimentally testable hypotheses for the design of MIPs. Additionally, from the theoretical point of view, the set of computational analyzes

presented in this paper constitutes a very useful protocol to predict optimal experimental conditions, which can considerably reduce the time and cost on the MIPs preparation.

Keywords: DFT, theoretical calculations, rational design, artificial receptors.

Introduction

Despite the many problems caused by psychoactive substances, those compounds are excessively and intentionally consumed around the world. It is estimated that more than 338 million people worldwide used drugs at least once in 2017. Of the drugs, 6.28% are ecstasy [1]. The content of ecstasy tablets has been changing over the years, but its main composition is MDMA (3,4-methylenedioxymethamphetamine). MDMA is a synthetic drug with potential to generate chemical dependence, and is commonly consumed as 1:1 racemate of (R) and (S) enantiomer, the (S)-enantiomer being more efficient in producing euphoria, sociability enhancement, increased mood, auditory and/or visual perceptions and energy boosting, due its stimulant effect on the central nervous system [2, 3]. Despite these desirable effects, MDMA also can be an contributor to neurotoxicity in humans, and can induce severe acute toxic symptoms, such as hepatotoxicity, tachycardia, hyperthermia, and even fatal intoxications [4]. The risk of adverse effects depends on a range of factors, such as frequency and amount of use, or administration route. Apart from those mental and physical health issues, there are still losses related to dependence or social problems [5].

From a public health perspective, the control of these substances is of great importance. Considering that point, many detection methods have been developed over the last 20 years aiming to analyze a small amount of this illicit drug [2, 6–14]. The development of chemical sensors based on polymers-biomimics, which are synthetic mimics of enzymes or antibodies, is one of the most effective approaches to small molecules detection, as they possess high selectivity and stability, when compared to biosensors based on natural molecules [11, 15–17]. Molecularly imprinted polymers (MIPs), prepared by polymerization methodology [18], are a novel class of high selectivity polymeric materials, which are synthesized in the presence of the target molecule, together with a functional monomer and cross-linking agent [19, 20]. The

presence of a template molecule during the synthesis allows the formation of specific cavities for the analyte, or molecules with high structural similarity [21–23]. Besides the spatial selectivity, there are also intermolecular interactions between template and the functional monomers that contribute to high selectivity of the material. After synthesis, template molecules are removed, and the resulting three-dimensional structure remains with the specific recognition sites, with chemical and steric hindrance selectivity to the analyte molecule [20, 24]. It is indicated that the monomer and template are joined only by non-covalent interactions, in order to facilitate the removal of the template from the cavity at the wash step [25].

As can be seen, the preparation of MIP is an easy, fast and efficient procedure for detecting molecules of interest [26]. However, gaining all important information prior to material synthesis, such as the best functional monomer, proper molar ratio, most suitable cross-linking agents, among others, is of utmost importance, but it is a time-consuming process [27]. In this context, computational methods have been largely used, and have enabled a faster and better rational design protocol for the preparation of high affinity MIPs [18, 22, 28–32]. The insightful microscopic rationalization for the design of molecularly imprinted polymers can demonstrate the power of joint experimental−computational strategies applied to technological problems [33–41]. By means of theoretical investigations, it is possible to not only obtain all of this information, but to also investigate what happens in the system at the molecular level, which can help save time in the process, in addition to making improvements in the materials already synthesized [25]. Thus, the goal of the present study was to perform a rational design for the preparation of an MIP for MDMA detection, gathering a set of alternatives of how the computational resources can be useful in the rational design in diverse stages of the MIP development and use process.
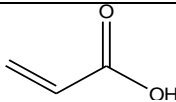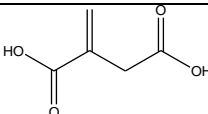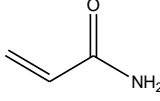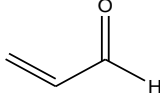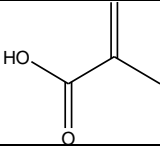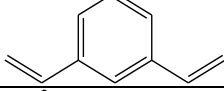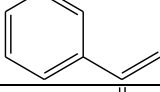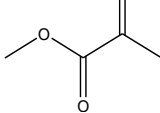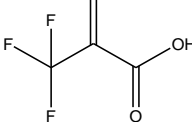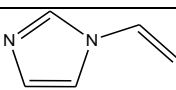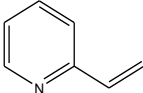
Methodology

- Selection of the most appropriate functional monomer

Density Functional Theory (DFT) method was employed in order to analyze the different types of information that can be obtained through the computational design of MIPs and to explore the many computational resources that can be employed for better understanding of the system at a molecular level. All of the calculations were performed

using B3LYP/6-31G(d,p)[18, 42, 43] level of theory, using Gaussian 09[44] software. Aiming to predict the possible interaction sites of the monomers (see Table 1) and the template molecule (MDMA) (Figure 1), the molecular electrostatic potentials (MEPs) of the molecules were created and analyzed. To investigate the most appropriate functional monomer for MIP design, all functional monomers presented in Table1 were tested. The systems were built at 1:1, 1:2 and 1:3 (template:monomer) molar ratios. After that, geometry optimization calculations were performed for the computation of interaction energy values (ΔE) of each system, employing the equation (1)[17].

Table 1 Functional monomers used for computational simulations

Name	Abbreviation	Structure
Acrylic acid	AA	
Itaconic acid	IA	
Acrylamide	ACL	
Acrolein	ACRO	
Metacrylic acid	MA	
Divinylbenzene	DVB	
Styrene	ST	
Methyl methacrylate	MMA	
Trifluoro methacrylate	TFMA	
Vinylimidazole	VI	

Vinylpiridine	VP	

$$\Delta E = E_C - [\Sigma E_M + E_T] \qquad \text{(Equation 1)}$$

Where E_c, E_M and E_T are the lowest theoretical interaction energies of the monomer-template complex, monomer and template, respectively.

Vibrational frequency calculations of the template: monomer complexes were performed at the same level of theory, and the theoretical Infra-Red spectra were subsequently analyzed, in order to investigate the nature of molecular interactions that occur among the involved molecules, by analyzing the change in the vibrational spectrum profile [45].

-Simulations in solvents

Experimentally, MIP for the MDMA detection has already been prepared using chloroform [18] and acetonitrile [46] as solvents. In spite of its great importance, to our knowledge, this is surprisingly the first application of theoretical methods for investigating this type of synthesis. Thus, using the best complex obtained in the previous steps, optimization calculations were performed in implicit solvent environment to analyze the system behavior and investigate which solvent is the most suitable for the construction of the pre-polymerization complex. To this end, considering their polarity, six solvents most commonly used for the preparation of MIPs, such as DMSO, water, methanol, chloroform, acetone and acetonitrile [47] were implicitly tested employing the integral equation formalism polarizable continuum model (IEFPCM) [48].
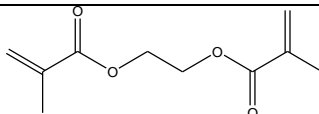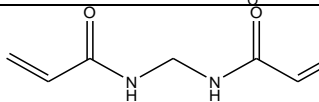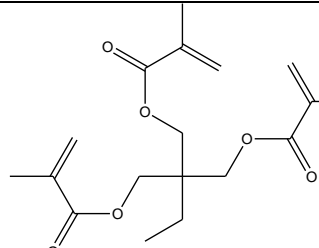
-Selection of proper cross-linking agent

The main function of the crosslinking agent in the entire molecular imprinting process is to copolymerize with the functional monomer to fix the three-dimensional structure of the monomer-model complex in space. An effective imprinting process is one in which functional residues are uniformly distributed across all cross-linked networks. In the pre-polymerization and copolymerization step, the crosslinking agent can form interference complexes with both the functional monomer and the template via

hydrogen bonding or electrostatic interactions, which are difficult to observe experimentally. Therefore, computational chemistry can be an ally to optimize the process and avoid undesirable factors [47].

Thus, the next step was the analysis of the proper cross-linking agent. For this goal, the three most experimentally used cross linking agents N,N-methylene bisacrylamide (NNMB)[49–51], trimethylolpropane trimethacrylate (TRIM) [52–54], and ethylene glycol dimethacrylate (EGDMA) [26, 55–59] were chosen. It should be kept in mind that EGDMA is the most commonly employed. However, cross-linking agents that possess more vinyl groups, such as trimethacrylate (TRIM), can generate a better resolution and selectivity to the studied polymer [47]. The three cross-linking agents were tested under the same conditions as the monomer simulations. The chemical structures of the three cross-linking agents are displayed in Table 2.

Table 2 Cross-linking agents used for computational simulations

Name	Abbreviation	Structure
Ethylene glycol dimethacrylate	EGDMA	
N,N-methylene bisacrylamide	NNMB	
Trimethylolpropane trimethacrylate	TRIM	

-Selectivity tests

The last step is to analyze, theoretically, the selectivity of the material. For this end, the three IA interacting monomers were kept frozen in the optimized position for the MDMA complex, in an attempt to simulate the solid cavity constructed for the specific template. For selectivity tests, eleven molecules with varying structural similarity to the MDMA were introduced in its cavity. The tested molecules were 3,4-methylenedioxyamphetamine (MDA), 3,4-metilendioxietilamfetamina (MDEA), amphetamine (AP), mescaline (MC), methamphetamine (MA), 3,4-methylenedioxy-N-

methylcathinone (MDMC), 2-(1H-Indol-3-yl)-N,N-dimethylethan-1-amine (DMT), 2,5-dimethoxy-4-methylphenethylamine (2C-D), 2,5-dimethoxy-4-methylthioamphetamine (ALEPH), 4-Bromo- 2,5 dimethoxyphenethylamine (2C-B) and 2,5-Dimethoxy-4-ethoxyamphetamine (MEM), whose structures are shown in Figure 1. The energy of each system was calculated by the same level of theory and with the equation (1) [60]. For better visualization of the difference between the energies, the relative interaction energy was calculated by equation (2), for each system, taking MDMA complex as the reference.

$$\Delta E_{rel} = \Delta E_{system} - \Delta E_{MDMA} \qquad \text{Equation (2)}$$

Where ΔE_{system} is the interaction energy for each system built, and ΔE_{MDMA} is the interaction energy of the system with MDMA as template.

Results

- Forecast of the Active Sites for the Template and Function Monomers

In order to predict the nature of the attractive forces, as well as the electrophilic and nucleophilic character of the template and monomer reactive sites, the MEP of each monomer and of the template were analyzed. MEP maps are very useful tools to determine the ability of molecule to, based on the local charge density. The results are shown in Figure 2. For the MDMA molecule, there is a concentration of negative charge in the two Oxygen atoms of the molecule, which can act as acceptors in two hydrogen bonds. Based on this information, it can be inferred that molar ratio 1:2 (template:monomer) is possibly more stable than the 1:1 molar ratio. Moreover, the Nitrogen atom can also act as acceptor or donor in one more hydrogen bond, which indicates that 1:3 molar ratio can be more stable than 1:2. In addition, the molecule also has an aromatic ring with a small concentration of electronic density, and can perform interactions with π bonds of the monomers. Based on these observations, the monomers AA, IA, ACL, MAA, TFMA may be the most appropriate, since they have positive hydrogen that can perform hydrogen bonds with the MDMA molecule, acting as proton donors, which indicates that these monomers possibly will form the most stable complexes for MDMA MIP design. Of these, itaconic acid was the monomer with most

positive hydrogen, so it can be inferred that this molecule will perform stronger hydrogen bonds than others, and consequently, form the most stable complex.

Fig. 1 Chemical structures of MDMA similar molecules used in recognition test calculations: 3,4-methylenedioxyamphetamine (MDA), 3,4-metilendioxietilamfetamina (MDEA), amphetamine (AP), mescaline (MC), methamphetamine (MA) and, 3,4-methylenedioxy-N-methylcathinone (MDMC), 2-(1H-Indol-3-yl)-N,N-dimethylethan-1-amine (DMT), 2,5-dimethoxy-4-methylphenethylamine (2C-D), 2,5-dimethoxy-4-methylthioamphetamine (ALEPH), 4-Bromo- 2,5 dimethoxyphenethylamine (2C-B) and 2,5-Dimethoxy-4-ethoxyamphetamine (MEM)


3,4-methylenedioxymethamphetamine (MDMA)

3,4- methylenedioxyamphetamine (MDA)

Methylenedioxyethylamphetamine (MDEA)

Mescaline (MC)

Methamphetamine (MA)

Amphetamine (AP)

3,4-methylenedioxy-N-methylcathinone (MDMC)

2-(1H-Indol-3-yl)-N,N-dimethylethan-1-amine (DMT)

2,5-dimethoxy-4-methylphenethylamine (2C-D)

2,5-dimethoxy-4-methylthioamphetamine (ALEPH)

2,5-dimethoxy-4-bromophenethylamine (2C-B)

2,5-Dimethoxy-4-ethoxyamphetamine (MEM)
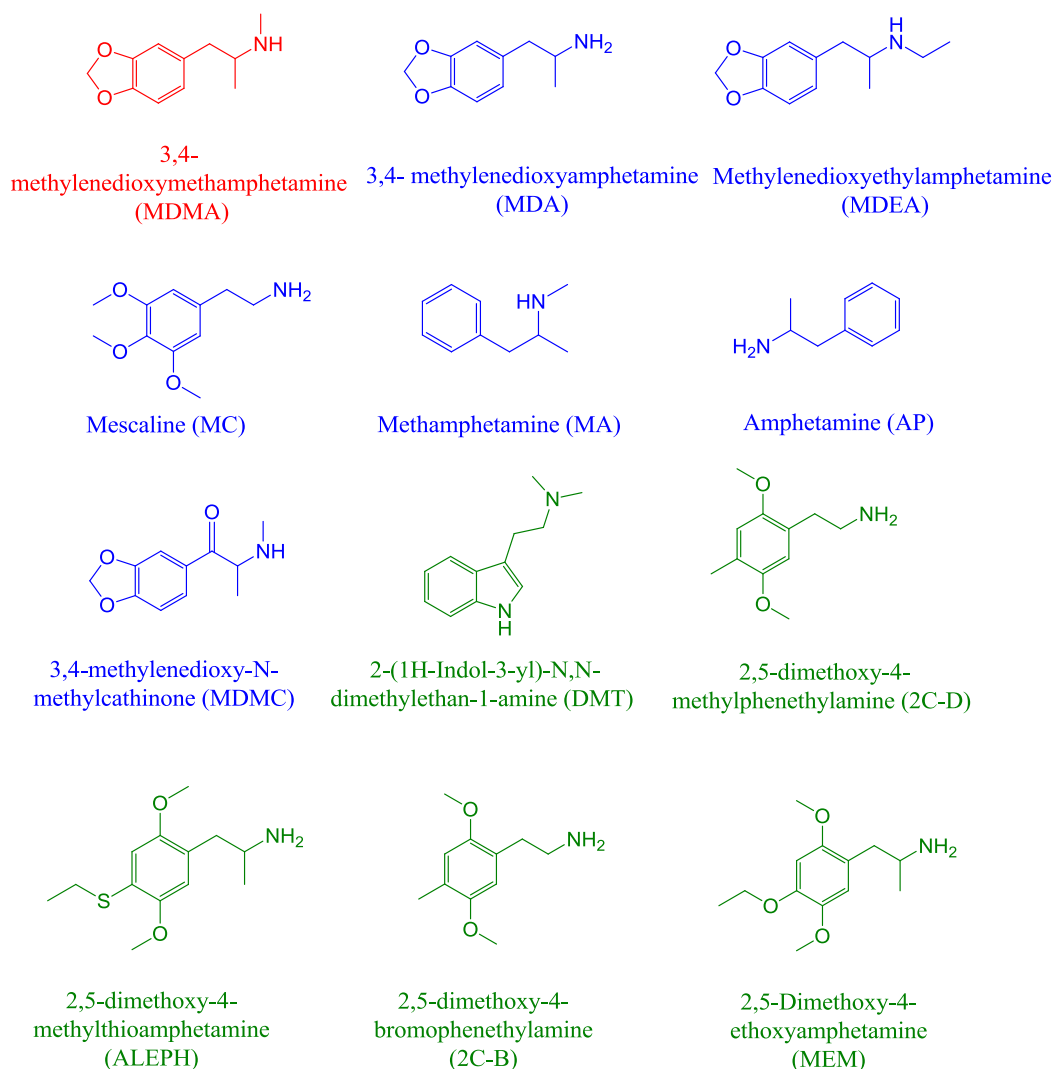
Legend:
Reference
Greater structural similarity
Lower structural similarity

Fig. 2 Molecular electrostatic potential (MEP) analysis of monomers and MDMA. (a) acrilic acid, (b) itaconic acid, (c) acrylamide, (d) acrolein, (e) metacrilic acid, (f) divinylbenzene, (g) styrene, (h) methyl methacrylate, (i) MDMA, (j) TFMA, (k) vinylimidazole and (l) vinylpiridine
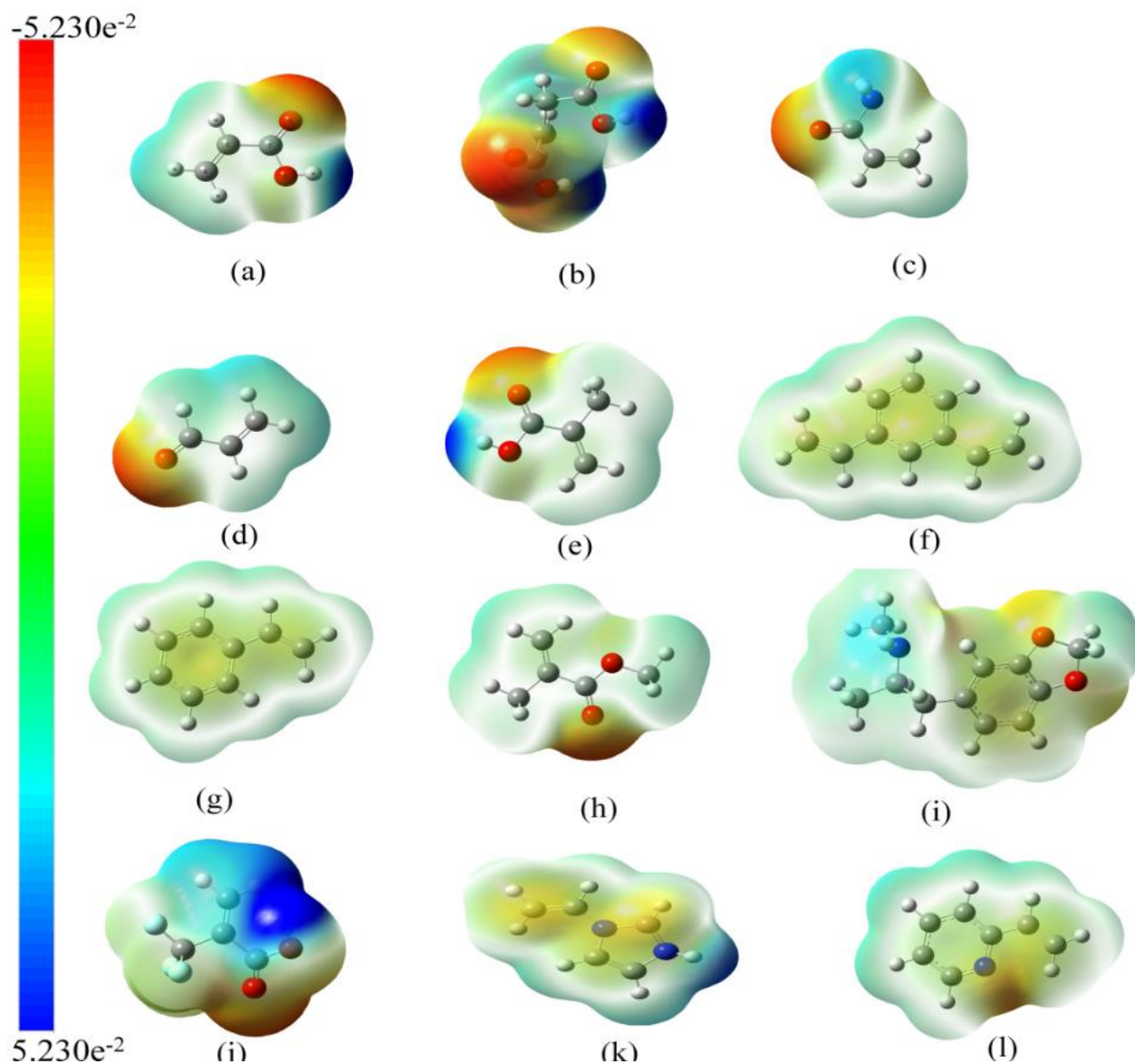
-Selection of the proper functional monomer and Template-monomer mole ratio

To give an idea of relative stability of different components of the system, as well as provide an appropriate guide for selection of the most suitable monomer and to investigate the most proper molar ratio, the interaction energies (ΔE) for the

complexation process at 1:1, 1:2 and 1:3 molar ratios were calculated and are presented in Table 3.

Table 3 Interaction energy variation (ΔE) values for each monomer-template complex at 1:1, 1:2 and 1:3 molar ratios

	ΔE (kcal.mol^{-1})		
Molar Ratio	1:1	1:2	1:3
AA	-176.58	-196.14	-220.82
IA	-192.42	-231.03	-285.01
MA	-174.79	-192.43	-215.65
ACL	-180.33	-201.61	-238.57
ACRO	-165.91	-176.34	-186.78
DVB	-167.58	-179.16	-189.13
ST	-163.16	-168.93	-176.13
MMA	-171.38	-184.59	-197.30
TFMA	-173.97	-194.80	-217.45
VI	-160.58	-161.03	-173.60
VP	-163.35	-166.33	-175.85

As expected from the MEP analysis and according to our calculated interaction energies, the most stable complexes are those formed with IA, ACL, AA, TFMA, and MA, being 1:3 the preferential molar ratio in most cases. The IA complexes were those for which the highest energy values were obtained, with values of -192.42, -231.03 and -285.01 kcal.mol-1 for 1:1, 1:2 and 1:3 molar ratios, respectively. These highest interaction energies mean that the strongest level of interaction occurs using itaconic acid (IA) as functional monomer in the MIP design for MDMA detection, which implies a better selectivity of MIP. The next strongest interaction occurs in the ACL-MDMA complex, and the interaction energy value differs by 46.44 kcal.mol-1 for the 1:3 molar ratio of both monomers.

-Identification of the interaction type between template and monomer

The next steps were carried out only for the IA complex with 1:3 (template:monomer) stoichiometry, considering that this compound had the best results in the previous steps. In order to better understand the complex formation as well as to

investigate the nature of the monomer-template interactions, the theoretical IR spectra of the complex and isolated molecules were analyzed. The theoretical IR analysis can be a valuable tool in the identification of intermolecular interactions within the monomer-template complex, as in the case of hydrogen bond formation, which can be easily discernible by means of changes in the stretching frequency of the O-H and N-H bonds [23]. Theoretical IR spectra reveal that there is substantial interaction and formation of the complex occurring between MDMA and IA, through specific and significant shifts, which can be used to validate this study and for future interpretations of experimental work.

As seen in Figure 3, there are additional peaks observed in the IA-MDMA complex, compared to monomer and template spectra. Formation of a strong hydrogen bond between the O-H group of itaconic acid and the nitrogen atom of MDMA molecule, is indicated by the presence of a high intensity peak at 2741.1 cm-1. In addition, the presence of two other intense peaks in the region of 3479.7 and 3521.1 cm-1 indicates that there are two other hydrogen bonds with the other two itaconic acid monomers. Thus, it may be suggested that three hydrogen bonds occur between MDMA and the IA monomers, as expected by MEP analysis.

-Simulations in solvents

This step is extremely important, taking into account that the most appropriate solvent for MIP preparation should solubilize all the components present in the synthesis as well as not affect the intermolecular interactions between the template and the monomers, or even attenuate these interactions. Aiming to investigate the most suitable solvent, optimization and frequency calculations were performed for IA-MDMA complex, employing the IEFPCM implicit solvation model at the same level of theory. For the choice of solvents, the dielectric constant values were used as criteria. Thus, it was attempted to investigate solvents of different dielectric constants values to investigate the behavior of the complex under these conditions. From Table4, it is possible to observe that besides the interaction energy decrease, when compared to the energy in the vacuum, there was not a great variation between the energies in relation to the different solvents. The decrease of ΔE value in the solvent can be attributed to the fact that interactions occur with the solvent molecules and these interactions compete with the interactions between monomer and template.

Fig. 3 Theoretical InfraRed Spectrum corresponding to template MDMA, functional monomer itaconic acid (IA) and the lowest energy system, MDMA-IA complex
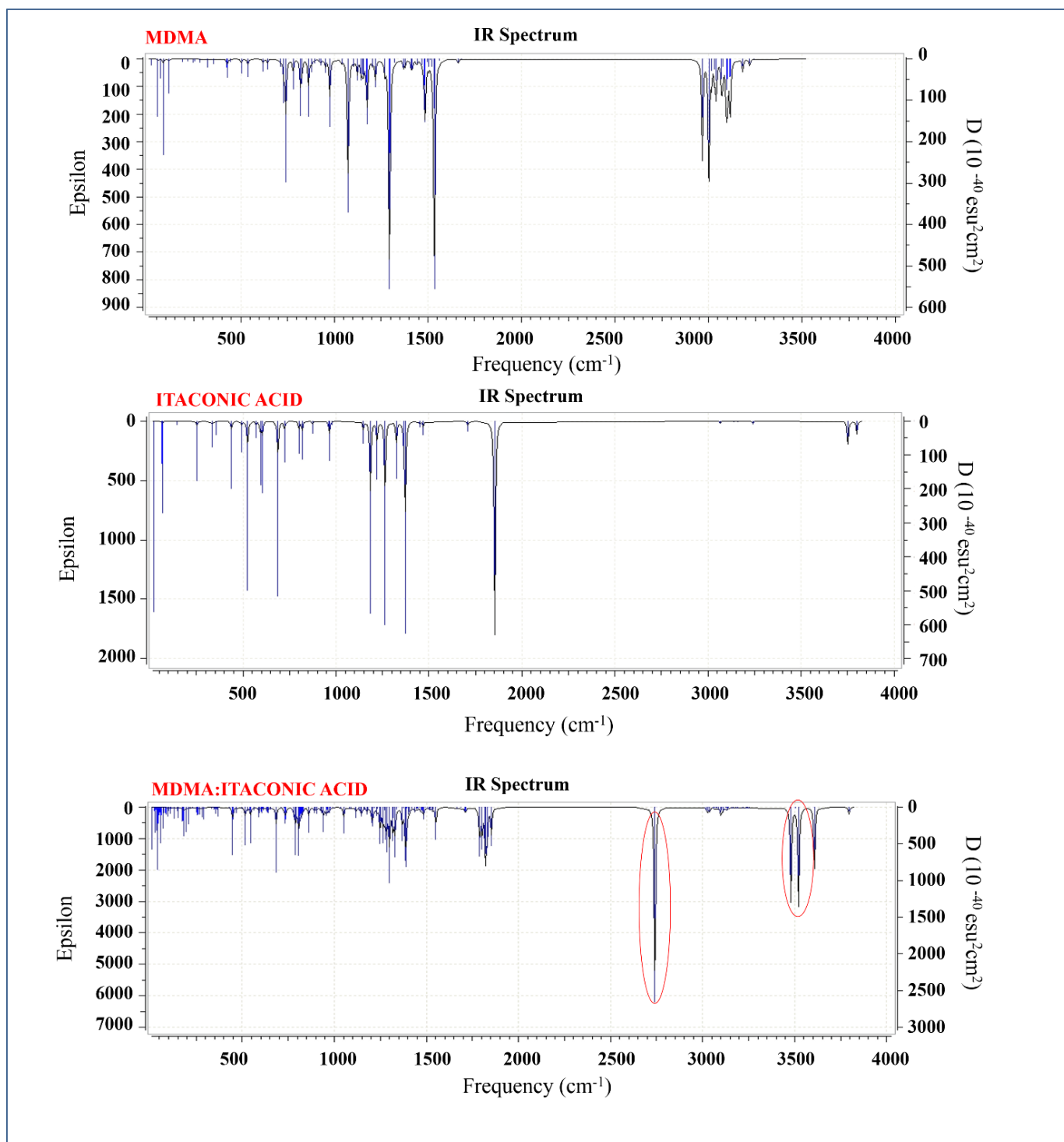
Table 4 Interaction energy variation (ΔE) values for Itaconic Acid-MDMA complex at a 1:3 molar ratio, according to each solvent

Solvent	Dielectric constant	ΔE (kcal.mol^{-1})
Water	80	-197.32
DMSO	45	-197.33
Acetonitrile	36	-197.35
Methanol	32	-197.36
Acetone	20	-197.45
Chloroform	4.8	-192.1

The interaction energies were very similar for all polar solvents, the highest stability being obtained for simulation in acetone, with a interaction energy value of -197.45 kcal.mol-1. The worse interaction energy value was obtained for the simulation in chloroform solvent, corresponding to -192.1 kcal.mol-1. From these results and analyzing the graph with ΔE vs. dielectric constant presented in Figure 4, it can be concluded that polar solvents are the most efficient. Among the polar solvents, acetone can better stabilize the complex since it is not a protic solvent. Protic solvents, such as water and methanol, can possibly compete with monomer for performing hydrogen bonds with the template, and this feature can decrease the interaction between monomer and template. In addition, it can be concluded that the stabilization of the complex is slightly affected for high polarity solvents, which can also be attributed to the competition of the solvent with monomer and the template when performing intermolecular interactions.

Fig. 4 Graph of interaction energy variation (ΔE) of the template-monomer complex IA-MDMA at a 3:1 molar ratio vs. dielectric constant values of the solvents
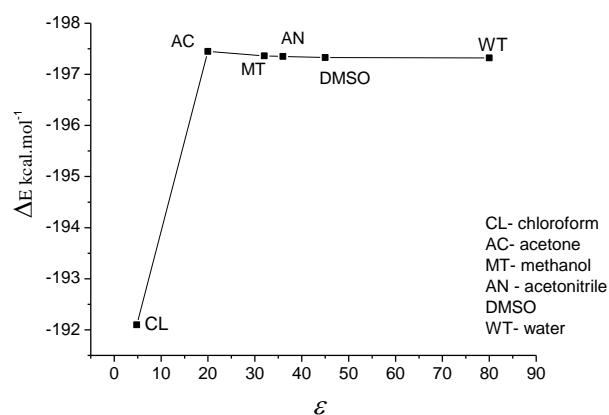
chloroform, acetone, methanol, acetonitrile, dimethylsulfoxide (DMSO) and water

- *Cross-linking selection*

The interaction energy values obtained from the optimization calculations for the cross-linking/template complexes are found in Table 4. As can be seen in Table 5, the interaction energy values do not differ significantly, and the lowest values were obtained for the cross-linking agent TRIM, with a value of -169.88 kcal.mol-1, followed by the EGDMA molecule, with an interaction energy value of -179.59 kcal.mol-1. The NNMB molecule is the least indicated because it has the highest interaction energy value. This can be explained by the fact that this molecule has Hydrogen bond donor sites and consequently interacts more strongly with the template. The TRIM and EGDMA molecules do not have these binding sites, which is advantageous, considering that the interactions between the cross-linking and the template should be as low as possible, so that cross-linking does not disrupt the template-monomer interactions. In this way, the most appropriate cross-linking molecule, considering the template chemical characteristics and the theoretical calculation results, would be the TRIM and then the EGDMA molecule.

Table 5 Interaction energy variation values (ΔE) in kcal.mol-1 for cross-linking agent simulations with template mdma. Ethylene glycol dimethacrylate (EGDMA), N,N-methylene bisacrylamide (NNMB) and trimethylolpropane trimethacrylate (TRIM)

Cross-linking agent	ΔE $(kcal.mol^{-1})$
EGDMA	-179.59
NNMB	-181.51
TRIM	-169.88

-*Recognition tests*

A theoretical prediction of the selectivity in synthetic receptors can also be made by means of theoretical techniques. The molecules tested have different degrees of similarity with the MDMA molecule, and by interaction energy results (Table 6) it is possible to observe that for very similar molecules the MIP was not so selective. This occurs because both the size and interaction sites are very similar. Furthermore, Figure 5 presents that there was a considerable variation in the interaction energy value for the most different molecules in the size and interaction points. So, the molecules MDA, MDEA and MDMC, which are very structurally similar, have close interaction energy

values, while the MEM, DMT and ALEPH molecules show higher interaction energy values compared to MDMA, which means that the MIP will possibly have selectivity in relation to these molecules. For AP, MD, MC, 2CB and 2CD molecules, intermediary interaction energy values were obtained. Despite the similar results for most similar molecules, the media in which the test will be performed can influence this value. It is also important to consider that the structural similarity can hide some differences in chemical properties, such as hydrophobicity [61]. Thus, if a more suitable solvent is chosen for MDMA, it is possible to increase the selectivity for the desired molecule, since the polarity of these compounds is different, despite the similarity in size and sites of interaction with the monomers.

Independent of the application of the MIP, some selectivity is expected for target compounds against other compounds and the selectivity needs to be tested in real life applications. There are many methods for selectivity verifications, and the desired selectivity will depend on the application [61] and flexibility [62, 63]. However, the theoretical values can give us a good prediction of the selectivity of the studied material.

Table 6 Interaction energy (ΔE) and relative interaction energy values (ΔE_{rel}) (kcal.mol-1 for templates in the selectivity test

Template	ΔE (kcal.mol^{-1})	ΔE_{rel}(kcal.mol^{-1})
AP	-113.64	15.29
MA	-114.13	14.80
MC	-119.34	9.59
MDA	-128.80	0.12
MDEA	-127.98	0.95
MDMC	-124.41	4.51
MDMA	-128.93	0.00
ALEPH	-108.84	20.08
2CB	-117.41	11.52
2CD	-118.54	10.39
DMT	-104.97	23.96
MEM	-105.48	23.45

Fig. 5 Variation of interaction energy for some templates: IA complex in relation to MDMA:IA complex
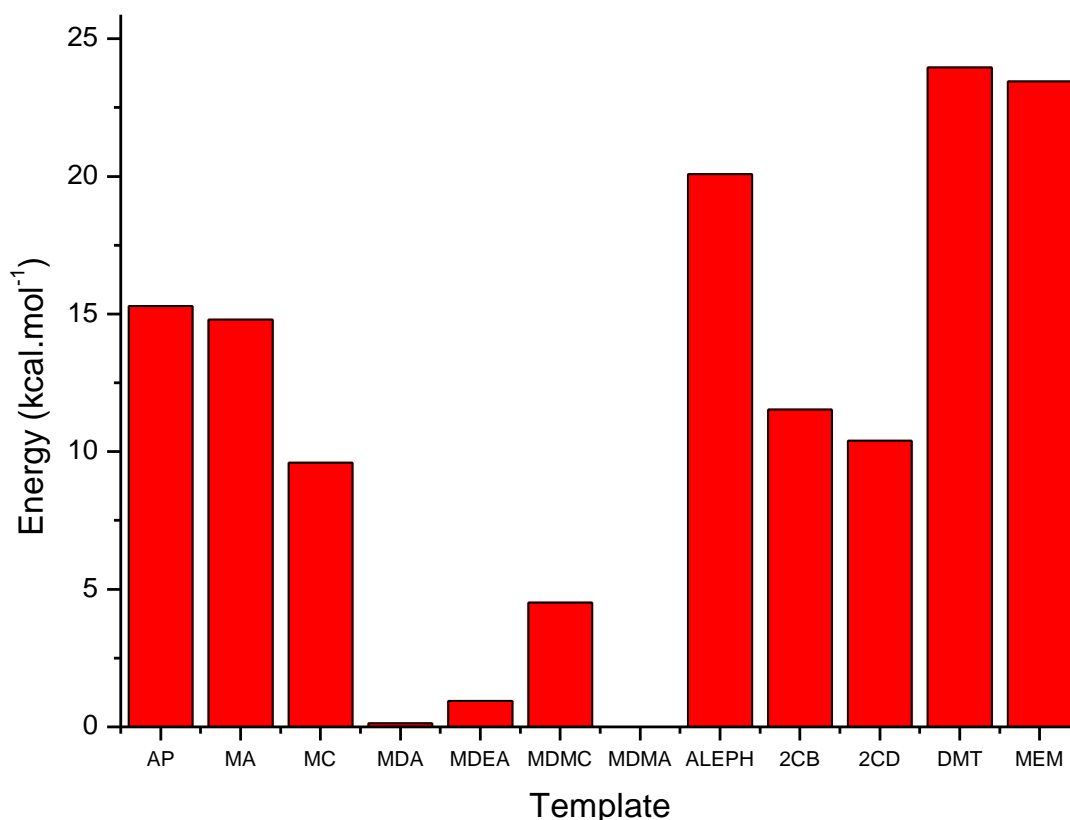
Conclusions

By means of computational resources, much information relevant to the preparation of molecularly printed polymers (MIP) can be obtained, thus saving financial resources and time during many steps of the process. In the rational design of a MIP for the detection of MDMA, it can be concluded that the best monomer to be employed in the MIP preparation is itaconic acid (IA), using the solvent acetone in the preparation of the complex pre-polymerization and synthesis of the polymer. In addition, the most suitable crosslinking agents are trimethylolpropane trimethacrylate (TRIM) and ethylene glycol dimethacrylate (EGDMA). In relation to the selectivity, it is possible to infer that the MIP constructed under the conditions explained above possesses a relative selectivity in relation to the molecules amphetamine (AP), mescaline (MC), methamphetamine (MA), 2-(1H-Indol-3-yl)-N,N-dimethylethan-1-amine (DMT), 2,5-dimethoxy-4-methylphenethylamine (2C-D), 2,5-dimethoxy-4-

methylthioamphetamine (ALEPH), 4-Bromo- 2,5 dimethoxyphenethylamine (2C-B) and 2,5-Dimethoxy-4-ethoxyamphetamine (MEM).

In comparison with other recognition tests, MIPs have many attractive features, as easy preparation, high physical stability, excellent robustness as well as low cost. Due to all of these advantages, this material has gained a lot of attention in several fields, mainly in chromatographic separation [16, 64–66], solid phase extraction (SPE) [67, 68], and sensing technologies [69–76]. In order to optimize the imprinting conditions, various approaches have been studied, and, from this study, the computational approach indicates to be an efficient optimization strategy. As can be seen, the theoretical measurement could drastically increase the speed of possible subtracts selection for their "optimal" laboratory preparation. Consequently, the time of the traditional try-and-error approach, as well as the amount of necessary chemicals and solvents can be considerably reduced. This is a great advantage not only for save time and money, but also for a lower environmental impact, obtaining the best material, with great robustness and selectivity.

Thus, a clear practical utility lies in the ability to predict the performance of unique substrate classes, thereby directing future synthetic efforts for MIPs.

Acknowledgments

References

1.UNODC (2019) United Nations Office of Drugs and Crime. https://dataunodc.un.org/drugs/prevalence_regional-2017#ecstasy. Accessed 10 Jul 2019

2. Silva ATM da, Bessa CDPB, Borges W de S, Borges KB (2018) Bioanalytical methods for determining ecstasy components in biological matrices: A review. TrAC Trends Anal Chem 108:323–346. https://doi.org/10.1016/J.TRAC.2018.08.001

3. Busardo FP, Pichini S, Pellegrini M, et al (2017) Correlation between Blood and Oral Fluid Psychoactive Drug Concentrations and Cognitive Impairment in Driving under the Influence of Drugs. Curr Neuropharmacol 16:84–96. https://doi.org/10.2174/1570159X15666170828162057

4. Monks TJ, Jones DC, Bai F, Lau SS (2004) The role of metabolism in 3,4-(+)-methylenedioxyamphetamine and 3,4-(+)-methylenedioxymethamphetamine (ecstasy) toxicity. Ther Drug Monit 26:132–6. https://doi.org/10.1097/00007691-200404000-00008

5. Gjerde H, Gjersing L, Furuhaugen H, Bretteville-Jensen AL (2019) Correspondence between Oral Fluid Drug Test Results and Self-Reported Illicit Drug Use among Music Festival Attendees. Subst Use Misuse 54:1337–1344. https://doi.org/10.1080/10826084.2019.1580295

6. Meyer MR, Wilhelm J, Peters FT, Maurer HH (2010) Beta-keto amphetamines: Studies on the metabolism of the designer drug mephedrone and toxicological detection of mephedrone, butylone, and methylone in urine using gas chromatography - Mass spectrometry. Anal Bioanal Chem 397:1225–1233. https://doi.org/10.1007/s00216-010-3636-5

7. Kawase K, Ogawa Y, Watanabe Y, Inoue H (2003) Non-destructive terahertz imaging of illicit drugs using spectral fingerprints. Opt Express 11:2549. https://doi.org/10.1364/oe.11.002549

8. Krauss ST, Woolf MS, Hadley KC, et al (2019) Centrifugal microfluidic devices using low-volume reagent storage and inward fluid displacement for presumptive drug detection. Sensors Actuators, B Chem 284:704–710. https://doi.org/10.1016/j.snb.2018.12.113

9. Ng TT, So PK, Hu B, Yao ZP (2019) Rapid detection and quantitation of drugs-of-abuse by wooden-tip electrospray ionization mass spectrometry. J Food Drug Anal 27:428–438. https://doi.org/10.1016/j.jfda.2018.09.002

10. Saar-Reismaa P, Tretjakova A, Mazina-Šinkar J, et al (2019) Rapid and sensitive capillary electrophoresis method for the analysis of Ecstasy in an oral fluid. Talanta 197:390–396. https://doi.org/10.1016/j.talanta.2019.01.029

11. Couto RAS, Costa SS, Mounssef B, et al (2019) Electrochemical sensing of ecstasy with electropolymerized molecularly imprinted poly(o-phenylenediamine)

polymer on the surface of disposable screen-printed carbon electrodes. Sensors Actuators, B Chem 290:378–386. https://doi.org/10.1016/j.snb.2019.03.138

12. Malaca S, Rosado T, Restolho J, et al (2019) Determination of amphetamine-type stimulants in urine samples using microextraction by packed sorbent and gas chromatography-mass spectrometry. J Chromatogr B Anal Technol Biomed Life Sci 1120:41–50. https://doi.org/10.1016/j.jchromb.2019.04.052

13. Zubaidi FA, Choo YM, Tan GH, et al (2019) A Novel Liquid Chromatography Tandem Mass Spectrometry Technique using Multi-Period-Multi-Experiment of MRM-EPI-MRM3 with Library Matching for Simultaneous Determination of Amphetamine Type Stimulants Related Drugs in Whole Blood, Urine and Dried Blood Stain (DBS)-Application to Forensic Toxicology Cases in Malaysia. J Anal Toxicol 43:528–535. https://doi.org/10.1093/jat/bkz017

14. Fabresse N, Aouad H, Knapp A, et al (2019) Development and validation of a liquid chromatography-tandem mass spectrometry method for simultaneous detection of 10 illicit drugs in oral fluid collected with FLOQSwabsTM and application to real samples. Drug Test Anal 11:824–832. https://doi.org/10.1002/dta.2563

15. Sergeyeva T, Yarynka D, Piletska E, et al (2019) Development of a smartphone-based biomimetic sensor for aflatoxin B1 detection using molecularly imprinted polymer membranes. Talanta 201:204–210. https://doi.org/10.1016/j.talanta.2019.04.016

16. Liu Q, Wan J, Cao X (2018) Synthesis of core-shell molecularly imprinted polymers (MIP) for spiramycin I and their application in MIP chromatography. Process Biochem 70:168–178. https://doi.org/10.1016/j.procbio.2018.04.001

17. Karim K, Cowen T, Guerreiro A, et al (2017) A Protocol for the Computational Design of High Affi nity Molecularly Imprinted Polymer Synthetic Receptors. Glob J Biotechnol Biomater Sci 3:1–7. https://doi.org/10.17352/gjbbs.000009

18. Ahmadi F, Ahmadi J, Rahimi-Nasrabadi M (2011) Computational approaches to design a molecular imprinted polymer for high selective extraction of 3,4-methylenedioxymethamphetamine from plasma. J Chromatogr A 1218:7739–7747. https://doi.org/10.1016/j.chroma.2011.08.020

19. Moreno-González D, Hamed AM, García-Campaña AM, Gámiz-Gracia L (2017) Evaluation of hydrophilic interaction liquid chromatography–tandem mass

spectrometry and extraction with molecularly imprinted polymers for determination of aminoglycosides in milk and milk-based functional foods. Talanta 171:74–80. https://doi.org/10.1016/j.talanta.2017.04.062

20. He T, Wang GN, Liu JX, et al (2019) Dummy molecularly imprinted polymer based microplate chemiluminescence sensor for one-step detection of Sudan dyes in egg. Food Chem 288:347–353. https://doi.org/10.1016/j.foodchem.2019.03.031

21. Farooq S, Nie J, Cheng Y, et al (2018) Molecularly imprinted polymers' application in pesticide residue detection. Analyst 143:3971–3989. https://doi.org/10.1039/C8AN00907D

22. Cowen T, Karim K, Piletsky S (2016) Computational approaches in the design of synthetic receptors – A review. Anal Chim Acta 936:62–74. https://doi.org/10.1016/J.ACA.2016.07.027

23. Khan MS, Wate PS, Krupadam RJ (2012) Combinatorial screening of polymer precursors for preparation of benzo[??] pyrene imprinted polymer: An ab initio computational approach. J Mol Model 18:1969–1981. https://doi.org/10.1007/s00894-011-1218-x

24. Li Z, Wang J, Chen X, et al (2019) A novel molecularly imprinted polymer-solid phase extraction method coupled with high performance liquid chromatography tandem mass spectrometry for the determination of nitrosamines in water and beverage samples. Food Chem 292:267–274. https://doi.org/10.1016/j.foodchem.2019.04.036

25. Sajini T, Thomas R, Mathew B (2019) Rational design and synthesis of photo-responsive molecularly imprinted polymers for the enantioselective intake and release of l-phenylalanine benzyl ester on multiwalled carbon nanotubes. Polymer (Guildf) 173:127–140. https://doi.org/10.1016/j.polymer.2019.04.031

26. Kuşçuoğlu CK, Güner H, Söylemez MA, et al (2019) A smartphone-based colorimetric PET sensor platform with molecular recognition via thermally initiated RAFT-mediated graft copolymerization. Sensors Actuators, B Chem 296:1266533. https://doi.org/10.1016/j.snb.2019.126653

27. Cowen T, Karim K, Piletsky S (2016) Computational approaches in the design of synthetic receptors – A review. Anal Chim Acta 936:62–74. https://doi.org/10.1016/j.aca.2016.07.027

28. Riahi S, Edris-Tabrizi F, Javanbakht M, et al (2009) A computational approach to studying monomer selectivity towards the template in an imprinted polymer. J Mol Model 15:829–836. https://doi.org/10.1007/s00894-008-0437-2

29. Nicholls IA, Chavan S, Golker K, et al (2015) Theoretical and Computational Strategies for the Study of the Molecular Imprinting Process and Polymer Performance. Springer, Cham, pp 25–50

30. Silva CF, Borges KB, Nascimento CS (2019) Computational study on acetamiprid-molecular imprinted polymer. J Mol Model 25:104. https://doi.org/10.1007/s00894-019-3990-y

31. Subrahmanyam S, Karim K, Piletsky SA (2012) Computational Approaches in the Design of Synthetic Receptors. Springer, Berlin, Heidelberg, pp 131–165

32. Bates F, Busato M, Piletska E, et al (2017) Computational design of molecularly imprinted polymer for direct detection of melamine in milk. Sep Sci Technol 52:1441–1453. https://doi.org/10.1080/01496395.2017.1287197

33. Ghiasuddin, Akram M, Adeel M, et al (2018) A combined experimental and computational study of 3-bromo-5-(2,5-difluorophenyl) pyridine and 3,5-bis(naphthalen-1-yl)pyridine: Insight into the synthesis, spectroscopic, single crystal XRD, electronic, nonlinear optical and biological properties. J Mol Struct 1160:129–141. https://doi.org/10.1016/j.molstruc.2018.01.100

34. Ahmad MS, Khalid M, Shaheen MA, et al (2018) Synthesis and XRD, FT-IR vibrational, UV–vis, and nonlinear optical exploration of novel tetra substituted imidazole derivatives: A synergistic experimental-computational analysis. J Phys Chem Solids 115:265–276. https://doi.org/10.1016/j.jpcs.2017.12.054

35. Shahid M, Salim M, Khalid M, et al (2018) Synthetic, XRD, non-covalent interactions and solvent dependent nonlinear optical studies of Sulfadiazine-Ortho-Vanillin Schiff base: (E)-4-((2-hydroxy-3-methoxy- benzylidene) amino)-N-(pyrimidin-2-yl)benzene-sulfonamide. J Mol Struct 1161:66–75. https://doi.org/10.1016/j.molstruc.2018.02.043

36. Jawaria R, Hussain M, Khalid M, et al (2019) Synthesis, crystal structure analysis, spectral characterization and nonlinear optical exploration of potent thiosemicarbazones based compounds: A DFT refine experimental study. Inorganica Chim Acta 486:162–171. https://doi.org/10.1016/j.ica.2018.10.035

37. Khalid M, Ullah MA, Adeel M, et al (2019) Synthesis, crystal structure analysis, spectral IR, UV–Vis, NMR assessments, electronic and nonlinear optical properties of potent quinoline based derivatives: Interplay of experimental and DFT study. J Saudi Chem Soc 23:546–560. https://doi.org/10.1016/j.jscs.2018.09.006

38. Tahir MN, Mirza SH, Khalid M, et al (2019) Synthesis, single crystal analysis and DFT based computational studies of 2,4-diamino-5-(4-chlorophenyl)-6-ethylpyrim idin-1-ium 3,4,5-trihydroxybenzoate -methanol (DETM). J Mol Struct 1180:119–126. https://doi.org/10.1016/j.molstruc.2018.11.089

39. Haroon M, Khalid M, Akhtar T, et al (2019) Synthesis, spectroscopic, SC-XRD characterizations and DFT based studies of ethyl2-(substituted-(2-benzylidenehydrazinyl))thiazole-4-carboxylate derivatives. J Mol Struct 1187:164–171. https://doi.org/10.1016/j.molstruc.2019.03.075

40. Rafiq M, Khalid M, Tahir MN, et al (2019) Synthesis, XRD, spectral (IR, UV–Vis, NMR) characterization and quantum chemical exploration of benzoimidazole-based hydrazones: A synergistic experimental-computational analysis. Appl Organomet Chem 33:. https://doi.org/10.1002/aoc.5182

41. Khan B, Khalid M, Shah MR, et al (2019) Efficient Synthesis by Mono-Carboxy Methylation of 4,4′-Biphenol, X-ray Diffraction, Spectroscopic Characterization and Computational Study of the Crystal Packing of Ethyl 2-((4′-hydroxy-[1,1′-biphenyl]-4-yl)oxy)acetate. ChemistrySelect 4:9274–9284. https://doi.org/10.1002/slct.201901422

42. Liang D, Wang Y, Li S, et al (2016) Study on dicyandiamide-imprinted polymers with computer-aided design. Int J Mol Sci 17:1–11. https://doi.org/10.3390/ijms17111750

43. Fonseca MC, Nascimento CS, Borges KB (2016) Theoretical investigation on functional monomer and solvent selection for molecular imprinting of tramadol. Chem Phys Lett 645:174–179. https://doi.org/10.1016/J.CPLETT.2015.12.061

44. M. J. Frisch, G. W. Trucks, H. B. Schlegel, G. E. Scuseria, M. A. Robb, J. R. Cheeseman, G. Scalmani, V. Barone, B. Mennucci, G. A. Petersson, H. Nakatsuji, M. Caricato, X. Li, H. P. Hratchian, A. F. Izmaylov, J. Bloino, G. Zheng, J. L. Sonnenberg, M. Had and DJF (2009) Gaussian 09. Gaussian, Inc., Wallingford CT

45. Khan MS, Pal S, Krupadam RJ (2015) Computational strategies for understanding the nature of interaction in dioxin imprinted nanoporous trappers. J Mol Recognit 28:427–437. https://doi.org/10.1002/jmr.2459

46. Djozan D, Farajzadeh MA, Sorouraddin SM, Baheri T (2012) Determination of methamphetamine, amphetamine and ecstasy by inside-needle adsorption trap based on molecularly imprinted polymer followed by GC-FID determination. Microchim Acta 179:209–217. https://doi.org/10.1007/s00604-012-0879-1

47. Zhang B, Fan X, Zhao D (2018) Computer-Aided Design of Molecularly Imprinted Polymers for Simultaneous Detection of Clenbuterol and Its Metabolites. Polymers (Basel) 11:17. https://doi.org/10.3390/polym11010017

48. Barone V, Cossi M, Tomasi J (1998) A new definition of cavities for the computation of solvation free energies by the polarizable continuum model. J Chem Phys 107:3210. https://doi.org/10.1063/1.474671

49. Yuan Y, Li Z, Liu Y, et al (2012) Hydrogel photonic sensor for the detection of 3-pyridinecarboxamide. Chem - A Eur J 18:303–309. https://doi.org/10.1002/chem.201102001

50. Wang LQ, Lin FY, Yu LP (2012) A molecularly imprinted photonic polymer sensor with high selectivity for tetracyclines analysis in food. Analyst 137:3502–3509. https://doi.org/10.1039/c2an35460h

51. Gai Q, Liu Q, Li W, et al (2008) Preparation of bovine hemoglobin-imprinted polymer beads via the photografting surface-modified method. Front Chem China 3:370–377. https://doi.org/10.1007/s11458-008-0089-x

52. Anirudhan TS, Alexander S (2014) Multiwalled carbon nanotube based molecular imprinted polymer for trace determination of 2,4-dichlorophenoxyaceticacid in natural water samples using a potentiometric method. Appl Surf Sci 303:180–186. https://doi.org/10.1016/j.apsusc.2014.02.139

53. Khan MS, Pal S (2018) Quantum mechanical studies on dioxin-imprinted polymer precursor composites: Fundamental insights to enhance the binding strength and selectivity of biomarkers. J Mol Recognit 31:e2736. https://doi.org/10.1002/jmr.2736

54. Ishkuh FA, Javanbakht M, Esfandyari-Manesh M, et al (2014) Synthesis and characterization of paclitaxel-imprinted nanoparticles for recognition and controlled

release of an anticancer drug. J Mater Sci 49:6343–6352. https://doi.org/10.1007/s10853-014-8360-7

55. Khan MS, Wate PS, Krupadam RJ (2012) Combinatorial screening of polymer precursors for preparation of benzo[α] pyrene imprinted polymer: an ab initio computational approach. J Mol Model 18:1969–1981. https://doi.org/10.1007/s00894-011-1218-x

56. Hassan SSM, Amr AEGE, El-Naby HA, et al (2019) Novel aminoacridine sensors based on molecularly imprinted hybrid polymeric membranes for static and hydrodynamic drug quality control monitoring. Materials (Basel) 12:3327–3340. https://doi.org/10.3390/ma12203327

57. Baezzat MR, Bagheri M, Abdollahi E (2019) Molecularly imprinted polymer based sensor for measuring of zileuton: Evaluation as a modifier for carbon paste electrode in electrochemically recognition. Mater Today Commun 19:23–31. https://doi.org/10.1016/j.mtcomm.2018.12.013

58. El-Kosasy AM, Kamel AH, Hussin LA, et al (2018) Mimicking new receptors based on molecular imprinting and their application to potentiometric assessment of 2,4-dichlorophenol as a food taint. Food Chem 250:188–196. https://doi.org/10.1016/j.foodchem.2018.01.014

59. Wei X, Xu G, Gong C, et al (2018) Fabrication and evaluation of sulfanilamide-imprinted composite sensors by developing a custom-tailored strategy. Sensors Actuators, B Chem 255:2697–2703. https://doi.org/10.1016/j.snb.2017.09.081

60. Douhaya Y V., Barkaline V V., Tsakalof A (2016) Computer-simulation-based selection of optimal monomer for imprinting of tri-O-acetyl adenosine in a polymer matrix: calculations for benzene solution. J Mol Model 22:1–8. https://doi.org/10.1007/s00894-016-3030-0

61. Dorkó Z, Nagy-Szakolczai A, Tóth B, Horvai G (2018) The Selectivity of Polymers Imprinted with Amines. Molecules 23:1298. https://doi.org/10.3390/molecules23061298

62. Gonçalves MA, Santos LS, Prata DM, et al (2017) Optimal wavelet signal compression as an efficient alternative to investigate molecular dynamics simulations: application to thermal and solvent effects of MRI probes. Theor Chem Acc 136:15. https://doi.org/10.1007/s00214-016-2037-z

63. Martins TLC, Ramalho TC, Figueroa-Villar JD, et al (2003) Theoretical and experimental13C and15N NMR investigation of guanylhydrazones in solution. Magn Reson Chem 41:983–988. https://doi.org/10.1002/mrc.1299

64. Zhang K, Zhou T, Kettisen K, et al (2019) Chromatographic separation of hemoglobin variants using robust molecularly imprinted polymers. Talanta 199:27–31. https://doi.org/10.1016/j.talanta.2019.01.125

65. Gomes CP, Dias RCS, Costa MRPFN (2019) Preparation of Molecularly Imprinted Adsorbents with Improved Retention Capability of Polyphenols and Their Application in Continuous Separation Processes. Chromatographia 82:893–916. https://doi.org/10.1007/s10337-019-03728-7

66. Song WF, Zhao QL, Zhou XJ, et al (2019) A star-shaped molecularly imprinted polymer derived from polyhedral oligomeric silsesquioxanes with improved site accessibility and capacity for enantiomeric separation via capillary electrochromatography. Microchim Acta 186:22. https://doi.org/10.1007/s00604-018-3151-5

67. Xie Z, Chen Y, Zhang L, Hu X (2019) Magnetic molecularly imprinted polymer combined with high performance liquid chromatography for selective extraction and determination of the metabolic content of quercetin in rat plasma. J Biomater Sci Polym Ed 1–19. https://doi.org/10.1080/09205063.2019.1675224

68. Zhao X, Mai Y, Chen D, et al (2019) Selective enrichment of clenbuterol onto molecularly imprinted polymer microspheres with tailor-made structure and oxygen functionalities. Polymers (Basel) 11:. https://doi.org/10.3390/polym11101635

69. Ertuğrul Uygun HD, Uygun ZO, Canbay E, et al (2020) Non-invasive cortisol detection in saliva by using molecularly cortisol imprinted fullerene-acrylamide modified screen printed electrodes. Talanta 206:. https://doi.org/10.1016/j.talanta.2019.120225

70. Bangaleh Z, Bagheri Sadeghi H, Ebrahimi SA, Najafizadeh P (2019) A New Potentiometric Sensor for Determination and Screening Phenylalanine in Blood Serum Based on Molecularly Imprinted Polymer. Iran J Pharm Res IJPR 18:61–71

71. Zhang G, Yu Y, Zhang L, et al (2020) Precise detection of prostate specific antigen in serum: A surface molecular imprinted sensor based on novel cooperated signal amplification strategy. Sensors Actuators, B Chem 302:1269982. https://doi.org/10.1016/j.snb.2019.126998

72. Wang X, Huang K, Zhang H, et al (2019) Preparation of molecularly imprinted polymers on hemin-graphene surface for recognition of high molecular weight protein. Mater Sci Eng C 105:110141. https://doi.org/10.1016/j.msec.2019.110141

73. Xia Y, Zhao F, Zeng B (2020) A molecularly imprinted copolymer based electrochemical sensor for the highly sensitive detection of L-Tryptophan. Talanta 206:120245. https://doi.org/10.1016/j.talanta.2019.120245.

74. Ramalho TC, Castro AA, Silva DR, et al (2016) Computational Enzymology and Organophosphorus Degrading Enzymes: Promising Approaches Toward Remediation Technologies of Warfare Agents and Pesticides. Current Medicinal Chemistry, 23:1041. https://doi.org/10.2174/0929867323666160222113504.

75. Xavier LPS, Dias AC, Baeta BEL et al (2019) Experimental and theoretical studies of solvent polarity influence on the preparation of molecularly imprinted polymers for the removal of estradiol from water. New Journal of Chemistry 43: 1775. https://doi.org/10.1039/C8NJ03639J

76. Ramalho TC, Martins TLC, Figueroa-Villar JD (2003) A Theoretical and Experimental 13C and 15N NMR Investigation of Guanylhydrazones in Solution. Magnetic Resonance in Chemistry, 41:983. https://doi.org/10.1002/mrc.1299.

2. ANIMAL HEALTH MONITORING

2.1. Patent: SENSOR SUBCUTÂNEO BASEADO EM POLÍMERO MAGNÉTICO MOLECULARMENTE IMPRESSO DE FERROXITA/POLIMETILMETACRILATO PARA DETECÇÃO E MONITORAMENTO DE NÍVEIS DE CONCENTRAÇÃO DE HORMÔNIOS REPRODUTIVOS NA CIRCULAÇÃO SANGUÍNEA DE FÊMEAS MAMÍFERAS

Patente depositada junto ao INPI. Número do processo: BR 10 2020 024389
Data: 30/11/2020

RESUMO

A presente invenção se trata de um sensor desenvolvido para detecção de progesterona e 17-β Estradiol em amostras biológicas, *in vivo e in vitro*. É constituído de um polímero molecularmente impresso de Polimetilmetacrilato (PMMA), magnetizado com nanopartículas de ferroxita (δ-FeOOH), como parte reconhecedora. Este material é parte constituinte de um sensor eletroquímico, e funciona como material reconhecedor do mesmo. Pode ser utilizado na indústria como sensor, podendo ser implantado em animais, para acompanhamento dos níveis hormonais, entre outras aplicações, como por exemplo para análise de amostras biológicas líquidas *in vitro*. Além da sua seletividade, estabilidade, baixo custo, fácil preparação e manuseio; o material possui propriedades magnéticas, o que facilita o controle de suas propriedades por meio externo, viabilizando assim sua implantação em animais, ou mesmo sua utilização em amostras biológicas líquidas.

RELATÓRIO DESCRITIVO

1.2 - Apresentação do invento ou campo de aplicação

Esta invenção pertence ao campo de materiais utilizados em sensores para detecção de compostos pelo uso de meios elétricos, eletroquímicos ou magnéticos; especificamente a campo dos materiais utilizados em dispositivos para análise de progesterona e 17-β Estradiol em materiais biológicos *in vivo* e em amostras líquidas. Também pode ser parte constituinte de sistemas em que o material é submetido a uma reação química, sendo o andamento ou o resultado da mesma investigado.

As principais funcionalidades desta invenção são:

1 - Monitoramento de concentração de progesterona e 17-β Estradiol no sangue de fêmeas mamíferas (em específico de fêmeas bovinas);

2 - Detectar, com alta precisão, o momento de ocorrência do pico de concentração de progesterona e 17-β Estradiol no sangue (início do cio do animal);

3 - Determinar, em quais animais foi verificada a ocorrência do pico de concentração de progesterona e 17-β Estradiol;

4 - Determinar, em quais animais 'não' foi verificada a ocorrência do pico de concentração de progesterona e 17-β Estradiol;

1.3 - Estado da técnica

Os sensores químicos são dispositivos empregados em diversos tipos de análises, e permitem o acompanhamento em tempo real e obtenção de informações *in situ*, uma vez que necessitam de manipulação mínima do sistema estudado. Além disso, possuem diversas vantagens, como portabilidade, facilidade de automação, baixo custo e possibilidade de miniaturização.

Um sensor químico é composto basicamente por um material reconhecedor, um transdutor e um detector, que interpretará o sinal. Para reconhecimento do analito de maneira seletiva são utilizados materiais que reagem especificamente com o analito, que são geralmente dispostos em uma membrana. Esta membrana é posicionada na extremidade do dispositivo, e deve ser fixada por um processo químico que viabilize a

transdução do sinal para o detector. Este sinal recebido é maximizado para minimizar os efeitos do ambiente no erro de detecção. Também devem ser consideradas aspectos referentes à robustez, sensibilidade e a estabilidade do sensor químico.

A classificação dos sensores é feita baseando-se tanto na constituição do material reconhecedor, quanto no sinal de transdução gerado. Biossensores empregam moléculas biológicas como bioreceptores, podendo ser biossensores enzimáticos ou imunobiossensores. Há também os sensores eletroquímicos, constituídos de um eletrodo que transforma o sinal gerado pela interação do analito com o material de reconhecimento em sinal eletrônico. Além destes, há também os sensores celulares, ópticos, acústicos e calorimétricos.

Uma das diversas justificativas para o desenvolvimento de novos sensores químicos é a necessidade de monitoramento *in vivo* de moléculas de importância biológica. Assim sendo, a nova geração de tecnologias de sensoriamento está intimamente ligada tanto ao desenvolvimento de novos materiais sintéticos om funcionalidades diversificadas, quanto expansão de novos recursos de hardware e software. O desenvolvimento e ampliamento destas tecnologias juntas, garantem então a ampla implementação, além da diminuição dos custos do produto final.

Atualmente, os sensores químicos são empregados em diversos campos, como o de análises químicas, segurança de alimentos, diagnóstico clínico, monitoramento ambiental, entre outros (Yang, B.; Li, J.; Deng, H.; Zhang, L.. Crit. Rev. Anal. Chem. 2016, 46, 469–481). Outro campo que vem sendo comtemplado com o uso de tecnologias de sensoriamento é o campo da pecuária, não apenas no manejo de animais, mas também em fornecimento de produtos de alta e consistente qualidade (Jorquera-Chavez, M. et al. Meat Science 156 (2019) 11–22).

1.3.1 - Problemas do estado da técnica

A maioria dos sensores já desenvolvidos possuem alto custo de produção, o processo de obtenção é muitas vezes complexo, apresentam baixa seletividade e são pouco estáveis, principalmente os biossensores enzimáticos e imunobiossensores. Além disso, a regeneração da superfície do sensor pode ser trabalhosa, o que inviabiliza sua reutilização. Afora todas estas desvantagens, os materiais inorgânicos desenvolvidos como sensores para utilização *in vivo* podem apresentar complicações relacionadas à

biocompatibilidade. Dessa forma, um material barato, de simples obtenção, estável, de fácil manuseio e biocompatível é de grande interesse da indústria. Porém, é importante ter em mente que o desenvolvimento de um material que atenda a todas essas exigências não é um processo fácil, por isso, materiais que venham a atender essa demanda são muito valorizados pelo mercado.

1.3.2 - Vantagens da invenção

Um material que atende a todos estes critérios é o polimetilmetacrilato (PMMA), importante membro da família dos poli (acrílico éster), obtido através da polimerização do metacrilato (Figura 1). Já é empregado em reposição de vidro, lentes intraoculares, próteses dentárias, entre outras. Este polímero é um material rígido de alta resistência à tração, compressão e flexão, elevado grau de transparência óptica e excelente estabilidade dimensional. Além disso, é resistente à hidrólise tanto em meio ácido quanto básico, o que favorece ainda mais seu uso para monitoramento *in vivo*.

A polimerização por impressão molecular é uma técnica de polimerização que tem sido empregada para sintetizar polímeros com cavidades de tamanhos específicos. Uma vantagem interessante de um sensor de PIMs é seu tempo de vida, uma vez que o polímero é de natureza robusta e essa propriedade confere facilidade na reutilização e regeneração da superfície do sensor. Os polímeros molecularmente impressos (PIMs) têm se destacado em relação à sua alta seletividade, uma vez que são polimerizados na presença do analito, este que é retirado após a polimerização. Dessa forma, as cavidades formadas possuem tamanho e forma específica, o que torna a adsorção seletiva para moléculas estruturalmente similares ao analito. Além da alta especificidade que é de interesse industrial, os polímeros 3D são mais viáveis do que as superfícies 2D de eletrodos modificados, uma vez que o processo de modificação na superfície de eletrodos gera uma instabilidade e piora a reprodutibilidade do material. Adicionalmente, materiais como o grafeno não são seletivos, o que faz com que a detecção tenha muitos interferentes.

Além de todas estas vantagens da utilização de impressão molecular utilizando PMMA, a presente invenção também conta com a possibilidade de controle do sensor por meio de campos externos, uma vez que nanopartículas de δ-FeOOH são empregadas

no processo de polimerização, conferindo propriedades magnéticas ao material. Essa possibilidade de controle por meio externo constitui uma propriedade importante no desenvolvimento de novas tecnologias na área biomedicinal.

O sensor desenvolvido na presente invenção é altamente específico para detecção dos níveis de progesterona e 17-β Estradiol, que são hormônios sexuais de concentrações detectáveis, presente nas fêmeas. Esse monitoramento é de suma importância, uma vez que torna a detecção do período fértil mais rápida e precisa. O termo "sensor " usado aqui se refere a um componente que compreende um ou mais meios reativos, estes que estão adaptados para detectar uma ou mais substâncias alvo (também chamadas de analitos), tais como microrganismos ou (bio) moléculas e além disso, ter a capacidade de fornecer um sinal da referida detecção para o usuário, cuidador ou um técnico.

1.4 - Objeto da invenção

A presente invenção enquadra-se no campo da pecuária de corte e de leite e refere-se à um polímero de PMMA, magnético, parte reconhecedora de um sistema eletrônico utilizado como sensor de progesterona e 17-β Estradiol, cujo propósito final consiste na promoção do incremento das taxas de concepção em métodos de Inseminação Artificial (IA) a partir do desenvolvimento de um método de alta precisão de detecção de pico destes hormônios no sangue de vacas.

1.5 - Descrição da invenção

De forma resumida, a elaboração da invenção ocorre em três partes:

(1) Desenvolvimento de um polímero molecularmente impresso de PMMA magnetizado com nanopartículas de ferroxita (δ-FeOOH), altamente seletivo para detecção de progesterona *in vivo* e em amostras biológicas líquidas.

(2) Acoplamento desse material a um eletrodo amperométrico de trabalho para transdução do sinal da molécula adsorvida no PIM.

(3) Vinculação deste aparato a um equipamento que envie o sinal elétrico a um detector a ser implantado no animal, este que enviará o sinal via wi-fi a uma coleira para o monitoramento em tempo real dos níveis hormonais do animal.

A construção do material consiste da polimerização na presença da progesterona/17-β Estradiol e de nanopartículas de ferroxita (δ-FeOOH), utilizando o monômero PMMA (polimetilmetaacrilato) (Figura 1), formando assim um polímero magnético. As propriedades magnéticas do material facilitam sua localização, o que pode ser vantajoso no caso da implantação deste minissistema em animais, para monitoramento em tempo real dos níveis hormonais. Além da propriedade magnética, o monômero empregado na produção do material possui biocompatibilidade, sendo usado inclusive como material de próteses. Por ser um polímero, é um material mais inerte, o que diminui sua interação com o organismo, sendo preferencial à alguns materiais inorgânicos utilizados em sensores hormonais, como é o caso do grafeno, que aumenta a produção de radicais livres no organismo. Adicionalmente, os polímeros são compostos estáveis, de fácil manuseio e baratos, tendo vantagem em relação aos biossensores enzimáticos, já que as enzimas são sensíveis à variação de pH e temperatura, entre outros fatores.

Para inserir nanopartículas magnéticas, estes componentes são pré-tratados com xileno, ácido oleico ou CDS (clorometil-feniletil-dimetilclorosilano), estes que fazem a modificação da superfície para aderência dos monômeros. Em seguida, estes aditivos modificados são dispersos sobre os monômeros de PMMA (3-(trimetóxi-silil)propil metacrilato ou TMSM). Como as nanopartículas de ferroxita (δ-FeOOH) possuem sítios de hidroxila, este pré tratamento não se faz necessário, o que confere outra vantagem ao material (Figura 2).

Após essa etapa, adiciona-se a solução contendo o analito alvo, que nesse caso é a progesterona /17-β estradiol. A mistura das soluções é feita para que a polimerização ocorra com a presença da molécula no meio, formando assim cavidades no local onde estas moléculas se encontrarem (cavidade para posterior adsorção e identificação do analito). Essa solução é denominada pré polimerização. Após a polimerização, as moléculas do hormônio são retiradas por meio de lavagens sucessivas, utilizando solução de etanol:ácido acético, liberando assim as cavidades com formatos específicos (Figura 3). Devido ao formato específico das cavidades, ocorre a adsorção de progesterona, ou moléculas com alta similaridade estrutural, o que garante a alta seletividade do sensor.

Por fim, para testar o material, foram realizadas análises eletroquímicas utilizando a técnica de Voltametria de Pulso Diferencial, empregando eletrodo de pasta

de carbono, contendo 5mg do PIM magnético (Figuras 5-10). Foram realizadas análises nas mesmas condições, utilizando o eletrodo de pasta de carbono (EPC) sem o material. A resposta do EPC foi na faixa de potencial de 0.3V, e não houve resposta na faixa onde o analito responde quando o eletrodo modoficado com o PIM foi utilizado, que é em torno de 0- 0.1 V. Essa é uma vantagem, já que na faixa de 0.3V, a chance de resposta de contaminantes é maior. A diminuição da faixa de potencial é uma característica vantajoas em relação à seletividade do material.

1.6 - Descrição das Figuras/Desenhos/Gráficos

A Figura 1 apresenta a estrutura monomérica (metilmetacrilato) que dá origem ao polímero utilizado nesta invenção. A Figura 2 apresenta um esquema de funcionalização das nanopartículas magnéticas para acoplamento dos monômeros. Na Figura 3, tem-se uma representação do processo geral de polimerização por impressão molecular. Inicialmente os monômeros são misturados ao analito, para formação de um complexo pré-polimerização. Esse complexo é então submetido ao processo de polimerização, na presença do analito. Após a polimerização, o polímero resultante é lavado para retirada das moléculas do analito, que serviram de molde para a formação de cavidades específicas no polímero. Essas cavidades serão depois utilizadas para detecção seletiva da molécula molde.

A Figura 4 representa um protótipo hipotético do sensor, constituído de uma parte eletrônica e pelo material reconhecedor, cuja tecnologia está descrita na presente invenção. As figuras 5-10 apresentam os resultados obtidos por meio de análises eletroquímicas, para detecção dos analitos.

Na Figura 5 encontram-se os resultados para a análise do material na detecção de Estradiol, em concentrações variando de 10 a 50 μM. Na figura 6, essas curvas foram corrigidas para a mesma linha base, e como pode ser melhor observado, houve um aumento da curvatura com a adição do analito. A Figura de número 7 e 8 comparam a detecção de estradiol e progesterona com o sinal obtido para a solução na ausência dos analitos (branco), sendo a última (8) com correção de linha base.

Na Figura 9, podem ser observadas as curvas para análise com o eletrodo de pasta de carbono sem o PIM. Como pode ser observado, não houve resposta na faixa onde o analito responde quando o eletrodo modoficado com o PIM foi utilizado, que é em torno de 0.1 Na figura 10 é possível ver a comparação do eletrodo sem modificação com o eletrodo modificado com o PIM. Como já mencionado, o eletrodo com o PIM mostra um sinal na faixa de 0-0.1, diferente do eletrodo de carbono. Isso pode ser vantajoso também para a seletividade, já que muitos compostos respondem em faixas de potencial maiores, em torno de 0.3.

Figura 1: Monômero de polimetilmetaacrilato (PMMA
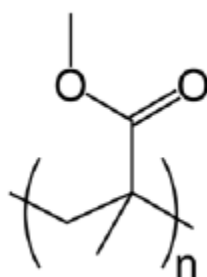
Figura 2: Esquema de magnetização dos monômeros

Moléculas de TMSM + Nanopartículas de δ-FeOOH → PMMA/δ-FeOOH (molécula)
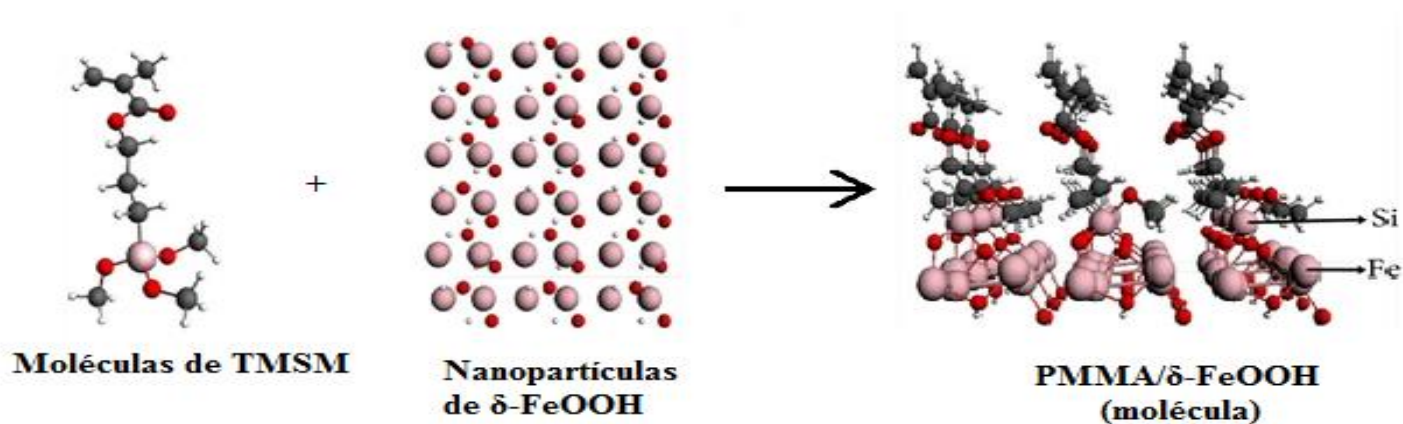
Figura 3: Preparação do PIM de PMMA com nanopartículas de δ-FeOOH em presença de progesterona.
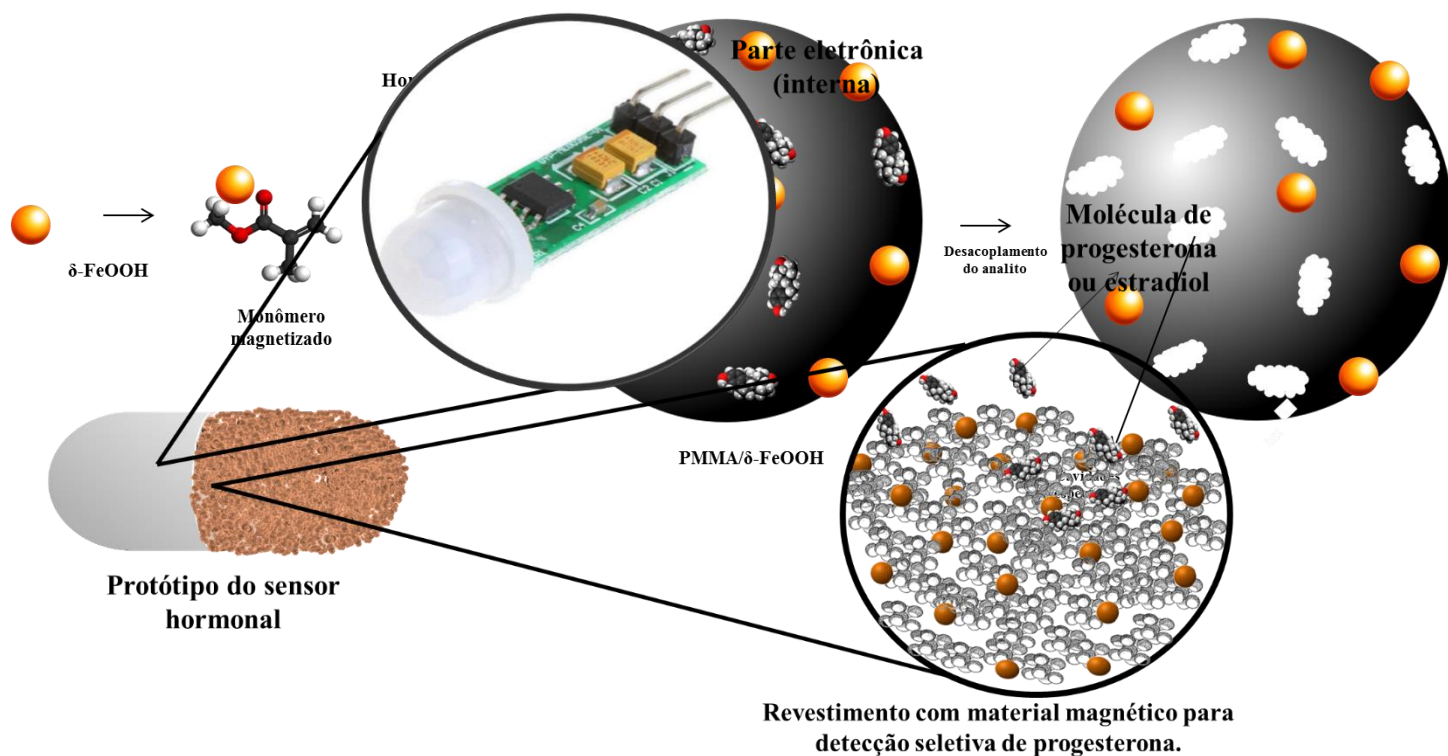
Figura 4: Protótipo do sensor montado

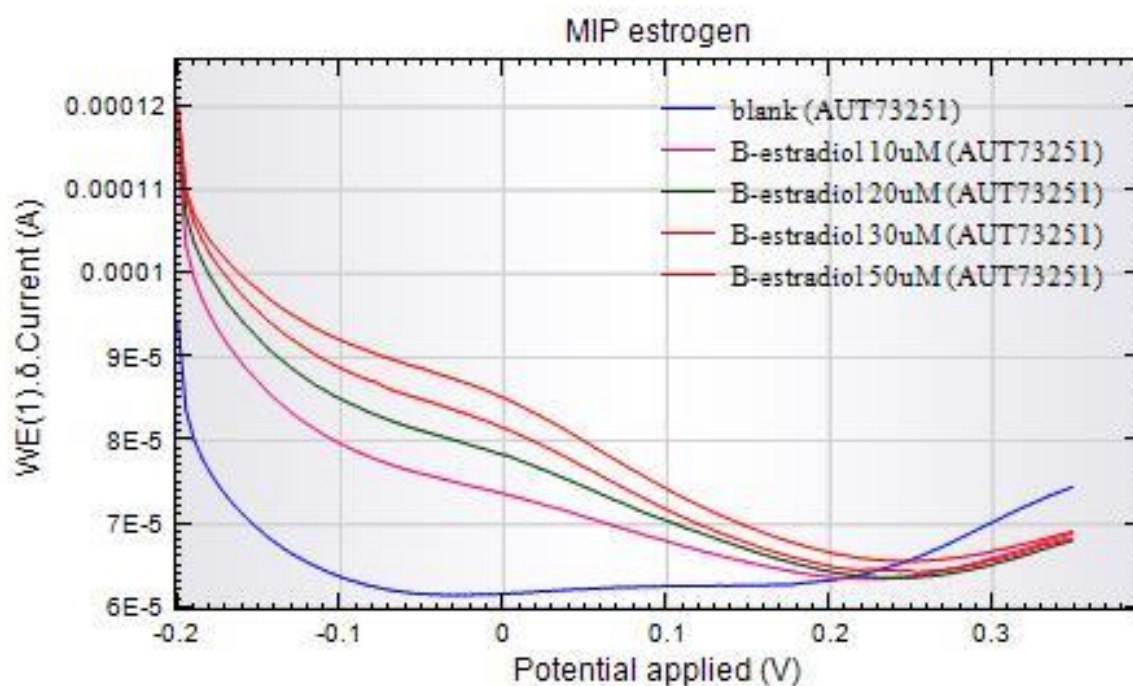**Figura 5:** Voltamograma PIM com adições de β-Estradiol

Figura 6: Voltamograma PIM com adições de β-Estradiol, com correção da linha base.
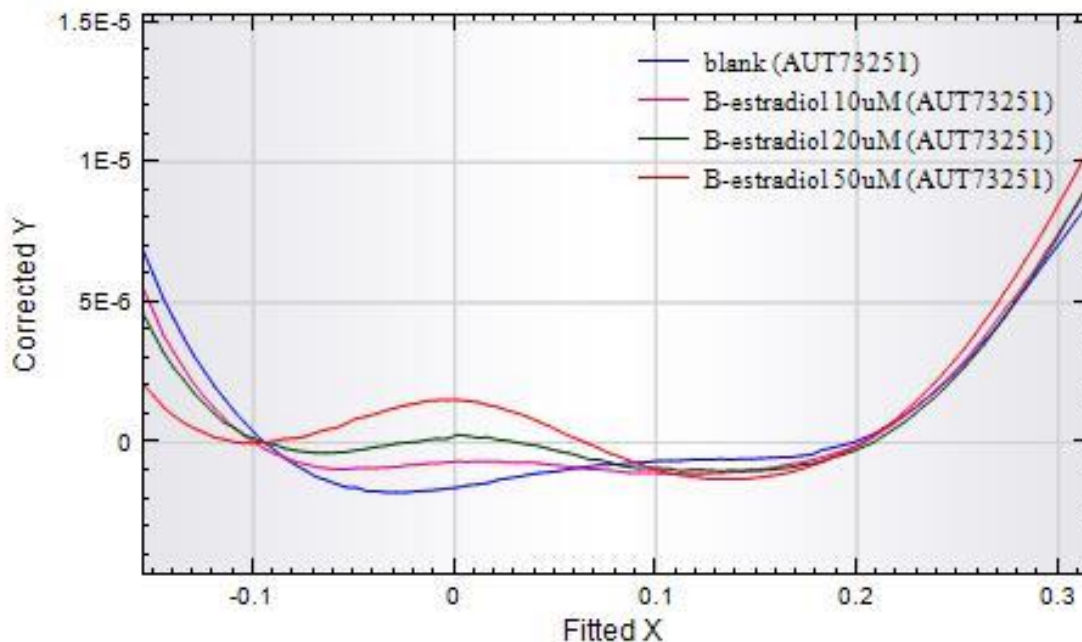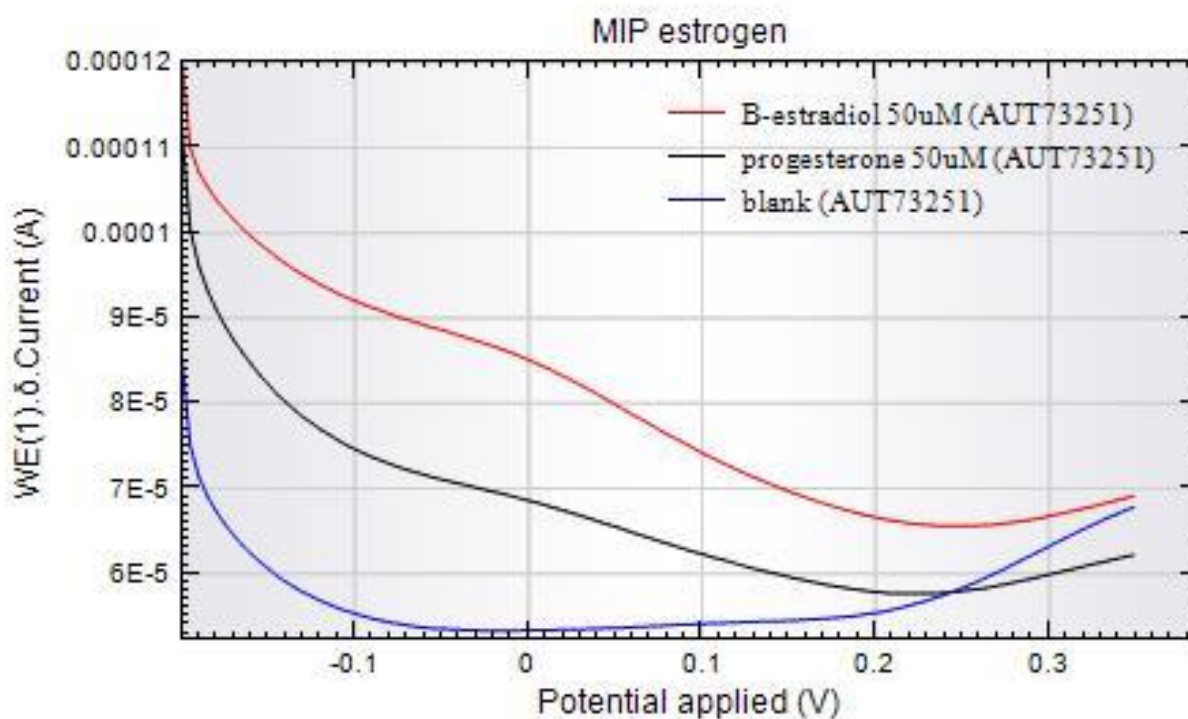

Figura 7: Voltamograma comparando as curvas para a mesma concentração de β-Estradiol e progesterona.

Figura8: Voltamograma comparando as curvas para a mesma concentração de β-Estradiol e progesterona, com correção da linha de base.
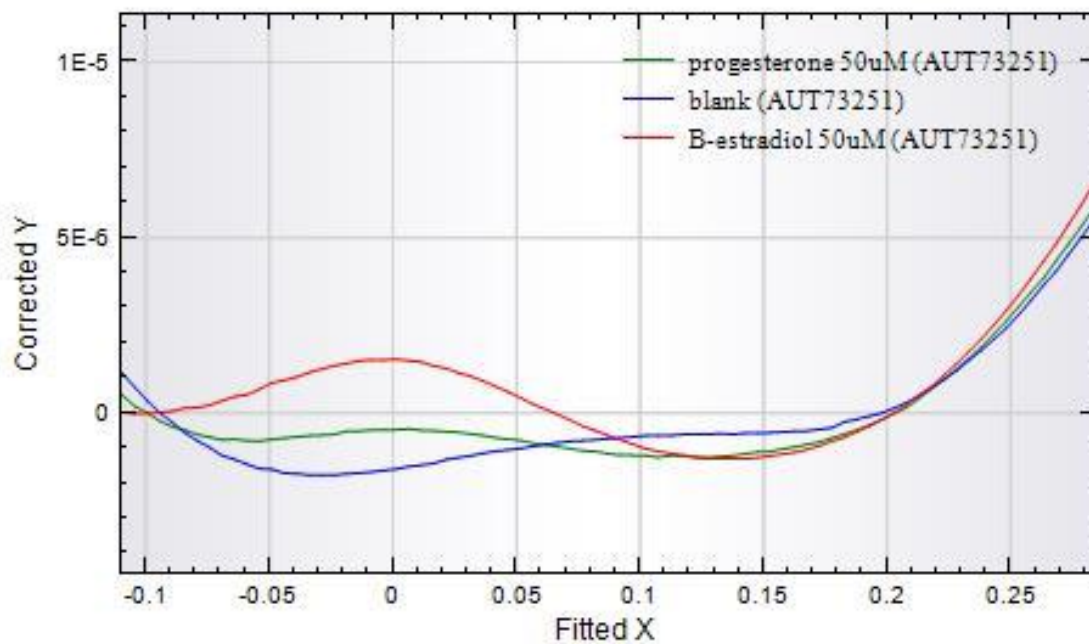
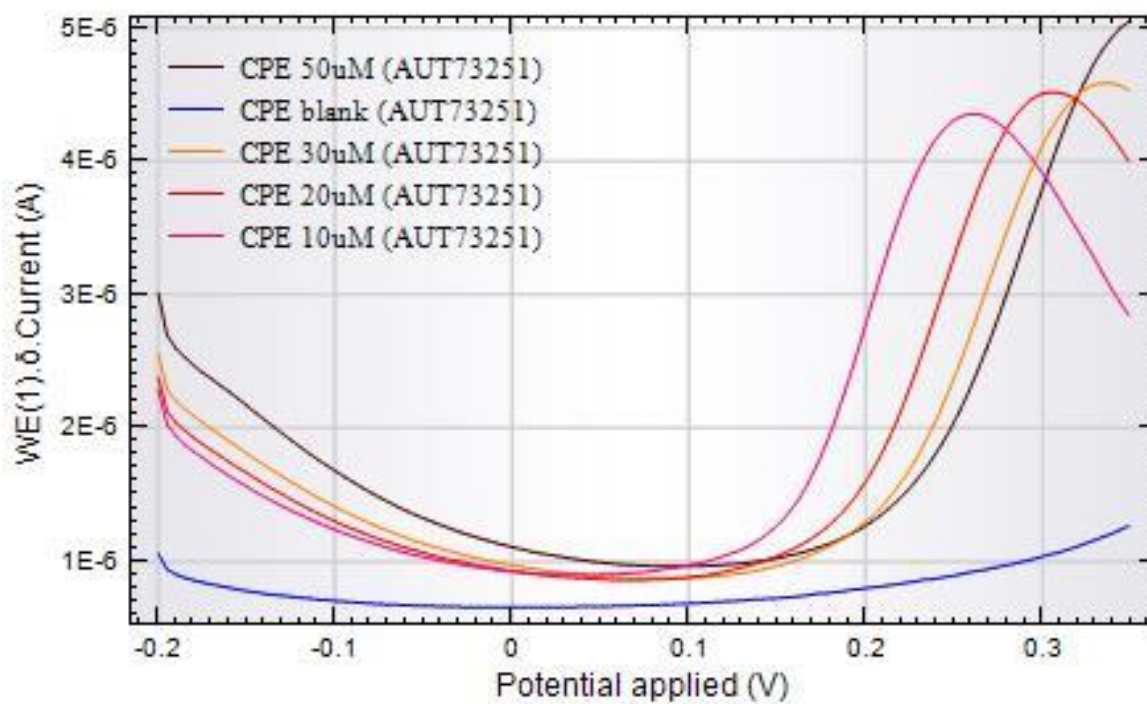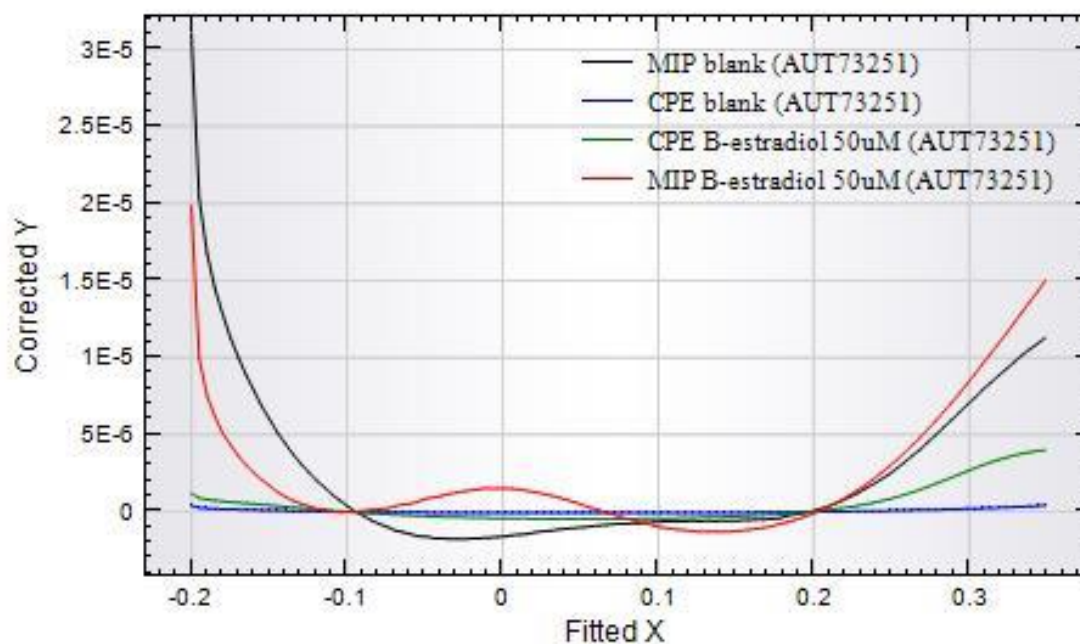**Figura 9:** Voltamograma eletrodo de pasta de carbono com β-Estradiol.

Figura 10: Voltamograma eletrodo de pasta de carbono com β-Estradiol comparado com o eletrodo com PIM.

REIVINDICAÇÕES

1- SENSOR SUBCUTÂNEO BASEADO EM POLÍMERO MAGNÉTICO MOLECULARMENTE IMPRESSO DE FERROXITA/POLIMETILMETACRILATO PARA DETECÇÃO E MONITORAMENTO DE NÍVEIS DE CONCENTRAÇÃO DE HORMÔNIOS REPRODUTIVOS NA CIRCULAÇÃO SANGUÍNEA DE FÊMEAS MAMÍFERAS **caracterizado por** ser parte constituinte de um sistema de detecção de hormônios a ser fixado em um aparato que faz a transdução do sinal.

2- SENSOR SUBCUTÂNEO BASEADO EM POLÍMERO MAGNÉTICO MOLECULARMENTE IMPRESSO DE FERROXITA/POLIMETILMETACRILATO PARA DETECÇÃO E MONITORAMENTO DE NÍVEIS DE CONCENTRAÇÃO DE HORMÔNIOS REPRODUTIVOS NA CIRCULAÇÃO SANGUÍNEA DE FÊMEAS MAMÍFERAS **caracterizado por** utilizar o PIM magnetizado como parte constituinte de sistemas em que o material é submetido a uma reação química, para investigação da variação de concentração dos reagentes, do andamento ou do resultado do processo.

3- SENSOR SUBCUTÂNEO BASEADO EM POLÍMERO MAGNÉTICO MOLECULARMENTE IMPRESSO DE FERROXITA/POLIMETILMETACRILATO PARA DETECÇÃO E MONITORAMENTO DE NÍVEIS DE CONCENTRAÇÃO DE HORMÔNIOS REPRODUTIVOS NA CIRCULAÇÃO SANGUÍNEA DE FÊMEAS MAMÍFERAS **caracterizado por** empregar os monômeros de PMMA como material base para construir sensor de polímero impresso molecularmente para detecção de progesterona.

4- SENSOR SUBCUTÂNEO BASEADO EM POLÍMERO MAGNÉTICO MOLECULARMENTE IMPRESSO DE FERROXITA/POLIMETILMETACRILATO PARA DETECÇÃO E MONITORAMENTO DE NÍVEIS DE CONCENTRAÇÃO DE HORMÔNIOS REPRODUTIVOS NA CIRCULAÇÃO SANGUÍNEA DE FÊMEAS MAMÍFERAS **caracterizado por** empregar os monômeros de PMMA como material base para construir sensor de polímero impresso molecularmente para detecção de 17-β Estradiol.

5- SENSOR SUBCUTÂNEO BASEADO EM POLÍMERO MAGNÉTICO MOLECULARMENTE IMPRESSO DE FERROXITA/POLIMETILMETACRILATO PARA DETECÇÃO E MONITORAMENTO DE NÍVEIS DE CONCENTRAÇÃO DE HORMÔNIOS REPRODUTIVOS NA CIRCULAÇÃO SANGUÍNEA DE FÊMEAS MAMÍFERAS **caracterizado por** empregar os monômeros de PMMA como material base para construir sensor magnético de polímero impresso molecularmente para detecção de hormônios.

6- SENSOR SUBCUTÂNEO BASEADO EM POLÍMERO MAGNÉTICO MOLECULARMENTE IMPRESSO DE FERROXITA/POLIMETILMETACRILATO PARA DETECÇÃO E MONITORAMENTO DE NÍVEIS DE CONCENTRAÇÃO DE HORMÔNIOS

REPRODUTIVOS NA CIRCULAÇÃO SANGUÍNEA DE FÊMEAS MAMÍFERAS **caracterizado por** utilizar a ferroxita (δ-FeOOH) como material magnético na preparação do polímero molecularmente impresso.

7- SENSOR SUBCUTÂNEO BASEADO EM POLÍMERO MAGNÉTICO MOLECULARMENTE IMPRESSO DE FERROXITA/POLIMETILMETACRILATO PARA DETECÇÃO E MONITORAMENTO DE NÍVEIS DE CONCENTRAÇÃO DE HORMÔNIOS REPRODUTIVOS NA CIRCULAÇÃO SANGUÍNEA DE FÊMEAS MAMÍFERAS **caracterizado por** construir um PIM utilizando ferroxita e PMMA para detecção de progesterona e 17-β Estradiol.

8- SENSOR SUBCUTÂNEO BASEADO EM POLÍMERO MAGNÉTICO MOLECULARMENTE IMPRESSO DE FERROXITA/POLIMETILMETACRILATO PARA DETECÇÃO E MONITORAMENTO DE NÍVEIS DE CONCENTRAÇÃO DE HORMÔNIOS REPRODUTIVOS NA CIRCULAÇÃO SANGUÍNEA DE FÊMEAS MAMÍFERAS **caracterizado por** ser seletivo para detecção de progesterona, sendo preparado utilizando esta molécula específica.

9- SENSOR SUBCUTÂNEO BASEADO EM POLÍMERO MAGNÉTICO MOLECULARMENTE IMPRESSO DE FERROXITA/POLIMETILMETACRILATO PARA DETECÇÃO E MONITORAMENTO DE NÍVEIS DE CONCENTRAÇÃO DE HORMÔNIOS REPRODUTIVOS NA CIRCULAÇÃO SANGUÍNEA DE FÊMEAS MAMÍFERAS **caracterizado por** ser seletivo para detecção de 17-β Estradiol, sendo preparado utilizando esta molécula específica.

10- SENSOR SUBCUTÂNEO BASEADO EM POLÍMERO MAGNÉTICO MOLECULARMENTE IMPRESSO DE FERROXITA/POLIMETILMETACRILATO PARA DETECÇÃO E MONITORAMENTO DE NÍVEIS DE CONCENTRAÇÃO DE HORMÔNIOS REPRODUTIVOS NA CIRCULAÇÃO SANGUÍNEA DE FÊMEAS

MAMÍFERAS **caracterizado por** ser um polímero biocompatível para implantação em animais, para monitoramento dos níveis hormonais.

11- SENSOR SUBCUTÂNEO BASEADO EM POLÍMERO MAGNÉTICO MOLECULARMENTE IMPRESSO DE FERROXITA/POLIMETILMETACRILATO PARA DETECÇÃO E MONITORAMENTO DE NÍVEIS DE CONCENTRAÇÃO DE HORMÔNIOS REPRODUTIVOS NA CIRCULAÇÃO SANGUÍNEA DE FÊMEAS MAMÍFERAS **caracterizado por** medir os níveis hormonais em fêmeas mamíferas.

12- SENSOR SUBCUTÂNEO BASEADO EM POLÍMERO MAGNÉTICO MOLECULARMENTE IMPRESSO DE FERROXITA/POLIMETILMETACRILATO PARA DETECÇÃO E MONITORAMENTO DE NÍVEIS DE CONCENTRAÇÃO DE HORMÔNIOS REPRODUTIVOS NA CIRCULAÇÃO SANGUÍNEA DE FÊMEAS MAMÍFERAS **caracterizado por** medir os níveis hormonais em fêmeas bovinas.

13- SENSOR SUBCUTÂNEO BASEADO EM POLÍMERO MAGNÉTICO MOLECULARMENTE IMPRESSO DE FERROXITA/POLIMETILMETACRILATO PARA DETECÇÃO E MONITORAMENTO DE NÍVEIS DE CONCENTRAÇÃO DE HORMÔNIOS REPRODUTIVOS NA CIRCULAÇÃO SANGUÍNEA DE FÊMEAS MAMÍFERAS **caracterizado por** otimizar as taxas de concepção em métodos de Inseminação Artificial (IA) por meio do acompanhamento hormonal utilizando sensor eletroquímico.

3. MEDICAL DIAGNOSIS

3.1. Probing thermal and solvent effects on the interaction between ciprofloxacin and human topoisomerase-II β enzyme: toward new NMR probes

Article submitted to Journal of Molecular Graphics and Modelling.

Abstract:

New tools for cancer diagnosis are being studied day by day, since early diagnosis can be crucial for a successful treatment. In this context, the use of NMR probes constitutes an efficient way of diagnosis. In this work, we investigated the use of ciprofloxacin to indirectly label the overexpression of topoisomerase-II enzymes by means of changes in ^{19}F NMR chemical shifts of ciprofloxacin. Using DFT calculations, a spectroscopy analysis of ciprofloxacin was performed in different chemical environments, evaluating the solvent and enzymatic effects. Our results point out that the ciprofloxacin forms a stable complex with the enzyme, and the main intermolecular interactions between ciprofloxacin and human topoisomerase-IIβ are hydrogen bonds, π-π stacking and electrostatic interactions. Also, a shift of 6.04 ppm occurs in the ^{19}F NMR signal when ciprofloxacin is interacting with the human topoisomerase-IIβ enzyme, and that this parameter may be a possible indirect marker to indicate the overexpression of this enzyme in the body.

Keywords: Spectroscopic probe, computational methods, drug repositioning, cancer diagnosis.

1. **Introduction**

Fluoroquinolones, introduced more than 20 years ago, are a derivative class of quinolones, known for their antibacterial activity [1]. One representative of this class of molecules is the commercialized antibacterial agent ciprofloxacin (CPX) [2–4]. These compounds exert antibacterial activity due to inhibition of two bacterial enzymes, which are DNA gyrase and topoisomerase II enzymes [5,6]. The later enzymes are under continuous investigation for the development of new anticancer drugs, once some evidences indicate increased levels of topoisomerase II in proliferating cancer cells [7–9]. Currently, cancer is one of the deadliest diseases in the world [10–13], and one factor that contributes for many deaths is the difficulty in diagnosing [14–16].

One of the challenges of image diagnosis is to develop a system capable of locating species in different environments to detect outbreaks of cancer in the surgical margins for clinical use with high resolution [14]. In this line, many spectroscopic techniques have been used for detecting tumor cells, as it is the case of Nuclear Magnetic Resonance (NMR) [15,17,18]. Molecules that interact with key enzymes can act as spectroscopic probes [19], and these molecules are

of great interest, once they are highly sensitive and easy to operate, enabling imaging in live systems in a fast way [20].

In CPX molecule, the presence of fluorine atom allows the application of ^{19}F NMR spectroscopy techniques. The large chemical shift range, together with the high sensitivity of the ^{19}F NMR spectroscopy makes ^{19}F NMR an extremely attractive proposition [21]. Naturally occurring fluorine compounds are scarce, and because of this, ^{19}F NMR spectroscopy offers an attractive option for investigating the interactions between proteins and other biomolecules, as well as structure and mechanisms of action of fluorinated inhibitors [22]. In addition to the already mentioned advantages of ^{19}F NMR, it is also worth noting that this technique is particularly useful for studying large proteins that cannot be easily probed by conventional NMR experiments [23].

Computational methods have been widely employed to predict spectroscopic properties of various compounds for various purposes [24–26]. In fact, theoretical methods offer a fast, efficient and practical way to investigate changes in the NMR properties of different compounds, which can be caused by several factors, such as changes in the chemical environment or structure of the molecule, caused by interactions with biological macromolecules [15,27]. In this context, the aim of this study is to investigate theoretically, the behavior of CPX in the human topoisomerase-II β (hTOPO-II) active site, evaluating how this interaction affects the ^{19}F NMR chemical shift of CPX to propose the use of CPX as a spectroscopic NMR probe for cancer diagnosis.

2. Methodology

2.1. Molecular dynamics simulations

The first MD simulation was performed with CPX in active site of hTopo-II enzyme. Therefore, the crystallographic structure of hTOPO-II in complex with DNA (PDB-ID 5ZAD) was obtained from Protein Data Bank [28] while CPX topology and charge data were taken from the Automated Topology Builder (ATB) Repository [29]. The simulation was performed employing GROMACS® Package [30] using Gromos 54a7 force field [31]. The system CPX:hTOPO-IIβ was solvated inside a cubic box with SPC water model. The algorithm steepest descent was employed for minimization step, stopping

minimization when the maximum force was under 10.0 kJ/mol. A heading step of 1 ps was performed in NVT ensemble and for equilibrium simulation in NPT ensemble, the temperature and pressure were respectively controlled by the v-rescale thermostat (300 K) and Berendsen barostat (1 bar). The last simulation step was the performance of 10 ns of MD simulation, using barostat and thermostat Parrinello-Rahman and v-rescale, respectivelly. Coordinates, velocities and energies were saved at 10.0 ps of simulation, obtaining 1000 frames at the end of simulation. For both steps, the leap-frog integrator was adopted.

Finally, to select the best conformations, the optimal wavelet signal compression algorithm (OWSCA) [32] was used. This algorithm is based on a wavelet compression strategy, in which an optimization algorithm is applied to compress the maximum number of wavelet coefficients, instead of using heuristically chosen parameters. A second MD simulation of free CPX in a water box (CPX:explicit water system) was also performed under the same conditions as mentioned above for comparison of ^{19}FNMR chemical shifts.

2.2. ^{19}F NMR chemical shift (δ) calculations

All ^{19}F NMR shielding constant calculations of this step were performed using GAUSIAN 09 software package [33] at DFT level with the B3LYP functional and Duning basis set [34] with diffuse function [35,36] aug-cc-pVDZ, by applying gauge-including atomic orbital (GIAO) method [37]. These levels of theory selected were based on previous parametrization studies performed about NMR calculations [38] for the CPX molecule [25]. QM calculations were made for CPX in the selected snapshots of two MD systems using the ONIOM model [39]. In CPX:explicit water system, the first solvation shell was maintained, and the obtained values were compared with the results obtained for the CPX:hTOPO-II system. Additionally, ^{19}F NMR shielding constants were calculated also for CPX in vacuum (CPX:vacuum), and using the IEF-PCM solvation model [40], employing water as solvent (CPX: implicit water). For both systems, the initial structures were generated from a conformational analysis in Spartan 14® software using molecular mechanics. After this step, ten lowest energy conformations obtained were directed to geometry optimization calculations in Gaussian software at B3LYP/aug-cc-pVDZ level of theory. After

that, NMR calculations were performed in the same way as for the previous systems.

The theoretical ^{19}F NMR chemical shifts were calculated in ppm according to Equation (1) [38]. The chemical shifts were reported relative to the external chemical shit reference CF₃COOH. Theoretical results obtained were compared with experimental data, where measurements were carried out using the same reference compound [41,42].

$$\delta_{teor} = \sigma_{ref}^{cal} - \sigma_{CPX}^{cal} \tag{1}$$

Where σ_{ref}^{cal} and σ_{CPX}^{cal} are the isotropic NMR shieldings of the reference compound (CF₃COOH) and the CPX frame, respectively. To analyze the agreement between theoretical values for chemical shifts and the experimental ^{19}F NMR chemical shifts data, the Δδ calculation was performed using equation 2 that follows [38]:

$$\Delta\delta = \delta_{exp} - \delta^{cal} \tag{2}$$

3. Results and Discussion

3.1. MD simulations

In order to analyze the influence of the chemical environment on the conformational change of CPX, two MD simulations were performed. One simulation was done with CPX in the hTOPO-II active site (CPX:hTOPO-II system) an the other MD simulation was performed with CPX only in a water box (CPX:explicit water). By the analysis of Root Mean Square Deviation (RMSD) of CPX in both systems (Figure 1), it is possible to observe that the systems reached equilibrium around 2000 ps of simulation, and this simulation time was used as a starting time for the selection of representative frames using OWSCA algorithm. As can also be seen in Figure 1, there is a slightly higher flexibility of CPX in the aqueous system, when compared to molecule in the enzyme active site. This makes sense, once that in the active site, the molecule has greater conformational restriction because of the presence of surrounding amino acids, with which it carries out intermolecular interactions. Additionally,

the RMSD levels, mainly for CPX in hTOPO-II active site, are around 0.1 nm (1Å), indicating high stability of the structures [43,44].

Figure 1: RMSD variation for ciprofloxacin molecule inside the active site (CPX:hTOPO-II) and out of the active site of Topoisomerase-II enzyme (CPX: explicit water).
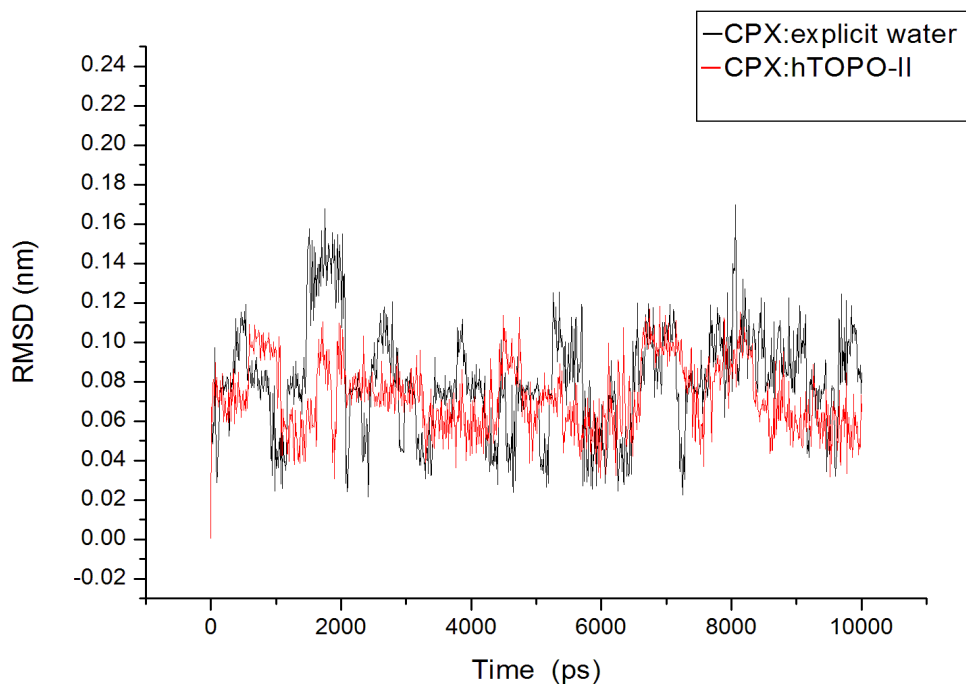
The total energy variation for CPX in both systems CPX:hTOPO-II and CPX:explicit water were got and can be seen in Figure 2. As observed, the values remain balanced over the course of the simulation, showing a stabilization of both systems. Regarding the ligand-protein interaction energy, in the CPX:hTOPO-II system, the total average value got was equal to -94.27 ± 1.02 kJ.mol^{-1}, which corresponds to the sum of the short-range electrostatic (coulombic) interactions, -36.27 ± 0.77 kJ.mol^{-1}, and the short-range Lennard-Jones interactions, whose average value obtained was equal to -58 ± 0.67 kJ.mol^{-1}.

Figure 2: Total Energy variation for CPX:hTOPO-II and CPX:explicit water systems.
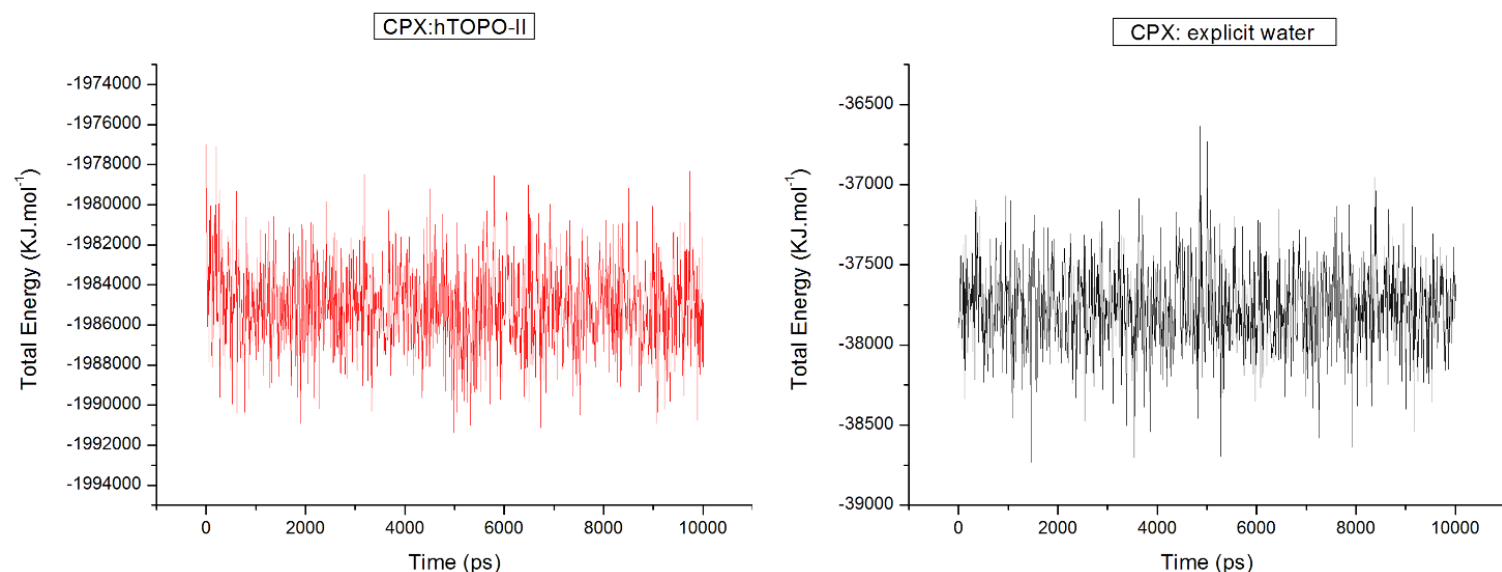
The hydrogen bonds performed between CPX and hTOPO-II were the main interactions responsible for the stability of the molecule in the enzyme active site, as showed in Table 1, which contains the residues that participated in the intermolecular interactions, for the representative conformations selected by OWSCA algorithm. Additionally, the number of hydrogen bonds performed during the MD simulation for all snapshots can be seen in Figure 3. By analyzing this figure, it can be observed that the CPX shows three hydrogen bonds with hTOPO-IIβ, two of which are quite frequent during most of the simulation time.

Table 1: Intermolecular interactions performed between human Topoisomerase-II β enzyme and ciprofloxacin molecule during molecular dynamics simulation.

Frame	Time (ps)	Residue	Interaction type
1	2000	Asn 520	HBond
2	2200	Asn 520	HBond
3	2300	Leu 507	HBond
4	2400	Asn 520	HBond
5	2600	Asn 520; Gln 516	HBond
6	3000	Asn 520	HBond
7	3100	Asn 520	HBond
8	3200	Glu 519; Asn 520; Ala 521	HBond
9	3700	Asn 520; Ala 521	HBond
10	3900	Asn 520; Ala 521	HBond

11	4200	Asn 520	HBond
12	4400	Asn 520; Ala 521	HBond
13	4700	Asn 520; Ala 521	HBond
14	5100	Asn 520; Ala 521	HBond
15	5500	Ala 521	HBond
16	7000	-	-
17	7300	Lys 505	π-π; HBond. Electrostatic
18	7500	-	-
19	7700	Arg 503	HBond
20	7900	Arg 503; Lis 505; Gly 504	π-π
21	8000	-	-
22	8250	Lys 505	HBond; π-π
23	8800	-	-
24	9000	Ile 506	HBond
25	9200	Ile 506	HBond
26	9400	Ile 506	HBond
27	9500	-	
28	9800	Ile 506	HBond
29	10000	Ile 506	HBond

Figure 3: Hydrogen bonds performed between CPX and hTOPO-II beta during the molecular dynamics simulation.
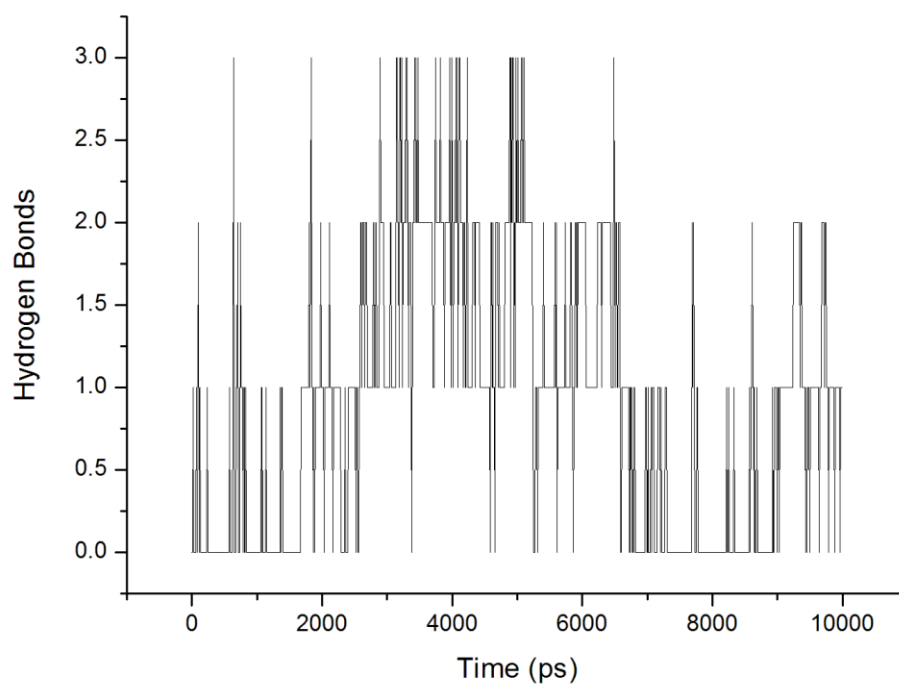
Figure 4-A shows the hydrogen bonds performed for frame 8, at 3200 ps of simulation, which is the time when the greatest number of hydrogen interactions can occur. The residues that take part in the interaction are the Glu 519, Asn 520 and Ala 521. It can also be seen in Figure (3-B), the π-π stacking interactions performed between CPX and amino acids residues Arg 503; Lis 505and Gly 504.

Figure 4: Intermolecular interactions performed during molecular dynamics simulation. A: Hydrogen bonds performed between CPX and the amino acids Glu 519, Asn 520 and Ala 521 at 3200 ps of simulation. B: π-π stacking interactions between CPX and amino acids Arg 503; Lis 505and Glu 504 at 7900 ps of simulation.
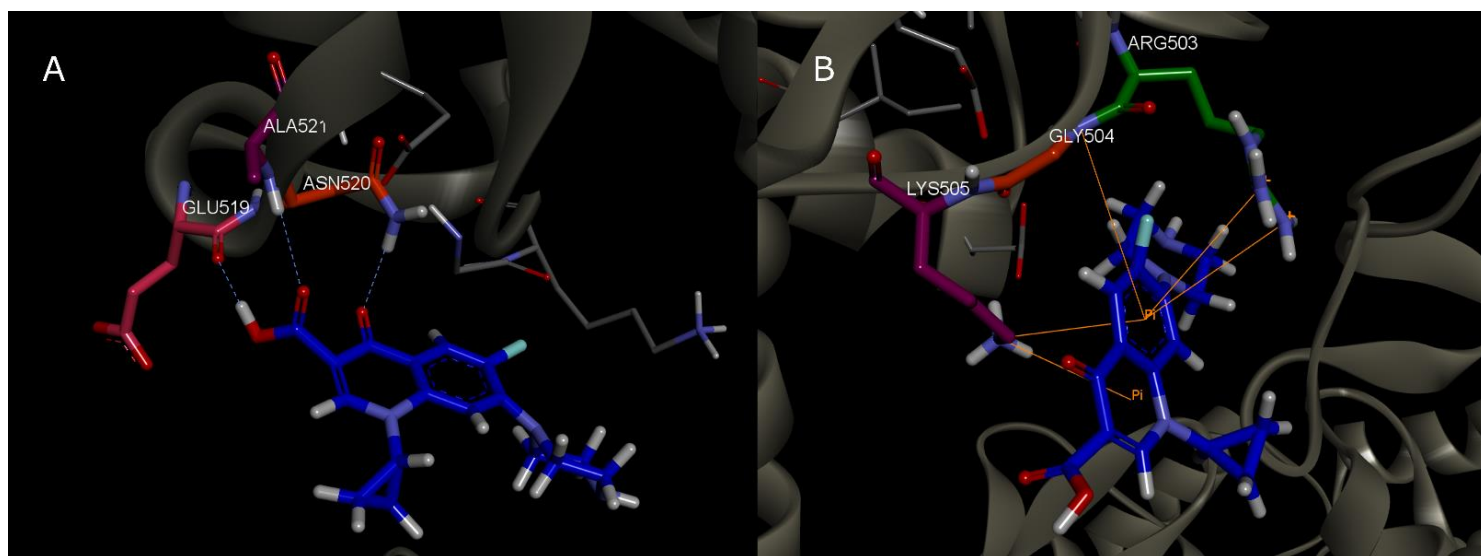
In the next step, the chemical shift calculation was performed for the representative configurations in both systems. For the CPX:explicit water system, the first solvation shell was maintained in order to represent explicit solvent molecules in the NMR calculation. For the CPX:hTOPO-II system, amino acid residues that are taking part in hydrogen interactions with CPX were maintained in order to represent the change in the chemical environment of the molecule inside the active site, since these were the main interactions observed in the MD simulation.

3.2. Spectroscopic parameters: ^{19}F- chemical shifts (δ)

Table 2 contains the average of the calculated values for theoretical ^{19}F NMR chemical shifts in all tested systems. The first point to highlight is the high

similarity between the experimental and the theoretical value obtained for CPX in the CPX:explicit water system. The low $\Delta\delta$ value indicates that the method and the level of theory selected are very accurate for this type of calculation [25]. Second, it is observed that the value obtained in the calculation using the implicit solvation model, CPX:implicit water, is very far from the experimental value. It is worth mentioning that results for the system CPX:implicit is similar to values obtained for CPX in vacuum. Such results show that explicit solvation is more adequate for representing the solvent effect on CPX. It can also be inferred that water molecules explicitly in the theoretical calculation is important since it creates the proper hydrogen bonding network of water molecules for calculating ^{19}F NMR spectroscopic parameters [45].

Table 2: Experimental vs. theoretically computed ^{19}F NMR chemical shifts at DFT/B3LYP/aug-cc-pVDZ level for CPX molecule.

System	^{19}F δ_{ppm}	$\Delta\delta_{ppm}$
CPX:Aqueous solution (experimental)	-43.70	0.00
CPX:Explicit water	-43.54	-0.16
CPX:hTOPO-II	-49.73	6.03
CPX:vacum	-55.11	11.41
CPX:Implicit water	-56.20	12.50

The fluorine nucleus has a high sensitivity compared to the ^{13}C and ^{15}N nuclei, being almost as sensitive as ^{1}H [46]. In this context, although solvent effects can be difficult to observe in nuclei, such as ^{13}C and ^{15}N NMR, for the ^{19}F nucleus, solvent-induced isotopic shifts can offer a very efficient way to probe solvent effects [47]. Now, analyzing the effect on the ^{19}F NMR chemical shifts caused by the interaction between CPX with hTOPO-II β (Table 2 and Figure5), it is observed that there is a variation of 6.03 ppm in relation to experimental/theoretical value for CPX in aqueous solution. This variation in the ^{19}F NMR chemical shift of CPX when it is interacting with the enzyme can provide important information regarding the occurrence of the ligand in the free form, and in the form complexed with the human topoisomerase-IIβ enzyme. The characteristic signal of CPX complexed with the enzyme, thus, constitutes an interesting form of indirect labeling of these proteins, helping to identify their overproduction in the body. Considering that this overexpression of

topoisomerase-II is related to the incidence of cancer [9,48,49]. These results point out CPX as a potential candidate for ^{19}F NMR probe, which can be an ally in the cancer diagnosis [15,21]. Furthermore, the application of fluorine probes is helpful, considering that the natural occurrence of fluorine in biological systems is scarce and the signals from ^{19}F NMR spectroscopy will not find any overlapping background signals to compete with the fluorine probes, making the spectra simpler and easier to analyze [22,23].

Figure 5: Schematic representation of the ^{19}F NMR chemical shift variation for ciprofloxacin when in with complex the human topoisomerase-IIβ enzyme.
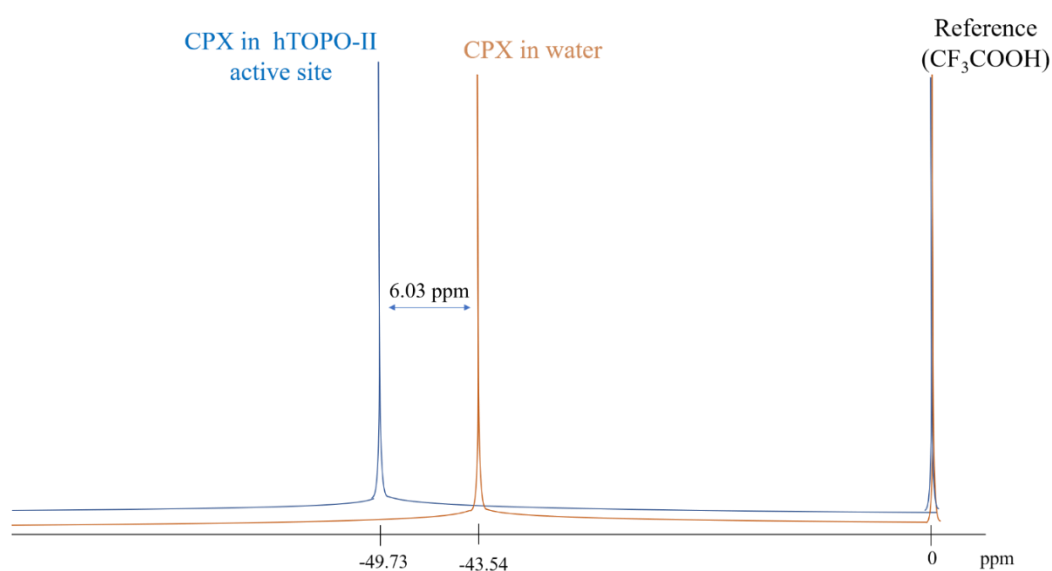
4. Conclusion

Our theoretical findings show that there is a possibility of interaction of the antibacterial agent ciprofloxacin with the human enzyme topoisomerase-IIβ since ciprofloxacin shows, from MD simulations, to form a stable complex with this enzyme. Furthermore, the main ligand-protein interactions that occur are hydrogen bonds. The results also point out that this interaction can alter the ^{19}F NMR chemical shifts signal of ciprofloxacin, when compared to the same parameter for the free molecule in water. Thus, this well-known antimicrobial agent constitutes a possible fluorine NMR probe, capable of indirectly labeling this enzyme in the body.

Regarding that, this molecule shows low toxicity, and it is a commercialized drug widely used worldwide, and can strongly interact with the topoisomerases-II enzyme, ciprofloxacin can be a promising molecule to be used

as an ally in cancer diagnosis, because the overexpression of topoisomerases-II enzymes is associated with cancer. We hope our results will stimulate new experimental and full-dimensional theoretical investigations that could assess the validity of this assumption. In fact, our theoretical findings will increase our understanding of the ciprofloxacin and human topoisomerase-II β enzyme and may provide new insights into how it exerts its anti-carcinogenic effect. This would further help in developing new tools for cancer diagnosis.

5. Acknowledgment

6. Conflicts of interest: Authors have no conflicts of interest.

7. Author Contributions: Sales, T.A. was responsible for methodology, planning and execution of experiments, data validation and analysis, and writing. Ramalho, T.C. was responsible for supervision, analysis, visualization, data validation, project and resource management, formal analysis and writing review.

9. References

[1]   S.K. Pitman, U.T.P. Hoang, C.H. Wi, M. Alsheikh, D.A. Hiner, K.M. Percival, Revisiting oral fluoroquinolone and multivalent cation drug-drug

interactions: Are they still relevant?, Antibiotics. 8 (2019). https://doi.org/10.3390/antibiotics8030108.

[2]   P. Qin, B. Su, R. Liu, Probing the binding of two fluoroquinolones to lysozyme: a combined spectroscopic and docking study, Mol. Biosyst. 8 (2012) 1222. https://doi.org/10.1039/c2mb05423j.

[3]   G.A.R.Y. Suaifan, A.A.M. Mohammed, Fluoroquinolones structural and medicinal developments (2013–2018): Where are we now?, Bioorganic Med. Chem. (2019). https://doi.org/10.1016/j.bmc.2019.05.038.

[4]   R. Ali, F.M. Alminderej, S. Messaoudi, S.M. Saleh, Ratiometric ultrasensitive optical chemisensor film based antibiotic drug for Al(III) and Cu(II) detection, Talanta. 221 (2021). https://doi.org/10.1016/j.talanta.2020.121412.

[5]   M. Abdel-Aziz, S.E. Park, G.E.D.A.A. Abuo-Rahma, M.A. Sayed, Y. Kwon, Novel N-4-piperazinyl-ciprofloxacin-chalcone hybrids: Synthesis, physicochemical properties, anticancer and topoisomerase i and II inhibitory activity, Eur. J. Med. Chem. 69 (2013) 427–438. https://doi.org/10.1016/j.ejmech.2013.08.040.

[6]   P.P. Majalekar, P.J. Shirote, Fluoroquinolones: Blessings Or Curses, Curr. Drug Targets. 21 (2020) 1354–1370. https://doi.org/10.2174/1389450121666200621193355.

[7]   H. Zhou, J. Tang, J. Zhang, B. Chen, J. Kan, W. Zhang, J. Zhou, H. Ma, A red lysosome-targeted fluorescent probe for carboxylesterase detection and bioimaging, J. Mater. Chem. B. 7 (2019) 2989–2996. https://doi.org/10.1039/C9TB00310J.

[8]   Kirk E. Hevenern, K.E.L. Tatsiana A. Verstak, J.W.M. Daniel L. Riggsbee, Recent developments in topoisomerase-targeted cancer chemotherapy, Acta Pharm. Sin. B. 8 (2018) 844–861. https://www.ncbi.nlm.nih.gov/pmc/articles/PMC6251812/pdf/main.pdf (accessed October 16, 2019).

[9]   M.A. Cinelli, Topoisomerase 1B poisons: Over a half-century of drug leads, clinical candidates, and serendipitous discoveries, Med. Res. Rev. 39 (2019) 1294–1337. https://doi.org/10.1002/med.21546.

[10]   S. Chaudhuri, B. Pahari, P.K. Sengupta, Ground and excited state proton transfer and antioxidant activity of 7-hydroxyflavone in model membranes:

Absorption and fluorescence spectroscopic studies, Biophys. Chem. 139 (2009) 29–36. https://doi.org/10.1016/J.BPC.2008.09.018.

[11] N. Dan, S. Setua, V. Kashyap, S. Khan, M. Jaggi, M. Yallapu, S. Chauhan, N. Dan, S. Setua, V.K. Kashyap, S. Khan, M. Jaggi, M.M. Yallapu, S.C. Chauhan, Antibody-Drug Conjugates for Cancer Therapy: Chemistry to Clinical Implications, Pharmaceuticals. 11 (2018) 32. https://doi.org/10.3390/ph11020032.

[12] F. Bray, J. Ferlay, I. Soerjomataram, R.L. Siegel, L.A. Torre, A. Jemal, Global cancer statistics 2018: GLOBOCAN estimates of incidence and mortality worldwide for 36 cancers in 185 countries, CA. Cancer J. Clin. 68 (2018) 394–424. https://doi.org/10.3322/caac.21492.

[13] A.E. Kassab, E.M. Gedawy, Novel ciprofloxacin hybrids using biology oriented drug synthesis (BIODS) approach: Anticancer activity, effects on cell cycle profile, caspase-3 mediated apoptosis, topoisomerase II inhibition, and antibacterial activity, Eur. J. Med. Chem. 150 (2018) 403–418. https://doi.org/10.1016/j.ejmech.2018.03.026.

[14] N. Lue, J.W. Kang, C.-C. Yu, I. Barman, N.C. Dingari, M.S. Feld, R.R. Dasari, M. Fitzmaurice, Portable Optical Fiber Probe-Based Spectroscopic Scanner for Rapid Cancer Diagnosis: A New Tool for Intraoperative Margin Assessment, PLoS One. 7 (2012) e30887. https://doi.org/10.1371/journal.pone.0030887.

[15] B.T.L. Pereira, M.A. Gonçalves, D.T. Mancini, K. Kuca, T.C. Ramalho, First attempts of the use of 195Pt NMR of phenylbenzothiazole complexes as spectroscopic technique for the cancer diagnosis, Molecules. 24 (2019). https://doi.org/10.3390/molecules24213970.

[16] E.P. da Rocha, H.A. Rodrigues, E.F.F. da Cunha, T.C. Ramalho, Probing kinetic and thermodynamic parameters as well as solvent and substituent effects on spectroscopic probes of 2-amino-1,4-naphthoquinone derivatives, Comput. Theor. Chem. 1096 (2016) 17–26. https://doi.org/10.1016/j.comptc.2016.09.028.

[17] H. Saleem, A. Maryam, S.A. Bokhari, A. Ashiq, S.A. Rauf, R.R. Khalid, F.A. Qureshi, A.R. Siddiqi, Design, synthesis, characterization and computational docking studies of novel sulfonamide derivatives, EXCLI J. 17 (2018) 169–180. https://doi.org/10.17179/EXCLI2017-886.

[18]   M.A. Gonçalves, B. Pereira, C. Tavares, T. Martins, E. Cunha, T. Ramalho, Value of contrast-enhanced Magnetic Resonance Imaging (MRI) in the diagnosis of breast cancer, Mini-Reviews Med. Chem. 21 (2021). https://doi.org/10.2174/1389557521666210521113155.

[19]   Z.-Y. Tang, Y. Zhang, Y.-T. Chen, Q. Yu, L.-K. An, The first small fluorescent probe as Tyrosyl-DNA phosphodiesterase 1 (TDP1) substrate, Dye. Pigment. 169 (2019) 45–50. https://doi.org/10.1016/J.DYEPIG.2019.05.010.

[20]   J. Zhou, H. Ma, Design principles of spectroscopic probes for biological applications,   Chem.   Sci.   7   (2016)   6309–6315. https://doi.org/10.1039/C6SC02500E.

[21]   P.D. Stanley, Principles and Topical Applications of 19F NMR Spectrometry,   Organofluorines.   (2002)   1–61. https://doi.org/10.1007/10721878_1.

[22]   E.N.G. Marsh, Y. Suzuki, Using 19F NMR to Probe Biological Interactions of Proteins and Peptides, ACS Chem. Biol. 9 (2014) 1242–1250. https://doi.org/10.1021/CB500111U.

[23]   D. Gimenez, A. Phelan, C.D. Murphy, S.L. Cobb, 19F NMR as a tool in chemical biology, Beilstein J. Org. Chem. 1728. 17 (2021) 293–318. https://doi.org/10.3762/BJOC.17.28.

[24]   R. Jawaria, M. Hussain, M. Khalid, M.U. Khan, M.N. Tahir, M.M. Naseer, A.A.C. Braga, Z. Shafiq, Synthesis, crystal structure analysis, spectral characterization and nonlinear optical exploration of potent thiosemicarbazones based compounds: A DFT refine experimental study, Inorganica Chim. Acta. 486 (2019) 162–171. https://doi.org/10.1016/j.ica.2018.10.035.

[25]   A. Koch, B. Stamboliyska, B. Mikhova, P. Breznica-Selmani, K. Mladenovska, E. Popovski, Calculations of 13C NMR chemical shifts and F–C coupling constants of ciprofloxacin, Magn. Reson. Chem. 57 (2019) S75–S84. https://doi.org/10.1002/MRC.4827.

[26]   D. Ghosh, S. Rhodes, D. Winder, A. Atkinson, J. Gibson, W. Ming, C. Padgett, S. Landge, K. Aiken, Spectroscopic investigation of bis-appended 1,2,3-triazole probe for the detection of Cu(II) ion, J. Mol. Struct. 1134 (2017) 638–648. https://doi.org/10.1016/J.MOLSTRUC.2016.12.096.

[27]   T.C. Ramalho, C.A. Taft, Thermal and solvent effects on the NMR and UV parameters of some bioreductive drugs, J. Chem. Phys. 123 (2005) 054319. https://doi.org/10.1063/1.1996577.

[28]   H.M. Berman, J. Westbrook, Z. Feng, G. Gilliland, T.N. Bhat, H. Weissig, I.N. Shindyalov, P.E. Bourne, The Protein Data Bank., Nucleic Acids Res. 28 (2000) 235–42. http://www.ncbi.nlm.nih.gov/pubmed/10592235 (accessed February 1, 2018).

[29]   A.K. Malde, L. Zuo, M. Breeze, M. Stroet, D. Poger, P.C. Nair, C. Oostenbrink, A.E. Mark, An Automated force field Topology Builder (ATB) and repository: Version 1.0, J. Chem. Theory Comput. 7 (2011) 4026–4037. https://doi.org/10.1021/ct200196m.

[30]   M.J. Abraham, T. Murtola, R. Schulz, S. Páll, J.C. Smith, B. Hess, E. Lindah, Gromacs: High performance molecular simulations through multi-level parallelism from laptops to supercomputers, SoftwareX. 1–2 (2015) 19–25. https://doi.org/10.1016/j.softx.2015.06.001.

[31]   M. Christen, P.H. Hünenberger, D. Bakowies, R. Baron, R. Bürgi, D.P. Geerke, T.N. Heinz, M.A. Kastenholz, V. Kräutler, C. Oostenbrink, C. Peter, D. Trzesniak, W.F. van Gunsteren, The GROMOS software for biomolecular simulation: GROMOS05, J. Comput. Chem. 26 (2005) 1719–1751. https://doi.org/10.1002/jcc.20303.

[32]   M.A. Gonçalves, L.S. Santos, D.M. Prata, F.C. Peixoto, E.F.F. da Cunha, T.C. Ramalho, Optimal wavelet signal compression as an efficient alternative to investigate molecular dynamics simulations: application to thermal and solvent effects of MRI probes, Theor. Chem. Acc. 136 (2017) 15. https://doi.org/10.1007/s00214-016-2037-z.

[33]   and D.J.F. M. J. Frisch, G. W. Trucks, H. B. Schlegel, G. E. Scuseria, M. A. Robb, J. R. Cheeseman, G. Scalmani, V. Barone, B. Mennucci, G. A. Petersson, H. Nakatsuji, M. Caricato, X. Li, H. P. Hratchian, A. F. Izmaylov, J. Bloino, G. Zheng, J. L. Sonnenberg, M. Had, Gaussian 09, Gaussian, Inc., Wallingford CT, 2009.

[34]   T.H.D. Jr., Gaussian basis sets for use in correlated molecular calculations. I. The atoms boron through neon and hydrogen, J. Chem. Phys. 90 (1998) 1007. https://doi.org/10.1063/1.456153.

[35]   R.A. Kendall, T.H.D. Jr., R.J. Harrison, Electron affinities of the first-row atoms revisited. Systematic basis sets and wave functions, J. Chem. Phys. 96 (1998) 6796. https://doi.org/10.1063/1.462569.

[36]   D.E. Woon, T.H.D. Jr., Gaussian basis sets for use in correlated molecular calculations. III. The atoms aluminum through argon, J. Chem. Phys. 98 (1998) 1358. https://doi.org/10.1063/1.464303.

[37]   K. Wolinski, J.F. Hinton, P. Pulay, Efficient implementation of the gauge-independent atomic orbital method for NMR chemical shift calculations, J.   Am.   Chem.   Soc.   112   (2002)   8251–8260. https://doi.org/10.1021/JA00179A005.

[38]   R. Mejía-Urueta, K. Mestre-Quintero, R. Vivas-Reyes, DFT-GIAO Calculation of Properties of 19 F NMR and Stability Study of Environmentally Relevant Perfluoroalkylsulfonamides (PFASAmide), Artic. J. Braz. Chem. Soc. 22 (2268).

[39]   S. Dapprich, I. Komáromi, K.S. Byun, K. Morokuma, M.J. Frisch, A new ONIOM implementation in Gaussian98. Part I. The calculation of energies, gradients, vibrational frequencies and electric field derivatives, J. Mol. Struct. THEOCHEM.   461–462   (1999)   1–21.   https://doi.org/10.1016/S0166-1280(98)00475-8.

[40]   A. V Marenich, C.J. Cramer, D.G. Truhlar, Universal Solvation Model Based on Solute Electron Density and on a Continuum Model of the Solvent Defined by the Bulk Dielectric Constant and Atomic Surface Tensions, (n.d.). https://doi.org/10.1021/jp810292n.

[41]   S. Trefi, V. Gilard, M. Malet-Martino, R. Martino, Generic ciprofloxacin tablets contain the stated amount of drug and different impurity profiles: A 19F, 1H and DOSY NMR analysis, J. Pharm. Biomed. Anal. 44 (2007) 743–754. https://doi.org/10.1016/j.jpba.2007.02.031.

[42]   F.-F. Zhang, M.-H. Jiang, L.-L. Sun, F. Zheng, L. Dong, V. Shah, W.-B. Shen, Y. Ding, Quantitative analysis of sitagliptin using the 19 F-NMR method: a universal technique for fluorinated compound detection, Analyst. 140 (2015) 280–286. https://doi.org/10.1039/C4AN01681E.

[43]   T.A. Sales, S. Marcussi, E.F.F. da Cunha, K. Kuca, T.C. Ramalho, Can inhibitors of snake venom phospholipases A$_2$ lead to new insights

into anti-inflammatory therapy in humans? A theoretical study, Toxins (Basel). 9 (2017). https://doi.org/10.3390/toxins9110341.

[44] W. Schreiner, R. Karch, B. Knapp, N. Ilieva, Relaxation estimation of RMSD in molecular dynamics immunosimulations, Comput. Math. Methods Med. 2012 (2012). https://doi.org/10.1155/2012/173521.

[45] E.Y.L. and, J.T. Gerig*, Origins of Fluorine NMR Chemical Shifts in Fluorine-Containing Proteins†, J. Am. Chem. Soc. 122 (2000) 4408–4417. https://doi.org/10.1021/JA992107W.

[46] M. Modo, 19F Magnetic Resonance Imaging and Spectroscopy in Neuroscience, Neuroscience. (2021). https://doi.org/10.1016/J.NEUROSCIENCE.2021.03.016.

[47] F. Evanics, J.L. Kitevski, I. Bezsonova, J. Forman-Kay, R.S. Prosser, 19F NMR studies of solvent exposure and peptide binding to an SH3 domain, Biochim. Biophys. Acta - Gen. Subj. 1770 (2007) 221–230. https://doi.org/10.1016/J.BBAGEN.2006.10.017.

[48] A.K. McClendon, N. Osheroff, DNA topoisomerase II, genotoxicity, and cancer., Mutat. Res. 623 (2007) 83–97. https://doi.org/10.1016/j.mrfmmm.2007.06.009.

[49] T. Idowu, F. Schweizer, Ubiquitous nature of fluoroquinolones: The oscillation between antibacterial and anticancer activities, Antibiotics. 6 (2017). https://doi.org/10.3390/antibiotics6040026.

3.2. Ciprofloxacin/Topoisomerase-II complex as a promising dual UV-Vis/fluorescent probe: accomplishments and opportunities for the cancer diagnosis

Article accepted for publication in Theoretical Chemistry Accounts Journal.

Abstract:

In this work, a dual UV-Vis/fluorescent probe to be used in cancer diagnosis is proposed, by theoretical investigations of the interaction of ciprofloxacin (CPX) molecule with human Topoisomerase-II β enzyme, and its respective excited state properties. Molecular docking simulations suggest CPX has similar inhibitory effects for human and bacteria Topoisomerase-II, and for human enzyme, CPX interacts preferentially in the same site of chemotherapeutic etoposide (EVP). In TD-DFT parametrization for CPX, it was found that Global Hybrid functionals containing exactly 25% of exact exchange contribution, as mPW1PW91 and PBE0, are most suitable to computing excitation energies for CPX and explicit solvent model calculations allows results closer to the real. For excited state properties, theoretical calculations show that there are changes in absorption energy of CPX, and the distance between Tyrosine 821 residue of human enzyme and CPX can also show a Fluorescence resonance energy transfer (FRET) between the two molecules. Therefore, it is suggested in this work that both the variation in the absorption energy of the CPX (UV-Vis spectra) and the variation in the excitation energy of Tyr (821) (Fluorescence spectra) can be used in a dual sensor to monitor the overexpression of hTOPO-II, constituting a promising tool in cancer diagnosis.

Keywords: dual probe, theoretical calculation, cancer diagnosis, drug repurposing.

Statements and Declarations

Competing interests: Authors have no conflicts of interest

1.Introduction

Cancer is the name given to a set of diseases, which has as fundamental characteristic the disordered growth of cells, and is a leading cause of morbidity and mortality, affecting populations worldwide [1]. There are around to 200 different known cancers [2] and just in 2020, the estimated number of cancer cases for both sexes and all ages by International Agency for Research on Cancer of Word Health Organization is approximately 9.5 million in Asia, 4.4 million for Europe, 2.5 million in North America, 1.5 million in Latin America and 1 million in Africa [3, 4].

Although there is no cure yet for cancer, an early and accurate diagnosis can be decisive in the disease's progression, helping in overall therapeutic outcome [5]. In this context, the improvement and development of effective new techniques for detecting tumor biomarkers is a constant concern in several research lines [6–9]. Fluorescence spectroscopy has been used in several medical subspecialties as a diagnostic tool, playing an important role for rapid and sensitive diagnosis [10, 11]. With cancer detection and treatment, the use of fluorescent probes was reported in 1990 [12], being widely studied until current days [13, 14]. Additionally to fluorescent probes, the possibility of a dual signaling by addition of UV-Vis parameters can improve the accuracy of the results, allowing mutual detection, which increases the sensibility and selectivity of the diagnostic technique, mainly in biological surroundings [15].

Considering the overexpression of topoisomerase-II enzymes in proliferating cancer cells [16–19], this enzyme can be used as an important cancer biomarker. Besides that, fluoroquinolones as ciprofloxacin (CPX), enrofloxacin, moxifloxacin and gatifloxacin are Topo-II inhibitors, and exhibit marked toxicity against many cancer cells [18]. CPX molecule, specifically, is widely reported in literature by its anticancer activity against lung cancer cells [20], breast cancer MDA-MB-231 cells [18, 21],

pancreatic cancer cells [22], among others. Regarding all available information, and that both Topo-II enzyme Tyr residue and CPX molecule presents fluorescence, it may be suggested that CPX/Topo-II complex can be a promising and powerful tool in the cancer diagnosis. In this context, the current work brings a theoretical investigation about CPX/human Topo-II interactions and the possibility of using these interactions as a target for the development of a dual signaling approach in the cancer diagnosis.

2.Methodology

The goal of this work was to analyze the possibility of using CPX/Topo-II enzyme complex as a dual UV-Vis/fluorescent probe for cancer diagnosis. For this, the strategy chosen was to evaluate CPX in different chemical environments (vacuum, water solvent and inside the enzyme interaction site) and to verify changes in UV-Vis or fluorescence properties of CPX and/or enzyme. Bearing this in mind, theoretical calculations were separated into three main sections, which are (i) computational methods validation, (ii) Docking calculations between CPX and Topo-II enzyme and (iii) theoretical calculations of UV-Vis/fluorescence parameters.

2.1. Validation of computational methods

2.1.1. Selection of the most appropriate DFT functional

The Time-dependent Density Theory (TD-DFT) was employed in the theoretical investigation of excited states of free CPX and CPX in complex with human Topo-II enzyme. To analyze best Exchange-correlation (EXC) functional to compute excited states properties, free CPX was submitted to a conformational analysis, employing water in explicit solvent model calculation, generating 25 different conformations. After this, single point energy (SPE) calculations were performed for the six first states of the obtained conformations, using 6-31g(d,p) basis set. For SPE calculations, six EXC functionals were tested, which are the GH functionals B3LYP (EE=20%), mPW1PW91 (EE=25%), PBE0 (EE=25%), and M05-2X (EE=56%); and the LCH functionals LC-ωPBE and ωB97X-D (both ω= 0.2 bohr-1). As selection criteria, the obtained absorption energy and the wavelength values for each conformation and functional were got and compared with the experimental absorption energy value for CPX in water [23,

24]. In addition, the hypothesis T test was performed for the analysis between theoretical and experimental values. A boxplot was also generated using the R program [25] to verify outliers between the calculated values.

2.1.2. Implicit vs. explicit solvent models

To investigate the solvation mode effects in theoretical results, the polarization continuum model (PCM) together with integral equation formalism polarization continuum model (IEF-PCM) was used and compared with results got with explicit water calculations of the previous step.

Initially, CPX was built in Spartan 14 program and a conformer distribution was performed using MMFF molecular mechanics to get the lowest energy conformers. This procedure generated 25 conformations, which were employed for geometry optimizations and SPE calculations using the IEF-PCM solvation model and water as solvent. Time-dependent DFT calculations, solved for the six first states, at PW1PW91/6-31G (d,p) level of theory were performed. Vacuum calculation was also carried out in the same conditions.

2.2. Molecular docking simulations for CPX/ human and bacterial Topo-II

Molecular docking calculations, employing Molegro Virtual Docker Program [26], were performed in order to investigate the interaction between CPX and human Topo-II enzyme (hTOPO-II), in comparison with the bacterial Topo-II enzyme (bTOPO-II). For analysis, crystallographic structure of hTOPO-II in complex with DNA and etoposide (EVP) ligand (PDB-ID 3QX3) as well as the Mycobacterium tuberculosis bTOPO-II in complex with CPX molecule (PDB-ID 5BTC) were obtained from Protein Data Bank [27]. Electrostatic charges of CPX were calculated in Gaussian 09 Software at the HF 6-31G level of theory.

Here, three docking simulations were performed. The first docking calculation was carried out with CPX in bTOPO-II. For this, residues within a radius of 10 Å of cavity were considered flexible, and the analysis was performed using a 7 Å sphere constraint and 30 runs. 30 different conformations were got and analyzed later using the best interaction energy and best overlap as criteria. The other two calculations were

performed with CPX in hTOPO-II, aiming to compare the interaction of the ligand in the both enzymes. One of them was done with CPX in the active site (AS1) of hTOPO-II. For this, residues in a radius of 8 Å of the active site were adopted as flexible and the calculation was performed in 30 steps, employing a sphere with 5 Å of radius as constraint (the cavity size was considered). The other was performed with the molecule in the active ligand (EVP) site (AS2), considering the residues in a radius of 10 Å around the cavity as flexible a constraint sphere of 7 Å and performing 30 runs. For both calculations, 30 conformations were obtained and analyzed using the same criteria as the previous analysis. The distance between CPX and Tyr aminoacid residue was analyzed for both conformations to investigate the possibility of FRET occurrence.

2.3. Spectroscopic properties

2.3.1. UV-Vis parameters

To establish a relationship between the environment and the CPX absorption energy, the best conformations obtained in molecular docking simulations were submitted to TD-DFT calculations. In order to simulate the proteic environment, main amino acids residues in the hTopo-II active site were kept. For theoretical UV-Vis calculation of CPX, the system was divided into two layers using ONIOM method in Gaussian 09 Software [28]. In low layer (CPX molecule), TD-DFT calculations were performed for both conformations. According to previous selection, the level of theory used was mPW1PW91 functional and 6-31g(d, p) basis set, for the six first states. The obtained results were compared with the theoretical and experimental results in water solution.

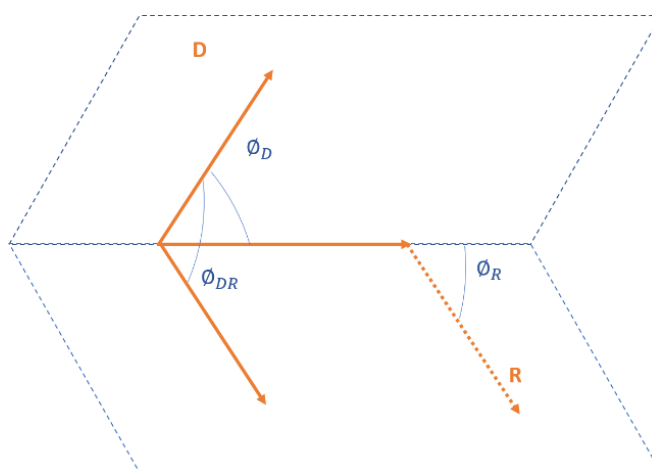### 2.3.2 Fluorescence resonance energy transfer (FRET)

The energy transfer model proposed by Förster [29] is a molecular non-radiative process that allows the transference of energy from an excited donor to an acceptor, due to long-range dipole-dipole interactions. For FRET occurrence, it is necessary a resonant condition between the oscillations of the excited state electrical field of the donor and ground state of the acceptor, besides the superposition between donor emission and acceptor absorption spectra, and also a favorable spatial orientation

between the electrical dipoles of the two states directly involved [30]. According to FRET energy transfer mechanism, K2 is the term that describes the orientation of the donor and the acceptor in the space, and is given for equation (1) [30]:

$$K^2 = cos\emptyset_{DR} - 3\ cos\emptyset_D cos\emptyset_R \tag{1}$$

Where $cos\emptyset_{DR}$ is the angle between the transition dipole moments of donor and receptor, $cos\emptyset_D$ the angle between donor dipole moment and vector that bind to receptor, and $cos\emptyset_R$ the angle between the receptor dipole moment and the vector that bind to donor (Figure 1), being the dipole moment a larger in excited state than in the ground state.

Fig. 1 Transition dipoles of donor (D) and receptor (R) and the dependence of orientation factor for FRET mechanism.

For analysis of the possibility of FRET occurrence between CPX and hTOPO-II enzyme, Förster fluorescence resonance energy transfer (FRET) theory was employed. FERT can evaluate the energy exchange between CPX and Tyr821. In fact, this analysis is related to center enlarged van der Waals spheres for interaction points between CPX and Tyr821, as proposed by Prandi, Ramalho and França (2019) [14]. Thus, we can use the superimposition volume as a preliminary study to have a clue about the probability of energy exchange.

3. Results & Discussion

This section was divided into three principal parts, following the order established in the method section. First, the validation of computational methods related

to (i) DFT EXC functional and (ii) solvation models for investigating spectroscopic parameters of CPX in solution. Second, the molecular docking studies between CPX and human and bacterial enzymes are discussed. In the third part, theoretical investigations about UV-Vis parameters of CPX when it is interacting with the human enzyme and the possibility of an intermolecular energy transfer between CPX and hTopo-II are reported.

3.1. Validation of Computational methods

3.1.1. DFT EXC functional analysis

TD-DFT is a very efficient tool to reproduce, predict and interpret the absorption and emission spectra of a wide variety of molecules in "real life" environments, being regularly applied as a "black box model" to complement experimental measurements, as well as to provide new applications for the technique [31]. However, one weakness of the adiabatic approach to TD-DFT is its exacerbated dependence on the selection of an adequate EXC functional [32]. Previous studies already indicate that pure functionals are less consistent, whereas functionals incorporating a larger fraction of exact exchange (EE) underestimate significantly the transition energies. In this way, the most accurate excitation energies estimates are got by using a Global Hybrids (GH) functionals, containing between 22% and 25% of exact exchange (EE) or a Long-range-corrected-hybrid (LCH) functional with a small damping parameter [33–35]. The choice of functionals for testing in this work was based on those considerations. The average λmax obtained for the 25 conformations was submitted to Test T and the observed results are displayed in Figure 2 and 3.

Among both functionals, theoretical λmax calculations for free CPX in explicit water employing the most popular B3LYP functional (λmax/B3LYP/Explicit water=295 nm) showed overestimating the experimental value (275 nm). On the other hand, calculations employing LCWPBE ((λmax/LCWPBE/Explicit water=241 nm), ωB97X-D (λmax/ωB97X-D/Explicit water=256 nm) and M05-2X (λmax/M05-2X/Explicit water=254 nm) functionals resulted in theoretical average λmax values below to the experimental value. Unlike the functionals mentioned above, th e theoretical average λmax obtained using the functionals mPW1PW91(λmax/mPW1PW91/Explicit water=278 nm) and PBE0 ((λmax/PBE0/Explicit water=278 nm) were statistically equivalent to experimental value (Figure 4). This implies that among the most suitable

functional for excitation energy calculations, GH functionals containing exactly 25% of EE contribution, as mPW1PW91 and PBE0, prove to be optimal for computing excitation energies for CPX, and possibly for fluoroquinolones in general, allowing more accurate results. Considering these results, the mPW1PW91 EXC functional was chosen for TD-DFT calculations of the next steps.

Fig. 2 Box plot for theoretical calculations of λmax in comparison with experimental value (275 nm).
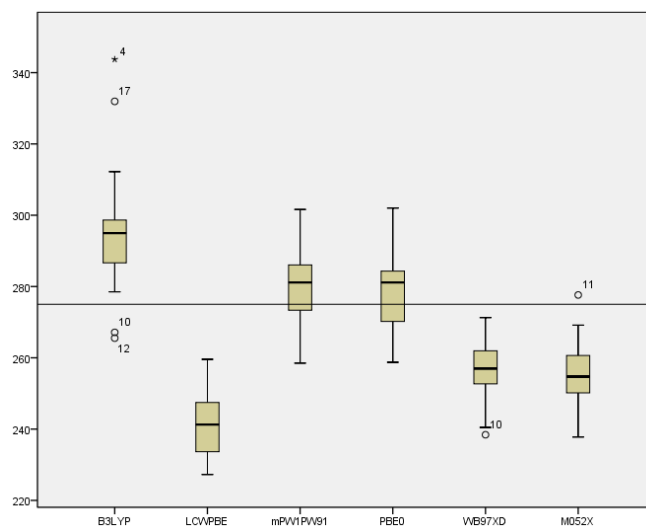

Fig. 3 Mean, standard deviation and standard error mean for λmax theoretical calculations, for each used EXC functional.

One-sample Statistics

b	N	Mean	Std. Deviation	Std. Error Mean
B3LYP	25	295.54	17.26	3.45
LCWPBE	25	241.22	9.02	1.80
mPW1PW91	25	278.96	10.18	2.04
PBE0	25	278.60	10.12	2;02
WB97XD	25	256.32	8.28	1.66
M052X	25	254.64	10.06	2.01

One-sample Test

	Test value =275					
	t	df	Sg. (2-tailed	Mean Diference	95% Confidence Interval of the Difference	
					Lower	Upper
B3LYP	5.95	24	.00	20.53	13.41	27.66
LCWPBE	-18.72	24	.00	-33.78	-37.50	-30.05
mPW1PW91	1.95	24	.06	3.96	-0.24	8.16
PBE0	1.78	24	.08	3.60	-0.57	7.78
WB97XD	-11.27	24	.00	-18.67	-22.09	-15.26
M052X	-10.12	24	.00	-20.36	-24.51	-16.21

3.1.2. Influence of the solvation model in TD-DFT calculations

UV-Vis spectra obtained in theoretical calculations in vacuum (λmax/mPW1PW91/Vacuum) and in the implicit solvent model (λmax/mPW1PW91/IEF-PCM/water) were compared with results of the explicit solvent model (λmax/mPW1PW91/Explicit water), which are plotted in Figure 4. The obtained value for λmax/mPW1PW91/IEF-PCM/water was equal to 307.93 nm, while for λmax/mPW1PW91/Vacuum, the obtained value was 306.23 nm. The two values are similar, being both higher than obtained value using the explicit solvent model (λmax/mPW1PW91/Explicit water = 278.96 nm). In addition, the two values were further from the experimental value (275 nm). The λmax/mPW1PW91/Vacuum and λmax/mPW1PW91/IEF-PCM/water are also different from theoretical calculations with the model λmax/mPW1PW91/Explicit water, which resulted in values very close to the experimental data. This indicates that, at least, one explicit solvent shell must be included in the system to guarantee more accurate results. In fact, our findings put in evidence that solvent effects play an important role in theoretical calculations of excited state properties.

Fig. 4 Theoretical UV-Vis spectra obtained in TD-DFT calculations for λmax/mPW1PW91/Explicit water, λmax/mPW1PW91/IEF-PCM/water and λmax/mPW1PW91/Vacuum.
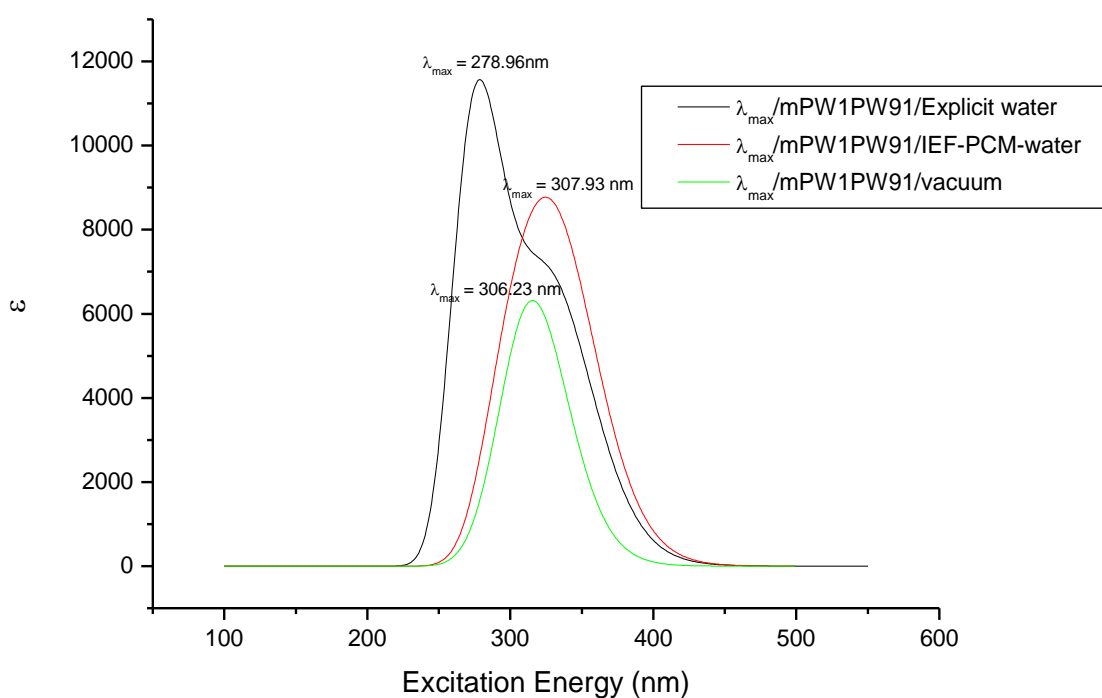
The presence of the first solvation shell is important to correctly predict intermolecular interactions that can occur between the molecules of interest and solvent molecules, which are crucial to explain specific solvent effects in shifts of absorption spectra [36]. In the case of CPX in water, dynamic simulations with explicit solvent model gave the most probable distribution of solvent molecules, and consequently gave a better description for the hydrogen bonds performed in the system. This hydrogen bonds are mostly responsible for the difference of λmax between vacuum and explicit water molecules.

3.3. Molecular docking calculations

CPX belongs to Fluoroquinolones (FQs) class, which represent one of the most highly prescribed antibiotic classes [37, 38]. Molecular target of FQs are the bacterial enzymes type II DNA topoisomerases, and their inhibitory action occurs by binding to the enzyme-DNA complex [39–41]. Topo-II enzyme is also present in humans and is associated with cancer disease [42–45]. In this context, several studies have reported the potential of FQs, such as CPX as anticancer drug, for several tumor cell lines [17, 18, 46, 47]. However, despite of these many promising experimental results, theoretical investigations about the mode of action of CPX molecule in hTOPO-II remain scarce in literature [48].

In order to better investigate the binding mode between CPX and hTOPO-II, molecular docking analysis were performed in two sites of the enzyme, (i) the active site (AS1), identified by Leu 826 residue; and (ii) the site in which the anticancer drug etoposide (EVP) acts (AS2). The obtained values for interaction energy and hydrogen bonds are in Table 1.

Table 1: Interaction energy (kcal.mol^{-1}) and hydrogen bonds energy (kcal.mol^{-1}) values from the docking analysis.

Ligand	Enzyme	Site	Interaction Energy (Kcal.mol^{-1})	HBond (Kcal.mol^{-1})
Ciprofloxacin	bTOPO-II	Active/interaction site	-77.11	-7.31
Ciprofloxacin	hTOPO-II	AS1	-64.54	0.00
Ciprofloxacin	hTOPO-II	AS2	-71.62	-4.21
EVP	hTOPO-II	AS2	-133.26	-9.51

Most stable interactions are found for EVP ligand in hTOPO-II, following by CPX in bTOPO-II. However, it is worth mentioning that a slight energy difference between CPX in bacteria and human (AS2) (Figure 5) enzymes was observed, which can suggest that CPX has similar inhibitory effects on both enzymes. As seen, CPX is more able to interact in AS2 than AS1 for the human enzyme. This suggests that CPX preferentially interacts in the same site as the chemotherapeutic EVP. It is also important to mention that no hydrogen bond was performed between CPX and hTOPO-II in AS1, while in AS2, the most stable conformations performed hydrogen bonds with Glu477, Tyr 821, Gln778 and Asp 479 amino acid residues.

Fig. 5 Molecular docking poses for **1)** Etoposide (EVP) docked in hTOPO-II enzyme; **2)** ciprofloxacin docked in AS2 of hTOPO-II enzyme, and **3)** ciprofloxacin docked into bTOPO-II enzyme.
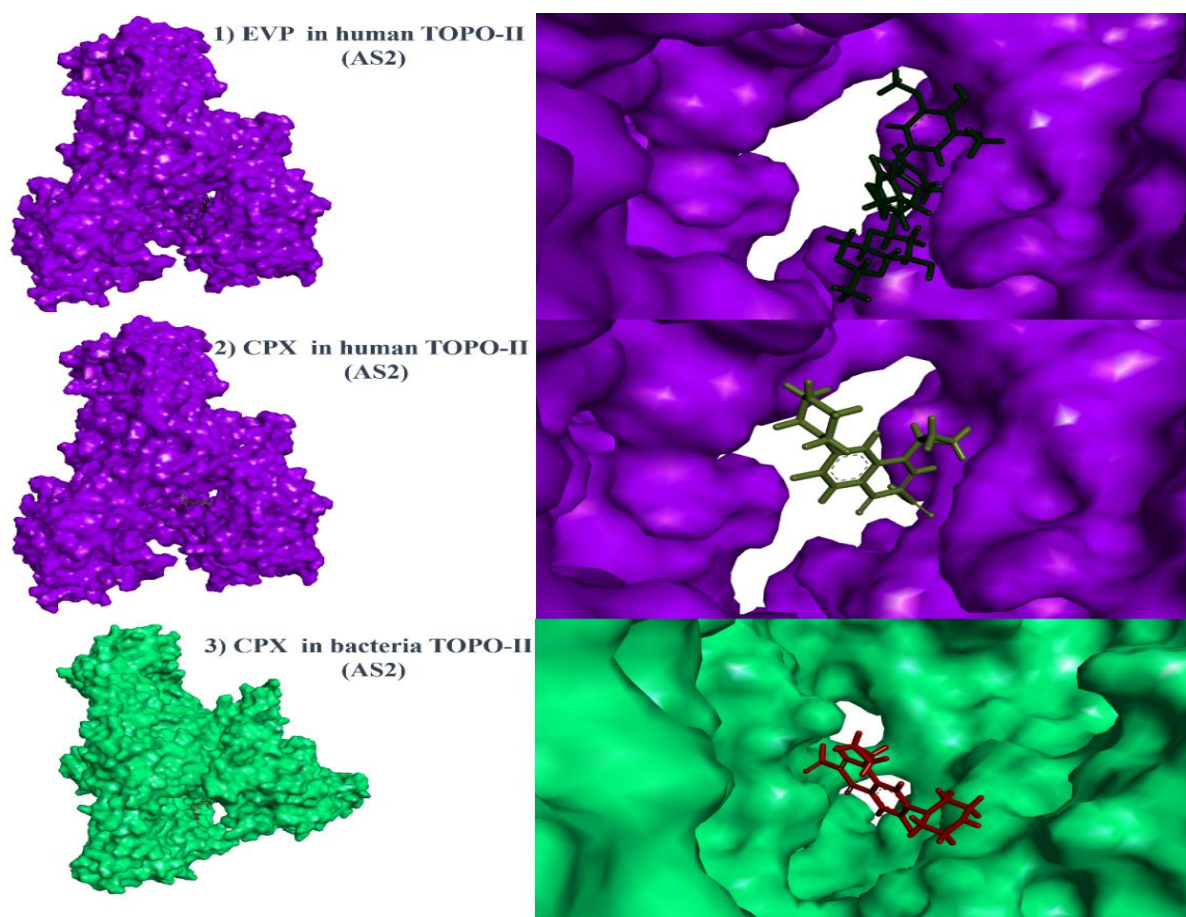

3.3. Spectroscopic parameters of CPX/Topo-II

3.3.1. UV-Vis parameters of CPX/hTopo-II

To establish λmax as one of the standard parameters for spectroscopic UV-Vis/fluorescent probe and identify the interaction of CPX with hTOPO-II, there must be a variation in λmax when the molecule is interacting with the enzyme. Keeping this in mind, UV-Vis spectra for CPX conformations, generated in docking simulation, were obtained considering its chemical environment within the human topo-II enzyme. The average λmax obtained for lower energy conformations was equal to 374 nm, against 278 nm for free CPX in water. For representative conformations, i.e. most stable conformations obtained in the docking simulation, λmax was equal to 380.35 nm. It is important to mention that despite the dispersion between λmax values for each conformation, reported in Figure 6, both values are above the obtained value for CPX in water. This result puts in evidence that, in general, when CPX is interacting with the hTOPO-II enzyme, there is an increase in λmax and a decrease in the absorption energy.

Decrease in the absorption energy can be attributed to the fact that CPX is already receiving energy from Tyr residue. Variations in λmax for each conformation can be attributed that there is a dependence of the dipole orientation of involved molecules to occur energy transfer, and different positions of CPX in AS2 can generate changes in spatial orientation of the electrical dipoles, and consequently, variations in energy exchange.

Fig. 6 λmax variation for CPX molecule in water and binding with human Topo-II
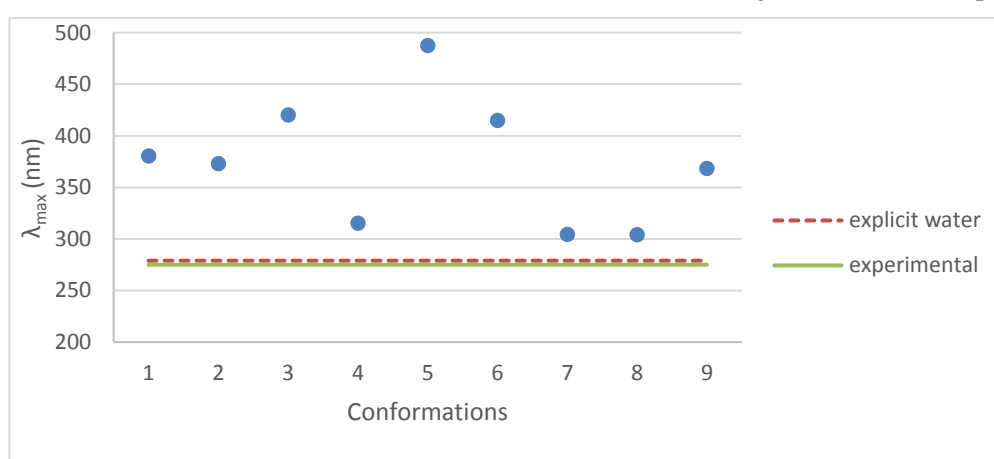
enzyme.

3.3.2. Fluorescence parameters of the CPX/hTopo-II complex

It is known that aromatic amino acid residues presents fluorescence, such as tryptophan (Trp), tyrosine (Tyr) and phenylalanine (Phe)[49]. Among them, Trp is the main exploited residue, because of its high quantum yield in proteins and sensitivity of its fluorescent properties to local environment [50]. To produce a change in fluorescence signal, it is needed to occur changes in microenvironment of the residue, caused by conformational changes in protein. However, when Trp residue is distant of the interaction site, there is no significant conformational change caused by binding of ligands, and consequently, fluorescence signal may remain unchanged. An alternative widely employed to solve this problem is to analyze other fluorescent residues that are closer to the interaction site, the Tyr residue, of the studied enzyme.

Considering that conformational changes of proteins can generate variations in the Tyr fluorescence, it is also possible to use this spectroscopic parameter for probing structural rearrangements of proteins, such as tryptophan [51]. With hTOPO-II, Tyr residue is the closest to the interaction site, and because of this feature, was chosen for the current analysis.

Therefore, to have a clue about the probability of energy exchange, an analysis of superimposition volume of distance constraint spheres of 3.5 Å, for interaction points between CPX and Tyr residue (Figure 7) was performed. The superimposition of the two spheres can be interpreted as a favorable orientation between donor and acceptor of energy [14]. By Figure 8, it can be seen that 63.3% of distance constraint spheres for all docking poses of are superimposed, which indicates a strong probability of energy transfer [14, 52]. This result in combination with previous theoretical findings of absorption energy for CPX can suggest that there is a non-radiative energy exchange by FRET mechanism, being Tyr residue the donor and CPX the acceptor.

Fig. 7 Superimposition of distance constraint for CPX and Tyr aminoacid residue of hTOPO-II enzyme, with 1.5 and 3.5 Å of distance for internal and external sphere, respectively.
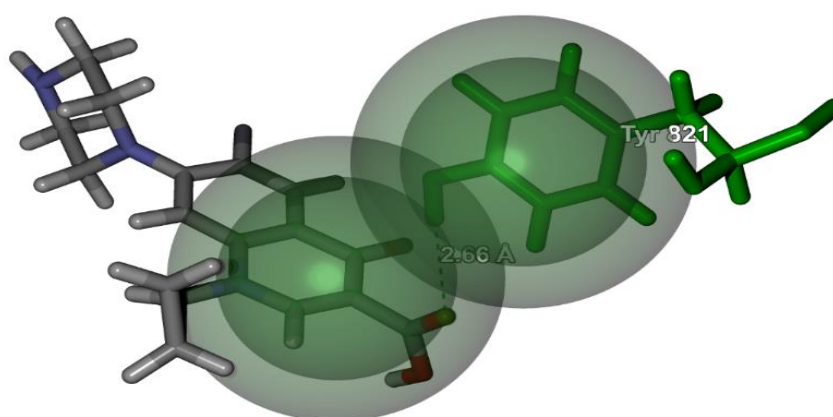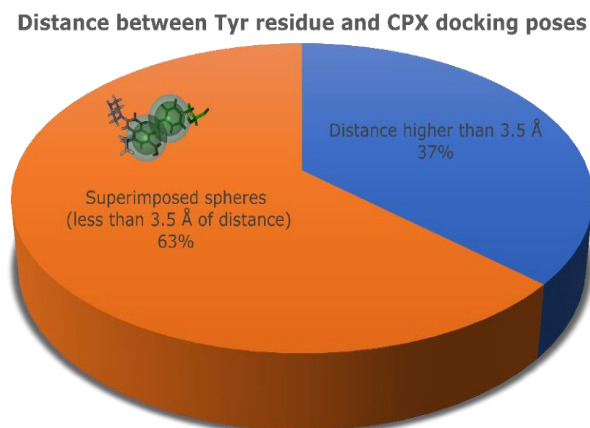
Fig. 8 Interlocked distance constraints for ciprofloxacin docking poses and Tyr (821) residue.

Distance between Tyr residue and CPX docking poses

Distance higher than 3.5 Å
37%

Superimposed spheres
(less than 3.5 Å of distance)
63%

4. Conclusion

By theoretical investigations, the interaction between CPX and hTOPO-II β, and the influence of this interaction in fluorescence/UV-Vis parameters, was analyzed. It was found that CPX is able to interact with the hTOPO-II enzyme at levels of interaction energy comparable with the interaction between CPX and the bTOPO-II enzyme. Additionally, the most probable site where CPX interacts with the human enzyme is in the same site that chemotherapeutic etoposide acts. For theoretical calculations of excited states, it was found that Global Hybrid functionals containing exactly 25% of EE contribution, as mPW1PW91 and PBE0, are the most suitable to provide accurate results for UV-Vis spectra of CPX molecule and possibly for fluoroquinolones. Considering the solvation model, explicit solvent calculations prove to be more appropriate, once solvent molecules are important to consider correctly the intermolecular interactions that may occur between molecule and solvent, in this case CPX and water molecules. Finally, UV-vis spectra of CPX in complex with the human enzyme showed a red shift in λmax, when compared with UV-Vis spectra for free CPX in water.

From these theoretical findings, it can be suggested that both Tyr fluorescence and CPX UV-Vis signal can be used as a marker for the development of a dual fluorescent/UV-Vis probe, based on the interaction between CPX and hTOPO-II enzyme, which can monitor the overexpression of human topoisomerase-II enzymes. Because this overexpression is associated with cancer disease, this system constitutes a promising alternative for cancer diagnosis. These results reveal very important data for future tests, considering that the cancer remains without cure, and the early diagnosis of

this disease can save many lives. Besides that, this study can also serve as a basis for future experiments and other theoretical studies, as a starting point for the development of compounds derived from ciprofloxacin antibiotic, which can act as even more efficient fluorescent probes, and with lower levels of toxicity.

5. References

1. INCA (2011) ABC do câncer: abordagens básicas para o controle do câncer

2. Shukla KK, Sankanagoudar S, Sanganeria BS, et al (2019) Recent Advances in Molecular Diagnostic Approaches for Cancer. In: Molecular Diagnostics in Cancer Patients. Springer Singapore, Singapore, pp 1–9

3. Siegel RL, Miller KD, Jemal A (2020) Cancer statistics, 2020. CA Cancer J Clin 70:7–30. https://doi.org/10.3322/caac.21590

4. Organization WHInA for research on C Cancer Today. https://gco.iarc.fr/today/online-analysis-multi-bars?v=2020&mode=population&mode_population=countries&population=900&populations=900&key=total&sex=0&cancer=39&type=0&statistic=5&prevalence=0&population_group=0&ages_group%5B%5D=0&ages_group%5B%5D=17&nb_ite. Accessed 28 Jan 2021

5. Bao S, Hu T, Liu J, et al (2021) Genomic instability-derived plasma extracellular vesicle-microRNA signature as a minimally invasive predictor of risk and unfavorable prognosis in breast cancer. J Nanobiotechnology 19:22. https://doi.org/10.1186/s12951-020-00767-3

6. Jia M, Mao Y, Wu C, et al (2019) A platform for primary tumor origin identification of circulating tumor cells via antibody cocktail-based in vivo capture and specific aptamer-based multicolor fluorescence imaging strategy. Anal Chim Acta 1082:136–145. https://doi.org/10.1016/j.aca.2019.07.051

7. Baxter GC, Selamoglu A, Mackay JW, et al (2021) A meta-analysis comparing the diagnostic performance of abbreviated MRI and a full diagnostic protocol in breast cancer. Clin Radiol 76:154.e23-154.e32. https://doi.org/10.1016/j.crad.2020.08.036

8. Yan J, Liang B, Lv Y, Li Y (2020) Monitoring and Analysis of Early Heart Structure of Fetus in Gynecology and Obstetrics Based on Ultrasound Image. J Med Imaging Heal Informatics 11:973–980. https://doi.org/10.1166/jmihi.2021.3350

9. Yuan Y, Lang N, Yuan H (2021) Rapid-kilovoltage-switching dual-energy computed tomography (CT) for differentiating spinal osteolytic metastases from spinal infections. Quant Imaging Med Surg 11:620–627. https://doi.org/10.21037/QIMS-20-334

10. Shahzad A, Knapp M, Edetsberger M, et al (2010) Diagnostic application of fluorescence spectroscopy in oncology field: Hopes and challenges. Appl Spectrosc Rev 45:92–99. https://doi.org/10.1080/05704920903435599

11. Pundi A, Chang CJ, Chen YS, et al (2021) An aniline trimer-based multifunctional sensor for colorimetric Fe^{3+}, Cu^{2+} and Ag^+ detection, and its complex for fluorescent sensing of L-tryptophan. Spectrochim Acta - Part A Mol Biomol Spectrosc 247:119075. https://doi.org/10.1016/j.saa.2020.119075

12. Russell AJ, Westwood IM, Crawford MHJ, et al (2009) Selective small molecule inhibitors of the potential breast cancer marker, human arylamine N-acetyltransferase 1, and its murine homologue, mouse arylamine N-acetyltransferase 2. Bioorganic Med Chem 17:905–918. https://doi.org/10.1016/j.bmc.2008.11.032

13. da Rocha EP, Rodrigues HA, da Cunha EFF, Ramalho TC (2016) Probing kinetic and thermodynamic parameters as well as solvent and substituent effects on spectroscopic probes of 2-amino-1,4-naphthoquinone derivatives. Comput Theor Chem 1096:17–26. https://doi.org/10.1016/j.comptc.2016.09.028

14. Prandi IG, Ramalho TC, França TCC (2019) Esterase 2 as a fluorescent biosensor for the detection of organophosphorus compounds: docking and electronic insights from molecular dynamics. Mol Simul 45:1432–1436. https://doi.org/10.1080/08927022.2019.1648808

15. Li R, Huang X, Lu G, Feng C (2018) A fluorescence and UV/vis absorption dual-signaling probe with aggregation-induced emission characteristics for specific detection of cysteine. RSC Adv 8:24346–24354. https://doi.org/10.1039/c8ra03756f

16. Zhou D-C, Lu Y-T, Mai Y-W, et al (2019) Design, synthesis and biological evaluation of novel perimidine o-quinone derivatives as non-intercalative topoisomerase II catalytic inhibitors. Bioorg Chem 91:103131. https://doi.org/10.1016/J.BIOORG.2019.103131

17. Kassab AE, Gedawy EM (2018) Novel ciprofloxacin hybrids using biology oriented drug synthesis (BIODS) approach: Anticancer activity, effects on cell cycle

profile, caspase-3 mediated apoptosis, topoisomerase II inhibition, and antibacterial activity. Eur J Med Chem 150:403–418. https://doi.org/10.1016/j.ejmech.2018.03.026

18. Beberok A, Wrześniok D, Minecka A, et al (2018) Ciprofloxacin-mediated induction of S-phase cell cycle arrest and apoptosis in COLO829 melanoma cells. Pharmacol Reports 70:6–13. https://doi.org/10.1016/j.pharep.2017.07.007

19. Idowu T, Schweizer F (2017) Ubiquitous nature of fluoroquinolones: The oscillation between antibacterial and anticancer activities. Antibiotics 6

20. Phiboonchaiyanan PP, Kiratipaiboon C, Chanvorachote P (2016) Ciprofloxacin mediates cancer stem cell phenotypes in lung cancer cells through caveolin-1-dependent mechanism. Chem Biol Interact 250:1–11. https://doi.org/10.1016/j.cbi.2016.03.005

21. Beberok A, Wrześniok D, Rok J, et al (2018) Ciprofloxacin triggers the apoptosis of human triple-negative breast cancer MDA-MB-231 cells via the p53/Bax/Bcl-2 signaling pathway. Int J Oncol 52:1727–1737. https://doi.org/10.3892/ijo.2018.4310

22. Yadav V, Varshney P, Sultana S, et al (2015) Moxifloxacin and ciprofloxacin induces S-phase arrest and augments apoptotic effects of cisplatin in human pancreatic cancer cells via ERK activation. BMC Cancer 15:581. https://doi.org/10.1186/s12885-015-1560-y

23. Senthilkumar M, Sheelarani B, Joshi RG, Dash S (2019) Solubilization and interaction of ciprofloxacin with pluronics and their mixed micelles. New J Chem 43:16530–16537. https://doi.org/10.1039/c9nj03383a

24. Alizadeh K, Mobarrez M, Ganjali MR, et al (2012) Spectrofluorimetric study of the interaction of ciprofloxacin with amino acids in aqueous solution following solvatochromic studies. Spectrochim Acta Part A Mol Biomol Spectrosc 94:72–77. https://doi.org/10.1016/j.saa.2012.03.053

25. Team RC (2019) R: A language and environment for statistical computing. In: R Found. Stat. Comput. Vienna, Austria

26. Giacoppo JOS, França TCC, Kuča K, et al (2015) Molecular modeling and in vitro reactivation study between the oxime BI-6 and acetylcholinesterase inhibited by different nerve agents. J Biomol Struct Dyn 33:2048–2058. https://doi.org/10.1080/07391102.2014.989408

27. Berman HM, Westbrook J, Feng Z, et al (2000) The Protein Data Bank. Nucleic Acids Res 28:235–42

28. Dapprich S, Komáromi I, Byun KS, et al (1999) A new ONIOM implementation in Gaussian98. Part I. The calculation of energies, gradients, vibrational frequencies and electric field derivatives. J Mol Struct THEOCHEM 461–462:1–21. https://doi.org/10.1016/S0166-1280(98)00475-8

29. Forster T (1946) Energiewanderung und Fluoreszenz. Naturwissenschaften 33:166–175. https://doi.org/10.1007/BF00585226

30. Souza ER, Sigoli FA (2012) Princípios fundamentais e modelos de transferência de energia inter e intramolecular. Quim Nova 35:1841–1847. https://doi.org/10.1590/S0100-40422012000900024

31. Ali R, Alminderej FM, Messaoudi S, Saleh SM (2021) Ratiometric ultrasensitive optical chemisensor film based antibiotic drug for Al(III) and Cu(II) detection. Talanta 221:. https://doi.org/10.1016/j.talanta.2020.121412

32. Jacquemin D, Adamo C (2015) Computational Molecular Electronic Spectroscopy with TD-DFT. In: Topics in current chemistry. pp 347–375

33. Jacquemin D, Wathelet V, Perpète EA, Adamo C (2009) Extensive TD-DFT Benchmark: Singlet-Excited States of Organic Molecules. J Chem Theory Comput 5:2420–2435. https://doi.org/10.1021/ct900298e

34. Jacquemin D MB and AC (2011) Excited-state calculations with TD-DFT: from benchmarks to simulations in complex environments. Phys Chem Chem Phys 13:16987–98

35. La Porta FA, Ramalho TC, Santiago RT, et al (2011) Orbital signatures as a descriptor of regioselectivity and chemical reactivity: The role of the frontier orbitals on 1,3-dipolar cycloadditions. J Phys Chem A 115:824–833. https://doi.org/10.1021/jp108790w

36. Martínez-Fernández L, Pepino AJ, Segarra-Martí J, et al (2016) Computing the Absorption and Emission Spectra of 5-Methylcytidine in Different Solvents: A Test-Case for Different Solvation Models. J Chem Theory Comput 12:4430–4439. https://doi.org/10.1021/acs.jctc.6b00518

37. Cdc R (2017) Outpatient Antibiotic Prescriptions — United States, 2017

38. Centers for Disease Control and Prevention (2016) OUTPATIENT ANTIBIOTIC PRESCRIPTIONS-United States

39. Fief CA, Hoang KG, Phipps SD, et al (2019) Examining the Impact of Antimicrobial Fluoroquinolones on Human DNA Topoisomerase IIα and IIβ. ACS Omega 4:4049–4055. https://doi.org/10.1021/acsomega.8b03428

40. Vance-Bryan K, Guay DRP, Rotschafer JC (1990) Clinical Pharmacokinetics of Ciprofloxacin. Clin Pharmacokinet 19:434–461. https://doi.org/10.2165/00003088-199019060-00003

41. Garoff L, Pietsch F, Huseby DL, et al (2020) Population Bottlenecks Strongly Influence the Evolutionary Trajectory to Fluoroquinolone Resistance in Escherichia coli. Mol Biol Evol 37:1637–1646. https://doi.org/10.1093/molbev/msaa032

42. Withoff S, De Jong S, De Vries EG, Mulder NH (1996) Human DNA topoisomerase II: biochemistry and role in chemotherapy resistance (review). Anticancer Res 16:1867–80

43. McClendon AK, Osheroff N (2007) DNA topoisomerase II, genotoxicity, and cancer. Mutat Res Mol Mech Mutagen 623:83–97. https://doi.org/10.1016/j.mrfmmm.2007.06.009

44. Kirk E. Hevenern, Tatsiana A. Verstak KEL, Daniel L. Riggsbee JWM (2018) Recent developments in topoisomerase-targeted cancer chemotherapy. Acta Pharm Sin B 8:844–861

45. Larsen AK, Escargueil AE, Skladanowski A (2003) Catalytic topoisomerase II inhibitors in cancer therapy. Pharmacol Ther 99:167–181. https://doi.org/10.1016/S0163-7258(03)00058-5

46. Beberok A, Wrześniok D, Rok J, et al (2018) Ciprofloxacin triggers the apoptosis of human triple-negative breast cancer MDA-MB-231 cells via the p53/Bax/Bcl-2 signaling pathway. Int J Oncol. https://doi.org/10.3892/ijo.2018.4310

47. Jaber DF, Jallad MAN, Abdelnoor AM (2017) The effect of ciprofloxacin on the growth of B16F10 melanoma cells. J Cancer Res Ther 13:956–960. https://doi.org/10.4103/0973-1482.180610

48. Abdel-Aziz AAM, Asiri YA, Al-Agamy MHM (2011) Design, synthesis and antibacterial activity of fluoroquinolones containing bulky arenesulfonyl fragment: 2D-QSAR and docking study. Eur J Med Chem 46:5487–5497. https://doi.org/10.1016/j.ejmech.2011.09.011

49. Yang H, Xiao X, Zhao X, Wu Y (2017) Intrinsic fluorescence spectra of tryptophan, tyrosine and phenyloalanine. In: Lv Y, Le J, Chen H, et al (eds) Selected Papers of the Chinese Society for Optical Engineering Conferences held October and November 2016. SPIE, p 102554M

50. Lakowicz JR (2006) Principles of fluorescence spectroscopy. Springer

51. Zhdanova NG, Shirshin EA, Maksimov EG, et al (2015) Tyrosine fluorescence probing of the surfactant-induced conformational changes of albumin. Photochem Photobiol Sci 14:897–908. https://doi.org/10.1039/c4pp00432a

52. Carullo P, Cetrangolo GP, Mandrich L, et al (2015) Fluorescence Spectroscopy Approaches for the Development of a Real-Time Organophosphate Detection System Using an Enzymatic Sensor. Sensors 15:3932–3951. https://doi.org/10.3390/s150203932

4. ATTACHMENTS

4.1. List of publications

1. *Ciprofloxacin/Topoisomerase-II complex as a promising dual UV-Vis/fluorescent probe: accomplishments and opportunities for the cancer diagnosis*

   <u>Sales, T. A.</u>; Ramalho, T.C.

   Accepted for publication

2. *Thermal and structural parameters of the interaction between ciprofloxacin and human topoisomerase-II β enzyme: Toward new MRI probes*

   <u>Sales, T. A.</u>; Ramalho, T.C.

   Submited

3. *Computational design of synthetic receptors for drug detection: interaction between molecularly imprinted polymers and MDMA (3,4-methylenedioxymethamphetamine)*

   <u>Sales, T. A</u>.; Ramalho, T. C.

   Theoretical Chemistry Accounts, v. 139, p. 31, 2020. DOI 10.1007/s00214-020-2543-x

4. *Vanillic acid as phospholipase A 2 and proteases inhibitor: In vitro and computational analyses.*

   Cesar, Pedro H. S.; Trento, Marcus V.; <u>Sales, Thais A</u>.; Simão, Anderson A.; Ramalho, Teodorico C.; Marcussi, Silvana.

   Biotechnology And Applied BiochemistrY, v. 00, p. 1-11, 2020. DOI 10.1002/bab.1943

5. *Current anti-inflammatory therapies and the potential of secretory Phospholipase A2 inhibitors in the design of new anti-inflammatory drugs: a review of 2012 – 2018.*

   <u>Sales, T. A.</u>; Marcussi, S.; Ramalho, Teodorico

   Current Medicinal Chemistry, v. 26, p. 1, 2019. DOI: 10.2174/0929867326666190201120646

6. *Recent Developments in Metal-Based Drugs and Chelating Agents for Neurodegenerative Diseases Treatments*

Thais A. Sales; Ingrid G. Prandi; Alexandre A. De Castro; Daniel H. S. Leal; Elaine F.F. Da Cunha; Kamil Kuca; Teodorico C. Ramalho

International Journal of Molecular Sciences, v. 20, p. 1829, 2019. DOI: 10.3390/ijms20081829

7. *Molecular interactions between p -coumaric acid and snake venom toxins*

Cesar, Pedro H. S.; Cardoso Trento, Marcus Vinícius; Sales, Thais A.; Marques, Tamara R.; Braga, Mariana A.; Ramalho, Teodorico C.; Marcussi, Silvana.

Journal of Cellular Biochemistry, v. 120, p. 14594-14603, 2019. DOI: 10.1002/jcb.28721

8. *Exploring the structural and functional aspects of the phospholipase A2 from Naja spp*

Trento, Marcus Vinícius Cardoso ; Sales, Thais Aparecida ; De Abreu, Tatiane Silva ; Braga, Mariana Aparecida ; Cesar, Pedro Henrique Souza ; Marques, Tamara Rezende ; Marcussi, Silvana

International Journal of Biological Macromolecules, v. 140, p. 49-58, 2019. DOI 10.1016/j.ijbiomac.2019.08.125

9. *Can Inhibitors of Snake Venom Phospholipases A2 Lead to New Insights into Anti-Inflammatory Therapy in Humans? A Theoretical Study*

Sales, Thaís; Marcussi, Silvana ; Da Cunha, Elaine ; Kuca, Kamil ; Ramalho, Teodorico

Toxins, v. 9, p. 341, 2017. DOI 10.3390/toxins9110341

10. *Essential Oils from the Leaves and Flowers of Callistemon viminalis: Chemical Characterization and Evaluation of the Insecticide and Antifungal Activities*

Sales, Thais Aparecida; Cardoso, Maria Das Graças ; Guimarães, Luiz Gustavo De Lima ; Camargo, Karen Caroline ; Rezende, Danúbia.A.C.S ; Brandão, Rafaela Magalhães ; Souza, Rafaela Vieira ; Ferreira, Vanúzia.R.F. ; Marques, Ana Ermelinda ; Magalhães, Maísa Lamounier; Nelson, David Lee

American Journal of Plant Sciences, v. 08, p. 2516-2529, 2017. DOI 10.4236/ajps.2017.810171

11. *Antimicrobial Activity of the Essential Oil from Hyptis carpinifolia Benth.*

Camargo, Karen Caroline ; Batista, Luís Roberto ; De Souza, Paulo Estevão ; Teixeira, Maria Luisa ; Sales, Thaís Aparecida ; Fernandes Ferreira, Vanuzia Rodrigues ; E Nogueira, Jéssica Oliveira ; Magalhães, Maísa Lamounier ; Caetano, Alex Rodrigues Silva ; Nelson, David Lee ; Das Graças Cardoso, Maria .

American Journal of Plant Sciences, v. 08, p. 2871-2877, 2017. DOI 10.4236/ajps.2017.811195

12. *Phytochemical Screening, Extraction of Essential Oils and Antioxidant Activity of Five Species of Unconventional Vegetables*

Sousa Carvalho, Marcos Schleiden ; Graças Cardoso, Maria Das ; Resende, Luciane Vilela ; Souza Gomes, Marcos De ; Marques Albuquerque, Luiz Roberto ; Silvestri Gomes, Anni Cristini ; Sales, Thaís Aparecida ; Camargo, Karen Caroline ; Nelson, David Lee ; Costa, Gabriele Mikami ; Espósito, Mariana Araújo ; Lima E Silva, Luis Felipe

American Journal of Plant Sciences, v. 06, p. 2632-2639, 2017. DOI 10.4236/ajps.2015.616265

13. *Light quality affects in vitro growth and essential oil profile in Lippia alba (Verbenaceae).*

Batista, Diego Silva ; De Castro, Kamila Motta ; Da Silva, Anderson Rodrigo ; Teixeira, Maria Luisa ; Sales, Thaís Aparecida ; Soares, Luana Isac ; Das Graças Cardoso, Maria ; De Oliveira Santos, Marcelo ; Viccini, Lyderson Facio ; Otoni, Wagner Campos

In Vitro Cellular & Developmental Biology - Plant, v. 1, p. 1-7, 2016. DOI 10.1007/s11627-016-9761-x

14. *Chemical Characterization and Application of the Essential Oils from Chenopodium ambrosioides and Philodendron bipinnatifidum in the Control of Diabrotica speciosa (Coleoptera: Chrysomelidae)*

Santiago, Juliana De Andrade ; Cardoso, Maria Das Graças ; Figueiredo, Ana Cristina Da Silva ; Moraes, Jair Campos De ; Assis, Franscinely Aparecida De ; Teixeira, Maria Luisa ; Santiago, Wilder Douglas ; Sales, Thaís Aparecida ; Camargo, Karen Caroline ; Nelson, David Lee

American Journal of Plant Sciences, v. 05, p. 3994-4002, 2014. DOI 10.4236/ajps.2014.526417